



UNIL | Université de Lausanne

Unicentre

CH-1015 Lausanne

<http://serval.unil.ch>

---

Year : 2019

## The Role of Novel Kinases in Adipose Tissue Biology

Nasrallah Anita

Nasrallah Anita, 2019, The Rôle of Novel Kinases in Adipose Tissue Biology

Originally published at : Thesis, University of Lausanne

Posted at the University of Lausanne Open Archive <http://serval.unil.ch>

Document URN : urn:nbn:ch:serval-BIB\_D66AA80EAC1B0

### **Droits d'auteur**

L'Université de Lausanne attire expressément l'attention des utilisateurs sur le fait que tous les documents publiés dans l'Archive SERVAL sont protégés par le droit d'auteur, conformément à la loi fédérale sur le droit d'auteur et les droits voisins (LDA). A ce titre, il est indispensable d'obtenir le consentement préalable de l'auteur et/ou de l'éditeur avant toute utilisation d'une oeuvre ou d'une partie d'une oeuvre ne relevant pas d'une utilisation à des fins personnelles au sens de la LDA (art. 19, al. 1 lettre a). A défaut, tout contrevenant s'expose aux sanctions prévues par cette loi. Nous déclinons toute responsabilité en la matière.

### **Copyright**

The University of Lausanne expressly draws the attention of users to the fact that all documents published in the SERVAL Archive are protected by copyright in accordance with federal law on copyright and similar rights (LDA). Accordingly it is indispensable to obtain prior consent from the author and/or publisher before any use of a work or part of a work for purposes other than personal use within the meaning of LDA (art. 19, para. 1 letter a). Failure to do so will expose offenders to the sanctions laid down by this law. We accept no liability in this respect.



**UNIL** | Université de Lausanne

Faculté de biologie  
et de médecine

**Centre de Génomique Intégrative (CIG)**

**The Role of Novel Kinases in Adipose Tissue Biology**

**Thèse de doctorat ès sciences de la vie (PhD)**

Programme Cardiovasculaire et Métabolisme

Présentée à la

Faculté de biologie et médecine  
De l'Université de Lausanne

par

**Anita NASRALLAH**

Biologiste diplômée du Master de  
Lebanese American University

**Jury**

Prof. Yvan Arsenijevic, Président  
Prof. Lluís Fajas Coll, Directeur de thèse  
Prof. Kei Sakamoto, Expert  
Prof. Bart Deplancke, Expert

Lausanne, 28 Mai 2019





**UNIL** | Université de Lausanne

Faculté de biologie  
et de médecine

**Centre de Génomique Intégrative (CIG)**

**The Role of Novel Kinases in Adipose Tissue Biology**

**Thèse de doctorat ès sciences de la vie (PhD)**  
Programme Cardiovasculaire et Métabolisme

Présentée à la

Faculté de biologie et médecine  
De l'Université de Lausanne

par

**Anita NASRALLAH**

Biologiste diplômée du Master de  
Lebanese American University

**Jury**

Prof. Yvan Arsenijevic, Président  
Prof. Lluis Fajas Coll, Directeur de thèse  
Prof. Kei Sakamoto, Expert  
Prof. Bart Deplancke, Expert

Lausanne, 28 Mai 2019

# Imprimatur

Vu le rapport présenté par le jury d'examen, composé de

<b>Président·e</b>	Monsieur	Prof.	Yvan	<b>Arsenijevic</b>
<b>Directeur·trice de thèse</b>	Monsieur	Prof.	Lluis	<b>Fajas Coll</b>
<b>Expert·e·s</b>	Monsieur	Prof.	Kei	<b>Sakamoto</b>
	Monsieur	Prof.	Bart	<b>Deplancke</b>

le Conseil de Faculté autorise l'impression de la thèse de

**Madame Anita Nasrallah**

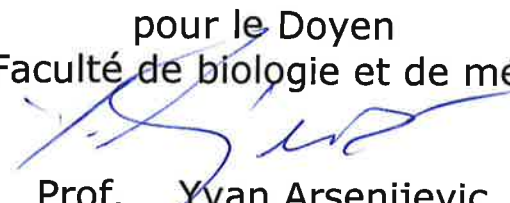
Master in Molecular Biology, Lebanese American University, Liban

intitulée

**The role of novel kinases in adipose tissue biology**

Lausanne, le 21 juin 2019

pour le Doyen  
de la Faculté de biologie et de médecine



Prof. Yvan Arsenijevic

*"Listen to advice and accept discipline, and at  
the end you will be counted among the wise"*

*Proverb 19:20*

*To my beloved parents Therese and Ibrahim*

*&*

*In loving memory of my cousin Aline*



---

# *Acknowledgements*

---

The past five years at UNIL, enduring the rigors of a challenging PhD, would not have been possible without the mentorship of my thesis advisor, Prof. Lluís Fajas Coll. I am grateful for his guidance, patience, and support during my studies. Thank you Lluís for believing in me and always driving me to do better.

Being a part of the Fajas lab is a badge I wear with pride. I am very lucky to have had the chance to share a lab life with amazing colleagues, present and former members, especially Laia, Judit, and Tiziana (an adopted Fajas lab member). Girls, you are truly a family. I will never forget our mini and maxi vacations, our crazy laughs, our gossip sessions, our foolish plans for the future, and of course our super-duper travels. I would like to thank our secretary Mrs. Carine Dovat for making my bureaucratic life easier.

It has been an enriching experience at the Department of Physiology and the Center for Integrative Genomics. It felt like home among amazing scientists. I was fortunate to meet my mentor Prof. Christian Fankhauser, who in time of need was by my side.

My life outside the lab was outstanding, thanks to an amazing bunch of friends. They were my refuge when I felt homesick. Louma, Nura and Zeina, my girl squad, thank you for helping me out in times of need, and more importantly, teaching me how to live a happy life away from home. Karim, Hassan, Mohammad and Hamid, thank you for showing me the true meaning of ambition. I am proud to have brothers like you (minus the shisha...).

Best friends are the spice of life they say. Perla, you are the sugar, the salt, and the pepper! You are the sister I've always wanted. You never stopped believing in me, and helped me believe in myself. Thank you for showing me what is really important in life. Nathalie, my partner in crime! Life had it tough on us, but we made it. We will always do. I will be waiting for you at the end of the tunnel, when you get your PhD. I am so lucky to have you both in my life, and I love you so much.

This whole journey would be a rutted road had it not been for my beloved parents, who stood by me every step of the way, and never ever put a ceiling to my ambition. I am eternally grateful, and it is to them that I owe everything that was, is, and will be. I love you more than life itself. Aline, my guardian angel, may your soul rest in peace.



---

# *Abstract*

---

Obesity, the accumulation of excess body fat, is an epidemic leading to numerous human metabolic diseases, such as type 2 diabetes (T2D). T2D is mainly characterized by hyperglycemia, accompanied by local (adipose tissue) and systemic insulin resistance. In the adipose tissue, insulin resistance involves alterations in the cross-talk of various signaling cascades, implicating numerous kinases and phosphatases. To identify molecular changes that occur during the development of insulin resistance, we have used here a new activity-based method to study the global kinase activity in human adipose tissue, the PamGene. Our study is based on the observation that some obese subjects do not develop insulin resistance. This population represents our control group, which avoids confounding results, due to obesity by itself rather than to insulin resistance. We found that a specific set of kinase activities are representative of insulin resistance in the obese population, such as PIM family, CHK2, and CDK10. In particular, we found that the Serine/Threonine kinase (STK) PIM-1, unlike the other PIM proteins, has increased activity in the visceral adipose tissue (VAT) of morbid obese diabetic (MOD) insulin resistant (IR) patients. We show that PIM-1 inhibition decreases the inflammatory capacity of bone marrow-derived macrophages in vitro, and leads to a decrease in the inflammatory profile in visceral adipose tissue (VAT), as well as to an increase in insulin sensitivity in diabetic mice. Furthermore, we found that CHK2 has higher activity in VAT of MOD patients, and we prove that the pharmaceutical inhibition of CHK2 in diabetic mice reduces their IR phenotype. Even though CDK10 was also found to be upregulated in VAT of MOD patients, it does not show any clear cut metabolic phenotype in CDK10 ablated knock out mice. Finally, the use of this innovative technique has paved the way to finding new kinases implicated in insulin resistance of the visceral adipose tissue, and to initiating new lines of research for further validation studies.



---

## Résumé

---

L'obésité, l'accumulation de l'excès de graisse corporelle, est une épidémie qui entraîne de nombreuses maladies métaboliques chez l'homme, telles que le diabète de type 2 (DT2). Le DT2 est principalement caractérisé par une hyperglycémie, accompagnée d'une résistance à l'insuline locale (tissu adipeux) et systémique. Dans le tissu adipeux, la résistance à l'insuline implique des modifications de la diaphonie de différentes cascades de signalisation, impliquant de nombreuses kinases et phosphatases. Pour identifier les changements moléculaires survenant au cours du développement de la résistance à l'insuline, nous avons utilisé ici une nouvelle méthode basée sur l'activité pour étudier l'activité de la kinase globale dans le tissu adipeux humain, le PamGene. Notre étude est basée sur l'observation que certains sujets obèses ne développent pas de résistance à l'insuline. Cette population représente notre groupe témoin, ce qui évite les résultats confondants, dus à l'obésité en soi plutôt qu'à la résistance à l'insuline. Nous avons constaté qu'un ensemble spécifique d'activités de kinases est représentatif de la résistance à l'insuline dans la population obèse, tel que la famille PIM, CHK2 et CDK10. En particulier, nous avons constaté que la protéine PIM-1 de la sérine / thréonine (STK), contrairement aux autres protéines de la protéine PIM, avait augmenté l'activité du tissu adipeux viscéral (VAT) des patients insulino-résistants (IR) morbides diabétiques obèses (MOD). Nous montrons que l'inhibition de PIM-1 diminue la capacité inflammatoire des macrophages dérivés de la moelle osseuse *in vitro* et conduit à une diminution du profil inflammatoire dans le tissu adipeux viscéral (TVA), ainsi qu'à une augmentation de la sensibilité à l'insuline chez la souris diabétique. De plus, nous avons constaté que la CHK2 a une activité plus élevée dans la TVA des patients MOD et nous prouvons que l'inhibition pharmaceutique de la CHK2 chez les souris diabétiques réduit leur phénotype IR. Même si CDK10 a également été retrouvée régulée à la hausse dans la TVA des patients MOD, elle ne montre aucun phénotype métabolique net chez les souris neutralisées par CDK10. Enfin, l'utilisation de cette technique innovante a ouvert la voie à la découverte de nouvelles kinases impliquées dans la résistance à l'insuline du tissu adipeux viscéral et au lancement de nouvelles lignes de recherche pour des études de validation ultérieures.



---

# *Table of Content*

---

<b>Acknowledgements</b>	<b>i</b>
<b>Abstract</b>	<b>iii</b>
<b>Résumé</b>	<b>v</b>
<b>List of Figures</b>	<b>xii</b>
<b>List of Tables</b>	<b>xiv</b>
<b>List of Abbreviations</b>	<b>xv</b>
<b>Objectives &amp; Overview</b>	<b>xix</b>
<b>1 Introduction</b>	<b>1</b>
1.1 Cell Signaling	1
1.2 Protein Kinases	1
1.2.1 Serine/Threonine Kinases (STKs)	3
1.2.2 Protein Tyrosine Kinases (PTKs)	3
1.2.3 Pseudo-kinases	4
1.3 Metabolic Regulation	5
1.4 Obesity and Diabetes	5
1.5 Adipose Tissue “Body Fat”	7
1.5.1 Brown Adipose Tissue (BAT)	8
1.5.2 White Adipose Tissue (WAT)	9
1.6 Kinome	12
<b>2 Materials and Methods</b>	<b>13</b>
2.1 Human Sampling	13
2.2 Isolation of mature adipocytes and stromal vascular fraction	13
2.3 Flow Cytometry	14
2.4 Kinome Profiling (PamGene)	14
2.5 STRING Analysis	15
2.6 Mouse Strains and Diet Information	15
2.7 Glucose and Insulin Tolerance Tests	16
2.8 Metabolic Phenocage of the PhenoMaster	16
2.9 Oxymax Open Circuit Indirect Calorimeter	16
2.10 Body Composition Analysis Using the EchoMRI	17
2.11 Immunohistochemistry (IHC)	17
2.12 3T3L1 Differentiation	17
2.13 3T3L1 Insulin Resistant Models and Treatment	17
2.14 BMDM Treatment	18
2.15 Protein Extraction and Western Blotting	18
2.16 RNA Extraction and RTqPCR	18
2.17 Data Analysis	19

<b>3</b>	<b>Kinome Profiling</b>	<b>21</b>
3.1	Results	23
3.2	Discussion	24
3.3	Figures	26
<b>4</b>	<b>PIM Family</b>	<b>27</b>
4.1	Results	29
4.1.1	<i>Pim-1</i> expression in VAT positively correlates with IR markers and is increased in different mouse models of insulin resistance	29
4.1.2	The effects of Pim-1 in insulin resistance are not mediated by adipocytes	30
4.1.3	Pim-1 expression and activity are increased in pro-inflammatory macrophages	30
4.1.4	SGL-1776 decreases pro-inflammatory markers in LPS-stimulated macrophages	31
4.1.5	Pim-1 inhibition improves insulin sensitivity in diabetic mice	31
4.1.6	PIM3KO Mice Are Leaner and Insulin Sensitive	32
4.2	Discussion	33
4.3	Figures	35
<b>5</b>	<b>CHK2</b>	<b>43</b>
5.1	Results	45
5.1.1	CHEK-2 expression in VAT is upregulated in IR mouse models	45
5.1.2	CHK2 kinase activity is upregulated in human VAT of MOD patients	45
5.1.3	CHK2 inhibition improves insulin sensitivity in diabetic mice	45
5.2	Discussion	46
5.3	Figures	48
<b>6</b>	<b>CDK10</b>	<b>51</b>
6.1	Results	53
6.1.1	CDK10 and CycM proteins are highly expressed in metabolic tissues, and their mRNA levels are higher upon fasting and HFD	53
6.1.2	CDK10 and CycM exhibit a role in thermogenic activity of mouse BAT	53
6.1.3	CDK10 and CycM mRNA might play a role in C57BAT differentiation and the $\beta$ 3 adrenergic pathway in pBAT	54
6.1.4	No difference in body weight, fasting glycemia and relative weight of tissues is observed	54
6.1.5	CDK10 deficiency in adipose tissue induces insulin resistance in mice	54
6.1.6	CDK10 floxed mice and CDK10 AdipoQCreERT2 mice manifest no difference in indirect calorimetry	54
6.1.7	No difference is observed in expression of BAT markers	55
6.2	Discussion	56
6.3	Figures	58

<b>7</b>	<b>Limitations of the Study</b>	<b>65</b>
	<b>Summary &amp; Outlook</b>	<b>67</b>
	<b>Bibliography</b>	<b>69</b>
	<b>Appendix A</b>	
	<b>Appendix B</b>	
	<b>Appendix C</b>	
	<b>Appendix D</b>	
	<b>Curriculum Vitae</b>	



---

## *List of Figures*

---

1.1	Enzyme-Substrate Recognition	4
1.2	WHO Report on Obesity	8
1.3	Adipose tissue dysfunction	8
1.4	The differences between metabolically healthy and unhealthy obese patients	9
1.5	The origin of different adipose tissue depots	10
1.6	Adipose Tissue Scheme	12
1.7	The crosstalk between adipocytes and macrophages plays an important role in adipose tissue homeostasis	13
3.1	Kinome profiling of human visceral adipose tissue (hVAT) samples from morbid obese diabetic (MOD) and morbid obese non-diabetic (MOND) patients	24
3.2	Many novel kinases are upregulated in human visceral adipose tissue (hVAT) of morbid obese diabetic (MOD) patients as seen in upstream score plot using kinexus-based analysis	28
4.1	Genetic Structures of the PIM family	29
4.2	Pim-1 gene expression positively correlates to IR markers in hVAT and is upregulated in mVAT of 2 IR mouse models	37
4.3	Pim-1 inhibition does not promote insulin sensitivity in TNF $\alpha$ -treated mature adipocytes	38
4.4	Pim-1 kinase activity and gene expression are upregulated in pro-inflammatory macrophages	39
4.5	Pim-1 kinase activity and gene expression are upregulated in pro-inflammatory macrophages	40
4.6	Pim-1 expression is high in LPS-stimulated macrophages, and its inhibition decreases expression of pro-inflammatory markers	41
4.7	db/db mice treated with SGI-1776 for 3 weeks have lower fat mass, increased glucose and insulin sensitivity, and decreased VAT inflammation	42
4.8	Pim3 <sup>-/-</sup> are leaner and insulin sensitive, with an insulin resistant WAT	43
5.1	Structures of the human CHK2 gene and protein	44

5.5	CHK2 Activation	45
5.3	CHEK2 gene expression does not correlate to IR markers in hVAT, but is upregulated in mVAT of 2 IR mouse models	49
5.4	CHK2 kinase activity is upregulated in hVAT	49
5.5	db/db mice treated with CCT241533 HCl for 2 weeks have lower fasting glycemia, and increased glucose and insulin sensitivity	50
6.1	Molecular Regulation of the Cycle by CDK-Cyclin Complexes	52
6.2	Schematic Diagram and Properties of CDK10 Isoforms	53
6.3	CDK10 and CycM proteins and mRNA are highly expressed in metabolic tissues	59
6.4	CDK10 and CycM exhibit a role in mouse BAT	60
6.5	CDK10 and CycM might play a role in the $\beta$ 3 adrenergic pathway	61
6.6	CDK10 <sup>fl/fl</sup> AdipoQCreERT2 do not differ in body weight or fasting glycemia	61
6.7	CDK10 deficiency induces insulin resistance in adipose tissue of KO mice	62
6.8	Indirect Calorimetry Studies show no difference between control and CDK10 ATKO mice	63
6.9	No difference is observed in the expression of BAT markers in the BAT of CDK10 ATKO mice	64

---

## *List of Tables*

---

1.1	Different characteristics of the 3 adipose tissue types	10
2.1	Cohort 1 (discovery cohort)	15
2.2	Cohort 2 (confirmatory cohort)	15
2.3	Primers used for qPCR analysis of housekeeping genes (human and mouse)	21
2.4	Primers used for qPCR analysis of kinases upregulated in VAT of MOD patients	21
2.5	Primers used for qPCR analysis of pro-inflammatory markers (mouse)	21
2.6	Primers used for qPCR analysis of BAT markers (mouse)	22



---

## *List of Abbreviations*

---

AKT	PI3K-protein kinase B
AMP	Adenosine Monophosphate
AMPK	AMP-activated Protein Kinase
ANP $\alpha$	Atrial natriuretic peptide 1
ATM	Adipose Tissue Derived Macrophages
ATM	Ataxia-Telangiectasia Mutated
ATP	Adenosine Triphosphate
ATR	ATM and Rad3-related
BAT	Brown Adipose Tissue
BCR	B-Cell Receptor
BeAT	Beige Adipose Tissue
BMDM	Bone Marrow Derived Macrophages
BMI	Body Mass Index
c-Myc	Avian myelocytomatosis virus oncogene cellular homolog
CAMK	Ca <sup>2+</sup> /Calmodulin-dependent kinase
CD	CHOW Diet
CDK	Cyclin-Dependent Kinase
CDKN1A	Cyclin-Dependent Kinase Inhibitor 1A
ChIP	Chromatin Immunoprecipitation
CHK2	Checkpoint Kinase 1
CK2	Casein Kinase 2
CPT1 $\beta$	Carnitine Palmitoyltransferase 1 $\beta$
CycM	Cyclin M
DNA	Deoxyribonucleic Acid
FACS	Fluorescence Activated Cell Sorting
FFA	Free Fatty Acid
FHA	Forkhead-Associated Domain
FRAP	FK506-binding protein 12- <i>rapamycin</i> -associated protein 1

GLUT1	Glucose Transporter 1
GTT	Glucose Tolerance Test
GWAS	Genome-Wide Association Study
HFD	High Fat Diet
I $\kappa$ B	Inhibitor of Kappa B
IKK	I $\kappa$ B Kinase
IL-2R	Interleukin-2 Receptor
IL-6	Interleukin-6
iNOS	Inducible Nitric Oxide Synthase
IR	Insulin Resistance
IRS1	Insulin Receptor Substrate 1
IRS2	Insulin Receptor Substrate 2
IS	Insulin Sensitive
ITT	Insulin Tolerance Test
KO	Knock Out
LDHA	Lactate Dehydrogenase A
LPS	Lipopolysaccharide
MAD	Mitotic Arrest Deficient
MAPK	Mitogen-activated Protein Kinase
MAPKK	Mitogen-activated Protein Kinase Kinase
MCP-1	Monocyte Chemoattractant Protein
MG	Methylglyoxal
MOD	Morbid Obese Diabetic
MOND	Morbid Obese Non Diabetic
mTOR	Mammalian Target of Rapamycin
NF $\kappa$ B	Nuclear Factor Kappa B
nRTK	Non-Receptor Tyrosine Kinase
PGC1 $\alpha$	PPAR gamma coactivator 1-alpha
PGK1	Phosphoglycerate kinase 1
pgWAT	Perigonadal White Adipose Tissue
PI3K	Phosphoinositide-3 Kinase

PIM	Proviral Integration Site for Moloney Murine Leukemia Virus
PKA	Protein Kinase A
PKB	Protein Kinase B
PKC	Protein Kinase C
PKD	Protein Kinase D
PKG	Protein Kinase G
PPAR $\alpha$	Peroxisome Proliferator-Activated Receptor
PRKX	Protein Kinase X
PRKY	Protein Kinase Y
PTK	Protein Tyrosine Kinase
RANKL	Receptor Activator of Nuclear Factor Kappa B Ligand
RNA	Ribonucleic Acid
RTK	Receptor Tyrosine Kinase
SAT	Subcutaneous Adipose Tissue
SNP	Single Nucleotide Polymorphism
STK	Serine Threonine Kinase
SVF	Stromal Vascular Fraction
T2DM	Type 2 Diabetes Mellitus
TCR	T Cell Receptor
TGF $\beta$	Tumor Growth Factor $\beta$
TNF $\alpha$	Tumor Necrosis Factor $\alpha$
UCP1	Uncoupled Protein 1
VAT	Visceral Adipose Tissue
WAT	White Adipose Tissue
WHO	World Health Organization



---

## *Objectives and Overview*

---

The main objective of this thesis is to shed light on a new technology, known as the PamGene. This technology, by combining experimental and computational approaches, helps in constructing a better understanding of functional kinases in the context of metabolic disease. This integrative kinome profiling approach presents the first-ever study to unravel differential kinase activity in human patients developing type 2 diabetes. Therefore, novel kinases implicating insulin resistance in adipose tissue of diabetic patients were found. The research was performed at Université de Lausanne from July 2014 until May 2019. The structure of the thesis is as follows:

*Chapter 1* is an introduction covering signaling pathways, including the different protein kinases and their implication in metabolic regulation. It also comprises of general information about obesity and diabetes, and the implication of adipose tissue with its different types in insulin resistance and inflammation, and finally kinome profiling.

*Chapter 2* covers all the materials and methods performed throughout this study.

*Chapter 3* extensively describes the PamGene, a new approach used throughout this study, which helps in finding putative upstream kinases. Results show that several kinases, of which are the Pim family, CHK2, and CDK10, are upregulated in the visceral fat of insulin resistant obese subjects. Further on, each chapter will cover each kinase, and its validation in other diabetic models.

*Chapter 4* presents the first-ever study showing that the Pim family of kinases is implicated in adipose tissue insulin resistance. Specifically, Pim-1 is depicted as a novel target for the treatment of insulin resistance in obese subjects. On the contrary, Pim-3 is shown to have opposite effects in diabetic models. The phenotypic implications of Pim-1 and Pim-3 inhibition have been demonstrated using a diabetic mouse model and a full knock out mouse model, respectively.

- Chapter 5* reveals CHK2 as a new kinase that is directly correlated to adipose tissue insulin resistance. It shows that the pharmaceutical inhibition of CHK2 renders diabetic mice metabolically “healthy”.
- Chapter 6* shows that, even though CDK10 was found to be within the top kinases upregulated in diabetic patients, CDK10 inhibition does not show any striking metabolic phenotype. Metabolic implications of CDK10 ablation have been exhibited using a tamoxifen-induced adipose tissue knock out mouse model.
- Chapter 7* deliberates the limitations of the kinome study. This chapter serves as a general discussion for the overall project.
- Chapter 8* summarizes the thesis and presents an outlook for future work in this field.
- Appendix* includes my contribution to other projects and the corresponding published articles.

---

# *Chapter 1: Introduction*

---

## **1.1. Cell Signaling**

Cellular signaling is at the basis of any communication process, governing fundamental cell activities and coordinating all cell actions. Cellular development, tissue repair, immunity, normal tissue homeostasis, etc. are all centered around the ability of cells to perceive and correctly respond to their microenvironment. Errors in signaling interactions and in processing cellular information are accountable to diseases such as cancer, autoimmunity, and diabetes (Solinas et al., 2007; Vlahopoulos et al., 2015; K. Wang, Grivennikov, & Karin, 2013). By realizing the prominence of cell signaling and studying its underlying structure, diseases may be treated more efficiently. Changes in cell signaling networks may disturb signal transduction, the flow and transmission of information. Exploring these networks requires both theoretical and experimental approaches, including the development and analysis of model organisms and disease simulations (Eungdamrong & Iyengar, 2004).

Cell signaling can be sorted as mechanical and biochemical categories, based on the signal type that is transmitted. Mechanical signals are the external and internal forces exerted on and by the cell, respectively (Miller & Davidson, 2013). Biochemical signals are subcategorized based on the distance between the interacting cells: autocrine, juxtacrine, paracrine, and endocrine signaling. These signals are transmitted through molecules, such as proteins, lipids, metabolites, etc. (Pandit & Soltis, 2012).

## **1.2. Protein Kinases**

Proteins, such as phosphatases and kinases, are also known as phosphotransferases. They catalyze the transfer of  $\gamma$ -phosphate from and to their protein substrates, respectively (Cheng, Qi, Paudel, & Zhu, 2011). These opposing reactions help in modulating the functions and structures of many cellular proteins. Thus, protein phosphorylation and dephosphorylation are the most prevalent post-translational modifications that regulate a wide spectrum of cellular processes (Ubersax & Ferrell,

2007). Phosphorylation induces conformational changes that might disrupt or create protein-protein interaction surfaces, consequently regulating protein activity (Cohen, 2000; Holt et al., 2009). Also, phosphorylation is able to modulate protein function without inducing any changes in the conformation, but by disrupting protein-ligand interactions (Manning, Plowman, Hunter, & Sudarsanam, 2002).

There are 2 types of interactions employed by protein kinases to specifically recognize their substrates: (A) the active site of the kinase recognizes a consensus phosphorylation sequence in its substrate, and (B) the docking motif that is separated from the phosphorylation site binds to the interaction motif that is separated from the active site of the kinase, leading to a distal interaction between the substrate and the kinase (Ubersax & Ferrell, 2007) (Figure 1.1).

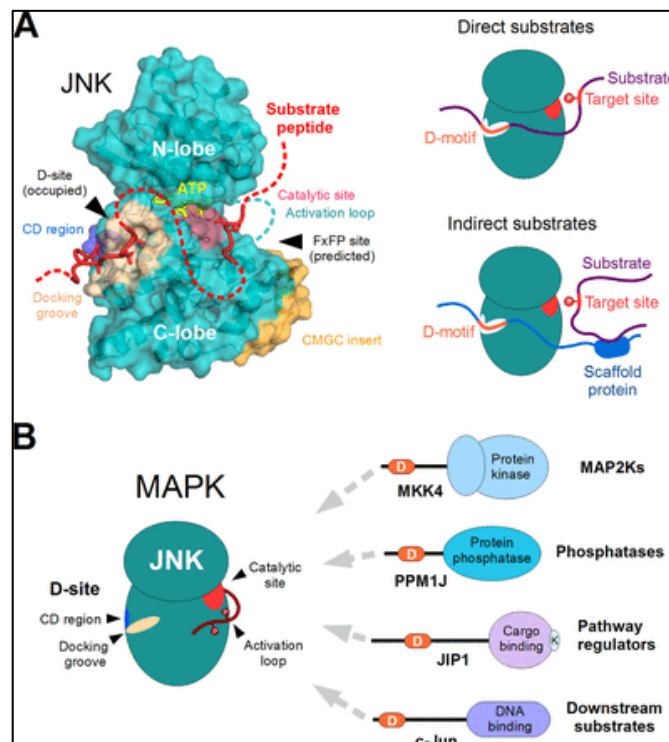


**Figure 1.1: Enzyme-Substrate Recognition.** The 2 types of interactions are either through direct substrates with the enzyme catalytic site (A) or through engagement of the recruitment site that is distinct from their catalytic site (B) (Zeke, Misheva, Remenyi, & Bogoyevitch, 2016).

The different types of protein kinases in mammals are serine/threonine kinases (STKs) and protein tyrosine kinases (PTKs) (Hanks & Hunter, 1995; Manning, Whyte, Martinez, Hunter, & Sudarsanam, 2002). Some kinases, such as Mitogen-Activated Protein Kinase Kinase (MAPKK), have both the STK and PTK activities (Mordret, 1993). These are known as dual specificity kinases. A less-studied type of kinases are catalytically inactive kinases, or pseudo-kinases (Raju & Shaw, 2015).

### **1.2.1. Serine/Threonine Kinases (STKs)**

Serine and threonine residues have similar sidechains, and can be phosphorylated on their hydroxyl group by specific enzymes. These protein enzymes are known as serine/threonine protein kinases (STKs) (Edelman, Blumenthal, & Krebs, 1987; Hanks & Hunter, 1995). As stated previously, kinases specifically recognize a consensus sequence. Thus, STKs do not phosphorylate any serine or threonine residues, only the ones within the phospho-acceptor consensus sites. STKs can function as receptors or as intracellular signaling peptides and proteins.

#### *Receptor Proteins*

The group of STK receptor proteins are known as adenosine triphosphate (ATP) receptor protein phosphotransferases. Proteins of this group participate in the regulation of cellular proliferation, differentiation and apoptosis (Manoharan, Seong, & Ha, 2018). Also, they play a paramount role in major metabolic pathways, such as Mitogen-Activated Protein Kinase (MAPK) (Medina-Castellanos, Esquivel-Naranjo, Heil, & Herrera-Estrella, 2014) and Tumor Growth Factor beta (TGF $\beta$ ) pathways (Massague & Chen, 2000; Takai et al., 2012; Wrana, Attisano, Wieser, Ventura, & Massague, 1994).

#### *Intracellular Signaling Proteins*

STKs functioning as intracellular signaling proteins are vastly studied, and are known to be majorly involved in canonical pathways, including cell migration (Di Blasio, Gagliardi, Puliafito, & Primo, 2017), proliferation (Lin et al., 2019), glucose metabolism (Abd Al Haleem & El-Bakly, 2019), angiogenesis (Lyu et al., 2018) and lysosomal biogenesis (Carroll & Dunlop, 2017). Examples of these proteins include Protein Kinases A (PKA), Protein Kinase B (PKB) also known as AKT, Protein Kinase C (PKC), Casein Kinase 2 (CK2), and Ca<sup>2+</sup>/Calmodulin-dependent protein kinase (CAMK). They show major functions in cancer, endocrine disorders, cardiovascular disease, metabolic diseases etc. (Turnham & Scott, 2016).

### **1.2.2. Protein Tyrosine Kinases (PTKs)**

Tyrosine kinases are enzymes that catalyze the transfer of the terminal phosphate from ATP to a protein, at one or several tyrosine residues located in specific consensus sites (Hanks & Hunter, 1995). There are two classes of PTKs in the human genome: the

receptor tyrosine kinases (RTKs) and the non-receptor (cytoplasmic) tyrosine kinases (nRTKs) (Robinson, Wu, & Lin, 2000).

#### *Receptor Tyrosine Kinases (RTKs)*

RTKs encompass an extracellular domain that binds to specific ligands, a transmembrane domain that propagates the signal, and an intracellular domain that is catalytic by binding and phosphorylating specific downstream substrates (Hubbard & Till, 2000). Around 20 classes of RTKs were identified, of which is the Insulin Receptor family that is known as RTK class II (Segaliny, Tellez-Gabriel, Heymann, & Heymann, 2015). RTK pathways coordinate a wide variety of cell functions, such as proliferation, differentiation, metabolism, motility, and apoptosis (Schlessinger, 2014). Thus, RTKs are tightly regulated by positive and negative feedback loops, to avoid cellular dysfunction that might lead to pathologies like cancer, neurodegenerative diseases, etc. (Bhise, Nalawade, & Wadhawa, 2004; Bublil & Yarden, 2007).

#### *Non Receptor Tyrosine Kinases (nRTKs)*

nRTKs are cytosolic enzymes that phosphorylate proteins at their tyrosine residue. They can either be cell membrane-bound or nuclear specific (Lahiry, Torkamani, Schork, & Hegele, 2010). In human cells, 32 nRTKs have been identified (Hubbard & Till, 2000). Their main function is in regulating the immune system (Pawson, 2002). nRTKs play important roles in activating B- and T-cells, through numerous receptors, i.e. T-cell receptor (TCR), B-cell receptor (BCR), and interleukin-2 receptor (IL-2R) (Weiss & Littman, 1994).

### **1.2.3. Pseudo-kinases**

Pseudo-kinases, such as PTENP1, even though they bind to ATP, have no measurable kinase activity. Just like active kinases, pseudo-kinases have been evolving (Raju & Shaw, 2015), and their mutations are implicated in several disorders (O'Sullivan et al., 2011; Simpson et al., 2007). They are known to act as substrates and scaffolds, used for the assembly of signaling complexes (Kroiher, Miller, & Steele, 2001; Morrison, 2001; Zervas & Brown, 2002). Several studies have shown that they are implicated in the regulation of the activity of other kinases, such as RAF kinases (Rajakulendran & Sicheri, 2010; Shaw,

Kornev, Hu, Ahuja, & Taylor, 2014). This type of regulation is known as allosteric regulation (Kornev, Taylor, & Ten Eyck, 2008).

### **1.3. Metabolic Regulation**

The regulation of metabolism stands at the intersection of major research fields, involving physiology, cell and molecular biology, biochemistry, and the study of disease pathogenesis. It is fundamental for the survival, growth and development of all organisms, requiring the coordination of many metabolic pathways (Somvanshi & Venkatesh, 2014). Recently, the interest in understanding the metabolic network has been rekindled, due to the discoveries linking cell signaling, metabolism, and the pathogenesis of disease (Cairns, Harris, & Mak, 2011; DeBerardinis & Thompson, 2012; Saltiel & Kahn, 2001). In order to meet the energy needs of the cell and maintain homeostasis, metabolic pathways are dynamically regulated. Dysregulation of these pathways is prominently linked to metabolic diseases, such as obesity and type 2 diabetes (T2D), as well as cancer and ageing (Goodpaster & Sparks, 2017).

### **1.4. Obesity and Diabetes**

The World Health Organization (WHO) has recently announced that worldwide obesity has almost tripled since 1975 (16 February 2018). Obesity is linked to numerous health problems, including insulin resistance, type 2 diabetes, hypertension, dyslipidemia, atherosclerosis, and cancer, among others (Figure 1.2) (Arroyo-Johnson & Mincey, 2016; Y. C. Wang, McPherson, Marsh, Gortmaker, & Brown, 2011; Weitzman & Gordon, 1990). Most obese patients suffer from an impaired adipose tissue function, caused by the interaction of environmental and genetic factors, leading in turn to adipocyte hypertrophy, hypoxia, a variety of stresses and inflammatory processes within the adipose tissue (Paniagua, 2016). Moreover, central obesity is at the heart of organ dysfunction, such as liver and muscle (Figure 1.3). Obesity will not only affect the metabolic state of the adipose tissue, but will also induce a systemic insulin resistant profile, leading to type 2 diabetes (T2D) (Paniagua, 2016).

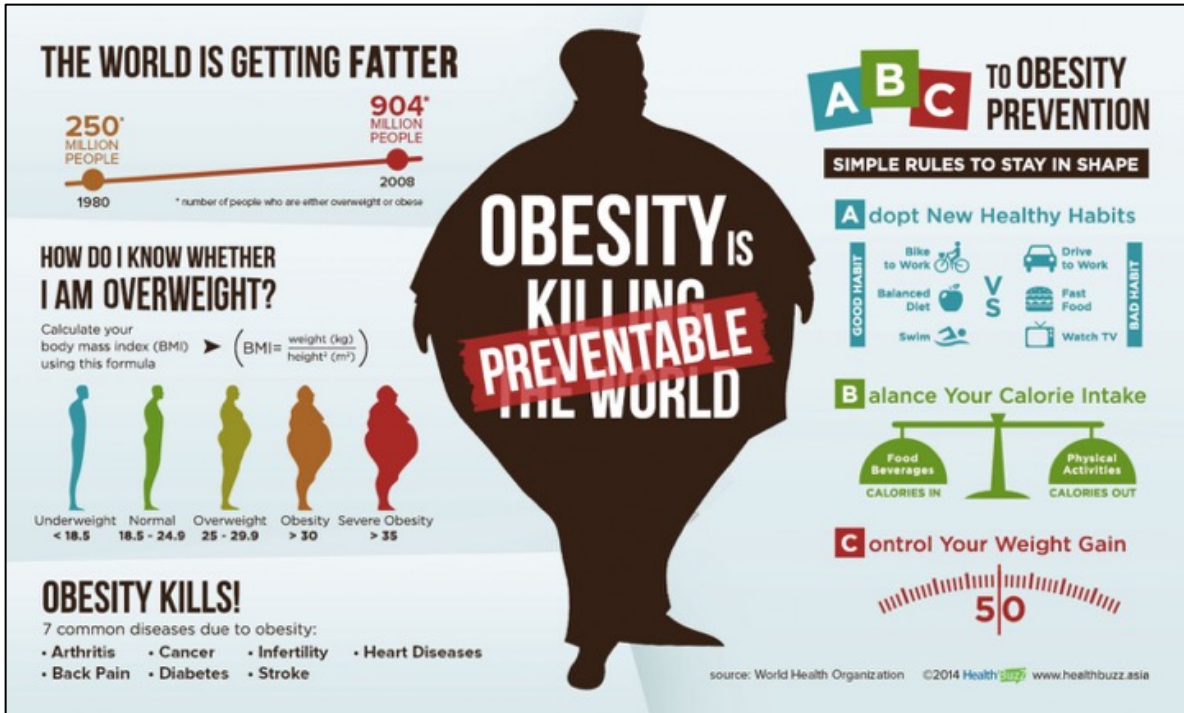


Figure 1.2: WHO report on obesity. Obesity has quadrupled during almost 30 years. Obese people have suffered from several diseases, such as diabetes, cancer, heart disorders, etc. Several new healthy habits should be adopted to evade weight gain and obesity.

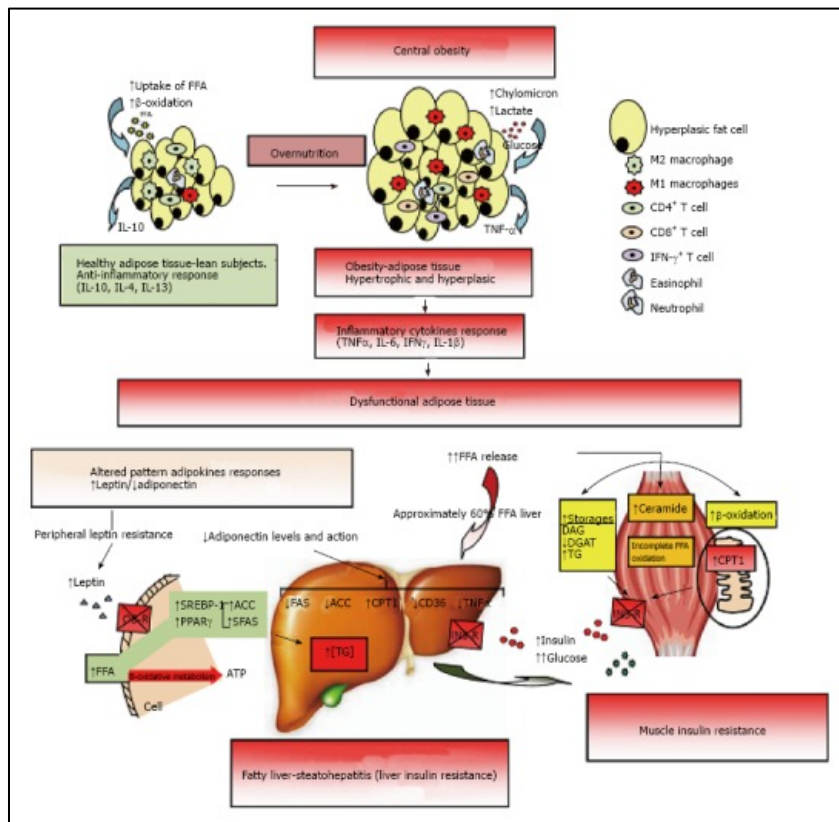
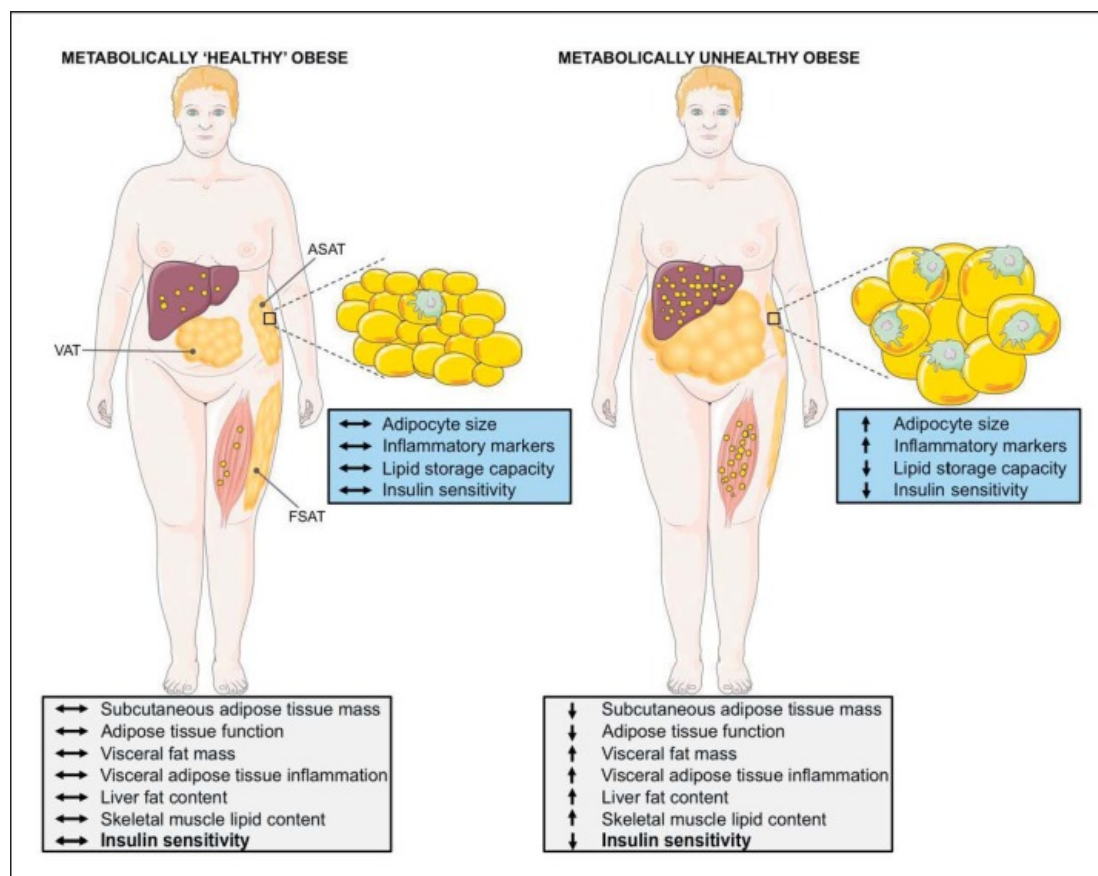


Figure 1.3: Adipose tissue dysfunction. Central obesity leads to dysfunctional adipose tissue, and consequently to insulin resistant fatty livers and muscles (Paniagua, 2016).

Together, the rising prevalence of obesity and the frequent co-morbidities in affected patients is an important challenge for health care systems. Nevertheless, recent data suggest that the total amount of body fat does not entirely explain the predisposition to cardio-metabolic risk (Figure 1.4) (Goossens, 2017; Wajchenberg, Giannella-Neto, da Silva, & Santos, 2002). Indeed, metabolic complications can be observed in a significant number of non-obese individuals. In sharp contrast, 10 to 35% of obese patients do not appear to develop such complications and are thus considered metabolically healthy (Wildman et al., 2008).



**Figure 1.4: The differences between metabolically healthy and unhealthy obese patients.** Adipocyte size and inflammatory markers increase, while lipid storage capacity and insulin sensitivity decrease in MUO patients as compared to MHO (Goossens, 2017).

### 1.5. Adipose Tissue or “Body Fat”

In mammals, there are three main types of differentiated adipose tissue. They are known as the white adipose tissue (WAT), the brown adipose tissue (BAT), and the beige or brite (brown in white) adipose tissue (BeAT) (Carobbio, Pellegrinelli, & Vidal-Puig, 2017). These different adipose tissue types have different characteristics, distributions, and

functions throughout the body (Table 1.1) (El Hadi, Di Vincenzo, Vettor, & Rossato, 2018; Hildebrand, Stumer, & Pfeifer, 2018; Paniagua, 2016; Virtanen et al., 2009).

**Table 1.1: Different characteristics of the 3 adipose tissue types.**

Characteristics	WAT	BAT	BeAT
Location in mice	Subcutaneous Intra-abdominal Epicardial Gonadal	Interscapular Subscapular Perirenal	Inguinal
Lipid Droplets	Single lipid droplet	Multiple small lipid droplets	After stimulation
Mitochondria	Few mitochondria	Many mitochondria	After stimulation
UCP1	None	High	After stimulation
Main function	Energy storage	Thermogenesis	Thermogenic capacity
Response to HFD	Hyperplasia Hypertrophy Inflammation	Hypertrophy	Heypertrophy

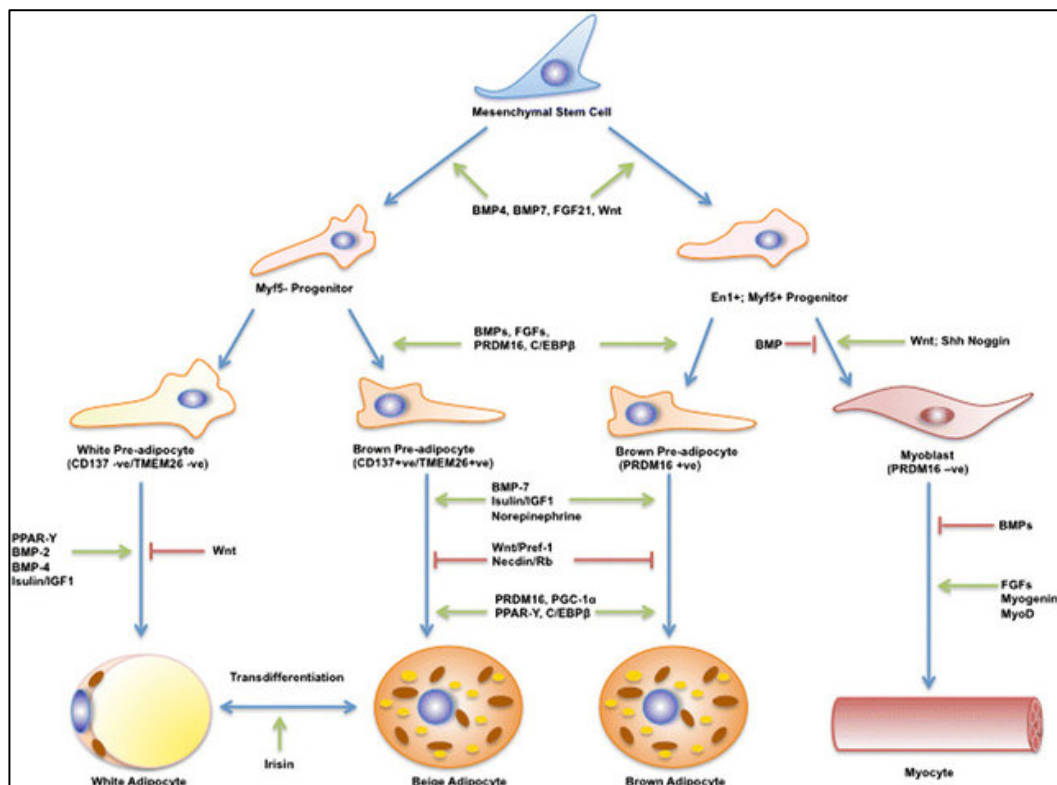


**Figure 1.5: The origin of different adipose tissue depots.** Multipotent mesenchymal stem cells give rise to the different adipose tissue depots, through a cascade of signaling pathways, triggered by morphogenic proteins and growth factors (Reddy, Tan, Barber, & Randeve, 2014).

Multipotent mesenchymal stem cells are triggered by growth factors and morphogenic proteins, leading to a cascade of pathways, which in turn result in fully developed WAT, BAT, and BeAT (Figure 1.5) (Reddy et al., 2014). In this work, we will focus on the first two types of adipose tissue.

### **1.1.1. Brown Adipose Tissue (BAT)**

BAT is a highly metabolic tissue composed of a specialized form of adipocytes that contains several multilocular lipid droplets. BAT is mainly involved in thermogenesis, manifested by the expenditure of energy and regulation of body weight (Virtanen et al., 2009). This process is stimulated by cold exposure and/or lipid-rich calorie food intake, and is mediated by activating of the mitochondrial Uncoupling Protein 1 (UCP1). UCP1 is ubiquitously expressed in the inner mitochondrial membrane, the site in which saturated ATP production is dissipated as heat. In mice, brown fat is able to utilize blood glucose and lipids and its expansion and/or activation results in elevated energy expenditure, improved glucose and lipid metabolism and reduced body weight (Cannon & Nedergaard, 2004).

In humans, the first evidence of BAT activity was related to the control of body temperature after birth and during early childhood (Lean, 1989). Active brown fat was also discovered in human adults (Cypess et al., 2009; Ouellet et al., 2011; Schulz et al., 2013; Zingaretti et al., 2009). Furthermore, some studies have shown a relationship between BAT activation and increased basal energy expenditure, lower BMI, and decreased onset of obesity and type 2 diabetes (Cypess & Kahn, 2010). BAT depots have been found in different amounts in the cervical and supraclavicular areas in human. These are known as the canonical BAT (Cypess et al., 2013). Consequently, the study of brown fat function and development has gained great interest in the recent years, in particular the identification of novel factors that regulate brown adipocyte differentiation and thermogenic activity for its potential therapeutic applications (S. H. Kim & Plutzky, 2016; Moonen, Nascimento, & van Marken Lichtenbelt, 2019; Pradhan et al., 2017).

### **1.1.2. White Adipose Tissue (WAT)**

WAT is a highly heterogenous adipose tissue depot that exists as adipocytes and stromal vascular fraction (SVF) (Cristancho & Lazar, 2011). The SVF contains pre-adipocytes, endothelial cells, fibroblasts, and macrophages (Figure 1.6). Pre-mature adipocytes have

a multipotent stem cell origin, and are able to generate new fat cells throughout the whole human life (Otto & Lane, 2005).

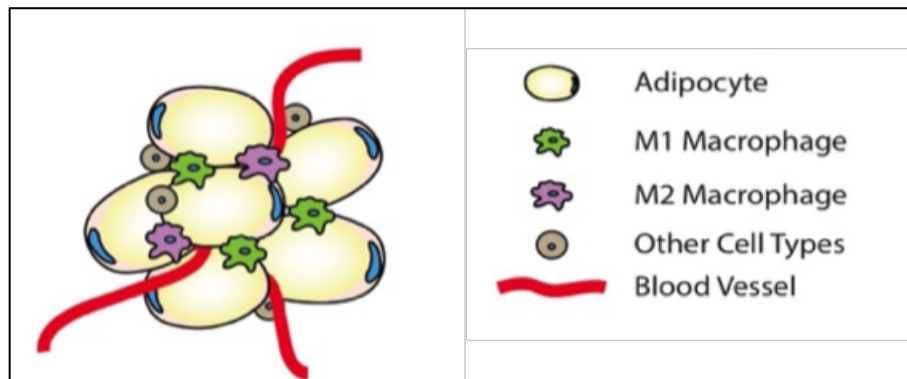


**Figure 1.6: Adipose Tissue Scheme.** Adipose tissue consists of mature adipocytes and other different cell types.

WAT's classical role is to cushion and insulate the body, store free fatty acids (FFA) after food intake, and to release them during fasting. This is mainly what ensures homeostatic energy status in the body. WAT has monumental capacity to expand, at which it becomes associated with increased risk of metabolic disorders (Bluher, 2009; Otto & Lane, 2005; Rosen & Spiegelman, 2014).

Main WAT depots are subcutaneous (SAT), and visceral (VAT) also known as abdominal adipose tissue. Both depots have common functions, such as TNF- $\alpha$  production (Fontana, Eagon, Trujillo, Scherer, & Klein, 2007). Nevertheless, they are known to be functionally divergent. SAT mainly produces leptin, while VAT highly expresses genes for fatty acid-binding and blood pressure regulation, secretes more adiponectin, and drains directly onto the portal circulation. Thus, VAT is thought to be responsible for lower adiponectin plasma levels in obese and insulin-resistant patients, while SAT is the major adiponectin source of those patients (Dusserre, Moulin, & Vidal, 2000; Gabrielsson et al., 2003; Motoshima et al., 2002). It is also known that during obesity, macrophage infiltration is higher in VAT than in SAT (Cancello et al., 2006). Moreover, adipokines produced by VAT directly influence liver function, such as TNF $\alpha$  and IL-6 (Smitka & Maresova, 2015). Both VAT and SAT are innervated by the autonomic nervous system. Parasympathetic stimulation leads to an anabolic state with reduced lipolysis, while sympathetic stimulation leads to a catabolic state with attenuated adipogenesis and stimulated lipolysis (Bartness, Liu, Shrestha, & Ryu, 2014).

In adipose tissue, insulin resistance is tightly correlated with inflammation as well as with the accumulation of proinflammatory macrophages (Lackey & Olefsky, 2016; McLaughlin, Ackerman, Shen, & Engleman, 2017). Immune cells found in the SVF of WAT include myeloid cells like macrophages and granulocytes, effector and memory T cells, regulatory T cells, and others (Huh, Park, Ham, & Kim, 2014). Macrophages, that are classified into anti-inflammatory (M2-like) and pro-inflammatory (M1-like) macrophages (Rosen & Spiegelman, 2014) are especially important for adipose tissue homeostasis (Figure 1.7). It is well known that, upon obesity, adipocytes secrete inflammatory mediators, such as MCP-1, inducing pro-inflammatory macrophage recruitment and activation through transcription factors, such as NFκB (Bhargava & Lee, 2012; Hotamisligil, Shargill, & Spiegelman, 1993; Nguyen et al., 2007; Weisberg et al., 2003; Xu et al., 2003). Indeed, an inflammatory reaction is a pre-requisite for insulin resistance, locally in the adipose tissue and systemically in the whole organism (Kanda et al., 2006; Patsouris et al., 2008).

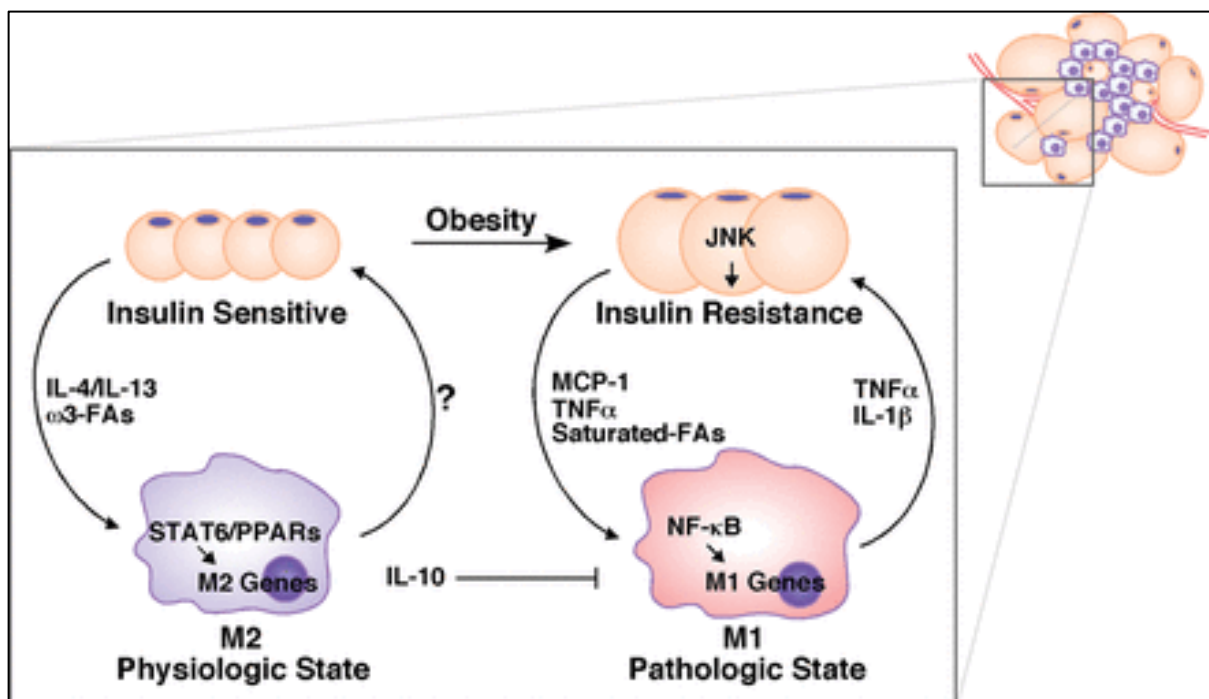


**Figure 1.7: The crosstalk between adipocytes and macrophages plays an important role in adipose tissue homeostasis.** In the physiological state, adipose tissue macrophages (ATMs) exhibit an M2 phenotype, mediated by the Th2 cytokines IL-4 and IL-13, and downstream transcription factors STAT6 and PPARδ/PPARγ. In obesity, stressed adipocytes produce inflammatory mediators (e.g. MCP-1, TNFα and saturated fatty acids) to induce M1 activation through inflammatory transcription factors, such as NF-κB. Macrophages respond by up-regulating inflammatory cytokines, which activate JNK and inhibit insulin signaling pathways in the adipocyte (Bhargava & Lee, 2012).

## 1.6. Kinases Involved in Insulin Resistance

Insulin sensitivity and resistance depend on the specific kinases such as AMP-activated protein kinase (AMPK), I $\kappa$ B kinase (IKK), protein kinase C (PKC), and mitogen-activated protein kinases (MAPKs) which act on the insulin receptor substrate (IRS) (McArdle, Finucane, Connaughton, McMorrow, & Roche, 2013; Nandipati, Subramanian, & Agrawal, 2017). Similarly, the role of Rho-associated coiled-coil containing protein kinase (ROCK) (D. H. Lee et al., 2009; S. H. Lee et al., 2014), and RNA-activated protein kinase (PKR) (Carvalho-Filho et al., 2012) in pathogenesis of insulin resistance has been documented. Insulin-mediated activation of intrinsic tyrosine kinase in the insulin receptor leads to tyrosine phosphorylation of IRS1. This further activates its substrates phosphatidylinositol 3-kinase (PI3K) and Akt, leading to increased glycogen synthesis, glucose uptake, and protein synthesis (Y. Li et al., 2004). AMPK is considered a positive regulator of insulin sensitivity. It is reported to be associated with increased Glucose Transporter 4 (GLUT4) translocation and subsequent glucose uptake (Fazakerley et al., 2010). Studies reported that dysregulation of AMPK as the central mechanism behind the insulin resistance mediated diabetes (Ruderman, Carling, Prentki, & Cacicedo, 2013).

The mitogen-activated protein kinases (MAPKs) are well known for their role in inflammatory responses through phosphorylation of serine/threonine residues of target proteins (Patterson, Nibbs, McInnes, & Siebert, 2014). The deficiency of MAPKs has been associated with reduced insulin sensitivity (de Boer et al., 2014). In insulin-resistant conditions, serine kinases such as I $\kappa$ B kinase (IKK) and JNK become activated by pro-inflammatory stimuli (Gual, Le Marchand-Brustel, & Tanti, 2005) and impair insulin sensitivity. Thus, understanding the interplay between inflammation, obesity and protein kinases, and identifying the specific protein kinases involved in phosphorylation may help in developing the targeted drug therapies to minimize the insulin resistance. This might play a key role in the prevention of diabetes.

## 1.7. Kinome

Describing the changes in the kinome is key to understanding the contributions of signaling cascades in normal or dysfunctional conditions, and therefore for the identification of signaling alterations leading to systemic diseases. The rapid

development of techniques, such as genome-wide association study (GWAS), RNA sequencing, or chromatin immunoprecipitation (ChIP) sequencing has paved the way for several scientific breakthroughs (Andersen et al., 2019; Gupta & Vadde, 2019; Ke et al., 2017; W. Sun et al., 2018).

Insulin signaling in adipocytes has been extensively studied *in vitro* and in animal models, with a particular focus on the effects of insulin receptor, insulin receptor substrates 1 and 2 (IRS1 and IRS2), and PI3K-protein kinase B (AKT) (Coppes & White, 2012). Other known protein kinases that have been involved in the onset of insulin resistance include, but are not limited to, AMP-activated protein kinase (AMPK), I $\kappa$ B kinase (IKK), protein kinase C (PKC), or mitogen-activated protein kinases (MAPKs) (Ye, 2013; Zhang, Zhou, & Li, 2009). However, an extensive study of protein phosphorylation or kinase function alterations in insulin resistance (IR) has not been performed in human white adipose tissue (WAT).

We have chosen here to use a novel technology developed by PamGene to perform a whole kinase activities profiling of human visceral adipose tissue from morbid obese non-diabetic subjects (MOND), compared to morbid-obese diabetic (MOD) patients. Identifying new and specific protein kinases involved in adipose tissue chronic inflammation and insulin resistance may help in developing targeted drug therapies and treatment strategies to minimize insulin resistance in patients.



---

## Chapter 2: Materials and Methods

---

### 2.1. Human Samples

All obese patients underwent biliopancreatic diversion of Scopinaro. Morbidly obese patients were excluded if they were receiving insulin or hypoglycemic agents, had cardiovascular disease, arthritis, acute inflammatory disease, infectious disease, or were receiving drugs that could alter the lipid profile or the metabolic parameters at the time of inclusion in the study. The non-obese patients were selected from among patients who underwent laparoscopic surgery for hiatus hernia or cholelithiasis with no alterations in lipid or glucose metabolism, with a similar age, and with the same selection criteria as those for the morbidly obese group. All of the patients were of Caucasian origin. All of the participants gave their written informed consent, and the study was reviewed and approved by the Ethics and Research Committee of Virgen de la Victoria Clinical University Hospital, Malaga, Spain.

**Table 2.1: Cohort 1 (discovery cohort)** Morbid obese non diabetic (MOND) and morbid obese diabetic (MOD)

Patients	n	Females	Males	Age (years)	BMI (kg/m <sup>2</sup> )	Insulinemia (mIU/mL)	Glycaemia (mg/dL)	HOMA-IR
MOND	23	16	7	47 ± 2	46.3 ± 1.0	17.8 ± 2.3	94.6 ± 2.6	4.4 ± 0.6
MOD	21	11	10	52 ± 2	48.5 ± 1.7	25.4 ± 4.8	133.5 ± 9.8	10.7 ± 2.7

**Table 2.2: Cohort 2 (confirmatory cohort)** Lean (L), obese (O) and morbid obese (MO)

Patients	n	Females	Males	Age (years)	BMI (kg/m <sup>2</sup> )	Insulinemia (mIU/mL)	Glycaemia (mg/dL)	HOMA-IR
L	20	13	7	55 ± 3	23.7 ± 0.4	7.5 ± 1.2	100.8 ± 4.2	1.9 ± 0.3
O	23	12	11	59 ± 3	32.8 ± 0.4	11.1 ± 1.4	110.8 ± 5.1	3.0 ± 0.4
MO	43	33	10	49 ± 1	46.6 ± 0.9	19.9 ± 2.3	114.4 ± 5.0	6.2 ± 1.0

### 2.2. Isolation of mature adipocytes and stromal vascular fraction

SVF was obtained from human adipose tissue biopsies as described (Ceperuelo-Mallafre et al., 2016; Serena et al., 2016; Serena et al., 2017). Briefly, sub-cutaneous white adipose tissue (scWAT) and visceral white adipose tissue (vWAT) was washed extensively with PBS to remove debris and treated with 0.1% collagenase in PBS and 1% BSA for 1 hr at

37°C with gentle agitation. Digested samples were centrifuged at  $300 \times g$  at 4°C for 5 min to separate adipocytes from the SVF. Adipocytes were directly used for RNA isolation and the cell pellet containing the SVF was resuspended in red-blood-cell lysis buffer (10 mM KHCO<sub>3</sub>, 150 mM NH<sub>4</sub>Cl, 0.1 mM EDTA) for 2 min, then washed with PBS and passed through a 40- $\mu$ m filter (Fisher Scientific). To isolate ultrapure ATMs, the SVF was incubated with F4/80 MicroBeads (130-110-443, MiltenyiBiotec S.L. Madrid, Spain) for 30 min and positive selection was performed with an autoMACS separator (MiltenyiBiotec).

### **2.3. Flow cytometry**

The SVF from scWAT and vWAT was isolated as described above. To isolate myeloid lineage cells, SVF was incubated with CD11b MicroBeads (130-049-601, MiltenyiBiotec) for 30 min, and positive selection was performed with an autoMACS separator. Magnetically isolated CD11b<sup>+</sup> cells were washed and incubated with the desired combination of fluorochrome-conjugated monoclonal antibodies, including FITC-anti-F4/80 (clone BM8), APC-anti-CD11c (clone N418), PE-anti-CD206 (clone MR6F3) and PE-Cy7-anti-Ly-6G (clone RB6-8C5) (all from eBiosciences, San Diego, CA) for 20 min. Data were acquired on a FACS Aria III (BD Biosciences) and analysis was performed using FACSDiva™ software (BD Biosciences).

### **2.4. Kinome Profiling (PamGene)**

For kinome analysis, serine/threonine (STK) kinase microarrays were purchased from PamGene International BV. Each array contains 140 phosphorylatable peptides, as well as 4 positive control peptides. Sample incubation, detection, and analysis were performed according to the manufacturer's instructions in a PamStation 12. Briefly, extracts from human adipose tissue were made using M-PER mammalian extraction buffer (Thermo Scientific) containing 1:50 Halt phosphatase inhibitor cocktail (Thermo Scientific) and 1:50 Halt protease inhibitor cocktail EDTA-free (Thermo Scientific) for 20 min on a spinning wheel at 4°C. The lysates were then centrifuged at 13,000 r.p.m. for 20 min to remove all debris. The supernatant was aliquoted, snap-frozen in liquid nitrogen, and stored at -80°C until further processing. Prior to incubation with the kinase reaction mix, the arrays were blocked with 2% BSA for 30 cycles and washed three times with PK assay buffer. Kinase reactions were performed over 1 h with 5  $\mu$ g total extract and 400

$\mu\text{M}$  ATP at 30°C. Phosphorylated peptides were detected with a secondary anti rabbit-FITC antibody that recognizes a pool of anti-phospho serine/threonine antibodies. The instrument contains a 12-bit CCD camera suitable for imaging of FITC-labelled arrays. The images obtained from the phosphorylated arrays were quantified using the bionavigator software (PamGene International BV). Generated heat maps and kinexus plots are further explained in the results and figures sections.

## 2.5. STRING Analysis

Based on the kinexus plot generated by the bionavigator software (PamGene International BV), we chose the top 20 kinases. The hit kinases were then used as input in the [STRING](#) software. A kinase interaction network was constructed with a minimum required interaction score or medium confidence of 0.4 and several criteria for linkage, i.e. co-expression, experimental evidence, existing databases, text mining, as well as co-occurrence and neighborhood. Further explanation is found in the figure legend.

## 2.6. Mouse Strains and Diet Information

BKS(D)-Lepr db/+JOrlRj and BKS(D)-Lepr db/db JOrlRj male mice were obtained from Janvier Labs. Animals were gavaged daily with 75mg/kg of vehicle or SGI-1776 (HY-13287) purchased from MedChemTronics, the European branch of MedChemExpress, for 21 consecutive days. Mice were acclimated and submitted to the PhenoMaster (metabolic phenocage) throughout the treatment, by which food intake was measured. Body weight was controlled daily. Following the protocol, mice were killed by cervical dislocation and tissues were isolated for analysis.

Our lab generated the following mouse models *Cdk10<sup>flox/flox</sup>* and *Cdk10<sup>flox/flox</sup> AdipoQCre-ERT2*, which is an inducible adipose-tissue specific knockout. At the age of 11 weeks, mice were gavaged with 2mg Tamoxifen in 100 $\mu\text{L}$  sunflower oil (20mg/mL) per day for 5 consecutive days. Mice were then subjected to different metabolic phenotyping experiments. Body weight was controlled weekly. Following the protocol, mice were killed by cervical dislocation, and tissues were isolated for analysis.

Other mouse strains used, include PIM3 KO mice (Olivier Staub lab, Switzerland) and SWJ/R mice (Villaroya lab, Spain).

Mice had free access to standard rodent chow diet and water, unless stated otherwise. They were housed 5 mice per cage in a 12h-day 12h-night cycle, unless stated differently. All animal care and treatment procedures were performed in accordance with Swiss guidelines and were approved by the Canton of Vaud, Service de la Consommation et des Affaires Vétérinaires (SCAV) (authorization VD 3121.g and VD3371.b).

### **2.7. Glucose and Insulin Tolerance Tests**

For the Glucose Tolerance Test, mice were starved for 16h and then injected intraperitoneally with glucose (2g/kg). Tail vein blood glucose was checked at the indicated time points. For the Insulin Tolerance Test, mice were fasted for 6h, after which they were injected intraperitoneally with 1.125 U/kg insulin and tail vein blood glucose was then measured at the indicated time.

### **2.8. Metabolic Phenocage of the PhenoMaster**

This special automated cage construct separates, collects and quantifies urine and feces of mice or rats and thus provides important information about the animal's energy balance. Dedicated urine and feces collection funnels direct urine and feces into standard lab tubes. Weighing sensors below the collection containers quantify urine and feces by amount and time. Before measurement, mice will be adapted for five days, after which the mice stay throughout the whole period of treatment. Individual mice are housed in a single test chamber (size, 8" x 5" x 4"). Animals have free access to food and water during the entire experiment period.

### **2.9. Oxymax Open Circuit Indirect Calorimeter**

Indirect calorimetry is a non-invasive method to study in vivo metabolic substrate utilization and basal metabolic rate of rodents. Basic calorimetry, activity, body temperature and food intake will be measured by the Oxymax from Columbus. Before measurement in the calorimetric chamber, mice will be adapted for two days, after which the actual experimental period is for two days. Individual mice are housed in a single test chamber (size, 8" x 5" x 4"). Maximum 10 animals can be used for each experiment at a time. Animals have free access to food and water during the entire experiment period. The Oxymax system will continuously measure and compute  $VO_2$ ,  $VCO_2$ , RER, Heat, and Activity during the entire experiment period.

### **2.10. Body Composition Analysis Using the EchoMRI**

Lean body mass, fat mass, free water, and total water were measured on live animals by quantitative magnetic resonance (QMR) using an EchoMRI instrument. Mice were not restrained nor anesthetized.

### **2.11. Immunohistochemistry**

Adipose Tissue samples were fixed overnight at 4°C with 4% paraformaldehyde, and then washed 3 times with cold PBS and embedded in paraffin. 4µm sections cut at 50µm intervals were mounted on charged glass slides, deparaffinized in xylene, and stained for expression of F4/80 as described by (Cecchini et al., 1994) with anti-F4/80 monoclonal antibody (ab6640) from Abcam, and hematoxylin and eosin as described in (Ni et al., 2018). Histological observation was done using light microscopy (Olympus Upright Motorized Microscope, Olympus Corporation, Tokyo, Japan). Image acquisition and processing was performed using the AxioVision software. 2 tissue sections were selected from each mouse, and 20 random non-overlapping fields at 10x magnification were taken. In a blinded manner, crown-like structures of the F4/80 staining were manually counted.

### **2.12. 3T3L1 Differentiation**

3T3-L1 were cultured in Dulbecco's modified Eagle's medium (DMEM) with 10% fetal bovine serum (FBS, PAA Laboratories) in 5% CO<sub>2</sub>. Two days after reaching confluence, they were differentiated with DMEM, 10% FBS, 0.5 mM 3-isobutyl-1-methylxanthine (IBMX), 1.7 µM insulin, 1 µM dexamethasone, and 1 µM rosiglitazone for 2 days. From day 3 onward, cells were incubated with DMEM, 10% FBS, 10 µg/ml insulin. Media was changed every 2 days until day 8 of differentiation. 3T3-L1 mature adipocytes were maintained in medium containing 10% FBS only.

### **2.13. 3T3L1 Insulin Resistant Models and Treatment**

After differentiation, mature 3T3L1 adipocytes were washed with PBS and incubated with or without 20 ng/ml TNFα in DMEM containing 0.2% bovine serum albumin (BSA). Insulin resistant mature adipocytes were treated overnight with DMSO, 0.1µM, 0.25µM, 0.5µM or 1µM SGI-1776 or CCT241533 HCl. Then, cells were starved and stimulated with

or without insulin, at 100 nM. Cells were washed with cold PBS and lysed as described later. SGI 1776 (HY-13287), the PIM inhibitor, and CCT241533 HCl (HY-14715B), the CHK2 inhibitor, were purchased from MedChemExpress.

#### **2.14. BMDM Treatment**

Bone marrow-derived macrophages (BMDMs) were seeded in 10cm petri-dishes. After cells attached, they were treated with control or 100ng/mL LPS for 6h or 24h. As for treatment with the inhibitor, BMDMs were seeded in 6-well plates. After they attached, BMDMs were treated with DMSO, 0.25 $\mu$ M or 0.5 $\mu$ M SGI-1776 for 24h, and then 100ng/mL LPS was added for 6h.

#### **2.15. Protein Extraction and Western Blotting**

For Western blot (WB) analysis, protein extraction from different mouse tissues, cell lysates, and human adipose tissue samples was obtained with M-PER mammalian extraction buffer (Thermo Scientific, USA) containing 1:100 Halt phosphatase inhibitor cocktail (Thermo Scientific, USA) and 1:100 Halt protease inhibitor cocktail, EDTA-free (Thermo Scientific, USA). Membranes were incubated over night at 4°C with the corresponding primary antibodies. The following day, membranes were washed and incubated with the corresponding secondary antibodies, washed and revealed with ECL in the Chemidoc or Fusion Fx. WB bands were quantified using ImageJ or Fiji software.

The following antibodies were used for Western blot analysis: anti-phospho AKT-T308 (244F9), anti AKT (9272), anti-PIM3 (D17EA), anti-phospho CHK2 T68 (2661T) from cell signaling, anti-phospho Bad-S112 (ab129192), anti-phospho p21-T145 (ab135553), anti-CDK10 (ab186912, ab72710, ab67828), and anti-FAM58A (ab81062) from Abcam, anti-PIM1 (AP7932d) from Abgent, anti-CDK10 (sc-51266) from Santa Cruz, anti-CDK10 (AP7516A-EV) from LuBioScience GmbH, and anti-Actin (A2066) and anti-Tubulin (T6199) from Sigma.

#### **2.16. RNA Extraction and RTqPCR:**

Samples were lysed using TRI-reagent (T9424, Sigma Aldrich), according to the manufacturer's instructions. An additional centrifugation step immediately after lysis was included in order to remove the lipid layer when adipose tissue samples or mature 3T3L1 adipocytes were extracted. For adipose tissue samples, a second chloroform wash

step, followed by an overnight precipitation using ammonium acetate and absolute ethanol, was performed to remove phenol contaminations. Quality check and quantification of the RNA was done using the Nanodrop. cDNA was prepared using 1µg of total RNA (unless stated otherwise), using Superscript II (Invitrogen). cDNAs were diluted 20 times and used for qPCR. qPCR experiments were done using the FastStart Universal SYBR Green Master (Rox) from Roche and a 7900HT Fast Real-Time PCR System (Applied Biosystems), with a mix of 10µM forward and reverse primers of the targeted genes. Relative mRNA expression levels were calculated from the comparative threshold cycle (Ct) values of the gene of interest relative to RS9 and actin mRNA (unless stated otherwise). Specific primer sequences are listed in Tables 2.3, 2.4, 2.5, and 2.6.

**Table 2.3: Primers used for qPCR analysis of housekeeping genes (human and mouse)**

Gene	Forward	Reverse
RS9	CACACTCTCCCAACGTTCT	ACCACCTGCTTGCGGACCCTGATA
Actin	TCCATCATGAAGTGTGACGT	TACTCCTGCTTGCTGATCCAC

**Table 2.4: Primers used for qPCR analysis of kinases upregulated in VAT of MOD patients**

Gene	Forward	Reverse
Pim-1 (human)	CCTGGGGATCCTGCTGTATG	CAGGGCCAAGCACCATCTAA
Pim-1 (mouse)	GCGGCGAAATCAAACCTCA	TCATAGAGCAGGATCCCAAG
Pim-2 (human)	AGCTCATCGACTTCGGTTTCG	TATCGTAGAGAAGCACGCCC
Pim-2 (mouse)	AGCTTTCGAGGCCGAATA	GGTTCGGGAGATTACTTTG
Pim-3 (human)	GTTCTGGTGCCTGCTTCAT	TGCATGGTACTGGTGTGCGAG
Pim-3 (mouse)	AGCTGAAGCTCATCGACT	GTAGAGCAGTACACCCAGA
PRKG1 (human)	ATCAGGCAAGGTGCAAGAGG	CCTGCAAGGCTTTCTCTCCA
PRKG2 (human)	TCCTGCACAATGGGAAGAGG	ATGGGGTAGCCTCTAGCAGT
CHK2 (human)	GCAGGTTTAGCGCCACTCTG	TCCGACTCCCGAGACATCAC
CHK2 (mouse)	TGAGAAGGACGGACAAGTA	CGTTTGCCTTTCCAATAAG
CDK10 (mouse)	ACGCCTGCGCGCTGGAAGAG	TGCCATAGGTGCCCTCGCCAAT
CycM (mouse)	TGTCGCACAGGTACTTTAACC	CGCAGAAGCTCGTAGCATAAG

**Table 2.5: Primers used for qPCR analysis of pro-inflammatory markers (mouse)**

Gene	Forward	Reverse
IL-1β	GCAACTGTTCCCTGAACTCAACT	ATCTTTTGGGGTCCGTCAACT
IL-6	TAGTCCTTCTACCCCAATTTCC	TTGGTCCTTAGCCACTCCTTC
iNOS	CCAAGCCCTCACCTACTTCC	CTCTGAGGGCTGACACAAGG
MCP-1	CCACTCACCTGCTGCTACTCA	TGGTGATCCTCTTGTAGCTCTCC
TNFα	ACGGCATGGATCTCAAAGAC	AGATAGCAAATCGGCTGACG

**Table 2.6: Primers used for qPCR analysis of BAT markers (mouse)**

Gene	Forward	Reverse
UCP1	TGCCCAACTGTGCAATGAA	TCGCAAGAAGGAAGGTACCAA
PGC1 $\alpha$	CCGATCACCATATTCCAGGTC	GTGTGCGGTGTCTGTAGTGG
PPAR $\alpha$	CGCATGTGAAGGCTGTAA	GGCAGTACTGGCATTGT
CPT1 $\beta$	CCGGAAAGGTATGGCCACTT	GAAGAAAATGCCTGTCGCCC

### **2.17. Data Analysis:**

All statistics are described in the figure legends. All *P*-values below 0.05 were considered significant. The results were expressed as means  $\pm$  standard error of the means (s.e.m). Statistical significance values were represented by asterisks corresponding to \* $p < 0.05$ , \*\* $p < 0.01$ , \*\*\* $p < 0.001$ , and \*\*\*\* $p < 0.0001$ .

---

## Chapter 3: Kinome Profiling

---

*This chapter is based on the manuscript under preparation “Global kinome analysis in obese subjects reveals PIM-1 as a novel target for the treatment of insulin resistance.”*

The main goal of our study is to identify novel kinases inducing insulin resistance in obese subjects. Since the VAT depot is well known to be predominantly implicated in adipose tissue inflammation upon obesity, leading to insulin resistance (Cancello et al., 2006), we decided to study the differential global kinase activity in human VAT from morbid obese non-diabetic (MOND) and morbid obese diabetic (MOD) patients (Table 2.1).

The insulin signaling cascade is dependent on the rapid activation of a series of tyrosine (TKs) and serine/threonine protein kinases (STKs). For this project, we decided to only study the kinase activities of STKs in the human samples, by using a new technology developed by PamGene. We used arrays that consist of 140 immobilized serine/threonine containing peptides and 4 control peptides (STK PamChips). These chips were incubated with the different adipose tissue lysates, and further analysis was done (Figure 3.1).

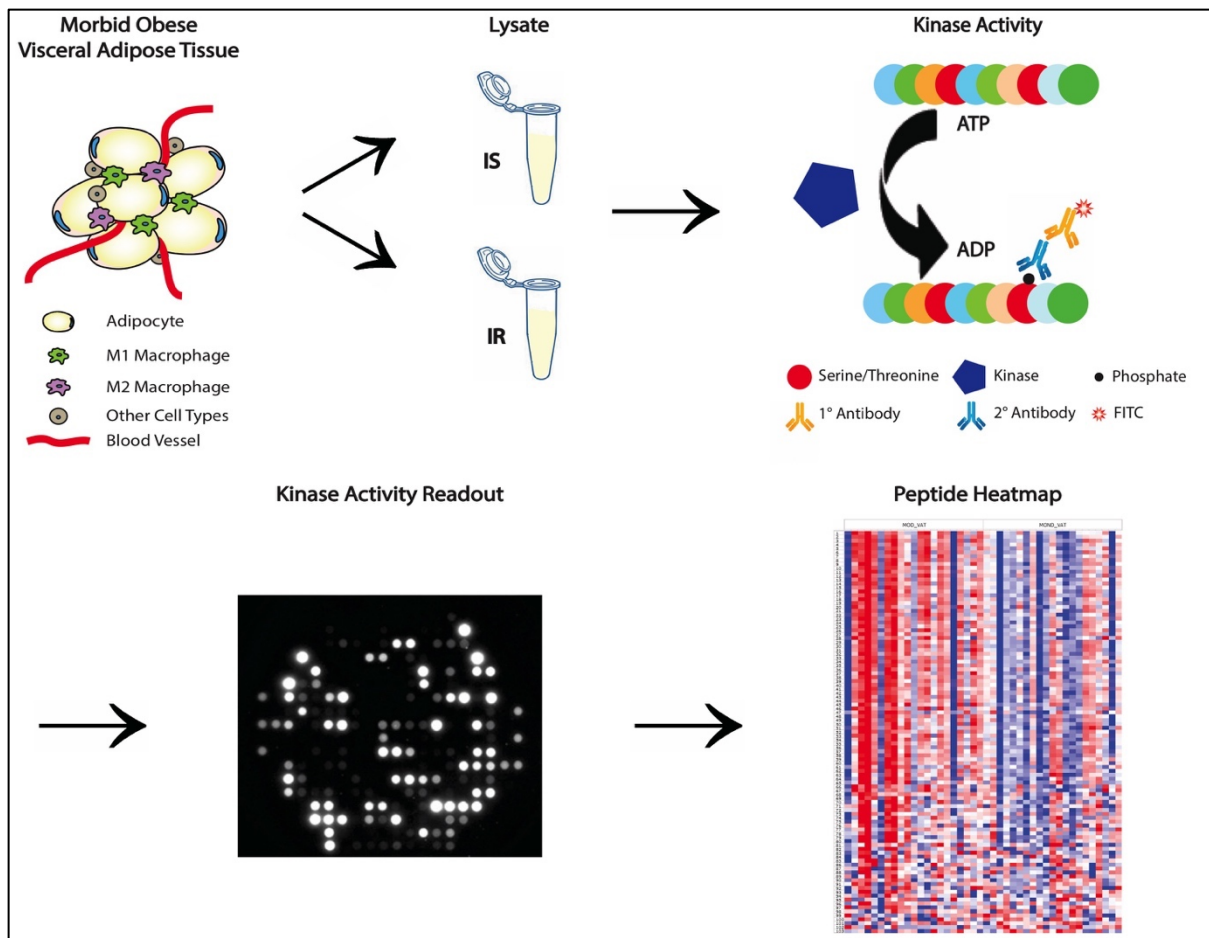


**Figure 3.1: Kinome profiling of human visceral adipose tissue (hVAT) samples from morbid obese diabetic (MOD) and morbid obese non-diabetic (MOND) patients.** The protein lysate was extracted from morbid obese visceral adipose tissue from IS and IR patients, and were passed into the PamStation, where the samples were incubated on PamChip Serine/Threonine kinase microarrays to detect kinase activity readout, by peptide phosphorylation and FITC labelling. The Log Data is then displayed as a heat map showing peptide phosphorylation.

### 3.1. Results

---

#### **Kinome profiling reveals distinct kinase activities in VAT from morbid obese diabetic, compared to non-diabetic subjects**

Differentially phosphorylated peptides, whose phosphorylation varied significantly between the MOND and MOD samples, were indicative of differential specific kinase activities. More than 60 peptides were highly phosphorylated specifically in the VAT of MOD patients, as compared to MOND patients (Figure 3.2A and Table 2.1). Putative upstream kinase analysis was done using the “STK upstream kinase analysis” Bionavigator software. This method takes into account the multiple parallel changes in peptide phosphorylation and both experimental kinase-substrate relationships ([Uniprot](#), [HPRD](#), [PhosphositePlus](#), [Phospho.ELM](#), and [Reactome](#) databases), and in silico predictions for upstream kinases ([phosphoNET](#) database). The kinases that were identified with “more confidence” using this method were AKT1/PKB $\alpha$ , AKT2/PKB $\beta$ , AMPK $\alpha$ 1, ANP $\alpha$ , CHK2, mTOR/FRAP, PIM1, PIM2, PIM3, PKA $\alpha$ , PKC ( $\alpha$ ,  $\delta$ ,  $\epsilon$ ,  $\eta$ ,  $\theta$ ), PKD1, PKG1, PKG2, PRKX and p70S6K $\beta$  (Figure 3.2B-C). Even though PRKY is shown as a kinase hit in the kinexus-based analysis (Figure 3.2B), however it is considered as a pseudogene, which is why it is not depicted in the String Plot (Figure 3.2C). Of note, during the course of this study, it was shown that the knockout of PKG1 in TNF $\alpha$ -induced mature adipocytes reverted the insulin resistant phenotype, by rescuing glucose uptake impairment (Ando et al., 2015). Importantly, PKA, PKC, AKT and AMPK have already been described as involved in the onset of insulin resistance (Huang, Liu, Guo, & Su, 2018; Mehta, 2014). These findings validated our experimental approach, and suggested that the increased activity of the above mentioned kinases can be either a cause or a consequence of the insulin resistance characterizing MOD subjects.

## 3.2. Discussion

---

The use of genomic, proteomic and transcriptomic techniques in the study of human pathologies has been rapidly expanding. Indeed, the recent identification of new key players in human type 2 diabetes mellitus (T2DM) is based on high throughput techniques. However, these approaches study potentially pathogenic mutations or SNPs, as well as the expression of protein coding genes and actual protein abundance. Functional proteomic methodologies bring more insight on protein activity and how cell signaling works. Indeed, in the past five years, proteomic studies have confirmed the importance of inflammatory pathways and cellular stress in the alterations found in adipose tissue of obese subjects (Garrison, Lastwika, Zhang, Li, & Lampe, 2017). A first prediction of upregulated kinases in adipose tissue in conditions of obesity and insulin resistance in mice was performed using phosphoproteomics. However, this study shows very limited overlap with our dataset (Shaik et al., 2016). The kinase activity-based assay from PamGene allows us to detect kinase function directly in order to perform kinome profiling on patients' biopsies.

The aim of our study was to discover new kinases whose activities are deregulated during the development of insulin resistance in obese subjects, independently of adiposity. To implement our strategy, we took advantage of a population of obese subjects that are protected from the development insulin resistance and other obesity-derived pathologies (Wildman et al., 2008). Comparing the global kinase activities in the adipose tissue of these subjects with the kinase activities of the obese diabetic patients allowed us to discover new kinases specifically active in the adipose tissue of the pathological group. This strategy allows us to overcome any confounding factors that could be related to obesity *per se*, and not to insulin resistance. Moreover, our results shed light on the mechanism behind the ability of a certain population of obese subjects to maintain metabolic health and evade metabolic complications.

We used three criteria to select specific kinase activities for further *in vivo* studies. First, the kinase activity should be significantly modified in validation studies. Second, specific kinase inhibitors should be available for further preclinical testing. And third, a role for the identified kinase in diabetes should not have been previously described. By performing a motif-based analysis of the differentially phosphorylated peptides in MOD

and MOND VAT samples, we identified that several putative kinases might be potentially upregulated in diabetic patients. We consequently validated our finding and propose a mechanism by which Pim-1 modulates insulin sensitivity by integrating cellular models, and diabetic mouse models with clinical data from our human cohort, as explained in Chapter 2.

### 3.3. Figures

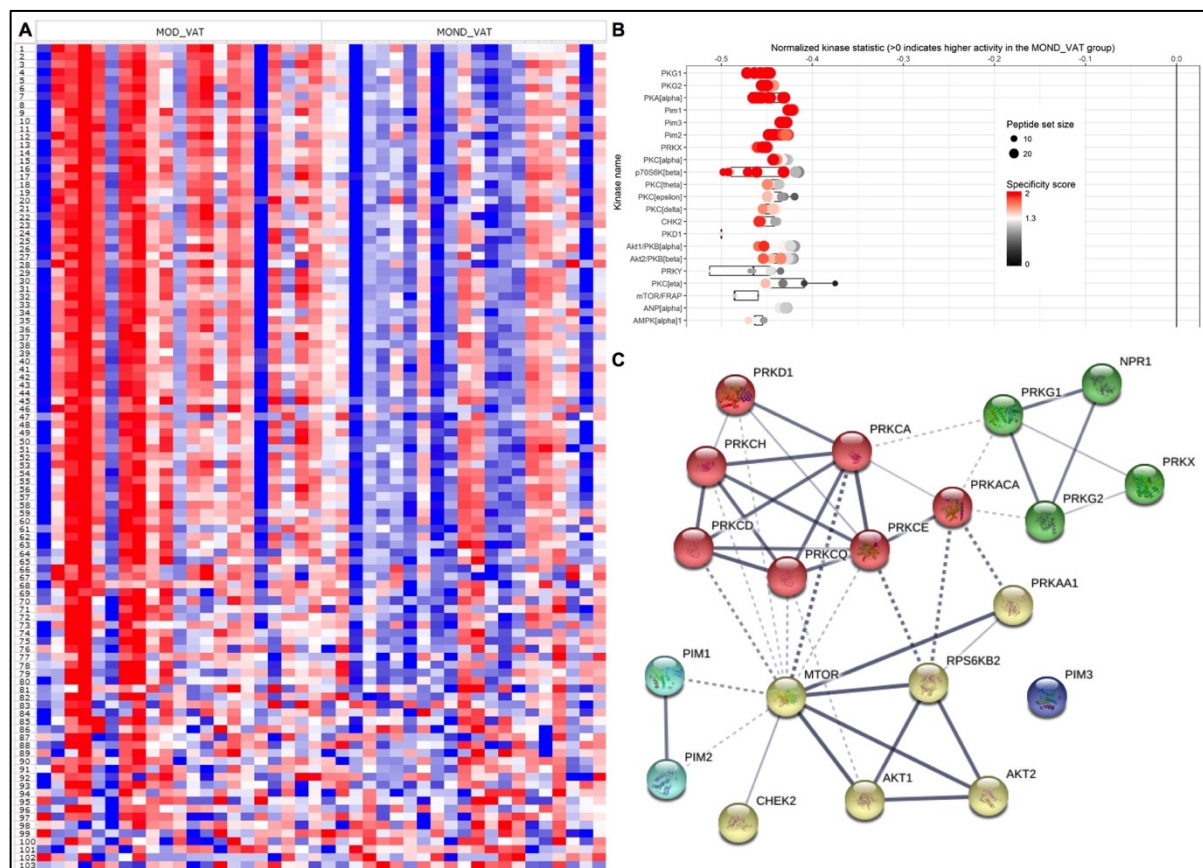


**Figure 3.2: Many novel kinases are upregulated in human visceral adipose tissue (hVAT) of morbid obese diabetic (MOD) patients as seen in upstream score plot using kinexus-based analysis.** The heatmap shows that more than 60 peptides were highly phosphorylated in visceral adipose tissue samples from morbid obese diabetic (IR) as compared to samples from morbid obese non-diabetic (IS) patients (A). Upstream kinase analysis was done using the Bionavigator software of the PamGene, which bases its assumption on kinexus. Peptide set size corresponding to each kinase is denoted by the size of the dot. As for the specificity of these peptides to the kinase, it ranges from black (0) to red (2). The darker the red color, the higher the specificity of the peptide set to the kinase. Negative values indicate higher kinase activity in the MOD group. As seen in this score plot, PKG1, PKG2, PKA, Pim-1, Pim-2, Pim-3, PRKX, PKC, p70S6K $\beta$ , CHK2, PKD1, Akt1/PKB, etc. have higher kinase activity in the hVAT samples from MOD patients, as compared to the hVAT samples from morbid obese non-diabetic (MOND) patients (B). An interaction network was constructed using the STRING tool and the selected kinases as input. The width of the interactions depends on the confidence score to each association in STRING, i.e. the thickness of the lines indicates the strength of the data support. Each color group of the kinases is attributed to a kinase cluster, giving a total of 5 different groups of interacting kinases (C). More detailed information is found in the Materials and Methods section. n = 21-24.

## Chapter 4: PIM Family

*This chapter is based on the manuscript under preparation “Global kinome analysis in obese subjects reveals PIM-1 as a novel target for the treatment of insulin resistance.”*

While analyzing the differences in the kinome of visceral WAT (VAT), we found that the activity of the PIM family of serine/threonine kinases was increased in the VAT of obese insulin resistant patients, compared to metabolically healthy obese subjects. The PIM family is composed of three kinases: PIM-1, PIM-2 and PIM-3, which are highly homologous (Keane, Reidy, Natoni, Raab, & O'Dwyer, 2015; J. Li et al., 2001). Pim AUG start codons result in the translation of one and two longer isoforms of Pim-1 and Pim-2, respectively (Figure 4.1). PIM proteins are auto-phosphorylated at an upstream serine 8 residue. PIM kinases are constitutively active since they lack a regulatory domain (Fox et al., 2003; Qian et al., 2005).

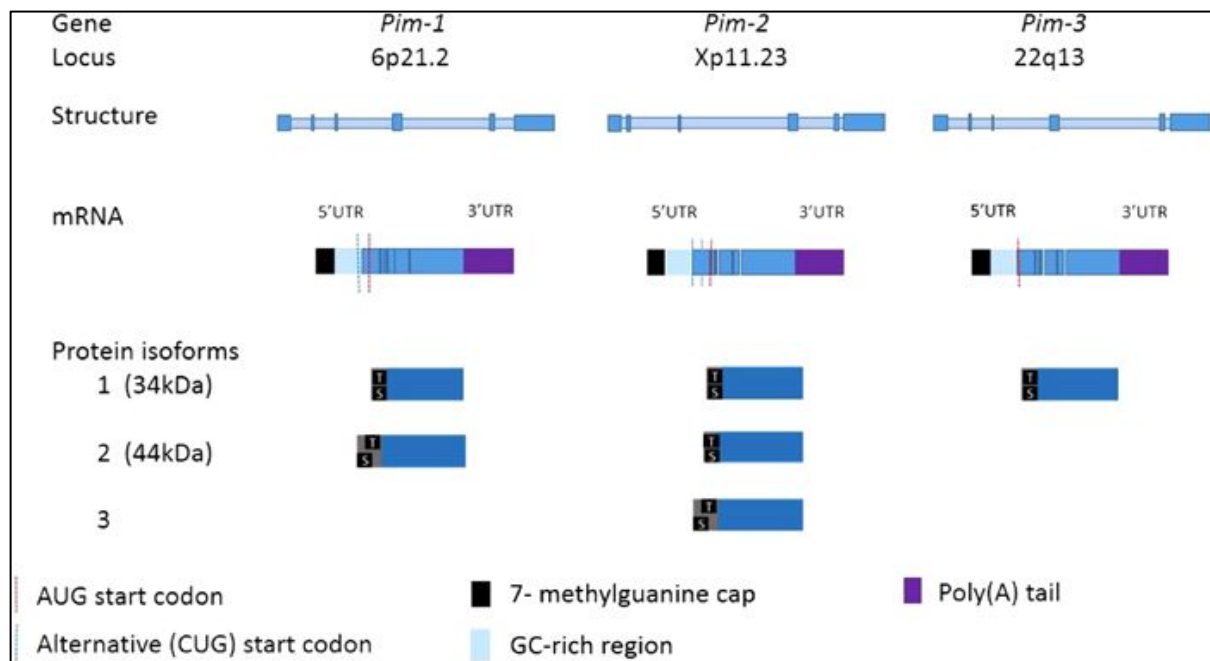


**Figure 4.1: Genetic Structures of the PIM family.** Each Pim gene contains 6 exons (depicted in darker blue). Pim mRNA contains a 5' untranslated region (UTR) which is comprised of a 7 methyl-guanine cap and GC-rich region which renders the Pims 'weak transcripts' requiring cap-dependent translation. The 3' UTR contains destabilizing AUUUA motifs which result in a short Pim mRNA half-life. The longer 44kDa isoform of Pim-1 is derived from use of an upstream CUG start codon at nucleotides 158–160 and localizes to the plasma membrane, with a role in chemotherapeutic resistance (Keane et al., 2015).

PIM kinases play vital roles in numerous cellular functions, such as proliferation, cell cycle progression, differentiation, apoptosis, and tumorigenesis (J. Li, Loveland, & Xing, 2011; Narlik-Grassow, Blanco-Aparicio, & Carnero, 2014; Warfel & Kraft, 2015). PIM kinases are important for growth factor signaling (Mikkers et al., 2004), by regulating B- and T- cell responses to cytokines and hematopoietic growth factors (An, Kraft, & Kang, 2013).

We show in this study that PIM-1 activity in the macrophage fraction of adipose tissue mediates their pro-inflammatory effects, thus promoting insulin resistance and type II diabetes. Moreover, we demonstrate that the pharmacological inhibition of PIM-1 alters macrophage polarization *in vitro* and ameliorates insulin resistance in a mouse model of obesity.

## 4.1. Results

---

### 4.1.1. *Pim-1* expression in VAT positively correlates with IR markers and is increased in different mouse models of insulin resistance.

We focused on the PIM family of kinases, because they were not previously described to be involved in insulin resistance or diabetes. PIM kinase activity is constitutively active (Warfel & Kraft, 2015). Thus, unlike other kinases, PIM kinase activity is regulated primarily at the transcriptional level, then by translation efficiency, and finally by proteasomal degradation (Amaravadi & Thompson, 2005). Functional redundancy, at the *in vitro* and *in vivo* levels, between the PIM kinases have been shown (Mikkers et al., 2004; Narlik-Grassow et al., 2012).

Thus, we used their transcriptional level as a readout for activity and measured the expression of the different novel kinases in the VAT of more than 80 human patients (Table 2.2). mRNA levels were correlated to the different IR markers, i.e. body mass index (BMI), insulinemia, and glycemia (Figure 4.2 A-I). Of all the identified kinases, *PIM-1* was the only one to show a positive correlation with all 3 variables (Figure 4.2 A-C). *PIM-2* was only correlated to BMI (Figure 4.2 D-F), while *PIM-3* did not correlate to any of the 3 parameters (Figure 4.2 G-I).

To validate if the increased expression of *PIM-1* upon insulin resistance is conserved in mice, we quantified mRNA levels in two different mouse models of type II diabetes: mice under high-fat diet (HFD), and db/db mice. Based on RNA sequencing data, *Pim-1* gene expression was significantly increased in the VAT of mice fed a HFD for 8 weeks, as compared to mice under normal chow diet (CD) (Figure 4.2J). This was further increased after 20 weeks of HFD (Figure 4.2 J). *Pim-2* expression did not change between the groups (Figure 4.2 K), while *Pim-3* expression significantly decreased in the VAT of mice under HFD (Figure 4.2 L). RTqPCR data showed that *Pim-1* mRNA is also significantly higher in VAT of db/db mice (Figure 4.2 M). However, *Pim-2* expression was also increased in VAT of db/db mice (Figure 4.2 N), while *Pim-3* expression was significantly decreased in the VAT of db/db mice (Figure 4.2 O). Overall, these results prove that *PIM-1* gene expression is increased in adipose tissue from diabetic human subjects and from mouse models of diabetes, suggesting that PIM-1 participates in the development of insulin resistance.

#### **4.1.2. The effects of Pim-1 in insulin resistance are not mediated by adipocytes.**

Next, we wanted to analyze the participation of PIM-1 in the onset of insulin-resistance in cellular models of white adipose tissue. Indeed, *Pim-1* is increasingly expressed during adipocyte differentiation in the 3T3L1 model (Figure 4.3 A). Mature 3T3L1 adipocytes treated with TNF $\alpha$  for 72h were used as a model for insulin resistance (Stephens, Lee, & Pilch, 1997). We stimulated these cells with 100nM insulin for 20 minutes and saw a significant decrease in the phosphorylation of AKT at Threonine 308, which is a readout of IS (Figure 4.3 B-C). We treated these insulin-resistant adipocytes with the Pim-1 inhibitor SGI-1776. The inhibition of PIM1 activity was validated by showing a dose-dependent decrease in the phosphorylation of Bad at Serine 112, which is a target of PIM1, upon SGI-1776 treatment starting from 0.25 $\mu$ M (Figure 4.3 D-F). The phosphorylation levels of AKT were, however, not increased with any of the tested doses of Pim-1 inhibitor, showing no rescue of the insulin resistant phenotype of TNF $\alpha$  treated 3T3L1 mature adipocytes (Figure 4.3 D-F). These results suggested that Pim-1 does not directly act on adipocytes to induce insulin resistance in the adipose tissue of obese subjects.

#### **4.1.3. Pim-1 expression and activity are increased in pro-inflammatory macrophages.**

Our initial kinome analysis was performed in whole VAT. In addition to adipocytes VAT contains fibroblasts, endothelial cells, and inflammatory cells. Out of those non-adipocyte cells, pro-inflammatory macrophages play a major role in the development of insulin resistance in this tissue. Therefore, we used bone marrow-derived macrophages (BMDMs) treated with lipopolysaccharide (LPS) for 6h, as an in vitro model of pro-inflammatory macrophages. Protein extracts from naive and 6h-LPS-stimulated cells were then submitted to PamChip serine/threonine kinase analyses (Figure 4.4 A). Pim-1 was among the kinases with increased activity in response to LPS treatment (Figure 4.4 B). Consistently, RNA sequencing data from naïve and LPS-treated macrophages showed an increase in *Pim-1* mRNA levels in the pro-inflammatory macrophages (Figure 4.5 A). Moreover, the expression of *Pim-1* was also increased in FACS sorted CD11c<sup>+</sup> adipose tissue-derived pro-inflammatory macrophages from mice under HFD, when compared to CD11c<sup>+</sup> macrophages from mice under chow diet (Figure 4.5 B), suggesting that our observations in BMDMs can be extended to adipose tissue macrophages.

#### **4.1.4. SGI-1776 decreases pro-inflammatory markers in LPS-stimulated macrophages.**

BMDMs were stimulated with LPS for 6h or 24h to induce a pro-inflammatory phenotype. Pro-inflammatory markers (*IL-1 $\beta$* , *IL-6*, *TNF $\alpha$* , *MCP-1* and *iNOS*) were significantly increased in LPS treated macrophages as compared to naïve macrophages as expected (Figure 4.6 A). *Pim-1* expression was also increased upon LPS-stimulation in BMDMs both at the mRNA and protein levels (Figure 4.6 B-D). The phosphorylation of the known Pim-1 targets pS112 Bad and pT146 p21 was also increased upon LPS stimulation (Figure 4.6 E), suggesting an increase in Pim-1 activity in pro-inflammatory macrophages.

The treatment of macrophages with the Pim-1 inhibitor SGI-1776 prior to LPS stimulation decreased the mRNA expression of several pro-inflammatory cytokines, such as *IL-1 $\beta$* , *TNF $\alpha$* , *MCP-1* and *iNOS* (Figure 4.6 F), as well as the expression of *Pim-1* (Figure 4.6 G). These results proved that Pim-1 has a direct role on pro-inflammatory macrophages, and this may participate in the onset of insulin resistance in WAT.

#### **4.1.5. Pim-1 inhibition improves insulin sensitivity in diabetic mice**

We next wanted to test the clinical relevance of our findings by treating the db/db diabetic mouse model with the SGI-1776 Pim-1 inhibitor. After 3 weeks of treatment, we did not observe changes in the food intake (Figure 4.7 A) or body weight (Figure 4.7 B). In contrast, the treatment elicits alterations in body composition; an increase of lean mass and a decrease of fat mass (Figure 4.7 C-D). This correlated with a decreased weight of WAT depots in SGI-1776-treated mice, whereas no differences were observed in the weight of other tissues, such as liver, heart or muscle (Figure 4.7 E). This suggests a specific effect of SGI-1776 on adipose tissue depots. Most important was the finding that the fasting glycemia of the db/db mice treated with the Pim-1 inhibitor was reduced after 3 weeks of treatment, when compared to the vehicle-treated group (Figure 4.7 F). Moreover, SGI-1776 treatment resulted in enhanced insulin sensitivity and glucose disposal, as measured by insulin and glucose tolerance tests (Figure 4.7 G-J).

Gene expression of several cytokines was next assessed. Pro-inflammatory markers, such as *MCP-1*, *TNF $\alpha$*  and *iNOS* decreased in the VAT of SGI-1776-treated mice (Figure 4.7 K). A higher expression of pro-inflammatory cytokines is often correlated with the aggregation of pro-inflammatory macrophages around dead adipocytes and is a

characteristic feature of inflammation in this tissue. These so-called crown-like structures were indeed apparent in the adipose tissue of vehicle-treated mice (Figure 4.7 L-M), but were much decreased in the VAT of db/db mice treated with SGI-1776 (Figure 4.7 L-M). These results proved that the inhibition of Pim-1 improves adipose tissue inflammation and the overall diabetic phenotype in the db/db mouse model.

#### **4.1.6. PIM3KO Mice Are Leaner and Insulin Sensitive.**

We metabolically phenotyped PIM3 full knock out mice (Figure 4.8 A-G). PIM3<sup>-/-</sup> are leaner (Figure 4.8 A), depicted by less scWAT and pgWAT masses (Figure 4.8 B). They show no difference in their fasting glycemia as compared to the wild type group (Figure 4.8 C). By testing their glucose tolerance, results show no difference (Figure 4.8 D). Nevertheless, their insulin tolerance test (ITT) displayed insulin sensitivity as compared to the wild type mice (Figure 4.8 D), which shows an insulin sensitive systemic phenotype of the PIM3<sup>-/-</sup> mice. This perfectly correlates with the PamGene data, which show that PIM3 is highly expressed in MOD samples (IR patients) as compared to MOND samples (IS patients). In other words, PIM3 activity inversely correlates with insulin resistance. However, phosphoT308 AKT decreased in the scWAT and pgWAT of PIM3<sup>-/-</sup> mice (Figure 4.8 F-G), which means the adipose tissue of the KO mice is insulin resistant. One explanation for this is that other tissues, such as the muscle and liver, might be playing a role in inducing this insulin sensitive phenotype in the PIM3 full knock out mice.

## 4.2. Discussion

---

Emerging evidence proves that PIM-1 is a promising drug target against many types of cancer. It is correlated with tumor aggressiveness and is a marker of poor prognosis in several tumor types, such as prostate cancer and leukemia (Dhanasekaran et al., 2001; H. T. Liu, Wang, Wang, & Li, 2010; Shah et al., 2008). Interestingly, in ovarian cancer cells, PIM-1 phosphorylates c-Myc, which in turn induces the expression of several metabolic enzymes: PGK1, LDHA, GLUT1, etc. (Wu et al., 2018), providing a first observation linking PIM-1 activity to the regulation of metabolism, at least in the context of cancer. Moreover, PIM-1 has been shown to play a role in diabetic cardiomyopathy and diabetic nephropathy, which are severe complications associated with diabetes (Agrawal & Kant, 2014; Kannel, Hjortland, & Castelli, 1974). However, PIM-1 has never been directly associated with adipose tissue insulin resistance in the context of T2D. An important role of PIM-1 that strongly places this kinase as a novel target for insulin resistance is its role in the inflammatory response. Indeed, PIM-1 has been linked to placental inflammation (Liong, Barker, & Lappas, 2017), to the stabilization of the p65 subunit of NF $\kappa$ B (Nihira et al., 2009), and to the immunosuppressive activity of human regulatory T cells (Z. Li et al., 2014). It is well established that pro-inflammatory cytokines, such as IL-6 and TNF- $\alpha$ , affect insulin signaling, which in turn is essential to maintain glucose homeostasis and regulate its metabolism in adipose tissue. We show here that PIM-1 kinase does not mediate cytokine-induced insulin resistance in adipocytes (Figure 4.3), but rather plays a key role in another cell type mediating insulin resistance in adipose tissue: pro-inflammatory macrophages.

PIM kinases are arising as significant mediators in cytokine signaling pathways. *Pim-1* is highly expressed in the bone marrow, spleen, thymus, fetal liver, and non-hematopoietic tissues such as hippocampus, prostate, and epithelia (Eichmann, Yuan, Breant, Alitalo, & Koskinen, 2000). *Pim-1* transcription is activated in response to numerous cytokines through JAK-STAT signaling (Brault et al., 2010). PIM-1 is also involved in myeloid cell differentiation, indeed when the levels of active PIM-1 are manipulated, the rate of differentiation of U937 cells is altered (Z. Wang et al., 2001). Importantly, PIM-1 has been shown to promote NF $\kappa$ B transactivation by preventing its degradation in HeLa cells (Nihira et al., 2009), and by promoting RANKL-induced NF $\kappa$ B transcriptional activity in

osteoclasts (K. Kim, Kim, Youn, Jin, & Kim, 2010). We propose here an additional role for PIM-1 in macrophage polarization in response to pro-inflammatory stimuli.

In conclusion, this study has identified a subset of novel kinases potentially involved in adipose tissue insulin resistance through an activity-based screen and elucidated yet another important role of PIM-1 kinase, linking its canonical role in cancer and inflammation to metabolism, specifically insulin resistance in diabetic patients. This will now pave the way for more studies, investigating the mechanisms by which PIM-1 participates in adipose tissue inflammation in obese subjects, and thus in the onset of T2D. This will also help develop new targeted drug therapies in the field of diabetes, a worldwide epidemic, with no clear therapeutic strategies yet.

### 4.3. Figures

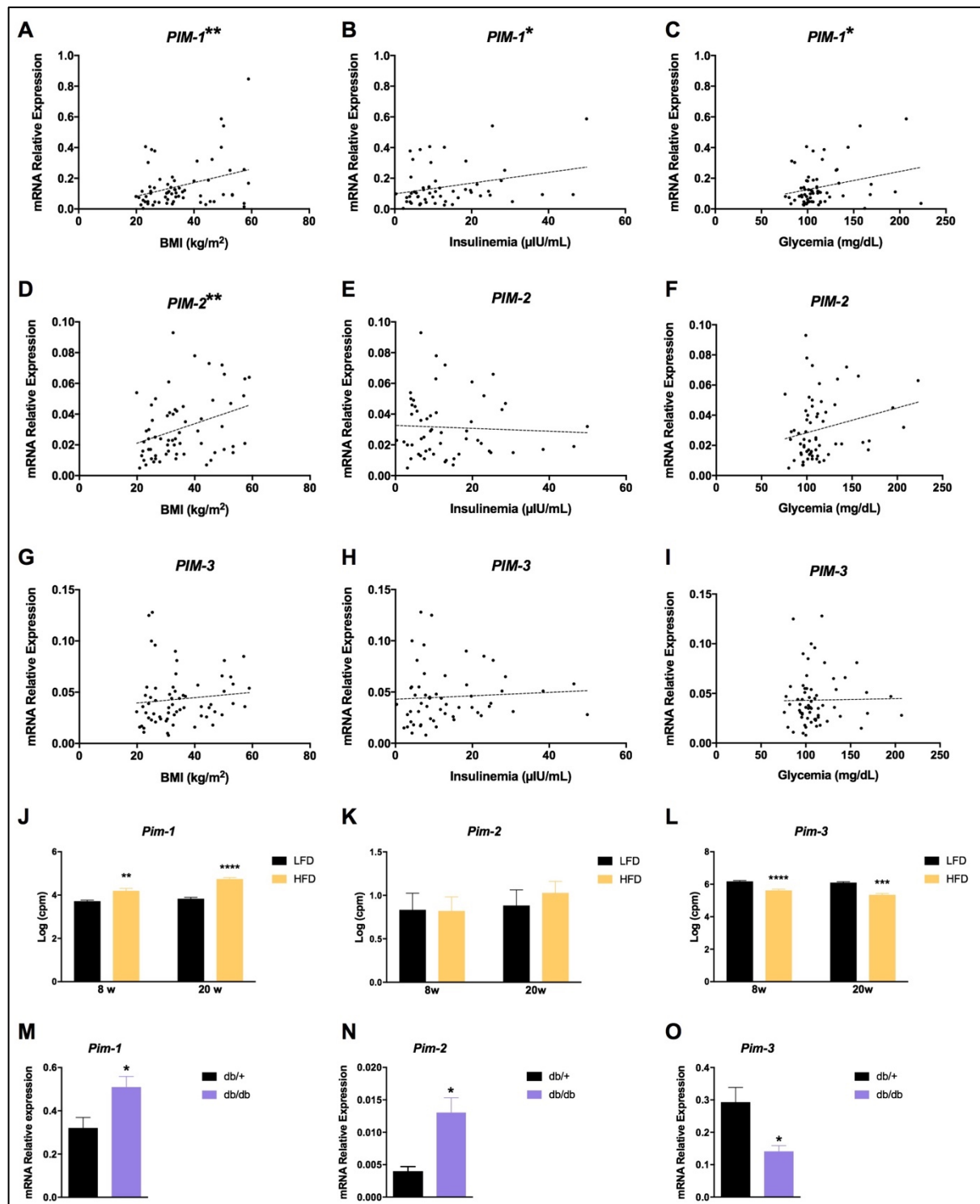


**Figure 4.2: *Pim-1* gene expression positively correlates to IR markers in hVAT and is upregulated in mVAT of 2 IR mouse models.** RTqPCR was performed on visceral adipose tissue samples taken from more than 80 lean, obese, and morbid obese healthy and diabetic patients. *Pim-1* relative gene expression positively correlates with BMI (A), insulinemia (B), and glycemia (C). *Pim-2* positively correlates with BMI (D), but not with insulinemia (E) or glycemia (F). *Pim-3* does not correlate with any of the three markers (G-I). *Pim* expression was also checked in visceral adipose tissue from 2 mouse models of insulin resistance (J-O). RNA sequencing data of VAT from mice under LFD or HFD (8 or 20 weeks) show that *Pim-1* expression was significantly increased in VAT of mice under HFD, with higher values in the 20 weeks' duration (J), *Pim-2* does not differ (K), and *Pim-3* significantly



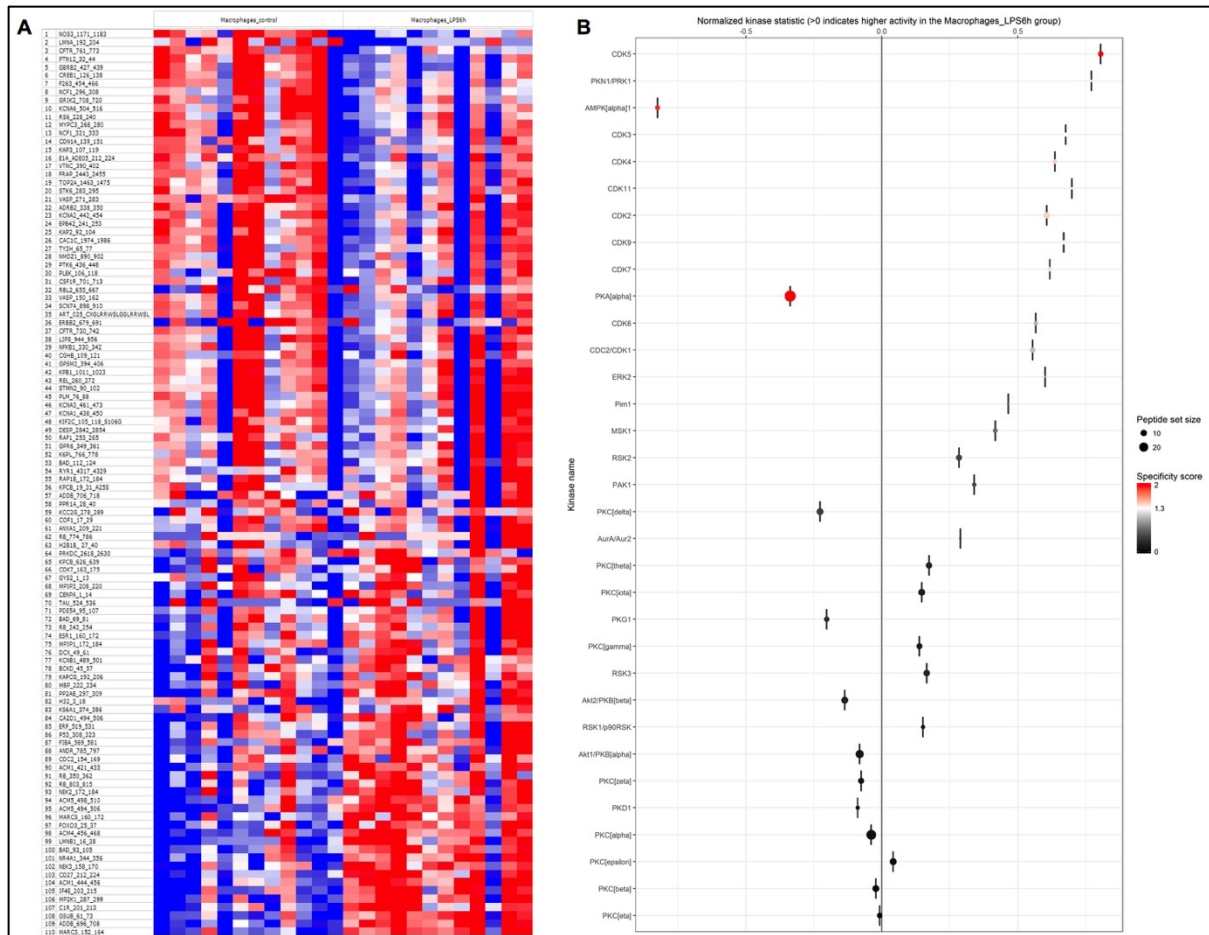


**Figure 4.4: Pim-1 kinase activity and gene expression are upregulated in pro-inflammatory macrophages.** Protein was extracted from naive and 6h-LPS-stimulated pro-inflammatory BMDMs, and then incubated on PamChip Serine/Threonine kinase microarrays to detect peptide phosphorylation. The heatmap shows that around 50 peptides were highly phosphorylated in LPS-treated macrophages, while around 60 were highly phosphorylated in the naïve macrophages (A). Upstream kinase analysis was done using the Bionavigator software of the PamGene, which bases its assumption on kinexus. Peptide set size corresponding to each kinase is denoted by the size of the dot. As for the specificity of these peptides to the kinase, it ranges from black (0) to red (2). The darker the red color, the higher the specificity of the peptide set to the kinase. Negative values indicate higher kinase activity in LPS-stimulated macrophages. As seen in the score plot, PKA, AMPK, several CDKs, and Pim-1 have higher kinase activity in the pro-inflammatory LPS-stimulated macrophages (B). PamGene results are the average of 3 independent experiments, each with 4 replicates.

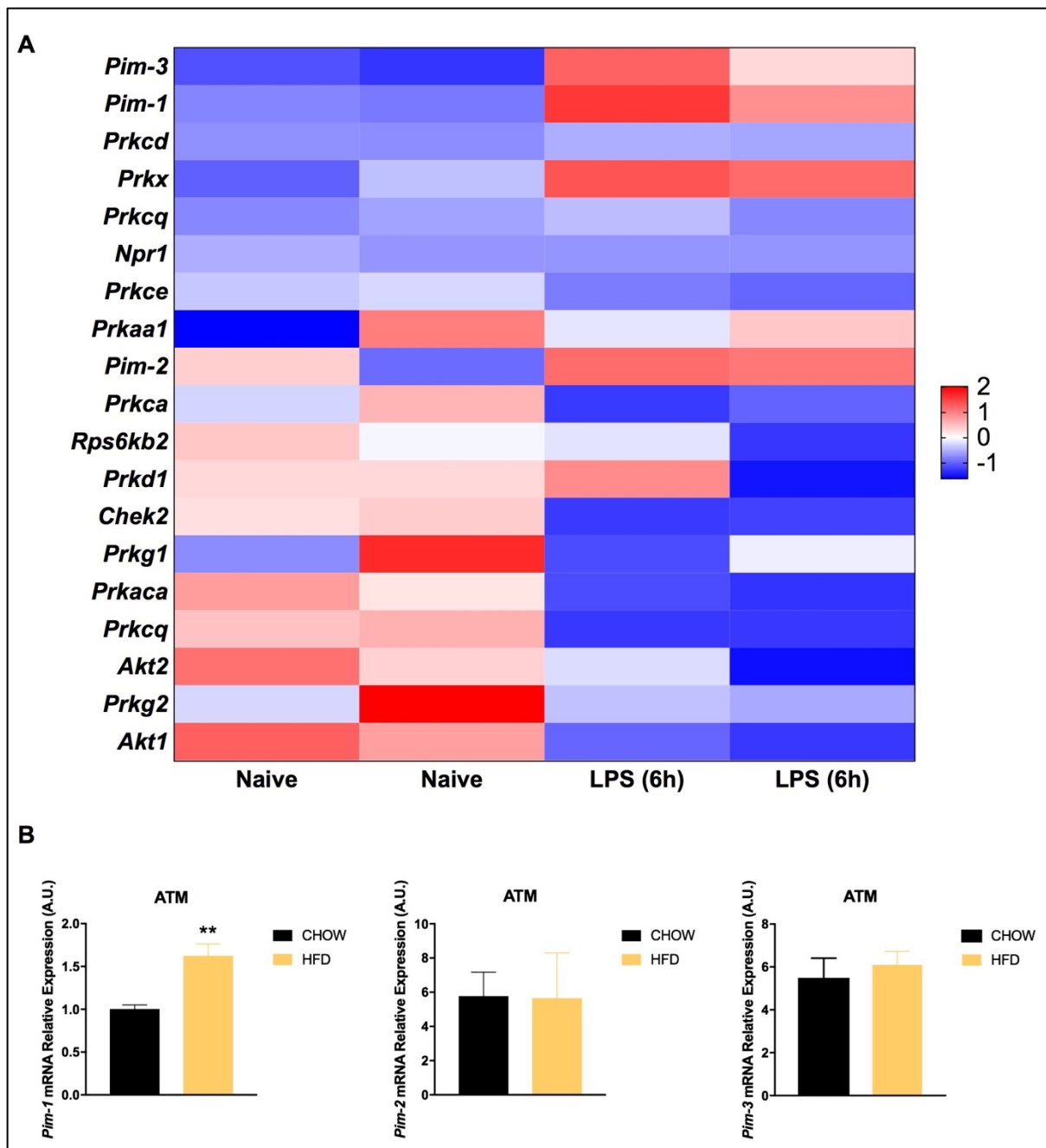


**Figure 4.5: *Pim-1* kinase activity and gene expression are upregulated in pro-inflammatory macrophages.** Heat map of the RNA sequencing data from naïve and LPS-treated macrophages show that *Pim-1* and *Pim-3* genes are significantly high in the pro-inflammatory as compared to naïve BMDMs (A). RTqPCR data show that only *Pim-1* mRNA expression is significantly higher in M1-sorted macrophages from VAT of HFD mice (B). B2M was used as the housekeeping gene in RTqPCR experiments, and results represent the average  $\pm$  SEM. Significance was determined using the Bonferroni-Dunn method, with \*\*  $p < 0.01$ .

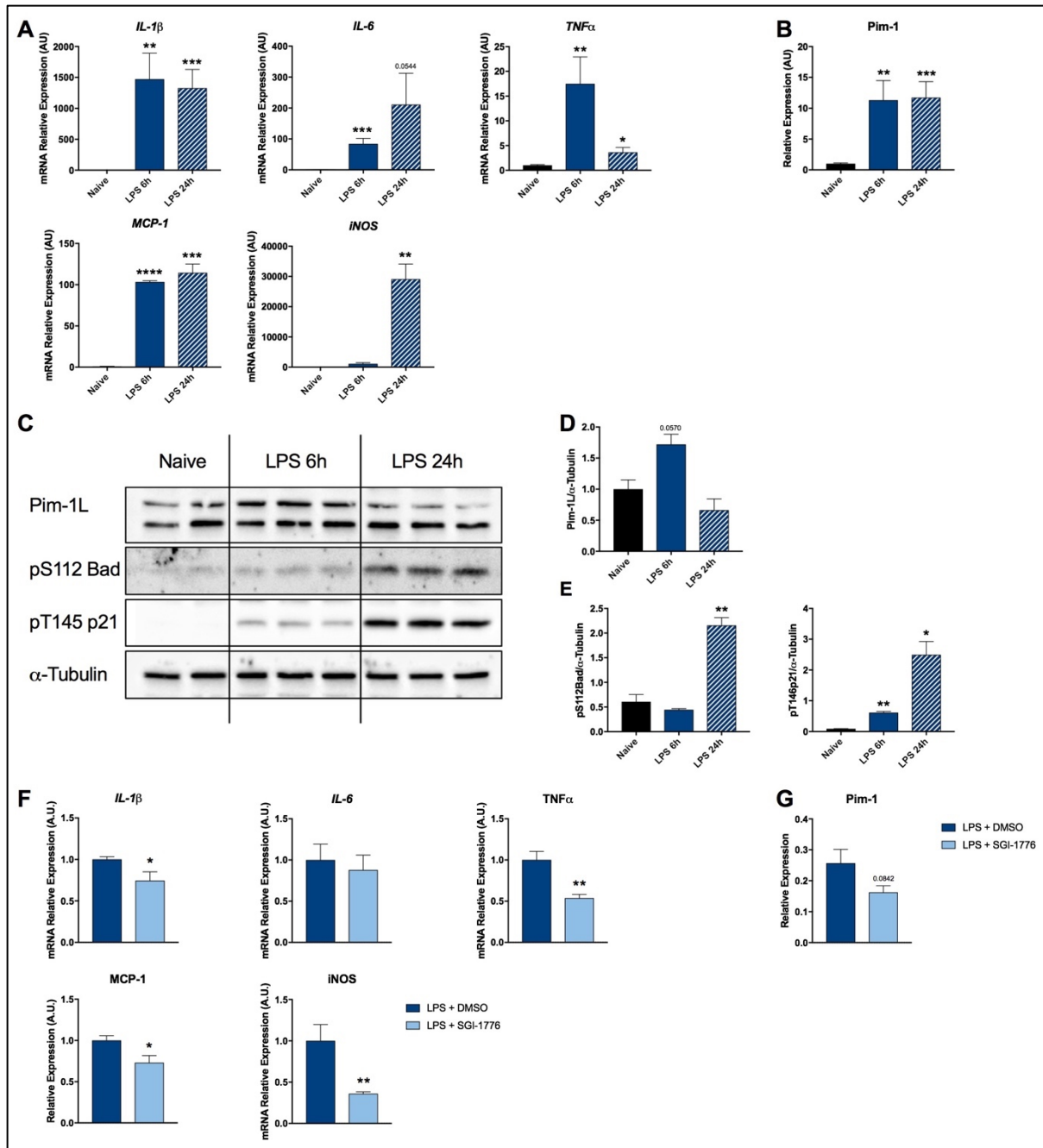


**Figure 4.6: Pim-1 expression is high in LPS-stimulated macrophages, and its inhibition decreases expression of pro-inflammatory markers.** RTqPCR was performed on naive and LPS-stimulated (6h, 24h) macrophages (A-B). Expression of pro-inflammatory markers IL-1 $\beta$ , IL-6, TNF $\alpha$ , and MCP-1 significantly increase in LPS-treated macrophages for 6h (A). Pim-1 expression is significantly high in LPS-treated pro-inflammatory macrophages (B). Western blot analysis of naïve and LPS-stimulated macrophages (6h, 24h) against Pim-1, pS112 Bad, and pT145 p21 (C). Pim-1 protein expression decreases in LPS-treated macrophages for 6h, while it increases back to normal levels in LPS-treated macrophages for 24h (D). pS112 Bad and pT145p21, Pim-1 phospho targets, significantly increase in LPS-treated macrophages (E). Pro-inflammatory macrophages that are LPS-stimulated for 6h were treated with DMSO or 0.25 $\mu$ M SGI-1776 for 24h. Pro-inflammatory markers IL-1 $\beta$ , TNF $\alpha$ , MCP-1, and iNOS gene expression significantly decrease upon inhibitor treatment (F). Pim-1 gene expression tends to decrease upon inhibitor treatment (G). RS9 and actin were used as housekeeping genes in RTqPCR experiments. 10 $\mu$ g of extracted protein was blotted, and  $\alpha$ -Tubulin was used as the loading control. Western blot quantification is done using ImageJ. Results represent the average  $\pm$  SEM. Significance was determined using the Bonferroni-Dunn method, with \*  $p < 0.05$ , \*\*  $p < 0.01$ , \*\*\*  $p < 0.001$ .

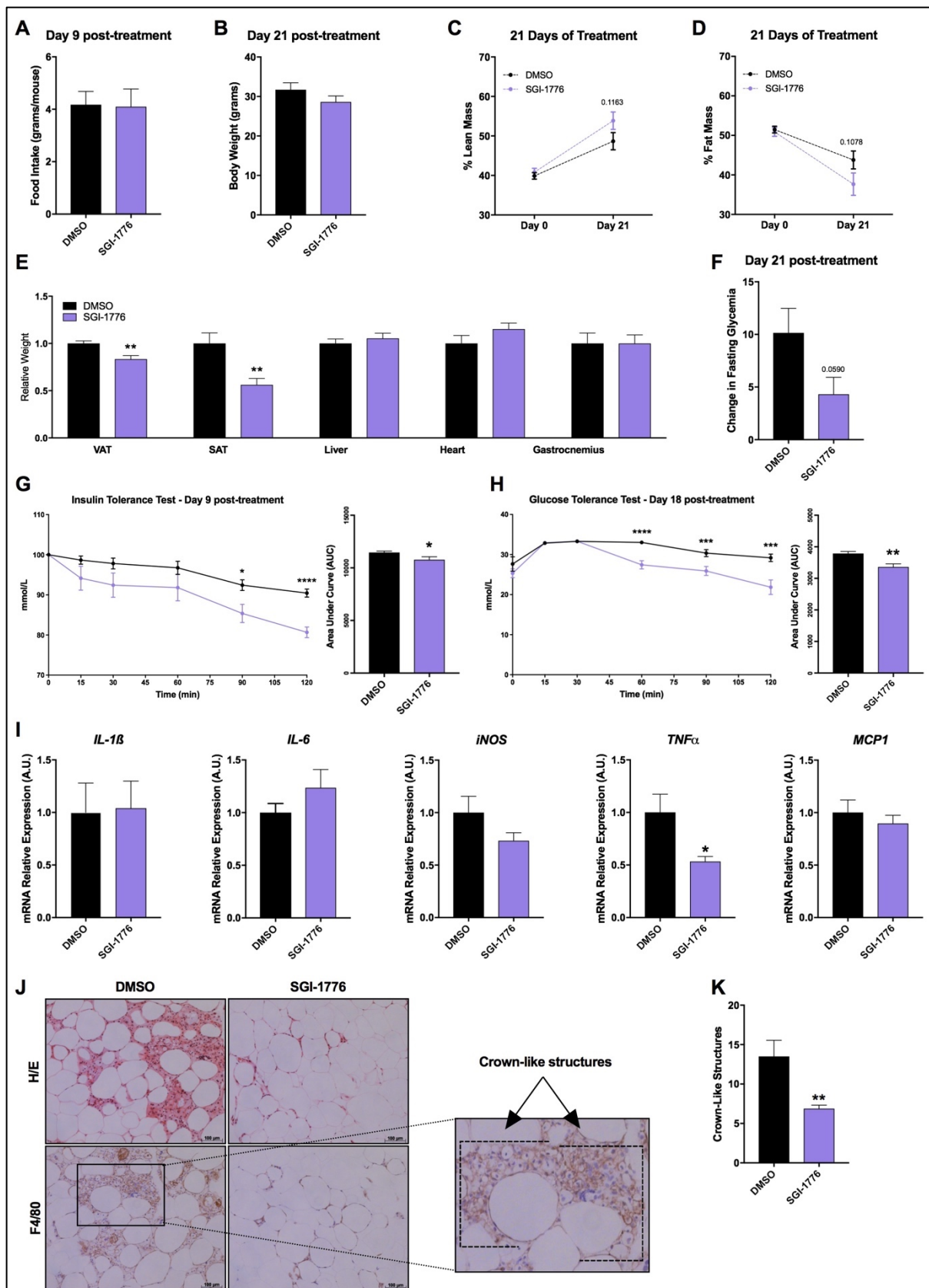


**Figure 4.7: *db/db* mice treated with SGI-1776 for 3 weeks have lower fat mass, increased glucose and insulin sensitivity, and decreased VAT inflammation.** Gavaged mice with DMSO or the Pim-1 inhibitor do not differ in food intake (A) or total body weight (B). However, their % lean mass increases more (C), and their % fat mass decreases more (D) as compared to the control group. The relative masses of VAT and SAT of treated mice significantly decrease in the treated group, while the relative masses of the liver, heart, and gastrocnemius do

not change between the groups (E). The % change in fasting glycemia before and after treatment tends to decrease in the treated group (F). Mice underwent an insulin tolerance test at day 9 post-treatment, in which the treated db/db mice became more insulin sensitive after 1h of insulin injection (G), and had a significant decrease in the Area Under Curve (H). Glucose tolerance test was done on both groups at day 18 post-treatment. Treated mice became more glucose tolerant after 30' of glucose injection (I), and had a significant decrease in the area under curve in SGI-1776-gavaged mice (J). RTqPCR was done on VAT of all mice, and gene expression of several pro-inflammatory macrophage markers was measured. iNOS, TNF $\alpha$ , and MCP-1 decrease in the SGI-1776-gavaged group, while IL-1 $\beta$  and IL-6 tend to increase (K). Cross-sections of the mVAT of control and treated mice were stained for H/E and F4/80, a macrophage marker (L). An example of a crown-like structure is depicted in the magnified image. For each mVAT sample, 20 images were taken and all crown-like structures were counted, and shown to be significantly decreased in mVAT of treated mice (M). Results represent the average  $\pm$  SEM, n = 8-9 mice. Significance was determined using the Bonferroni-Dunn method, with \* p < 0.05, \*\* p < 0.01, \*\*\* p < 0.001, \*\*\*\* p < 0.0001.

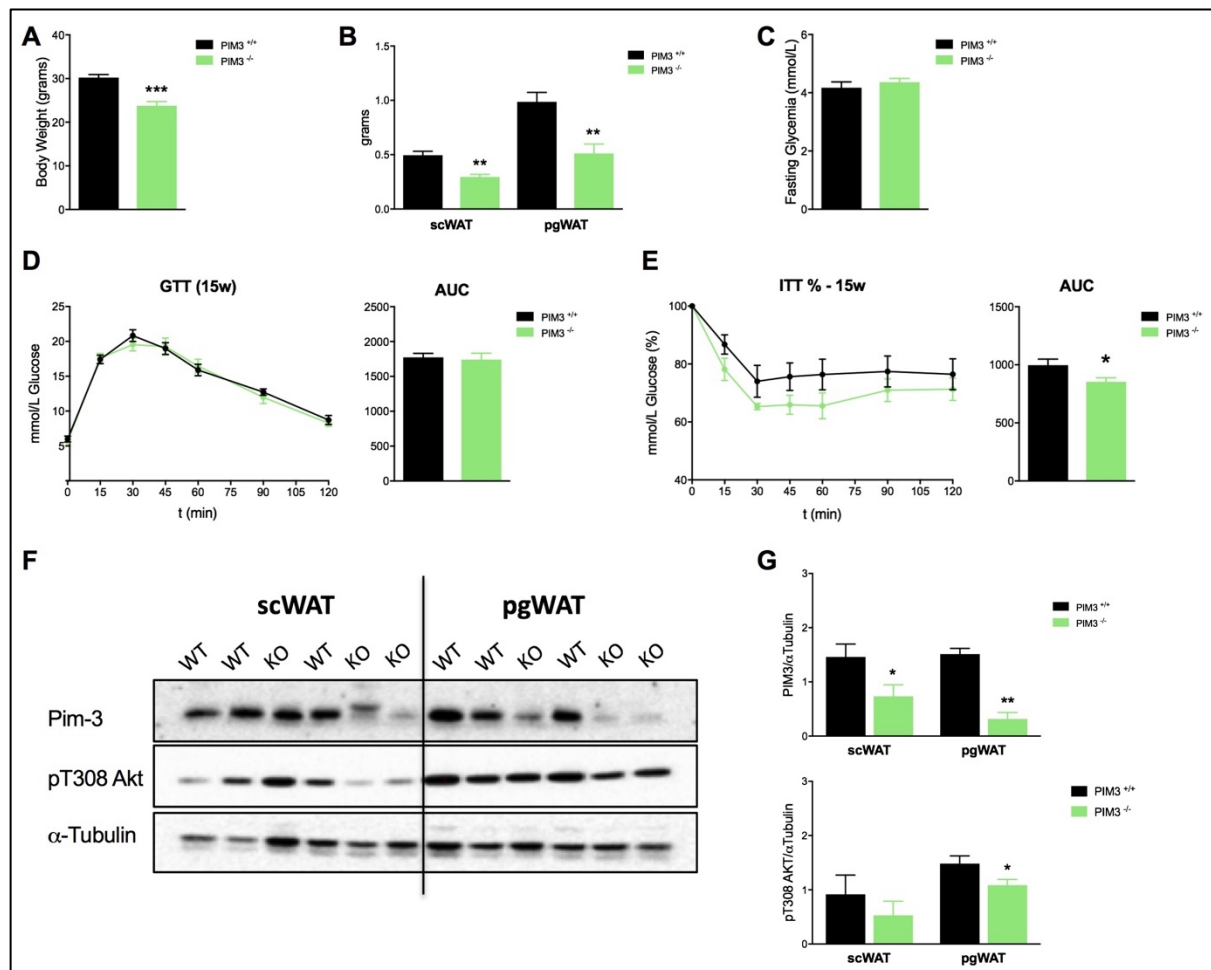


**Figure 4.8: *Pim3*<sup>-/-</sup> are leaner and insulin sensitive, with an insulin resistant WAT.** *Pim3*<sup>-/-</sup> mice are leaner (A), with less scWAT and pgWAT (B), but have no change in fasting glycemia (A). *Pim3*<sup>-/-</sup> mice have the same GTT profile as the *Pim3*<sup>+/+</sup> mice (D), but they are more insulin sensitive as seen from the ITT (E). Western blot analysis of different AT depots from wildtype and knock-out mice, against Pim-3 and pT308 Akt (F). Pim-3 protein expression is indeed decreased in the samples of the knockout mice, and pT308 AKT is significantly decreased in pgWAT of *Pim3*<sup>-/-</sup> mice, as compared to *Pim3*<sup>+/+</sup> (G). 10 $\mu$ g of extracted protein was blotted, and  $\alpha$ -Tubulin was used as the loading control. Western blot quantification was done using ImageJ. Results represent the average  $\pm$  SEM, n = 6-7 mice. Significance was determined using the unpaired t-test, with \* p < 0.05, \*\* p < 0.01, and \*\*\* p < 0.001.



## Chapter 5: CHK2

Another hit kinase from our kinome profiling experiment is Checkpoint kinase 2 (CHK2). The *CHK-2* gene was first identified in mammals by 5 groups (Blasina et al., 1999; Brown et al., 1999; Matsuoka, Huang, & Elledge, 1998; Tominaga et al., 1999). It is highly conserved throughout eukaryotic evolution. This is mainly due to the fact that CHK2 has fundamental roles in genome-surveillance pathways, coordinating cell-cycle progression with DNA repair and cell survival (Bartek, Falck, & Lukas, 2001).

At the protein level and as depicted in Figure 5.1, CHK2 consists of the SQ/TQ motif, the site of phosphorylation by ATM/ATR (ataxia-telangiectasia-mutated/ataxia-telangiectasia and Rad3-related) kinases (Kastan & Lim, 2000). Also, it has a forkhead-associated domain (FHA) that binds to phospho-threonine residues and is involved in protein-protein interactions (Durocher, Henckel, Fersht, & Jackson, 1999; Durocher et al., 2000; J. Li, Smith, & Walker, 1999; Z. Sun, Hsiao, Fay, & Stern, 1998). Additionally, CHK2 has a kinase domain at its carboxy-terminal, including the activation loop (Bartek et al., 2001).

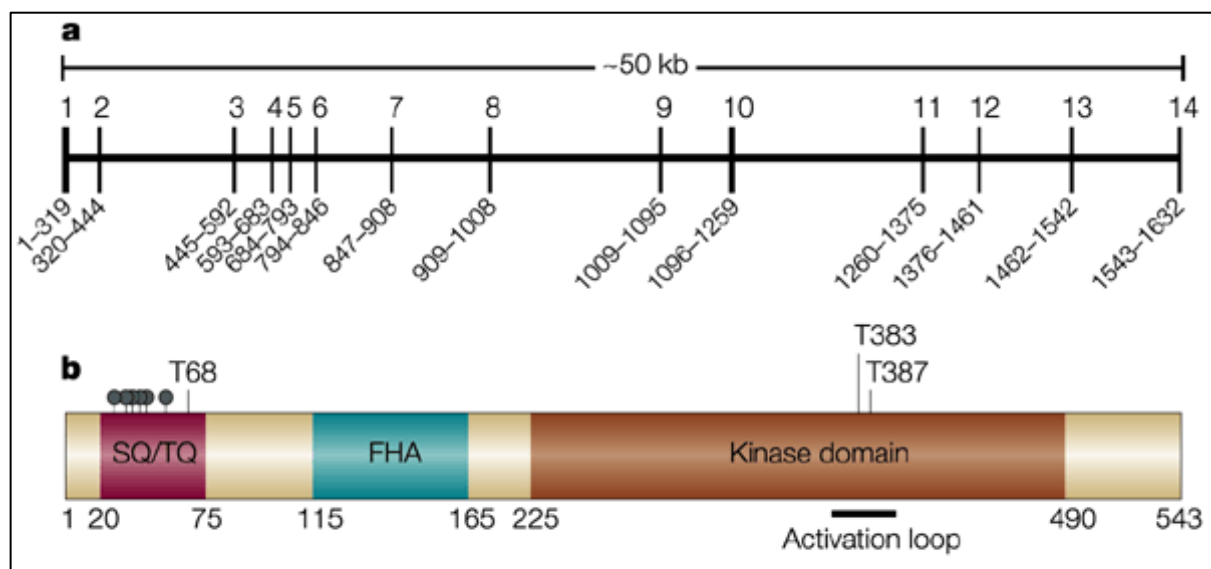


**Figure 5.1: Structures of the human *CHK2* gene and protein.** The *CHK2* gene localizes to chromosome 22q12.1, which spans approximately 50 kilobases (kb), and consists of 14 exons (black boxes). Numbers below the bars indicate the base-pair (bp) range of each exon. Highly homologous fragments of the gene that include exons 11 to 14 are found on chromosomes 2, 7, 10, 13, 15, 16, X and Y. b | Structure of the human CHK2 protein, with the

SQ/TQ-rich, forkhead-associated (FHA) and kinase domains shown in maroon, blue and brown, respectively. Pinheads indicate putative ATM/ATR phosphorylation sites in the SQ/TQ-rich region. *In vivo* phosphorylations of CHK2 on threonine 68 (by ATM/ATR) and threonines 383 and 387 in the activation loop (autocatalytic) are indicated (Bartek et al., 2001).

As illustrated in Figure 5.2, human CHK2 activation is carried out by the ATM kinase in response to double-stranded DNA strands, which phosphorylates CHK2 at Thr68 (Bartek et al., 2001). This first phosphorylation event is required for the autophosphorylation of CHK2 at Thr383 and Thr387 found in the activation loop of the kinase domain (C. H. Lee & Chung, 2001).

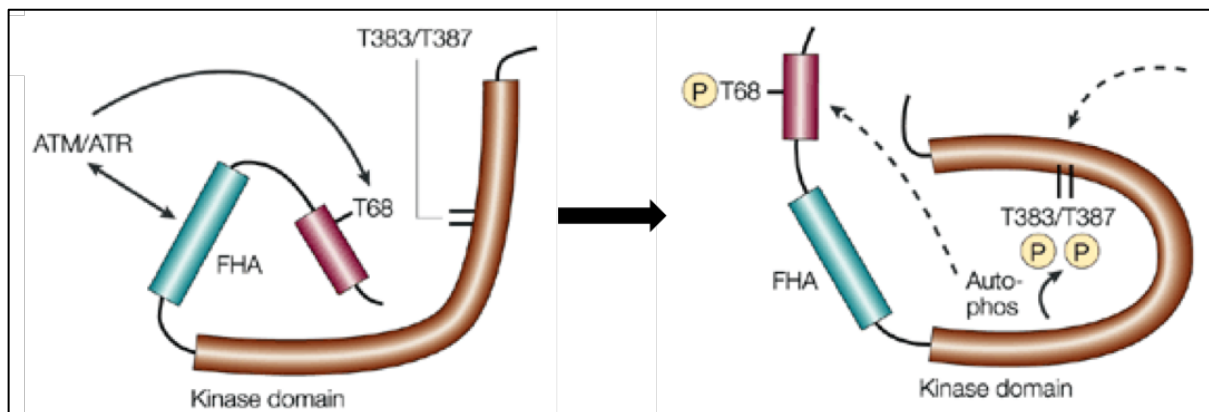


**Figure 5.2: CHK2 Activation.** In mammalian CHK2, forkhead-associated (FHA)-domain-mediated phosphorylation by ATM/ATR on threonine 68 (T68) probably induces conformational changes in the protein (dashed arrows). This makes threonines 383 and 387 in the activation loop accessible for autophosphorylation, an event required for full activation of Chk2. This model accounts for the observed sequential order of phosphorylations in which phosphorylation of T68 is required for subsequent phosphorylation of T383/387 (Bartek et al., 2001).

Defects in Chk2 contribute to the development of both hereditary and sporadic human cancers, and earmark this kinase as a candidate tumor suppressor (Bartek et al., 2001). However, it was never attributed to insulin resistance or adipose tissue defects. For this reason, we decided to study its effect on diabetic mice.

## 5.1. Results

---

### 5.1.1. CHEK-2 expression in VAT is upregulated in IR mouse models.

We focused on the CHK2 kinase, since it was not previously described to be involved in insulin resistance or diabetes. First, we checked its expression in the VAT of more than 80 human patients (Table 2.2). mRNA levels were not correlated to the different IR markers, i.e. body mass index (BMI), insulinemia, and glycemia (Figure 5.3 A-C).

We then quantified mRNA levels in two different mouse models of type II diabetes: mice under high-fat diet (HFD), and db/db mice. RTqPCR data showed that *CHEK-2* mRNA is significantly higher in VAT of db/db mice (Figure 5.3 D). Based on RNA sequencing data, *CHEK-2* gene expression was also significantly increased in the VAT of mice fed a HFD for 8 weeks and 20 weeks, as compared to mice under normal chow diet (CD) (Figure 5.3 E). Overall, these results prove that *CHEK-2* gene expression is increased in adipose tissue from mouse models of diabetes, suggesting that CHK2 participates in the development of insulin resistance.

### 5.1.2. CHK2 kinase activity is upregulated in human VAT of MOD patients.

As previously stated, one known readout for the kinase activity of CHK2 is its autophosphorylation at the T308 residue. Accordingly, CHK2 kinase activity significantly increases in hVAT of MOD patients (Figure 5.4 A-B).

### 5.1.3. CHK2 inhibition improves insulin sensitivity in diabetic mice.

We next wanted to test the clinical relevance of our findings by treating the db/db diabetic mouse model with the CCT241533 HCl CHK2 inhibitor. After 2 weeks of treatment, we did not observe changes in the body weight (Figure 5.5 A) or in the relative weight of different tissues (Figure 5.5 B). The principle finding was that the fasting glycemia of the db/db mice treated with the CHK2 inhibitor was significantly reduced after 2 weeks of treatment, when compared to the vehicle-treated group (Figure 5.5 C). Moreover, CCT241533 HCl treatment resulted in enhanced insulin sensitivity and glucose disposal, as measured by insulin and glucose tolerance tests (Figure 5.5 D-E).

## 5.2. Discussion

---

Another kinase of our interest is the Checkpoint Kinase 2 (CHK2). Even though CHK2 has never been directly correlated to insulin resistance in adipose tissue, other checkpoint regulators, such as p21 (also known as CDKN1A: Cyclin-dependent kinase inhibitor 1A), MAD2 (mitotic arrest deficient 2) and BUBR1 (also known as MAD3: mitotic arrest deficient 3), are proven to directly control insulin signaling and metabolic homeostasis (Choi, Zhang, Xing, & Yu, 2016), linking the guardians of chromosome stability to nutrient metabolism.

CHK2 has always been studied as an important player in cell-cycle progression, DNA repair, and cell survival, downstream from the ATM signaling network (Ronco, Martin, Demange, & Benhida, 2017; Zannini, Delia, & Buscemi, 2014), as well as a tumor suppressor (Bartek et al., 2001; Ronco et al., 2017). DNA damage triggers the activation of ATM that phosphorylates and activates CHK2, which in turn leads to the accumulation of phospho p53 and eventually G<sub>1</sub> arrest (Chen & Sanchez, 2004; Melchionna, Chen, Blasina, & McGowan, 2000).

DNA damage, the main trigger behind CHK2 activation, has been implicated in the early onset of obesity in mice under HFD, inducing p53 activation, and affecting insulin signaling, resulting in adipose tissue inflammation and adipocyte insulin resistance (Vergoni et al., 2016). Studies have shown that diabetes induces DNA damage, and not vice versa. Maternal diabetes triggers DNA damage, CHK2 activation, and phospho p53 accumulation in embryos, through oxidative stress (Dong et al., 2015).

Another study on oxidative stress signaling and diabetes elucidates the implication of CHK2 on methylglyoxal-induced cell-cycle arrest (Kani et al., 2007). Under hyperglycemic conditions, Methylglyoxal (MG) formation is known to increase, provoking oxidative stress signaling. It is implicated in the development of diabetic complications (Beisswenger et al., 2001; McLellan, Thornalley, Benn, & Sonksen, 1994). MG elicited DNA damage, and was proved to activate ATM and CHK2, leading to G<sub>2</sub>/M cell cycle arrest (Kani et al., 2007).

Yang and Kastan provided evidence that the kinase activity of the ATM protein is also activated by insulin (Yang & Kastan, 2000). Furthermore, it is upregulated in the liver lysates of obese *foz/foz* mice, accompanied by hepatic inflammation (Arfianti et al., 2016).

Since ATM is activated by insulin on one hand, and phosphorylates and activates CHK2 at T68 on another hand (C. H. Lee & Chung, 2001), this is a further link between insulin resistance and CHK2 kinase activity, shown to be higher in MOD VAT samples (Figure 5.2).

### 5.3. Figures

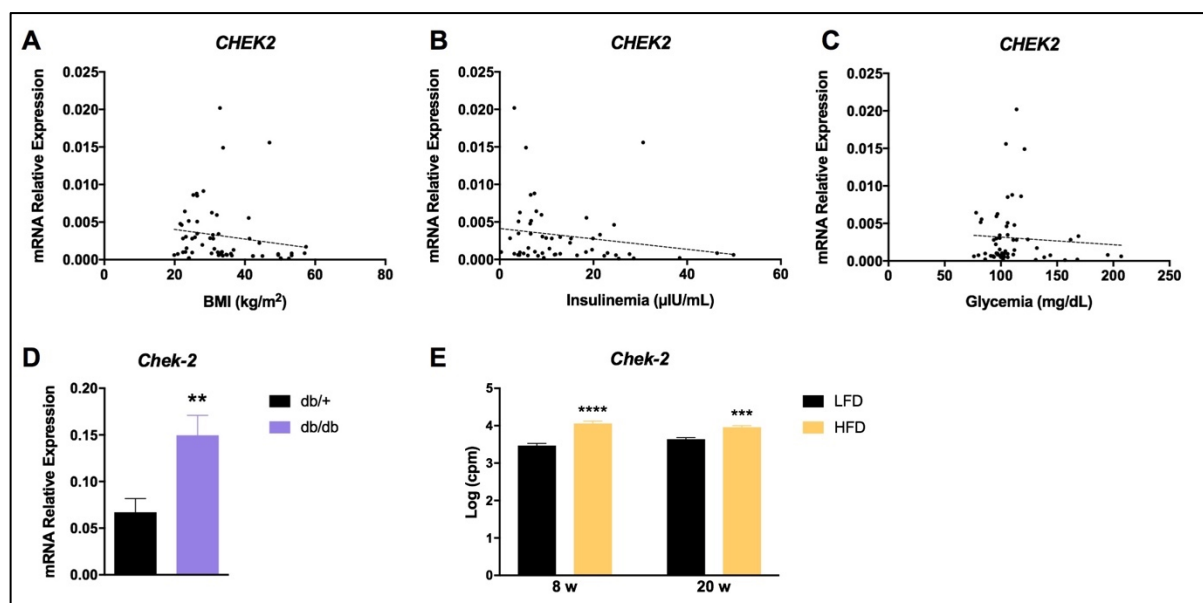


**Figure 5.3: *CHEK2* gene expression does not correlate to IR markers in hVAT, but is upregulated in mVAT of 2 IR mouse models.** RTqPCR was performed on visceral adipose tissue samples taken from more than 80 lean, obese, and morbid obese healthy and diabetic patients. *CHEK2* relative gene expression does not correlate with BMI (A), insulinemia (B), and glycemia (C). *Chek2* expression was also checked in visceral adipose tissue from 2 mouse models of insulin resistance (D-E). *Chek2* gene expression significantly increases in VAT of db/db mice (D). RNA sequencing data of VAT from mice under LFD or HFD (8 or 20 weeks) show that *Chek2* expression was significantly increased in VAT of mice under HFD (E). RS9 and 18S were used as a housekeeping genes. Significance of the correlation data panels A-C was determined using the Pearson correlation coefficients, with \*  $p < 0.05$ . Results of panels D-E represent the average  $\pm$  SEM.  $n = 5-7$  mice. Significance was determined using the Bonferroni-Dunn method, with \*  $p < 0.05$ , \*\*  $p < 0.01$ , \*\*\*  $p < 0.001$ , \*\*\*\*  $p < 0.0001$ .

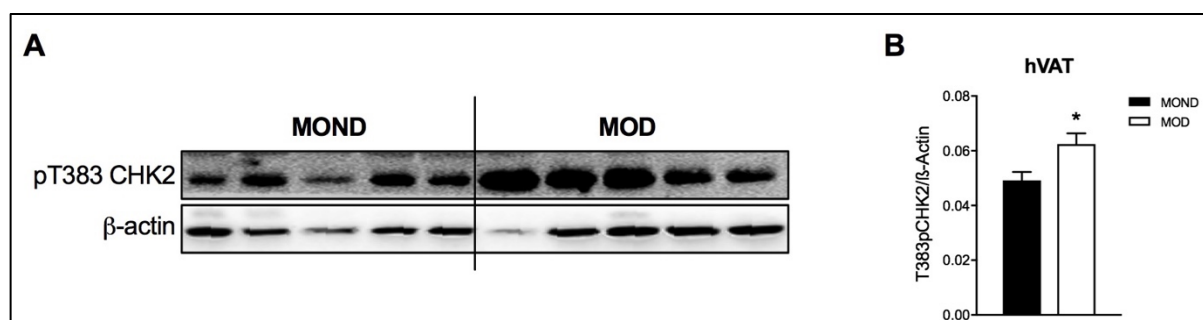


**Figure 5.4: *CHK2* kinase activity is upregulated in hVAT.** Western blot analysis of VAT from MOND and MOD patients, against pT383 *CHK2* (A). *CHK2* phosphorylation at Thr 308 is increased in the samples of the diabetic insulin resistant, as compared to the non-diabetic insulin sensitive patients (B). 10μg of extracted protein was blotted, and  $\beta$ -actin was used as the loading control. Western blot quantification was done using ImageJ. Results represent the average  $\pm$  SEM,  $n = 10$ . Significance was determined using the unpaired t-test, with \*  $p < 0.05$ .

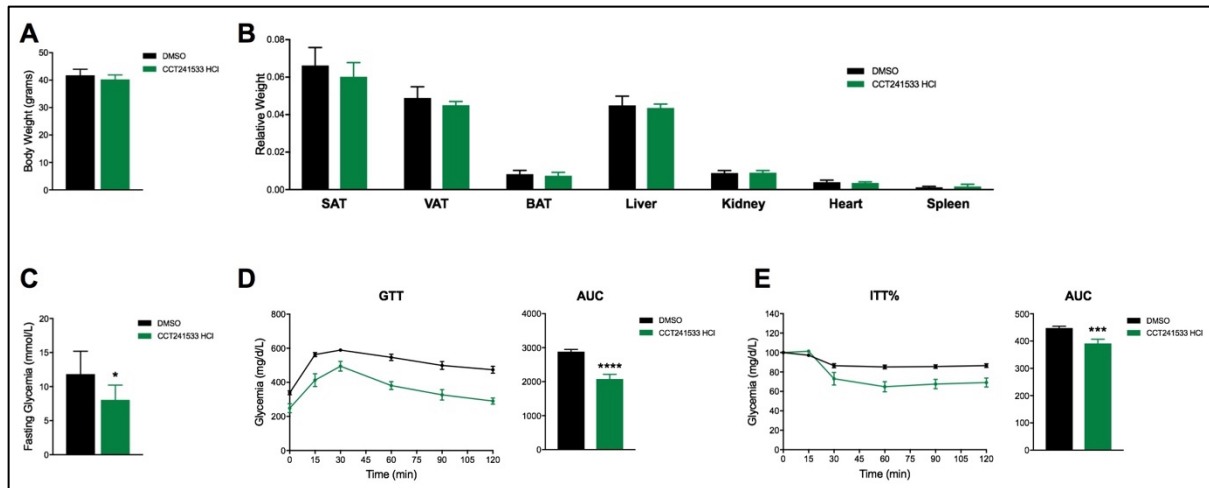


**Figure 5: *db/db* mice treated with CCT241533 HCl for 2 weeks have lower fasting glycemia, and increased glucose and insulin sensitivity.** Gavaged mice with DMSO or the Chk2 inhibitor do not differ in total body weight (A), or relative weight of their tissues (B). However, their fasting glycemia decreases significantly in the treated group (C). Glucose tolerance test was done on both groups post-treatment. Treated mice became more glucose tolerant and had a significant decrease in the area under curve (D). Mice underwent an insulin tolerance test post-treatment, in which the treated *db/db* mice became more insulin sensitive and had a significant decrease in the Area Under Curve (E). Results represent the average  $\pm$  SEM,  $n = 7-9$  mice. Significance was determined using the Bonferroni-Dunn method, with \*  $p < 0.05$ , \*\*  $p < 0.01$ , \*\*\*  $p < 0.001$ , \*\*\*\*  $p < 0.0001$ .



## Chapter 6: CDK10

Cyclin-dependent kinases (CDKs) form a family of heterodimeric Serine/Threonine kinases that play central roles in the regulation of cell cycle progression (Hanks, 1987). Depending on the CDK-Cyclin combination, complexes have had consistent functional specialization during evolution. This led to the division of the CDK family into cell-cycle-related subfamilies (Figure 6.1) and transcriptional subfamilies (Aguilar & Fajas, 2010; Malumbres, 2014; Murray, 2004). CDK2, CDK4 and CDK6 are known to orchestrate the cell cycle progression from the G<sub>1</sub> phase to the S phase (Malumbres & Barbacid, 2005). These same CDK/Cyclin complexes, in addition to newly discovered ones, have been implicated in transcriptional regulation, splicing patterns, and mRNA processing. Those are generally known as the atypical CDKs, such as CDK2, CDK4, CDK7, CDK8, CDK9, CDK11, and CKD20 (Loyer, Trembley, Katona, Kidd, & Lahti, 2005; Malumbres, 2014).

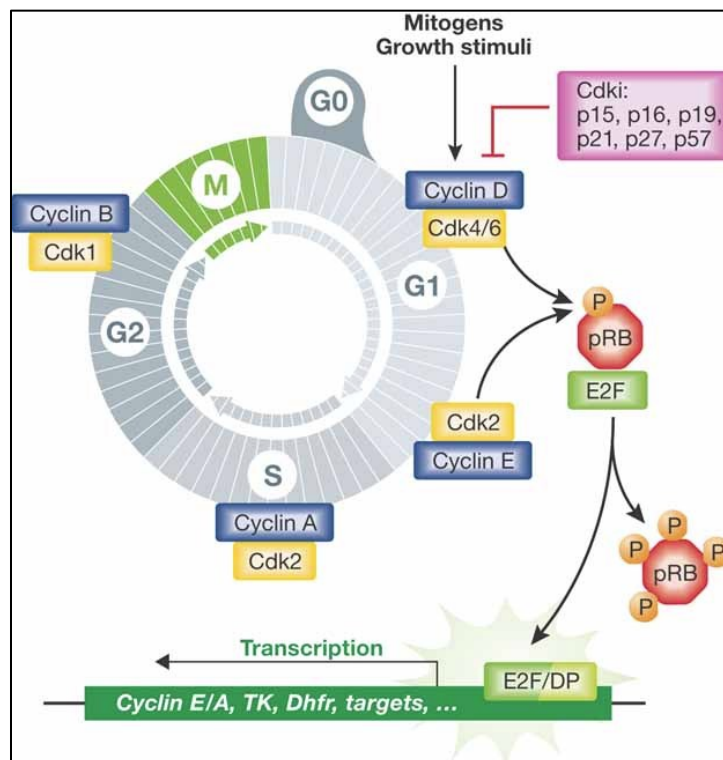
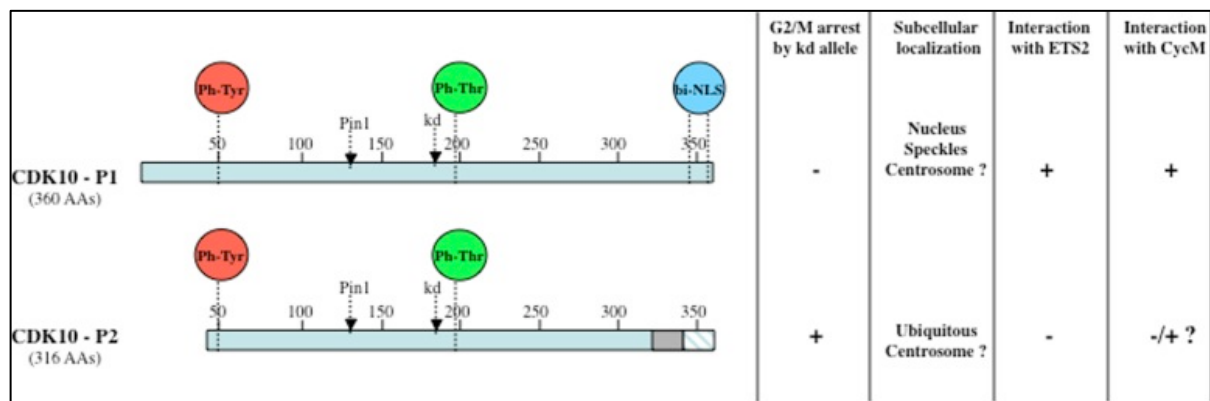


Figure 6.1: Molecular Regulation of the Cycle by CDK-Cyclin Complexes. (Aguilar & Fajas, 2010)

Many of these proteins play vital roles in metabolism, cardiovascular function, or neuron biology (Malumbres, 2011). Our laboratory and others have shown that members of the CDK family, such as CDK4 and CDK9, respond to nutritional status and are also key factors in the regulation of metabolism independently from cell proliferation, and that their activities are altered especially under pathological conditions contributing to obesity and diabetes (Abella et al., 2005; Annicotte et al., 2009; Denechaud, Lopez-Mejia, & Fajas, 2016; Fajas, Blanchet, & Annicotte, 2010; Lagarrigue et al., 2016; Rane et al., 1999).

*CDK10* is found on chromosome 16, in a region that is highly altered in breast and prostate cancers (Crawford et al., 1999; S. Li et al., 1995). *CDK10* has 2 isoforms, both containing the regulatory domain and the activation loop. Only the longer isoform has also a nuclear localization sequence (NLS) (Figure 6.2).



**Figure 6.2: Schematic Diagram and Properties of CDK10 Isoforms.** (Guen, Gamble, Lees, & Colas, 2017)

It has been shown that *CDK10* is upregulated in some cancers, such as lung adenocarcinoma, follicular lymphoma, and seminoma, while it is downregulated in others, such as breast, hepatocellular carcinoma, keloid skin, and biliary tract cancer (Iorns et al., 2008; Singhal et al., 2003). *CDK10* has been shown to participate in different processes and functions such as cell cycle progression, proliferation, migration, colony formation, and anchorage-independent growth (Husson et al., 2002; Y. Liu et al., 2012; Zhong et al., 2012). CDKs, as their name suggests, need a Cyclin partner. The only partner described for *CDK10* is Cyclin M. Murine *Cdk10* shows high similarity to the human isoform (Guen et al., 2013). However, its functions and/or binding partners are still unknown.

Based on our kinome profiling, we decided to study the role of *CDK10* in adipose tissue and global homeostasis, by generating adipose tissue-specific *CDK10* knockout mice.

## 6.1. Results

---

### 6.1.1. CDK10 and CycM proteins are highly expressed in metabolic tissues, and their mRNA levels are higher upon fasting and HFD.

Upon screening different tissues from fasted wild type mice, CDK10 and CycM protein expressions were higher in metabolically active tissues, i.e. BAT, muscle and heart for CDK10, while BAT, heart, kidney, and liver for CycM (Figure 6.3 A). Another screening method was checking mRNA levels of those two genes. Results further emphasized the previous protein expression screening, in which CDK10 and CycM mRNA levels were shown to be highly expressed in the muscle (quadriceps), liver and BAT. Surprisingly, we noticed that opposite to protein, their mRNA levels were the highest in the brain tissue and then in the perigonadal WAT (pgWAT) (Figure 6.3 B). These results suggest that both CDK10 and CycM must play a role in metabolism and thermogenesis.

### 6.1.2. CDK10 and CycM exhibit a role in thermogenic activity of mouse BAT.

Next, we checked the mRNA levels of CDK10 and CycM under different metabolic conditions. After 24h of fasting, both mRNA levels significantly increased, contrary to UCP1 mRNA, which was used as a thermogenic activity marker (Figure 6.4 A). However, when testing samples from wild type mice under high fat diet (HFD), CycM mRNA levels were significantly higher than the control ones, same as UCP1 level, contrary to CDK10 mRNA levels, which exhibited no difference (Figure 6.4 B). Wild type mice were put in an acute cold exposure (24h) and another group in a chronic cold exposure (21days). We noticed that CDK10 mRNA levels tend to increase respectively, however with no major significance. On the other hand, CycM levels significantly increased during acute cold exposure, and even reached higher levels in chronic cold exposure conditions (Figure 6.4 C). Another situation where thermogenesis is highly activated due to cold exposure is at the early developmental stages of mice. We found that CDK10 mRNA levels is the lowest in a 12h-old pup, after which this increases until it doubles in a 21 days-old pup. CycM mRNA has a different profile. It is the lowest in an 18-days old fetus. It steadily increases until it doubles after 21 days of birth (Figure 6.4 D). All these data show that CDK10 is inversely correlated to UCP1, thus might be a negative regulator of thermogenesis.

### **6.1.3. CDK10 and CycM mRNA might play a role in the $\beta$ 3 adrenergic pathway in pBAT.**

Moving into a cellular system, our aim was to check the profiles of CDK10 and CycM during cAMP and noradrenaline time-course stimulation, which are activators of the  $\beta$ 3-adrenergic pathway. Under both stimulations, CDK10 and CycM mRNA profiles seemed to be opposite to UCP1. They reached their lowest values after 6h of stimulation when UCP1 peaked, after which all mRNA levels were recuperated to control values (Figure 6.5 A-B). This nicely fits with the data from Figure 6.4.

### **6.1.4. No difference in body weight, fasting glycemia and relative weight of tissues is observed.**

During 8 months, we kept track of the body weight, fasting glycemia, %lean mass, and % fat mass in both groups. No difference was observed at any timepoint (Figure 6.6A-D). Upon sacrifice, relative weight of different tissues was calculated, and also no difference was detected (Figure 6.6 E).

### **6.1.5. CDK10 deficiency in adipose tissue induces insulin resistance in mice.**

CDK10 AdipoQCreERT2 (KO) mice were generated, and metabolically phenotyped as compared to CDK10<sup>fl<sub>ox</sub>fl<sub>ox</sub></sup> mice. Glucose Tolerance Test (GTT) was performed at different ages. KO mice had no differences. However, at the age of 21 weeks, 11 weeks after adipose tissue knock-out induction through tamoxifen gavage, Adipose-tissue CDK10 KO mice were significantly glucose intolerant (Figure 6.7 A). In contrast, adipose tissue knockout mice exhibited an insulin resistance, especially at the ages of 25 weeks (14 weeks after tamoxifen gavage) and 33 weeks (22 weeks after gavage) (Figure 6.7B).

### **6.1.6. CDK10 floxed mice and CDK10 AdipoQCreERT2 mice manifest no difference in indirect calorimetry.**

To further metabolically phenotype those mice, we measured their indirect calorimetry. Figure 6.8 A shows no difference in respiration, denoted by the RER, the ratio of O<sub>2</sub> volume to CO<sub>2</sub>. Similarly, heat dissipated by each mouse during experimentation did not differ between groups (Figure 6.8 B). Also, the total movement of each mouse and the ambulatory movement, to fetch food, also manifested no difference among the groups (Figure 6.8 C-D).

### **6.1.7. No difference is observed in expression of BAT markers.**

CDK10 KO was validated in Figure 6.9 A. However, no difference is observed in CycM (Figure 6.9 A) and several BAT markers, i.e. UCP1, PGC1 $\alpha$ , PPAR $\alpha$ , and CPT1 $\beta$  (Figure 6.9 B).

## 6.2. Discussion

---

Cyclin-dependent kinases (CDKs) mainly regulate cell cycle progression (Hanks, 1987). In our laboratory, we have shown that members of the CDK family respond to nutritional status and greatly regulate metabolism independently from cell proliferation, and that their activities are altered especially under pathological conditions contributing to obesity and diabetes (Abella et al., 2005; Annicotte et al., 2009; Denechaud et al., 2016; Lagarrigue et al., 2016).

As shown by our data, brown adipose tissue has the highest expression as compared to other adipose depots. Given that CDK10 is differentially expressed in brown adipose compared to white adipose depots, we hypothesize that CDK10 could play a role in thermogenesis in this key metabolic tissue.

It is well-established that in order to maintain body temperature, active BAT produces heat through non-shivering thermogenesis. This happens mainly through the key component UCP1 (Enerback et al., 1997; Foster & Frydman, 1978). Adaptive thermogenic activity of BAT can be inhibited or activated in response to many factors, including developmental stages, environmental conditions, and dietary intake (Loyd & Obici, 2014; Townsend & Tseng, 2014; S. Wang et al., 2015). Consistently, activation of BAT by cold-exposure increased whole-body energy expenditure, glucose homeostasis and insulin sensitivity in humans (Saito et al., 2009; van Marken Lichtenbelt et al., 2009). During cold exposure, plasma insulin levels are relatively low, and glucose tolerance increases. This is mainly due to the high glucose uptake of the activated BAT (Orava et al., 2011).

Since CDK10 was shown to be expressed in highly metabolic tissues (Figure 6.3 A-B), we focused on its effect in BAT biology. Based on the literature, we hypothesized that since CDK10 is highly expressed in the BAT, the best way to target and study its function is by knocking it out specifically in the adipose tissue. We used the AdipoQCreERT2 model to knock out CDK10 only in adipose tissue, through daily tamoxifen gavaging in 11 weeks old mice (Jeffery et al., 2014). We expected that this tissue-specific CDK10 knockout will have a striking phenotype in one or more of the following aspects: metabolic activity, non-shivering thermogenesis, indirect calorimetry, etc. However, as shown previously in the Results section, these mice did not show a striking phenotype. They do not show any difference in body weight, lean mass, or fat mass. They also did not exhibit any difference in their total or ambulatory movement. This further proves the fact that they do not

exhibit differences in energy expenditure under CHOW diet, and/or normal housing conditions (22°C). Furthermore, the metabolic phenotypes outlined by the ITT and GTT do not seem to correlate. As previously stated in our results, glucose intolerance and insulin resistance inconsistently change with age. At 25 weeks of age, 14 weeks after gavage, CDK10 KO mice exhibited insulin resistance, but no effect on glucose tolerance, similarly to the phenotype of the AS160 deficient mice (H. Y. Wang et al., 2013). This could be explained by problems in the glucose secretion mechanism. However, we were not able to have a strong phenotype with our mice. This was a problematic approach towards analyzing and understanding the overall role of CDK10 in adipose tissue.

For these reasons, we decided not to dwell further on this project and focus on other novel kinases in the adipose tissue, as revealed in the previous chapters.

### 6.3. Figures

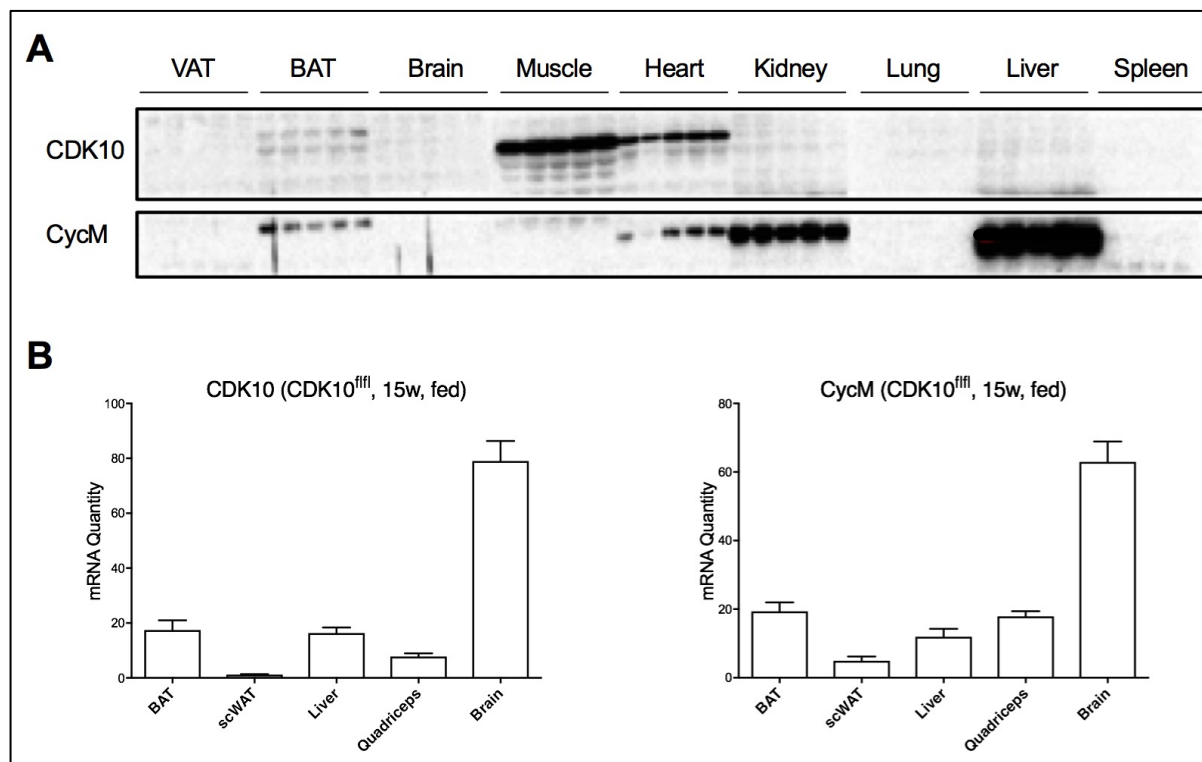


**Figure 6.3: CDK10 and CycM proteins and mRNA are highly expressed in metabolic tissues.** Western blot analysis of different tissue lysates from CDK10<sup>fl/fl</sup> mice show higher protein levels of CDK10 in muscle and heart, while CycM in liver and kidney (A). RTqPCR was performed on different tissue samples from CDK10<sup>fl/fl</sup>, showing that mRNA levels of CDK10 and CycM are highest in the brain, and then in metabolic tissue, BAT, Liver and quadriceps (B). Results represent the average  $\pm$  SEM, n = 5 mice.

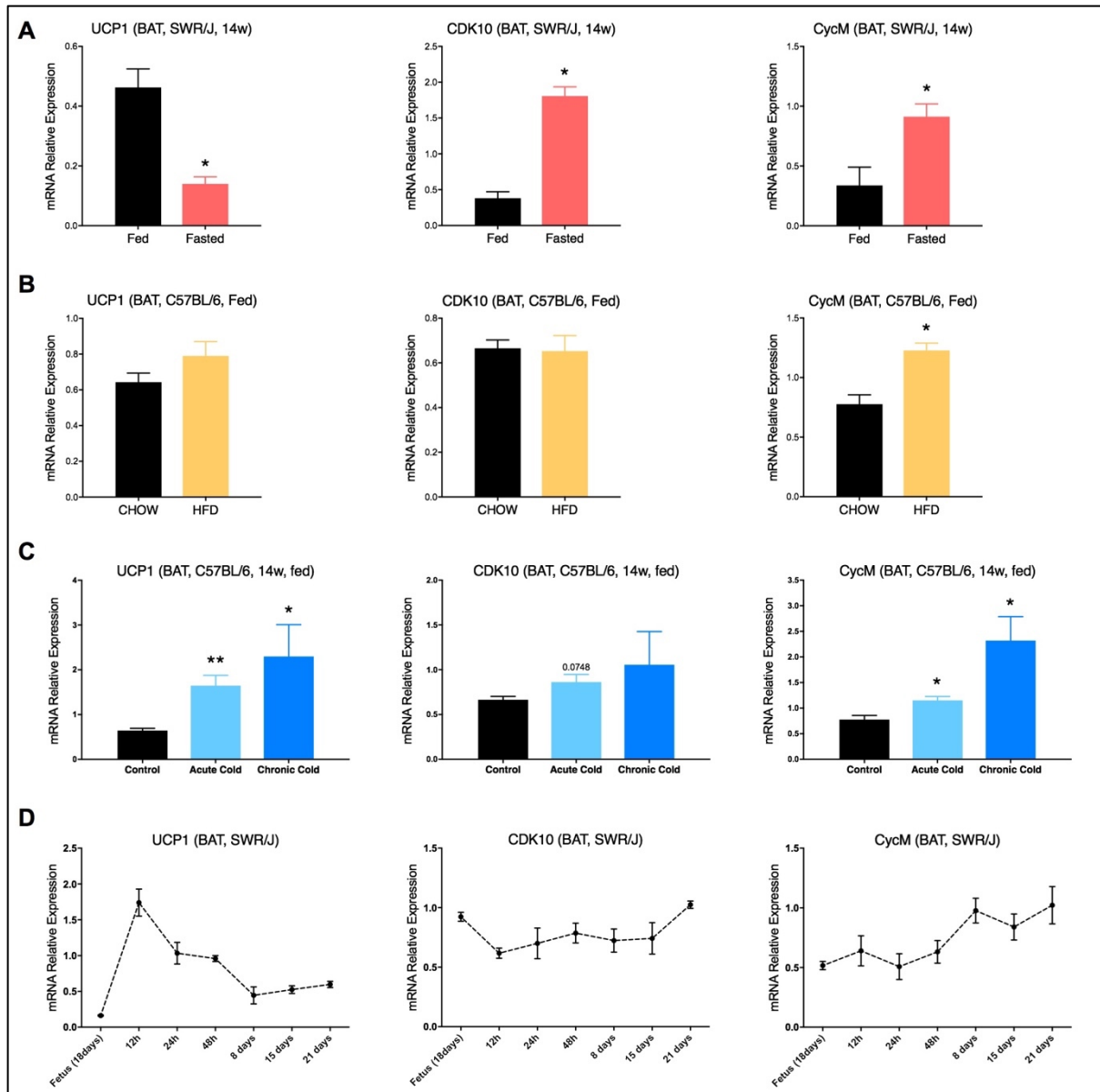


**Figure 6.4: *CDK10* and *CycM* exhibit a role in mouse BAT.** RTqPCR was performed on BAT samples from different mouse models under different metabolic conditions (A-D). UCP-1 mRNA expression significantly decreases in BAT of fasted SWR/J mice, while CDK10 and CycM significantly increase (A). CycM mRNA expression significantly increases in BAT of C57BL/6 mice, while UCP1 and CDK10 do not change (B). UCP1 and CycM significantly increase in BAT of C57BL/6 mice in acute and chronic cold exposure, and CDK10 tends to increase in both conditions (C). BAT samples of SWJ/R mice at different developmental stages were checked for UCP1, CDK10 and CycM gene expression. UCP1 peaks at 12h postpartum. CDK10 expression does not change, but CycM increases as fetus grows (D). RS9 was used as a housekeeping gene. Results represent the average  $\pm$  SEM,  $n = 5$  mice. Significance was determined using the Bonferroni-Dunn method, with \*  $p < 0.05$  and \*\*  $p < 0.01$ .

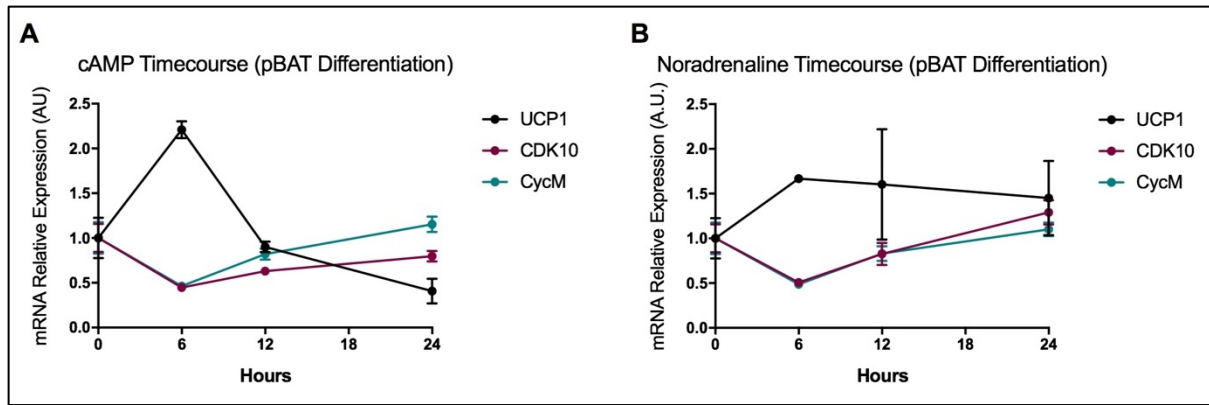


**Figure 6.5: *CDK10* and *CycM* might play a role in the  $\beta_3$  adrenergic pathway.** pBAT cells were stimulated with cAMP or noradrenaline, and mRNA levels of UCP1, CDK10 and CycM were checked every 6h for 24h. UCP1 peaks at 6h post-stimulation, while CDK10 and CycM reach their lowest expression throughout the timecourse. UCP1 expression is the least at the end, while CDK10 and CycM reach their highest expression (A-B). RS9 was used as a housekeeping gene. Results represent the average  $\pm$  SEM, n = 5 mice.

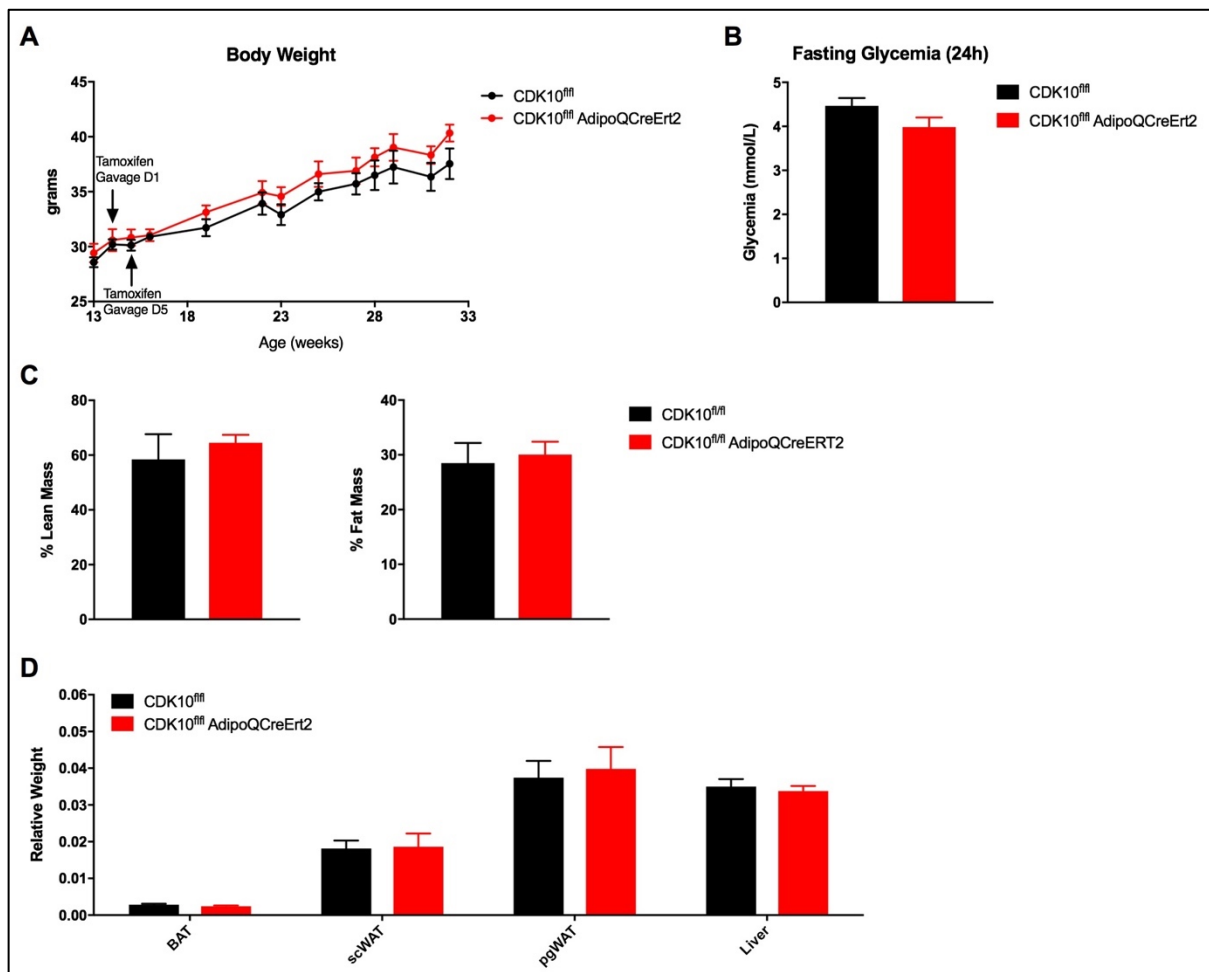


**Figure 6.6: *CDK10<sup>fl/fl</sup> AdipoQCreERT2* do not differ in body weight or fasting glycemia.** CDK10 ATKO mice have same body weight (A), fasting glycemia (B), % lean mass, % fat mass (C), and relative weight of different metabolic tissues: scWAT, pgWAT, BAT, and liver (D). Results represent the average  $\pm$  SEM, n = 8 mice. Significance was determined using the unpaired t-test, with \* p < 0.05.

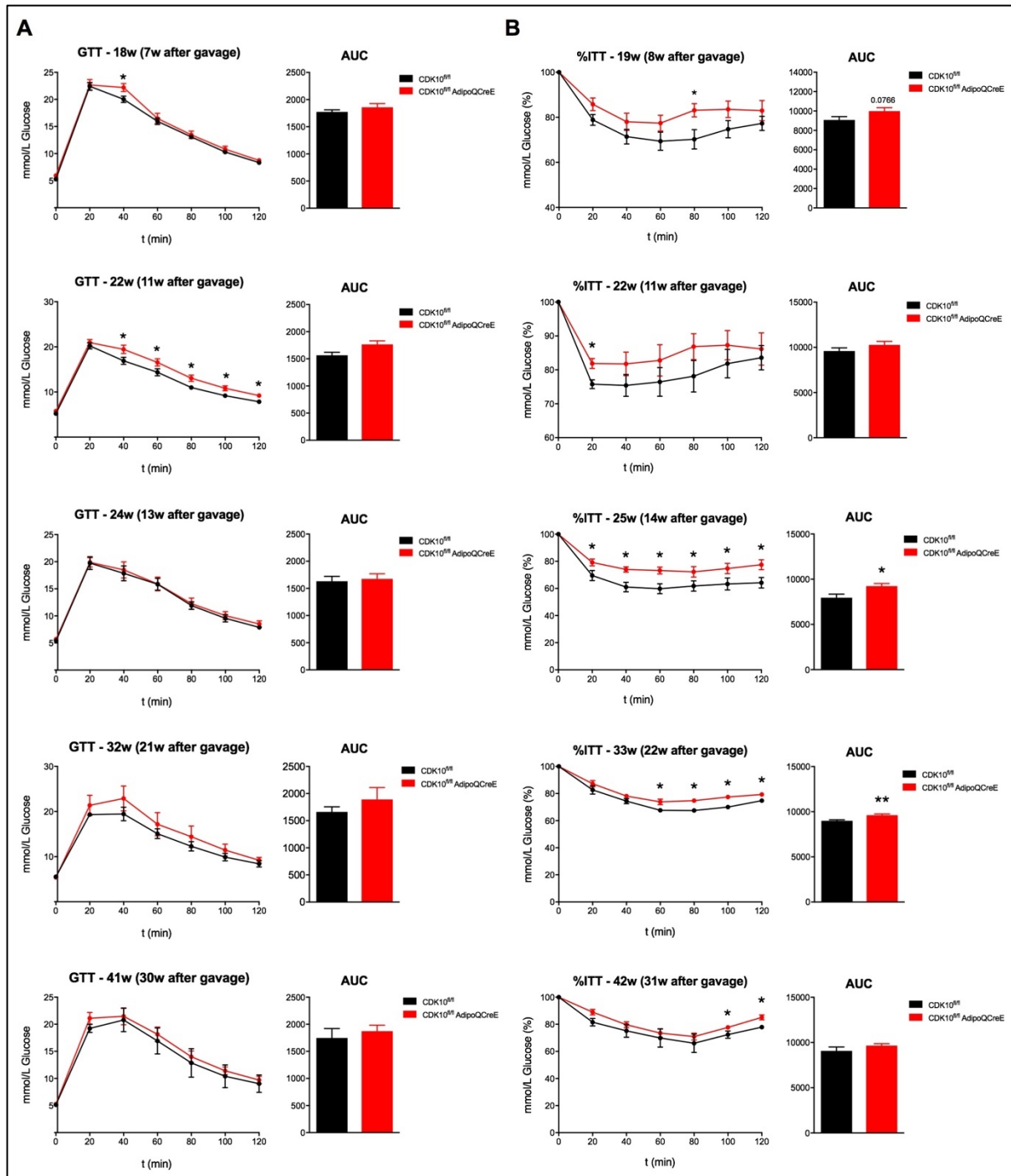


**Figure 6.7: CDK10 deficiency induces insulin resistance in adipose tissue of KO mice.** GTT was performed on control and CDK10 ATKO mice at different ages, showing that the KO mice glucose intolerant at the age of 22w (11w after gavage), after which they lose this phenotype and revert back to their normal metabolic state (A). ITT was also performed on these mice at different ages, showing that the KO mice are normal at the beginning but then they develop insulin resistance at the age of 25w (14w after gavage) until the age of 42w, when they start losing this phenotype (B). Results represent the average  $\pm$  SEM, n = 10 mice. Significance was determined using the unpaired t-test, with \* p < 0.05 and \*\* p < 0.01.

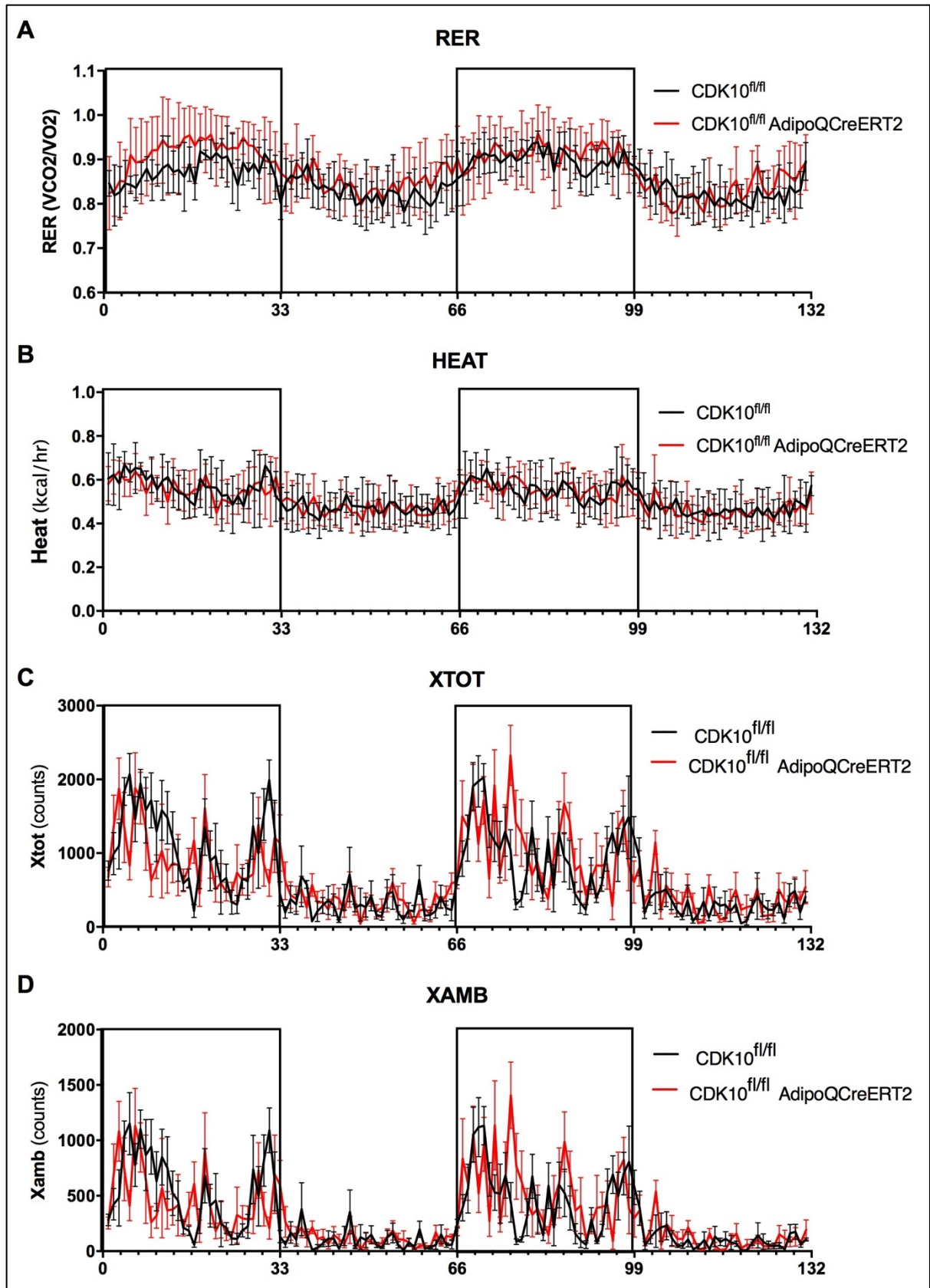


**Figure 6.8: Indirect Calorimetry Studies show no difference between control and CDK10 ATKO mice.** RER (A), heat (B), X total movement (C), and X amb (Ambulatory movement) (D) show no differences between CDK10<sup>fl/fl</sup> and CDK10<sup>fl/fl</sup> AdipoQCreERT2 mice. Results represent the average  $\pm$  SEM, n = 10 mice. Significance was determined using the unpaired t-test, with \* p < 0.05.

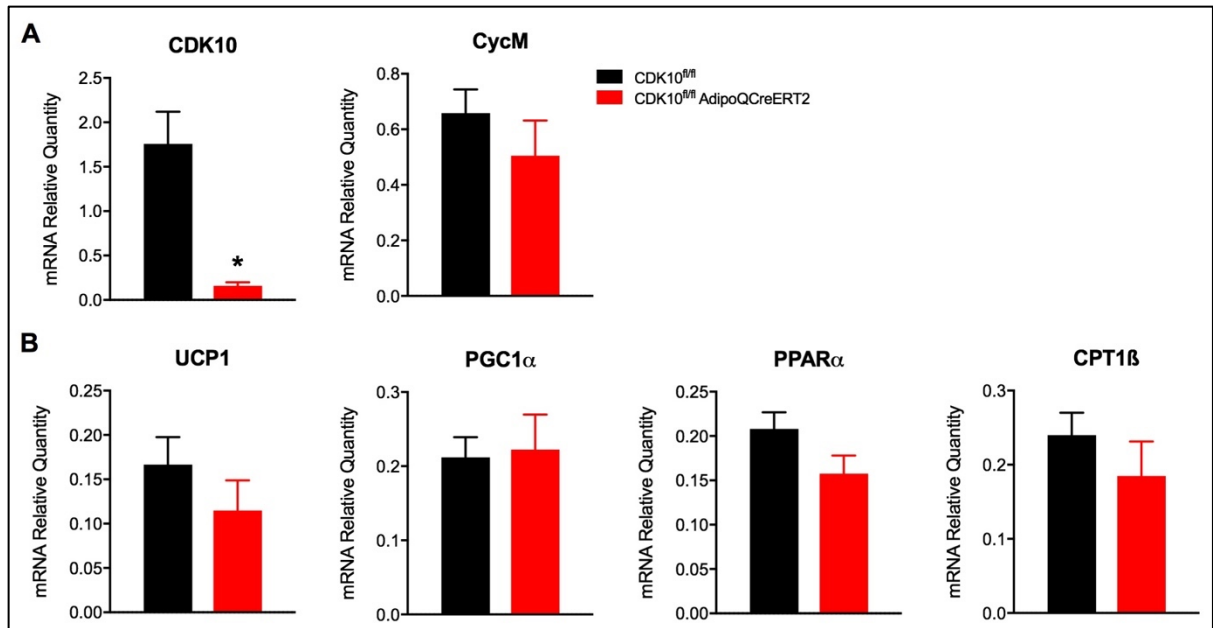


**Figure 6.9: No difference is observed in the expression of BAT markers in the BAT of CDK10 ATKO mice.** CDK10 is knocked out, and CycM tends to decrease in the ATKO mice (A). UCP1, PPAR $\alpha$ , and CPT1 $\beta$  tend to decrease in the BAT of ATKO mice. However, none of the observed changes are significant (B). Results represent the average  $\pm$  SEM, n = 10 mice. Significance was determined using the unpaired t-test, with \* p < 0.05.



---

## *Chapter 7: Limitations of the Kinome Study*

---

The purpose of this work is to discover new kinases with differential activity during insulin resistance development in obese patients. The novel kinase activity-based assay from PamGene helped us to directly detect kinase function from patients' biopsies. However, as in any research method, it is important to mention the limitations of the study.

PamGene is a well-established method tailored for cancer studies. Most of its projects are in oncology, and the technology is oriented towards biomarker research (Cato et al., 2019). Serine/Threonine Kinase PamChip® Array consists of 144 peptides. Each peptide represents a 15-amino-acid sequence, of which 13 residues are derived from a putative phosphorylation site in human proteins. Peptide sequences are derived from literature. Thus, the pathways covered by the BioNavigator software analysis are mainly signaling cascades implicated in cancer research, and not necessarily in metabolic studies. As stated previously, our group was among the first who used the PamGene for metabolic studies. For this reason, most of the kinase hits we obtained are tumor suppressors or proto-oncogenes.

Peptide sequences are correlated with one or multiple upstream kinases. While all STKs phosphorylate serine or threonine residues in their substrates, they choose specific residues in the consensus sequence to phosphorylate (de Oliveira et al., 2016). Since these residues of a target substrate only make contact with several key amino acids within the catalytic cleft of the kinase, a kinase is usually not specific to a single substrate, but instead can phosphorylate a whole substrate family, which share common recognition sequences (Munk, Refsgaard, Olsen, & Jensen, 2016). While the catalytic domain of these kinases is highly conserved, the sequence variation that is observed in the kinome provides for the recognition of distinct substrates (de Oliveira et al., 2016). However, barely 20% of the known phosphosites are assigned to a kinase, initiating various bioinformatics efforts that attempt to predict the responsible kinases. These algorithms employ different approaches to predict kinase consensus sequence motifs, mostly based on large scale in vivo and in vitro experiments (Munk et al., 2016).

Therefore, the criteria we used in our upstream kinase analysis might be confined by the bias in literature, which in turn may restrict the kinase hits by the kinome profiling.

---

## *Summary and Outlook*

---

In my work during the past five years, I have found novel kinases implicated in insulin resistance of obese patients, using a new technology known as the PamGene. The integrative kinome profiling approach illustrated in this thesis, helped us unravel potential targets for diabetic studies.

PIM-1, out of the PIM family of kinases, was shown to be a main player in the onset of insulin resistance in the adipose tissue, specifically by inducing inflammation and macrophage infiltration. We hypothesize that PIM-1 assists the translocation of NF $\kappa$ B into the nucleus, inducing a pro-inflammatory phenotype in the macrophages. This is still under development, and several experiments are ongoing to proof this idea. Metabolic phenotyping of mice under HFD treated with the vehicle or the PIM inhibitor is ongoing, in order to further prove the role of PIM-1 in a model that is more related to obesity, inflammation and diabetes in human patients.

CHK2 was depicted as a kinase directly correlated to adipocytes during adipose tissue insulin resistance. Treating diabetic mice with its inhibitor rendered them healthy. However, other studies in different tissues have shown that CHK2 activity is a result of insulin resistance and not what causes insulin resistance. Therefore, the adipose tissue specific knockout has to be generated, and the mice should be metabolically phenotyped and challenged under HFD.

CDK10 was also found as a top hit in the kinome analysis. However, our data showed that it is more implicated in the brown adipose tissue rather than white adipose tissue. No major findings were depicted in the adipose tissue induced knock out mouse model. This might be due to the fact that the upstream kinase analysis is based on motifs and consensus sequences, rather than actual experimentations. Hence, CDK10 was a “false positive” kinase hit.

The last chapter of this thesis shed light on the limitations of our kinome study, serving as a general discussion for the overall project. We showed that PamGene is a very useful technology to be used. Nevertheless, the analysis of the raw data has to still be optimized and fine-tuned.



---

## Bibliography

---

- Abd Al Haleem, E. N., & El-Bakly, W. M. (2019). The role of MAPK signaling pathway in selenium amelioration of high fat/high cholesterol diet-induced tauopathy in rats. *Chem Biol Interact*, 302, 108-116. doi:10.1016/j.cbi.2019.01.022
- Abella, A., Dubus, P., Malumbres, M., Rane, S. G., Kiyokawa, H., Sicard, A., . . . Fajas, L. (2005). Cdk4 promotes adipogenesis through PPARgamma activation. *Cell Metab*, 2(4), 239-249. doi:10.1016/j.cmet.2005.09.003
- Agrawal, N. K., & Kant, S. (2014). Targeting inflammation in diabetes: Newer therapeutic options. *World J Diabetes*, 5(5), 697-710. doi:10.4239/wjd.v5.i5.697
- Aguilar, V., & Fajas, L. (2010). Cycling through metabolism. *EMBO Mol Med*, 2(9), 338-348. doi:10.1002/emmm.201000089
- Amaravadi, R., & Thompson, C. B. (2005). The survival kinases Akt and Pim as potential pharmacological targets. *J Clin Invest*, 115(10), 2618-2624. doi:10.1172/JCI26273
- An, N., Kraft, A. S., & Kang, Y. (2013). Abnormal hematopoietic phenotypes in Pim kinase triple knockout mice. *J Hematol Oncol*, 6, 12. doi:10.1186/1756-8722-6-12
- Andersen, E., Ingerslev, L. R., Fabre, O., Donkin, I., Altintas, A., Versteyhe, S., . . . Barres, R. (2019). Preadipocytes from obese humans with type 2 diabetes are epigenetically reprogrammed at genes controlling adipose tissue function. *Int J Obes (Lond)*, 43(2), 306-318. doi:10.1038/s41366-018-0031-3
- Ando, Y., Shinozawa, Y., Iijima, Y., Yu, B. C., Sone, M., Ooi, Y., . . . Takahashi, S. (2015). Tumor necrosis factor (TNF)-alpha-induced repression of GKAP42 protein levels through cGMP-dependent kinase (cGK)-Ialpha causes insulin resistance in 3T3-L1 adipocytes. *J Biol Chem*, 290(9), 5881-5892. doi:10.1074/jbc.M114.624759
- Annicotte, J. S., Blanchet, E., Chavey, C., Iankova, I., Costes, S., Assou, S., . . . Fajas, L. (2009). The CDK4-pRB-E2F1 pathway controls insulin secretion. *Nat Cell Biol*, 11(8), 1017-1023. doi:10.1038/ncb1915
- Arfianti, E., Larter, C. Z., Lee, S., Barn, V., Haigh, G., Yeh, M. M., . . . Farrell, G. C. (2016). Obesity and diabetes accelerate hepatocarcinogenesis via hepatocyte proliferation independent of NF-kappaB or Akt/mTORC1. *J Clin Transl Res*, 2(1), 26-37. Retrieved from <https://www.ncbi.nlm.nih.gov/pubmed/30873458>
- Arroyo-Johnson, C., & Mincey, K. D. (2016). Obesity Epidemiology Worldwide. *Gastroenterol Clin North Am*, 45(4), 571-579. doi:10.1016/j.gtc.2016.07.012
- Bartek, J., Falck, J., & Lukas, J. (2001). CHK2 kinase--a busy messenger. *Nat Rev Mol Cell Biol*, 2(12), 877-886. doi:10.1038/35103059
- Bartness, T. J., Liu, Y., Shrestha, Y. B., & Ryu, V. (2014). Neural innervation of white adipose tissue and the control of lipolysis. *Front Neuroendocrinol*, 35(4), 473-493. doi:10.1016/j.yfrne.2014.04.001
- Beisswenger, P. J., Howell, S. K., O'Dell, R. M., Wood, M. E., Touchette, A. D., & Szwegold, B. S. (2001). alpha-Dicarbonyls increase in the postprandial period and reflect the degree of hyperglycemia. *Diabetes Care*, 24(4), 726-732. Retrieved from <https://www.ncbi.nlm.nih.gov/pubmed/11315838>

- Bhargava, P., & Lee, C. H. (2012). Role and function of macrophages in the metabolic syndrome. *Biochem J*, 442(2), 253-262. doi:10.1042/BJ20111708
- Bhise, S. B., Nalawade, A. D., & Wadhawa, H. (2004). Role of protein tyrosine kinase inhibitors in cancer therapeutics. *Indian J Biochem Biophys*, 41(6), 273-280. Retrieved from <https://www.ncbi.nlm.nih.gov/pubmed/22900354>
- Blasina, A., de Weyer, I. V., Laus, M. C., Luyten, W. H., Parker, A. E., & McGowan, C. H. (1999). A human homologue of the checkpoint kinase Cds1 directly inhibits Cdc25 phosphatase. *Curr Biol*, 9(1), 1-10. Retrieved from <https://www.ncbi.nlm.nih.gov/pubmed/9889122>
- Bluher, M. (2009). Adipose tissue dysfunction in obesity. *Exp Clin Endocrinol Diabetes*, 117(6), 241-250. doi:10.1055/s-0029-1192044
- Brault, L., Gasser, C., Bracher, F., Huber, K., Knapp, S., & Schwaller, J. (2010). PIM serine/threonine kinases in the pathogenesis and therapy of hematologic malignancies and solid cancers. *Haematologica*, 95(6), 1004-1015. doi:10.3324/haematol.2009.017079
- Brown, A. L., Lee, C. H., Schwarz, J. K., Mitiku, N., Piwnica-Worms, H., & Chung, J. H. (1999). A human Cds1-related kinase that functions downstream of ATM protein in the cellular response to DNA damage. *Proc Natl Acad Sci U S A*, 96(7), 3745-3750. Retrieved from <https://www.ncbi.nlm.nih.gov/pubmed/10097108>
- Bublil, E. M., & Yarden, Y. (2007). The EGF receptor family: spearheading a merger of signaling and therapeutics. *Curr Opin Cell Biol*, 19(2), 124-134. doi:10.1016/j.ceb.2007.02.008
- Cairns, R. A., Harris, I. S., & Mak, T. W. (2011). Regulation of cancer cell metabolism. *Nat Rev Cancer*, 11(2), 85-95. doi:10.1038/nrc2981
- Cancello, R., Tordjman, J., Poitou, C., Guilhem, G., Bouillot, J. L., Hugol, D., . . . Clement, K. (2006). Increased infiltration of macrophages in omental adipose tissue is associated with marked hepatic lesions in morbid human obesity. *Diabetes*, 55(6), 1554-1561. doi:10.2337/db06-0133
- Cannon, B., & Nedergaard, J. (2004). Brown adipose tissue: function and physiological significance. *Physiol Rev*, 84(1), 277-359. doi:10.1152/physrev.00015.2003
- Carobbio, S., Pellegrinelli, V., & Vidal-Puig, A. (2017). Adipose Tissue Function and Expandability as Determinants of Lipotoxicity and the Metabolic Syndrome. *Adv Exp Med Biol*, 960, 161-196. doi:10.1007/978-3-319-48382-5\_7
- Carroll, B., & Dunlop, E. A. (2017). The lysosome: a crucial hub for AMPK and mTORC1 signalling. *Biochem J*, 474(9), 1453-1466. doi:10.1042/BCJ20160780
- Carvalho-Filho, M. A., Carvalho, B. M., Oliveira, A. G., Guadagnini, D., Ueno, M., Dias, M. M., . . . Saad, M. J. (2012). Double-stranded RNA-activated protein kinase is a key modulator of insulin sensitivity in physiological conditions and in obesity in mice. *Endocrinology*, 153(11), 5261-5274. doi:10.1210/en.2012-1400
- Cato, L., de Tribolet-Hardy, J., Lee, I., Rottenberg, J. T., Coleman, I., Melchers, D., . . . Brown, M. (2019). ARV7 Represses Tumor-Suppressor Genes in Castration-Resistant Prostate Cancer. *Cancer Cell*, 35(3), 401-413 e406. doi:10.1016/j.ccell.2019.01.008
- Cecchini, M. G., Dominguez, M. G., Mocci, S., Wetterwald, A., Felix, R., Fleisch, H., . . . Stanley, E. R. (1994). Role of colony stimulating factor-1 in the establishment and regulation of tissue macrophages during postnatal development of the mouse. *Development*, 120(6), 1357-1372. Retrieved from <https://www.ncbi.nlm.nih.gov/pubmed/8050349>
- Ceperuelo-Mallafre, V., Ejarque, M., Serena, C., Duran, X., Montori-Grau, M., Rodriguez, M. A., . . . Fernandez-Veledo, S. (2016). Adipose tissue glycogen accumulation is associated with obesity-linked inflammation in humans. *Mol Metab*, 5(1), 5-18. doi:10.1016/j.molmet.2015.10.001

- Chen, Y., & Sanchez, Y. (2004). Chk1 in the DNA damage response: conserved roles from yeasts to mammals. *DNA Repair (Amst)*, 3(8-9), 1025-1032. doi:10.1016/j.dnarep.2004.03.003
- Cheng, H. C., Qi, R. Z., Paudel, H., & Zhu, H. J. (2011). Regulation and function of protein kinases and phosphatases. *Enzyme Res*, 2011, 794089. doi:10.4061/2011/794089
- Choi, E., Zhang, X., Xing, C., & Yu, H. (2016). Mitotic Checkpoint Regulators Control Insulin Signaling and Metabolic Homeostasis. *Cell*, 166(3), 567-581. doi:10.1016/j.cell.2016.05.074
- Cohen, P. (2000). The regulation of protein function by multisite phosphorylation--a 25 year update. *Trends Biochem Sci*, 25(12), 596-601. Retrieved from <https://www.ncbi.nlm.nih.gov/pubmed/11116185>
- Copps, K. D., & White, M. F. (2012). Regulation of insulin sensitivity by serine/threonine phosphorylation of insulin receptor substrate proteins IRS1 and IRS2. *Diabetologia*, 55(10), 2565-2582. doi:10.1007/s00125-012-2644-8
- Crawford, J., Ianzano, L., Savino, M., Whitmore, S., Cleton-Jansen, A. M., Settasatian, C., . . . Savoia, A. (1999). The PISLRE gene: structure, exon skipping, and exclusion as tumor suppressor in breast cancer. *Genomics*, 56(1), 90-97. doi:10.1006/geno.1998.5676
- Cristancho, A. G., & Lazar, M. A. (2011). Forming functional fat: a growing understanding of adipocyte differentiation. *Nat Rev Mol Cell Biol*, 12(11), 722-734. doi:10.1038/nrm3198
- Cypess, A. M., & Kahn, C. R. (2010). The role and importance of brown adipose tissue in energy homeostasis. *Curr Opin Pediatr*, 22(4), 478-484. doi:10.1097/MOP.0b013e32833a8d6e
- Cypess, A. M., Lehman, S., Williams, G., Tal, I., Rodman, D., Goldfine, A. B., . . . Kahn, C. R. (2009). Identification and importance of brown adipose tissue in adult humans. *N Engl J Med*, 360(15), 1509-1517. doi:10.1056/NEJMoa0810780
- Cypess, A. M., White, A. P., Vernochet, C., Schulz, T. J., Xue, R., Sass, C. A., . . . Tseng, Y. H. (2013). Anatomical localization, gene expression profiling and functional characterization of adult human neck brown fat. *Nat Med*, 19(5), 635-639. doi:10.1038/nm.3112
- de Boer, J. F., Dikkers, A., Jurdzinski, A., von Felden, J., Gaestel, M., Bavendiek, U., & Tietge, U. J. (2014). Mitogen-activated protein kinase-activated protein kinase 2 deficiency reduces insulin sensitivity in high-fat diet-fed mice. *PLoS One*, 9(9), e106300. doi:10.1371/journal.pone.0106300
- de Oliveira, P. S., Ferraz, F. A., Pena, D. A., Pramio, D. T., Morais, F. A., & Schechtman, D. (2016). Revisiting protein kinase-substrate interactions: Toward therapeutic development. *Sci Signal*, 9(420), re3. doi:10.1126/scisignal.aad4016
- DeBerardinis, R. J., & Thompson, C. B. (2012). Cellular metabolism and disease: what do metabolic outliers teach us? *Cell*, 148(6), 1132-1144. doi:10.1016/j.cell.2012.02.032
- Denechaud, P. D., Lopez-Mejia, I. C., & Fajas, L. (2016). [Cell cycle regulators CDK4 and E2F1 control glucose and lipid homeostasis]. *Med Sci (Paris)*, 32(10), 815-818. doi:10.1051/medsci/20163210008
- Dhanasekaran, S. M., Barrette, T. R., Ghosh, D., Shah, R., Varambally, S., Kurachi, K., . . . Chinnaiyan, A. M. (2001). Delineation of prognostic biomarkers in prostate cancer. *Nature*, 412(6849), 822-826. doi:10.1038/35090585
- Di Blasio, L., Gagliardi, P. A., Puliafito, A., & Primo, L. (2017). Serine/Threonine Kinase 3-Phosphoinositide-Dependent Protein Kinase-1 (PDK1) as a Key Regulator of Cell Migration and Cancer Dissemination. *Cancers (Basel)*, 9(3). doi:10.3390/cancers9030025

- Dong, D., Yu, J., Wu, Y., Fu, N., Villela, N. A., & Yang, P. (2015). Maternal diabetes triggers DNA damage and DNA damage response in neurulation stage embryos through oxidative stress. *Biochem Biophys Res Commun*, *467*(2), 407-412. doi:10.1016/j.bbrc.2015.09.137
- Durocher, D., Henckel, J., Fersht, A. R., & Jackson, S. P. (1999). The FHA domain is a modular phosphopeptide recognition motif. *Mol Cell*, *4*(3), 387-394. Retrieved from <https://www.ncbi.nlm.nih.gov/pubmed/10518219>
- Durocher, D., Taylor, I. A., Sarbassova, D., Haire, L. F., Westcott, S. L., Jackson, S. P., . . . Yaffe, M. B. (2000). The molecular basis of FHA domain:phosphopeptide binding specificity and implications for phospho-dependent signaling mechanisms. *Mol Cell*, *6*(5), 1169-1182. Retrieved from <https://www.ncbi.nlm.nih.gov/pubmed/11106755>
- Dusserre, E., Moulin, P., & Vidal, H. (2000). Differences in mRNA expression of the proteins secreted by the adipocytes in human subcutaneous and visceral adipose tissues. *Biochim Biophys Acta*, *1500*(1), 88-96. Retrieved from <https://www.ncbi.nlm.nih.gov/pubmed/10564721>
- Edelman, A. M., Blumenthal, D. K., & Krebs, E. G. (1987). Protein serine/threonine kinases. *Annu Rev Biochem*, *56*, 567-613. doi:10.1146/annurev.bi.56.070187.003031
- Eichmann, A., Yuan, L., Breant, C., Alitalo, K., & Koskinen, P. J. (2000). Developmental expression of pim kinases suggests functions also outside of the hematopoietic system. *Oncogene*, *19*(9), 1215-1224. doi:10.1038/sj.onc.1203355
- El Hadi, H., Di Vincenzo, A., Vettor, R., & Rossato, M. (2018). Food Ingredients Involved in White-to-Brown Adipose Tissue Conversion and in Calorie Burning. *Front Physiol*, *9*, 1954. doi:10.3389/fphys.2018.01954
- Enerback, S., Jacobsson, A., Simpson, E. M., Guerra, C., Yamashita, H., Harper, M. E., & Kozak, L. P. (1997). Mice lacking mitochondrial uncoupling protein are cold-sensitive but not obese. *Nature*, *387*(6628), 90-94. doi:10.1038/387090a0
- Eungdamrong, N. J., & Iyengar, R. (2004). Modeling cell signaling networks. *Biol Cell*, *96*(5), 355-362. doi:10.1016/j.biocel.2004.03.004
- Fajas, L., Blanchet, E., & Annicotte, J. S. (2010). CDK4, pRB and E2F1: connected to insulin. *Cell Div*, *5*(1), 6. doi:10.1186/1747-1028-5-6
- Fazakerley, D. J., Holman, G. D., Marley, A., James, D. E., Stockli, J., & Coster, A. C. (2010). Kinetic evidence for unique regulation of GLUT4 trafficking by insulin and AMP-activated protein kinase activators in L6 myotubes. *J Biol Chem*, *285*(3), 1653-1660. doi:10.1074/jbc.M109.051185
- Fontana, L., Eagon, J. C., Trujillo, M. E., Scherer, P. E., & Klein, S. (2007). Visceral fat adipokine secretion is associated with systemic inflammation in obese humans. *Diabetes*, *56*(4), 1010-1013. doi:10.2337/db06-1656
- Foster, D. O., & Frydman, M. L. (1978). Nonshivering thermogenesis in the rat. II. Measurements of blood flow with microspheres point to brown adipose tissue as the dominant site of the calorogenesis induced by noradrenaline. *Can J Physiol Pharmacol*, *56*(1), 110-122. Retrieved from <https://www.ncbi.nlm.nih.gov/pubmed/638848>
- Fox, C. J., Hammerman, P. S., Cinalli, R. M., Master, S. R., Chodosh, L. A., & Thompson, C. B. (2003). The serine/threonine kinase Pim-2 is a transcriptionally regulated apoptotic inhibitor. *Genes Dev*, *17*(15), 1841-1854. doi:10.1101/gad.1105003
- Gabrielsson, B. G., Johansson, J. M., Lonn, M., Jernas, M., Olbers, T., Peltonen, M., . . . Carlsson, L. M. (2003). High expression of complement components in omental adipose tissue in obese men. *Obes Res*, *11*(6), 699-708. doi:10.1038/oby.2003.100

- Garrison, C. B., Lastwika, K. J., Zhang, Y., Li, C. I., & Lampe, P. D. (2017). Proteomic Analysis, Immune Dysregulation, and Pathway Interconnections with Obesity. *J Proteome Res*, *16*(1), 274-287. doi:10.1021/acs.jproteome.6b00611
- Goodpaster, B. H., & Sparks, L. M. (2017). Metabolic Flexibility in Health and Disease. *Cell Metab*, *25*(5), 1027-1036. doi:10.1016/j.cmet.2017.04.015
- Goossens, G. H. (2017). The Metabolic Phenotype in Obesity: Fat Mass, Body Fat Distribution, and Adipose Tissue Function. *Obes Facts*, *10*(3), 207-215. doi:10.1159/000471488
- Gual, P., Le Marchand-Brustel, Y., & Tanti, J. F. (2005). Positive and negative regulation of insulin signaling through IRS-1 phosphorylation. *Biochimie*, *87*(1), 99-109. doi:10.1016/j.biochi.2004.10.019
- Guen, V. J., Gamble, C., Flajolet, M., Unger, S., Thollet, A., Ferandin, Y., . . . Colas, P. (2013). CDK10/cyclin M is a protein kinase that controls ETS2 degradation and is deficient in STAR syndrome. *Proc Natl Acad Sci U S A*, *110*(48), 19525-19530. doi:10.1073/pnas.1306814110
- Guen, V. J., Gamble, C., Lees, J. A., & Colas, P. (2017). The awakening of the CDK10/Cyclin M protein kinase. *Oncotarget*, *8*(30), 50174-50186. doi:10.18632/oncotarget.15024
- Gupta, M. K., & Vadde, R. (2019). Identification and characterization of differentially expressed genes in Type 2 Diabetes using in silico approach. *Comput Biol Chem*, *79*, 24-35. doi:10.1016/j.compbiolchem.2019.01.010
- Hanks, S. K. (1987). Homology probing: identification of cDNA clones encoding members of the protein-serine kinase family. *Proc Natl Acad Sci U S A*, *84*(2), 388-392. Retrieved from <https://www.ncbi.nlm.nih.gov/pubmed/2948189>
- Hanks, S. K., & Hunter, T. (1995). Protein kinases 6. The eukaryotic protein kinase superfamily: kinase (catalytic) domain structure and classification. *FASEB J*, *9*(8), 576-596. Retrieved from <https://www.ncbi.nlm.nih.gov/pubmed/7768349>
- Hildebrand, S., Stumer, J., & Pfeifer, A. (2018). PVAT and Its Relation to Brown, Beige, and White Adipose Tissue in Development and Function. *Front Physiol*, *9*, 70. doi:10.3389/fphys.2018.00070
- Holt, L. J., Tuch, B. B., Villen, J., Johnson, A. D., Gygi, S. P., & Morgan, D. O. (2009). Global analysis of Cdk1 substrate phosphorylation sites provides insights into evolution. *Science*, *325*(5948), 1682-1686. doi:10.1126/science.1172867
- Hotamisligil, G. S., Shargill, N. S., & Spiegelman, B. M. (1993). Adipose expression of tumor necrosis factor-alpha: direct role in obesity-linked insulin resistance. *Science*, *259*(5091), 87-91. Retrieved from <https://www.ncbi.nlm.nih.gov/pubmed/7678183>
- Huang, X., Liu, G., Guo, J., & Su, Z. (2018). The PI3K/AKT pathway in obesity and type 2 diabetes. *Int J Biol Sci*, *14*(11), 1483-1496. doi:10.7150/ijbs.27173
- Hubbard, S. R., & Till, J. H. (2000). Protein tyrosine kinase structure and function. *Annu Rev Biochem*, *69*, 373-398. doi:10.1146/annurev.biochem.69.1.373
- Huh, J. Y., Park, Y. J., Ham, M., & Kim, J. B. (2014). Crosstalk between adipocytes and immune cells in adipose tissue inflammation and metabolic dysregulation in obesity. *Mol Cells*, *37*(5), 365-371. doi:10.14348/molcells.2014.0074
- Husson, H., Carideo, E. G., Neuberger, D., Schultze, J., Munoz, O., Marks, P. W., . . . Freedman, A. S. (2002). Gene expression profiling of follicular lymphoma and normal germinal center B cells using cDNA arrays. *Blood*, *99*(1), 282-289. Retrieved from <https://www.ncbi.nlm.nih.gov/pubmed/11756183>

- Iorns, E., Turner, N. C., Elliott, R., Syed, N., Garrone, O., Gasco, M., . . . Ashworth, A. (2008). Identification of CDK10 as an important determinant of resistance to endocrine therapy for breast cancer. *Cancer Cell*, *13*(2), 91-104. doi:10.1016/j.ccr.2008.01.001
- Jeffery, E., Berry, R., Church, C. D., Yu, S., Shook, B. A., Horsley, V., . . . Rodeheffer, M. S. (2014). Characterization of Cre recombinase models for the study of adipose tissue. *Adipocyte*, *3*(3), 206-211. doi:10.4161/adip.29674
- Kanda, H., Tateya, S., Tamori, Y., Kotani, K., Hiasa, K., Kitazawa, R., . . . Kasuga, M. (2006). MCP-1 contributes to macrophage infiltration into adipose tissue, insulin resistance, and hepatic steatosis in obesity. *J Clin Invest*, *116*(6), 1494-1505. doi:10.1172/JCI26498
- Kani, S., Nakayama, E., Yoda, A., Onishi, N., Sougawa, N., Hazaka, Y., . . . Minami, Y. (2007). Chk2 kinase is required for methylglyoxal-induced G2/M cell-cycle checkpoint arrest: implication of cell-cycle checkpoint regulation in diabetic oxidative stress signaling. *Genes Cells*, *12*(8), 919-928. doi:10.1111/j.1365-2443.2007.01100.x
- Kannel, W. B., Hjortland, M., & Castelli, W. P. (1974). Role of diabetes in congestive heart failure: the Framingham study. *Am J Cardiol*, *34*(1), 29-34. Retrieved from <https://www.ncbi.nlm.nih.gov/pubmed/4835750>
- Kastan, M. B., & Lim, D. S. (2000). The many substrates and functions of ATM. *Nat Rev Mol Cell Biol*, *1*(3), 179-186. doi:10.1038/35043058
- Ke, M., Wu, H., Zhu, Z., Zhang, C., Zhang, Y., & Deng, Y. (2017). Differential proteomic analysis of white adipose tissues from T2D KKAY mice by LC-ESI-QTOF. *Proteomics*, *17*(5). doi:10.1002/pmic.201600219
- Keane, N. A., Reidy, M., Naton, A., Raab, M. S., & O'Dwyer, M. (2015). Targeting the Pim kinases in multiple myeloma. *Blood Cancer J*, *5*, e325. doi:10.1038/bcj.2015.46
- Kim, K., Kim, J. H., Youn, B. U., Jin, H. M., & Kim, N. (2010). Pim-1 regulates RANKL-induced osteoclastogenesis via NF-kappaB activation and NFATc1 induction. *J Immunol*, *185*(12), 7460-7466. doi:10.4049/jimmunol.1000885
- Kim, S. H., & Plutzky, J. (2016). Brown Fat and Browning for the Treatment of Obesity and Related Metabolic Disorders. *Diabetes Metab J*, *40*(1), 12-21. doi:10.4093/dmj.2016.40.1.12
- Kornev, A. P., Taylor, S. S., & Ten Eyck, L. F. (2008). A helix scaffold for the assembly of active protein kinases. *Proc Natl Acad Sci U S A*, *105*(38), 14377-14382. doi:10.1073/pnas.0807988105
- Kroiher, M., Miller, M. A., & Steele, R. E. (2001). Deceiving appearances: signaling by "dead" and "fractured" receptor protein-tyrosine kinases. *Bioessays*, *23*(1), 69-76. doi:10.1002/1521-1878(200101)23:1<69::AID-BIES1009>3.0.CO;2-K
- Lackey, D. E., & Olefsky, J. M. (2016). Regulation of metabolism by the innate immune system. *Nat Rev Endocrinol*, *12*(1), 15-28. doi:10.1038/nrendo.2015.189
- Lagarigue, S., Lopez-Mejia, I. C., Denechaud, P. D., Escote, X., Castillo-Armengol, J., Jimenez, V., . . . Fajas, L. (2016). CDK4 is an essential insulin effector in adipocytes. *J Clin Invest*, *126*(1), 335-348. doi:10.1172/JCI81480
- Lahiry, P., Torkamani, A., Schork, N. J., & Hegele, R. A. (2010). Kinase mutations in human disease: interpreting genotype-phenotype relationships. *Nat Rev Genet*, *11*(1), 60-74. doi:10.1038/nrg2707
- Lean, M. E. (1989). Brown adipose tissue in humans. *Proc Nutr Soc*, *48*(2), 243-256. Retrieved from <https://www.ncbi.nlm.nih.gov/pubmed/2678120>

- Lee, C. H., & Chung, J. H. (2001). The hCds1 (Chk2)-FHA domain is essential for a chain of phosphorylation events on hCds1 that is induced by ionizing radiation. *J Biol Chem*, *276*(32), 30537-30541. doi:10.1074/jbc.M104414200
- Lee, D. H., Shi, J., Jeoung, N. H., Kim, M. S., Zabolotny, J. M., Lee, S. W., . . . Kim, Y. B. (2009). Targeted disruption of ROCK1 causes insulin resistance in vivo. *J Biol Chem*, *284*(18), 11776-11780. doi:10.1074/jbc.C900014200
- Lee, S. H., Huang, H., Choi, K., Lee, D. H., Shi, J., Liu, T., . . . Kim, Y. B. (2014). ROCK1 isoform-specific deletion reveals a role for diet-induced insulin resistance. *Am J Physiol Endocrinol Metab*, *306*(3), E332-343. doi:10.1152/ajpendo.00619.2013
- Li, J., Loveland, B. E., & Xing, P. X. (2011). Anti-Pim-1 mAb inhibits activation and proliferation of T lymphocytes and prolongs mouse skin allograft survival. *Cell Immunol*, *272*(1), 87-93. doi:10.1016/j.cellimm.2011.09.002
- Li, J., Peet, G. W., Balzarano, D., Li, X., Massa, P., Barton, R. W., & Marcu, K. B. (2001). Novel NEMO/IkappaB kinase and NF-kappa B target genes at the pre-B to immature B cell transition. *J Biol Chem*, *276*(21), 18579-18590. doi:10.1074/jbc.M100846200
- Li, J., Smith, G. P., & Walker, J. C. (1999). Kinase interaction domain of kinase-associated protein phosphatase, a phosphoprotein-binding domain. *Proc Natl Acad Sci U S A*, *96*(14), 7821-7826. Retrieved from <https://www.ncbi.nlm.nih.gov/pubmed/10393905>
- Li, S., MacLachlan, T. K., De Luca, A., Claudio, P. P., Condorelli, G., & Giordano, A. (1995). The cdc-2-related kinase, PISLRE, is essential for cell growth and acts in G2 phase of the cell cycle. *Cancer Res*, *55*(18), 3992-3995. Retrieved from <https://www.ncbi.nlm.nih.gov/pubmed/7664269>
- Li, Y., Soos, T. J., Li, X., Wu, J., Degennaro, M., Sun, X., . . . Polakiewicz, R. D. (2004). Protein kinase C Theta inhibits insulin signaling by phosphorylating IRS1 at Ser(1101). *J Biol Chem*, *279*(44), 45304-45307. doi:10.1074/jbc.C400186200
- Li, Z., Lin, F., Zhuo, C., Deng, G., Chen, Z., Yin, S., . . . Li, B. (2014). PIM1 kinase phosphorylates the human transcription factor FOXP3 at serine 422 to negatively regulate its activity under inflammation. *J Biol Chem*, *289*(39), 26872-26881. doi:10.1074/jbc.M114.586651
- Lin, C., Bai, S., Du, T., Lai, Y., Chen, X., Peng, S., . . . Huang, H. (2019). Polo-like kinase 3 is associated with poor prognosis and regulates proliferation and metastasis in prostate cancer. *Cancer Manag Res*, *11*, 1517-1524. doi:10.2147/CMAR.S176762
- Liong, S., Barker, G., & Lappas, M. (2017). Placental Pim-1 expression is increased in obesity and regulates cytokine- and toll-like receptor-mediated inflammation. *Placenta*, *53*, 101-112. doi:10.1016/j.placenta.2017.04.010
- Liu, H. T., Wang, N., Wang, X., & Li, S. L. (2010). Overexpression of Pim-1 is associated with poor prognosis in patients with esophageal squamous cell carcinoma. *J Surg Oncol*, *102*(6), 683-688. doi:10.1002/jso.21627
- Liu, Y., Xiao, Z., Yang, D., Ren, L., Liu, G., & Yang, L. (2012). Effects of the cyclin-dependent kinase 10 (CDK10) on the tamoxifen sensitivity of keloid samples. *Molecules*, *17*(2), 1307-1318. doi:10.3390/molecules17021307
- Lopez-Mejia, I. C., Lagarrigue, S., Giralt, A., Martinez-Carreres, L., Zanou, N., Denechaud, P. D., . . . Fajas, L. (2017). CDK4 Phosphorylates AMPKalpha2 to Inhibit Its Activity and Repress Fatty Acid Oxidation. *Mol Cell*, *68*(2), 336-349 e336. doi:10.1016/j.molcel.2017.09.034
- Loyd, C., & Obici, S. (2014). Brown fat fuel use and regulation of energy homeostasis. *Curr Opin Clin Nutr Metab Care*, *17*(4), 368-372. doi:10.1097/MCO.0000000000000063

- Loyer, P., Trembley, J. H., Katona, R., Kidd, V. J., & Lahti, J. M. (2005). Role of CDK/cyclin complexes in transcription and RNA splicing. *Cell Signal*, *17*(9), 1033-1051. doi:10.1016/j.cellsig.2005.02.005
- Lyu, X., Wang, J., Guo, X., Wu, G., Jiao, Y., Faleti, O. D., . . . Li, X. (2018). EBV-miR-BART1-5P activates AMPK/mTOR/HIF1 pathway via a PTEN independent manner to promote glycolysis and angiogenesis in nasopharyngeal carcinoma. *PLoS Pathog*, *14*(12), e1007484. doi:10.1371/journal.ppat.1007484
- Malumbres, M. (2011). Physiological relevance of cell cycle kinases. *Physiol Rev*, *91*(3), 973-1007. doi:10.1152/physrev.00025.2010
- Malumbres, M. (2014). Cyclin-dependent kinases. *Genome Biol*, *15*(6), 122. Retrieved from <https://www.ncbi.nlm.nih.gov/pubmed/25180339>
- Malumbres, M., & Barbacid, M. (2005). Mammalian cyclin-dependent kinases. *Trends Biochem Sci*, *30*(11), 630-641. doi:10.1016/j.tibs.2005.09.005
- Manning, G., Plowman, G. D., Hunter, T., & Sudarsanam, S. (2002). Evolution of protein kinase signaling from yeast to man. *Trends Biochem Sci*, *27*(10), 514-520. Retrieved from <https://www.ncbi.nlm.nih.gov/pubmed/12368087>
- Manning, G., Whyte, D. B., Martinez, R., Hunter, T., & Sudarsanam, S. (2002). The protein kinase complement of the human genome. *Science*, *298*(5600), 1912-1934. doi:10.1126/science.1075762
- Manoharan, R., Seong, H. A., & Ha, H. (2018). Dual Roles of Serine-Threonine Kinase Receptor-Associated Protein (STRAP) in Redox-Sensitive Signaling Pathways Related to Cancer Development. *Oxid Med Cell Longev*, *2018*, 5241524. doi:10.1155/2018/5241524
- Martinez-Carreres, L., Nasrallah, A., & Fajas, L. (2017). Cancer: Linking Powerhouses to Suicidal Bags. *Front Oncol*, *7*, 204. doi:10.3389/fonc.2017.00204
- Massague, J., & Chen, Y. G. (2000). Controlling TGF-beta signaling. *Genes Dev*, *14*(6), 627-644. Retrieved from <https://www.ncbi.nlm.nih.gov/pubmed/10733523>
- Matsuoka, S., Huang, M., & Elledge, S. J. (1998). Linkage of ATM to cell cycle regulation by the Chk2 protein kinase. *Science*, *282*(5395), 1893-1897. Retrieved from <https://www.ncbi.nlm.nih.gov/pubmed/9836640>
- McArdle, M., Finucane, O., Connaughton, R., McMorrow, A., & Roche, H. (2013). Mechanisms of Obesity-Induced Inflammation and Insulin Resistance: Insights into the Emerging Role of Nutritional Strategies. *Frontiers in Endocrinology*, *4*(52). doi:10.3389/fendo.2013.00052
- McLaughlin, T., Ackerman, S. E., Shen, L., & Engleman, E. (2017). Role of innate and adaptive immunity in obesity-associated metabolic disease. *J Clin Invest*, *127*(1), 5-13. doi:10.1172/JCI88876
- McLellan, A. C., Thornalley, P. J., Benn, J., & Sonksen, P. H. (1994). Glyoxalase system in clinical diabetes mellitus and correlation with diabetic complications. *Clin Sci (Lond)*, *87*(1), 21-29. Retrieved from <https://www.ncbi.nlm.nih.gov/pubmed/8062515>
- Medina-Castellanos, E., Esquivel-Naranjo, E. U., Heil, M., & Herrera-Estrella, A. (2014). Extracellular ATP activates MAPK and ROS signaling during injury response in the fungus *Trichoderma atroviride*. *Front Plant Sci*, *5*, 659. doi:10.3389/fpls.2014.00659
- Mehta, K. D. (2014). Emerging role of protein kinase C in energy homeostasis: A brief overview. *World J Diabetes*, *5*(3), 385-392. doi:10.4239/wjdv5.i3.385
- Melchionna, R., Chen, X. B., Blasina, A., & McGowan, C. H. (2000). Threonine 68 is required for radiation-induced phosphorylation and activation of Cds1. *Nat Cell Biol*, *2*(10), 762-765. doi:10.1038/35036406

- Mikkers, H., Nawijn, M., Allen, J., Brouwers, C., Verhoeven, E., Jonkers, J., & Berns, A. (2004). Mice deficient for all PIM kinases display reduced body size and impaired responses to hematopoietic growth factors. *Mol Cell Biol*, 24(13), 6104-6115. doi:10.1128/MCB.24.13.6104-6115.2004
- Miller, C. J., & Davidson, L. A. (2013). The interplay between cell signalling and mechanics in developmental processes. *Nat Rev Genet*, 14(10), 733-744. doi:10.1038/nrg3513
- Moonen, M. P. B., Nascimento, E. B. M., & van Marken Lichtenbelt, W. D. (2019). Human brown adipose tissue: Underestimated target in metabolic disease? *Biochim Biophys Acta Mol Cell Biol Lipids*, 1864(1), 104-112. doi:10.1016/j.bbalip.2018.05.012
- Mordret, G. (1993). MAP kinase kinase: a node connecting multiple pathways. *Biol Cell*, 79(3), 193-207. Retrieved from <https://www.ncbi.nlm.nih.gov/pubmed/8004006>
- Morrison, D. K. (2001). KSR: a MAPK scaffold of the Ras pathway? *J Cell Sci*, 114(Pt 9), 1609-1612. Retrieved from <https://www.ncbi.nlm.nih.gov/pubmed/11309192>
- Motoshima, H., Wu, X., Sinha, M. K., Hardy, V. E., Rosato, E. L., Barbot, D. J., . . . Goldstein, B. J. (2002). Differential regulation of adiponectin secretion from cultured human omental and subcutaneous adipocytes: effects of insulin and rosiglitazone. *J Clin Endocrinol Metab*, 87(12), 5662-5667. doi:10.1210/jc.2002-020635
- Munk, S., Refsgaard, J. C., Olsen, J. V., & Jensen, L. J. (2016). From Phosphosites to Kinases. *Methods Mol Biol*, 1355, 307-321. doi:10.1007/978-1-4939-3049-4\_21
- Murray, A. W. (2004). Recycling the cell cycle: cyclins revisited. *Cell*, 116(2), 221-234. Retrieved from <https://www.ncbi.nlm.nih.gov/pubmed/14744433>
- Nandipati, K. C., Subramanian, S., & Agrawal, D. K. (2017). Protein kinases: mechanisms and downstream targets in inflammation-mediated obesity and insulin resistance. *Mol Cell Biochem*, 426(1-2), 27-45. doi:10.1007/s11010-016-2878-8
- Narlik-Grassow, M., Blanco-Aparicio, C., & Carnero, A. (2014). The PIM family of serine/threonine kinases in cancer. *Med Res Rev*, 34(1), 136-159. doi:10.1002/med.21284
- Narlik-Grassow, M., Blanco-Aparicio, C., Cecilia, Y., Peregrina, S., Garcia-Serelde, B., Munoz-Galvan, S., . . . Carnero, A. (2012). The essential role of PIM kinases in sarcoma growth and bone invasion. *Carcinogenesis*, 33(8), 1479-1486. doi:10.1093/carcin/bgs176
- Nguyen, M. T., Favelyukis, S., Nguyen, A. K., Reichart, D., Scott, P. A., Jenn, A., . . . Olefsky, J. M. (2007). A subpopulation of macrophages infiltrates hypertrophic adipose tissue and is activated by free fatty acids via Toll-like receptors 2 and 4 and JNK-dependent pathways. *J Biol Chem*, 282(48), 35279-35292. doi:10.1074/jbc.M706762200
- Ni, X., Zhang, L., Peng, M., Shen, T. W., Yu, X. S., Shan, L. Y., . . . Ma, K. T. (2018). Hydrogen Sulfide Attenuates Hypertensive Inflammation via Regulating Connexin Expression in Spontaneously Hypertensive Rats. *Med Sci Monit*, 24, 1205-1218. Retrieved from <https://www.ncbi.nlm.nih.gov/pubmed/29485979>
- Nihira, K., Ando, Y., Yamaguchi, T., Kagami, Y., Miki, Y., & Yoshida, K. (2009). Pim-1 controls NF-κB signalling by stabilizing RelA/p65. *Cell Death And Differentiation*, 17, 689. doi:10.1038/cdd.2009.174  
<https://www.nature.com/articles/cdd2009174#supplementary-information>
- O'Sullivan, J., Bitu, C. C., Daly, S. B., Urquhart, J. E., Barron, M. J., Bhaskar, S. S., . . . Dixon, M. J. (2011). Whole-Exome sequencing identifies FAM20A mutations as a cause of amelogenesis imperfecta and gingival hyperplasia syndrome. *Am J Hum Genet*, 88(5), 616-620. doi:10.1016/j.ajhg.2011.04.005

- Orava, J., Nuutila, P., Lidell, M. E., Oikonen, V., Noponen, T., Viljanen, T., . . . Virtanen, K. A. (2011). Different metabolic responses of human brown adipose tissue to activation by cold and insulin. *Cell Metab*, *14*(2), 272-279. doi:10.1016/j.cmet.2011.06.012
- Otto, T. C., & Lane, M. D. (2005). Adipose development: from stem cell to adipocyte. *Crit Rev Biochem Mol Biol*, *40*(4), 229-242. doi:10.1080/10409230591008189
- Ouellet, V., Routhier-Labadie, A., Bellemare, W., Lakhal-Chaieb, L., Turcotte, E., Carpentier, A. C., & Richard, D. (2011). Outdoor temperature, age, sex, body mass index, and diabetic status determine the prevalence, mass, and glucose-uptake activity of 18F-FDG-detected BAT in humans. *J Clin Endocrinol Metab*, *96*(1), 192-199. doi:10.1210/jc.2010-0989
- Pandit, N. K., & Soltis, R. P. (2012). *Introduction to the pharmaceutical sciences : an integrated approach* (2nd ed.). Baltimore, MD: Lippincott Williams & Wilkins.
- Paniagua, J. A. (2016). Nutrition, insulin resistance and dysfunctional adipose tissue determine the different components of metabolic syndrome. *World J Diabetes*, *7*(19), 483-514. doi:10.4239/wjd.v7.i19.483
- Patsouris, D., Li, P. P., Thapar, D., Chapman, J., Olefsky, J. M., & Neels, J. G. (2008). Ablation of CD11c-positive cells normalizes insulin sensitivity in obese insulin resistant animals. *Cell Metab*, *8*(4), 301-309. doi:10.1016/j.cmet.2008.08.015
- Patterson, H., Nibbs, R., McInnes, I., & Siebert, S. (2014). Protein kinase inhibitors in the treatment of inflammatory and autoimmune diseases. *Clin Exp Immunol*, *176*(1), 1-10. doi:10.1111/cei.12248
- Pawson, T. (2002). Regulation and targets of receptor tyrosine kinases. *Eur J Cancer*, *38 Suppl 5*, S3-10. Retrieved from <https://www.ncbi.nlm.nih.gov/pubmed/12528767>
- Pradhan, R. N., Bues, J. J., Gardeux, V., Schwalie, P. C., Alpern, D., Chen, W., . . . Deplancke, B. (2017). Dissecting the brown adipogenic regulatory network using integrative genomics. *Sci Rep*, *7*, 42130. doi:10.1038/srep42130
- Qian, K. C., Wang, L., Hickey, E. R., Studts, J., Barringer, K., Peng, C., . . . Farmer, B. (2005). Structural basis of constitutive activity and a unique nucleotide binding mode of human Pim-1 kinase. *J Biol Chem*, *280*(7), 6130-6137. doi:10.1074/jbc.M409123200
- Rajakulendran, T., & Sicheri, F. (2010). Allosteric protein kinase regulation by pseudokinases: insights from STRAD. *Sci Signal*, *3*(111), pe8. doi:10.1126/scisignal.3111pe8
- Raju, S., & Shaw, A. S. (2015). What is the point of pseudokinases? *Elife*, *4*, e07771. doi:10.7554/eLife.07771
- Rane, S. G., Dubus, P., Mettus, R. V., Galbreath, E. J., Boden, G., Reddy, E. P., & Barbacid, M. (1999). Loss of Cdk4 expression causes insulin-deficient diabetes and Cdk4 activation results in beta-islet cell hyperplasia. *Nat Genet*, *22*(1), 44-52. doi:10.1038/8751
- Reddy, N. L., Tan, B. K., Barber, T. M., & Randevara, H. S. (2014). Brown adipose tissue: endocrine determinants of function and therapeutic manipulation as a novel treatment strategy for obesity. *BMC Obes*, *1*, 13. doi:10.1186/s40608-014-0013-5
- Robinson, D. R., Wu, Y. M., & Lin, S. F. (2000). The protein tyrosine kinase family of the human genome. *Oncogene*, *19*(49), 5548-5557. doi:10.1038/sj.onc.1203957
- Ronco, C., Martin, A. R., Demange, L., & Benhida, R. (2017). ATM, ATR, CHK1, CHK2 and WEE1 inhibitors in cancer and cancer stem cells. *Medchemcomm*, *8*(2), 295-319. doi:10.1039/c6md00439c
- Rosen, E. D., & Spiegelman, B. M. (2014). What we talk about when we talk about fat. *Cell*, *156*(1-2), 20-44. doi:10.1016/j.cell.2013.12.012

- Ruderman, N. B., Carling, D., Prentki, M., & Cacicedo, J. M. (2013). AMPK, insulin resistance, and the metabolic syndrome. *J Clin Invest*, *123*(7), 2764-2772. doi:10.1172/JCI67227
- Saito, M., Okamatsu-Ogura, Y., Matsushita, M., Watanabe, K., Yoneshiro, T., Nio-Kobayashi, J., . . . Tsujisaki, M. (2009). High incidence of metabolically active brown adipose tissue in healthy adult humans: effects of cold exposure and adiposity. *Diabetes*, *58*(7), 1526-1531. doi:10.2337/db09-0530
- Saltiel, A. R., & Kahn, C. R. (2001). Insulin signalling and the regulation of glucose and lipid metabolism. *Nature*, *414*(6865), 799-806. doi:10.1038/414799a
- Schlessinger, J. (2014). Receptor tyrosine kinases: legacy of the first two decades. *Cold Spring Harb Perspect Biol*, *6*(3). doi:10.1101/cshperspect.a008912
- Schulz, T. J., Huang, P., Huang, T. L., Xue, R., McDougall, L. E., Townsend, K. L., . . . Tseng, Y. H. (2013). Brown-fat paucity due to impaired BMP signalling induces compensatory browning of white fat. *Nature*, *495*(7441), 379-383. doi:10.1038/nature11943
- Segaliny, A. I., Tellez-Gabriel, M., Heymann, M. F., & Heymann, D. (2015). Receptor tyrosine kinases: Characterisation, mechanism of action and therapeutic interests for bone cancers. *J Bone Oncol*, *4*(1), 1-12. doi:10.1016/j.jbo.2015.01.001
- Serena, C., Keiran, N., Ceperuelo-Mallafre, V., Ejarque, M., Fradera, R., Roche, K., . . . Fernandez-Veledo, S. (2016). Obesity and Type 2 Diabetes Alters the Immune Properties of Human Adipose Derived Stem Cells. *Stem Cells*, *34*(10), 2559-2573. doi:10.1002/stem.2429
- Serena, C., Keiran, N., Madeira, A., Maymo-Masip, E., Ejarque, M., Terron-Puig, M., . . . Vendrell, J. (2017). Crohn's Disease Disturbs the Immune Properties of Human Adipose-Derived Stem Cells Related to Inflammasome Activation. *Stem Cell Reports*, *9*(4), 1109-1123. doi:10.1016/j.stemcr.2017.07.014
- Shah, N., Pang, B., Yeoh, K. G., Thorn, S., Chen, C. S., Lilly, M. B., & Salto-Tellez, M. (2008). Potential roles for the PIM1 kinase in human cancer - a molecular and therapeutic appraisal. *Eur J Cancer*, *44*(15), 2144-2151. doi:10.1016/j.ejca.2008.06.044
- Shaik, A. A., Qiu, B., Wee, S., Choi, H., Gunaratne, J., & Tergaonkar, V. (2016). Phosphoprotein network analysis of white adipose tissues unveils deregulated pathways in response to high-fat diet. *Sci Rep*, *6*, 25844. doi:10.1038/srep25844
- Shaw, A. S., Kornev, A. P., Hu, J., Ahuja, L. G., & Taylor, S. S. (2014). Kinases and pseudokinases: lessons from RAF. *Mol Cell Biol*, *34*(9), 1538-1546. doi:10.1128/MCB.00057-14
- Simpson, M. A., Hsu, R., Keir, L. S., Hao, J., Sivapalan, G., Ernst, L. M., . . . Crosby, A. H. (2007). Mutations in FAM20C are associated with lethal osteosclerotic bone dysplasia (Raine syndrome), highlighting a crucial molecule in bone development. *Am J Hum Genet*, *81*(5), 906-912. doi:10.1086/522240
- Singhal, S., Amin, K. M., Kruklitis, R., DeLong, P., Friscia, M. E., Litzky, L. A., . . . Albelda, S. M. (2003). Alterations in cell cycle genes in early stage lung adenocarcinoma identified by expression profiling. *Cancer Biol Ther*, *2*(3), 291-298. Retrieved from <https://www.ncbi.nlm.nih.gov/pubmed/12878869>
- Smitka, K., & Maresova, D. (2015). Adipose Tissue as an Endocrine Organ: An Update on Pro-inflammatory and Anti-inflammatory Microenvironment. *Prague Med Rep*, *116*(2), 87-111. doi:10.14712/23362936.2015.49
- Solinas, G., Vilcu, C., Neels, J. G., Bandyopadhyay, G. K., Luo, J. L., Naugler, W., . . . Karin, M. (2007). JNK1 in hematopoietically derived cells contributes to diet-induced inflammation and insulin

- resistance without affecting obesity. *Cell Metab*, 6(5), 386-397. doi:10.1016/j.cmet.2007.09.011
- Somvanshi, P. R., & Venkatesh, K. V. (2014). A conceptual review on systems biology in health and diseases: from biological networks to modern therapeutics. *Syst Synth Biol*, 8(1), 99-116. doi:10.1007/s11693-013-9125-3
- Stephens, J. M., Lee, J., & Pilch, P. F. (1997). Tumor necrosis factor-alpha-induced insulin resistance in 3T3-L1 adipocytes is accompanied by a loss of insulin receptor substrate-1 and GLUT4 expression without a loss of insulin receptor-mediated signal transduction. *J Biol Chem*, 272(2), 971-976. Retrieved from <https://www.ncbi.nlm.nih.gov/pubmed/8995390>
- Sun, W., Yao, S., Tang, J., Liu, S., Chen, J., Deng, D., & Zeng, C. (2018). Integrative analysis of super enhancer SNPs for type 2 diabetes. *PLoS One*, 13(1), e0192105. doi:10.1371/journal.pone.0192105
- Sun, Z., Hsiao, J., Fay, D. S., & Stern, D. F. (1998). Rad53 FHA domain associated with phosphorylated Rad9 in the DNA damage checkpoint. *Science*, 281(5374), 272-274. Retrieved from <https://www.ncbi.nlm.nih.gov/pubmed/9657725>
- Takai, E., Tsukimoto, M., Harada, H., Sawada, K., Moriyama, Y., & Kojima, S. (2012). Autocrine regulation of TGF-beta1-induced cell migration by exocytosis of ATP and activation of P2 receptors in human lung cancer cells. *J Cell Sci*, 125(Pt 21), 5051-5060. doi:10.1242/jcs.104976
- Tominaga, K., Morisaki, H., Kaneko, Y., Fujimoto, A., Tanaka, T., Ohtsubo, M., . . . Nakanishi, M. (1999). Role of human Cds1 (Chk2) kinase in DNA damage checkpoint and its regulation by p53. *J Biol Chem*, 274(44), 31463-31467. Retrieved from <https://www.ncbi.nlm.nih.gov/pubmed/10531348>
- Townsend, K. L., & Tseng, Y. H. (2014). Brown fat fuel utilization and thermogenesis. *Trends Endocrinol Metab*, 25(4), 168-177. doi:10.1016/j.tem.2013.12.004
- Turnham, R. E., & Scott, J. D. (2016). Protein kinase A catalytic subunit isoform PRKACA; History, function and physiology. *Gene*, 577(2), 101-108. doi:10.1016/j.gene.2015.11.052
- Ubersax, J. A., & Ferrell, J. E., Jr. (2007). Mechanisms of specificity in protein phosphorylation. *Nat Rev Mol Cell Biol*, 8(7), 530-541. doi:10.1038/nrm2203
- van Marken Lichtenbelt, W. D., Vanhommerig, J. W., Smulders, N. M., Drossaerts, J. M., Kemerink, G. J., Bouvy, N. D., . . . Teule, G. J. (2009). Cold-activated brown adipose tissue in healthy men. *N Engl J Med*, 360(15), 1500-1508. doi:10.1056/NEJMoa0808718
- Vergoni, B., Cornejo, P. J., Gilleron, J., Djedaini, M., Ceppo, F., Jacquet, A., . . . Cormont, M. (2016). DNA Damage and the Activation of the p53 Pathway Mediate Alterations in Metabolic and Secretory Functions of Adipocytes. *Diabetes*, 65(10), 3062-3074. doi:10.2337/db16-0014
- Virtanen, K. A., Lidell, M. E., Orava, J., Heglind, M., Westergren, R., Niemi, T., . . . Nuutila, P. (2009). Functional brown adipose tissue in healthy adults. *N Engl J Med*, 360(15), 1518-1525. doi:10.1056/NEJMoa0808949
- Vlahopoulos, S. A., Cen, O., Hengen, N., Agan, J., Moschovi, M., Critselis, E., . . . Chrousos, G. P. (2015). Dynamic aberrant NF-kappaB spurs tumorigenesis: a new model encompassing the microenvironment. *Cytokine Growth Factor Rev*, 26(4), 389-403. doi:10.1016/j.cytogfr.2015.06.001
- Wajchenberg, B. L., Giannella-Neto, D., da Silva, M. E., & Santos, R. F. (2002). Depot-specific hormonal characteristics of subcutaneous and visceral adipose tissue and their relation to the metabolic syndrome. *Horm Metab Res*, 34(11-12), 616-621. doi:10.1055/s-2002-38256

- Wang, H. Y., Ducommun, S., Quan, C., Xie, B., Li, M., Wasserman, D. H., . . . Chen, S. (2013). AS160 deficiency causes whole-body insulin resistance via composite effects in multiple tissues. *Biochem J*, *449*(2), 479-489. doi:10.1042/BJ20120702
- Wang, K., Grivennikov, S. I., & Karin, M. (2013). Implications of anti-cytokine therapy in colorectal cancer and autoimmune diseases. *Ann Rheum Dis*, *72 Suppl 2*, ii100-103. doi:10.1136/annrheumdis-2012-202201
- Wang, S., Liang, X., Yang, Q., Fu, X., Rogers, C. J., Zhu, M., . . . Du, M. (2015). Resveratrol induces brown-like adipocyte formation in white fat through activation of AMP-activated protein kinase (AMPK) alpha1. *Int J Obes (Lond)*, *39*(6), 967-976. doi:10.1038/ijo.2015.23
- Wang, Y. C., McPherson, K., Marsh, T., Gortmaker, S. L., & Brown, M. (2011). Health and economic burden of the projected obesity trends in the USA and the UK. *Lancet*, *378*(9793), 815-825. doi:10.1016/S0140-6736(11)60814-3
- Wang, Z., Bhattacharya, N., Meyer, M. K., Seimiya, H., Tsuruo, T., Tonani, J. A., & Magnuson, N. S. (2001). Pim-1 negatively regulates the activity of PTP-U2S phosphatase and influences terminal differentiation and apoptosis of monoblastoid leukemia cells. *Arch Biochem Biophys*, *390*(1), 9-18. doi:10.1006/abbi.2001.2370
- Warfel, N. A., & Kraft, A. S. (2015). PIM kinase (and Akt) biology and signaling in tumors. *Pharmacol Ther*, *151*, 41-49. doi:10.1016/j.pharmthera.2015.03.001
- Weisberg, S. P., McCann, D., Desai, M., Rosenbaum, M., Leibel, R. L., & Ferrante, A. W., Jr. (2003). Obesity is associated with macrophage accumulation in adipose tissue. *J Clin Invest*, *112*(12), 1796-1808. doi:10.1172/JCI19246
- Weiss, A., & Littman, D. R. (1994). Signal transduction by lymphocyte antigen receptors. *Cell*, *76*(2), 263-274. Retrieved from <https://www.ncbi.nlm.nih.gov/pubmed/8293463>
- Weitzman, S. A., & Gordon, L. I. (1990). Inflammation and cancer: role of phagocyte-generated oxidants in carcinogenesis. *Blood*, *76*(4), 655-663. Retrieved from <https://www.ncbi.nlm.nih.gov/pubmed/2200535>
- Wildman, R. P., Muntner, P., Reynolds, K., McGinn, A. P., Rajpathak, S., Wylie-Rosett, J., & Sowers, M. R. (2008). The obese without cardiometabolic risk factor clustering and the normal weight with cardiometabolic risk factor clustering: prevalence and correlates of 2 phenotypes among the US population (NHANES 1999-2004). *Arch Intern Med*, *168*(15), 1617-1624. doi:10.1001/archinte.168.15.1617
- Wrana, J. L., Attisano, L., Wieser, R., Ventura, F., & Massague, J. (1994). Mechanism of activation of the TGF-beta receptor. *Nature*, *370*(6488), 341-347. doi:10.1038/370341a0
- Wu, Y., Deng, Y., Zhu, J., Duan, Y., Weng, W., & Wu, X. (2018). Pim1 promotes cell proliferation and regulates glycolysis via interaction with MYC in ovarian cancer. *Onco Targets Ther*, *11*, 6647-6656. doi:10.2147/OTT.S180520
- Xu, H., Barnes, G. T., Yang, Q., Tan, G., Yang, D., Chou, C. J., . . . Chen, H. (2003). Chronic inflammation in fat plays a crucial role in the development of obesity-related insulin resistance. *J Clin Invest*, *112*(12), 1821-1830. doi:10.1172/JCI19451
- Yang, D. Q., & Kastan, M. B. (2000). Participation of ATM in insulin signalling through phosphorylation of eIF-4E-binding protein 1. *Nat Cell Biol*, *2*(12), 893-898. doi:10.1038/35046542
- Ye, J. (2013). Mechanisms of insulin resistance in obesity. *Front Med*, *7*(1), 14-24. doi:10.1007/s11684-013-0262-6
- Zannini, L., Delia, D., & Buscemi, G. (2014). CHK2 kinase in the DNA damage response and beyond. *J Mol Cell Biol*, *6*(6), 442-457. doi:10.1093/jmcb/mju045

- Zeke, A., Misheva, M., Remenyi, A., & Bogoyevitch, M. A. (2016). JNK Signaling: Regulation and Functions Based on Complex Protein-Protein Partnerships. *Microbiol Mol Biol Rev*, 80(3), 793-835. doi:10.1128/MMBR.00043-14
- Zervas, C. G., & Brown, N. H. (2002). Integrin adhesion: when is a kinase a kinase? *Curr Biol*, 12(10), R350-351. Retrieved from <https://www.ncbi.nlm.nih.gov/pubmed/12015134>
- Zhang, B. B., Zhou, G., & Li, C. (2009). AMPK: an emerging drug target for diabetes and the metabolic syndrome. *Cell Metab*, 9(5), 407-416. doi:10.1016/j.cmet.2009.03.012
- Zhong, X. Y., Xu, X. X., Yu, J. H., Jiang, G. X., Yu, Y., Tai, S., . . . Cui, Y. F. (2012). Clinical and biological significance of Cdk10 in hepatocellular carcinoma. *Gene*, 498(1), 68-74. doi:10.1016/j.gene.2012.01.022
- Zingaretti, M. C., Crosta, F., Vitali, A., Guerrieri, M., Frontini, A., Cannon, B., . . . Cinti, S. (2009). The presence of UCP1 demonstrates that metabolically active adipose tissue in the neck of adult humans truly represents brown adipose tissue. *FASEB J*, 23(9), 3113-3120. doi:10.1096/fj.09-133546

---

# *Appendix A*

---

## **Cancer: Linking Powerhouses to Suicidal Bags**

(Martinez-Carreres, Nasrallah, & Fajas, 2017)

Throughout my PhD studies, I had the chance to co-author a review that shed light on the crosstalk between the mitochondria and the lysosomes in cancer. We covered the different signaling pathways, as well as the available therapeutic approaches targeting both organelles. We also provided an insight for future perspectives in the field.





# Cancer: Linking Powerhouses to Suicidal Bags

Laia Martinez-Carreres<sup>†</sup>, Anita Nasrallah<sup>†</sup> and Lluís Fajas<sup>\*</sup>

Cancer and Metabolism Laboratory, Center for Integrative Genomics, University of Lausanne, Lausanne, Switzerland

Membrane-bound organelles are integrated into cellular networks and work together for a common goal: regulating cell metabolism, cell signaling pathways, cell fate, cellular maintenance, and pathogen defense. Many of these interactions are well established, but little is known about the interplay between mitochondria and lysosomes, and their deregulation in cancer. The present review focuses on the common signaling pathways of both organelles, as well as the processes in which they both physically interact, their changes under pathological conditions, and the impact on targeting those organelles for treating cancer.

## OPEN ACCESS

### Edited by:

Cristina Mammucari,  
University of Padua, Italy

### Reviewed by:

Valeria Poli,  
University of Turin, Italy  
Darren Boehning,  
University of Texas Health Science  
Center at Houston, United States  
Manuela Côrte-Real,  
University of Minho, Portugal

### \*Correspondence:

Lluís Fajas  
lluís.fajas@unil.ch

<sup>†</sup>These authors have contributed  
equally to this work.

### Specialty section:

This article was submitted to  
Molecular and Cellular Oncology,  
a section of the journal  
Frontiers in Oncology

Received: 16 June 2017

Accepted: 21 August 2017

Published: 06 September 2017

### Citation:

Martinez-Carreres L, Nasrallah A and  
Fajas L (2017) Cancer: Linking  
Powerhouses  
to Suicidal Bags.  
Front. Oncol. 7:204.  
doi: 10.3389/fonc.2017.00204

**Keywords:** cancer, mitochondria, lysosomes, mammalian target of rapamycin, Rab7, AMP-activated protein kinase, mitophagy, lysosomal membrane permeabilization

## INTRODUCTION

Cancer is characterized by the unrestricted cellular growth and proliferation of abnormal cells. It exhibits properties of motility, invasion, angiogenesis, and metastasis. Recent studies identified diverse mechanisms of metabolic plasticity in cancer cells. These include increased glucose uptake in most tumors, elevated glycolytic intermediates, increased pentose phosphate pathway activities, increased glutamine catabolism, and increased use of lactate as a fuel in selective tumors (1).

According to the American Cancer Society, it is estimated that, in the US, almost 1.7 million new cases of cancer will be diagnosed in 2017. Mostly, general cancer treatments are limited to radiation, chemotherapy, and surgery. However, these treatments encounter non-specific distribution of chemotherapeutic agents, insufficient drug concentrations to reach the tumor, and restricted ability to survey therapeutic responses (2). More efforts are targeted to find new therapies to help overpass these obstacles. Subcellular targeting is beneficial for therapy in several scenarios (3): (1) basic organelle malfunctions could be targeted, making the process more selective; (2) the quantity of drug required could be significantly reduced because of its specificity, which eventually helps in decreasing side effects; and (3) most importantly, intracellular drug targeting may surpass dangerous drawbacks of drug actions in cancer therapy, i.e., multidrug resistance (4, 5).

In most of the mechanisms of cancer initiation and progression, different organelles are involved, especially mitochondria and lysosomes, for their relevance in energy homeostasis and cell death (6). The purpose of this review is to shed light on the roles of mitochondria and lysosomes in cancer, as well as them being prominent targets for cancer therapy.

## THE ROLE OF MITOCHONDRIA IN CANCER

Mitochondria, also called “powerhouses” of cells, are double membrane organelles, with their own genome, thought to have been originated from an ancient symbiosis that resulted when a nucleated cell engulfed an aerobic prokaryote. Through evolution, mitochondria conserved only a small part of prokaryotic bacterial genes, including the ones encoding 13 proteins of the respiratory chain (7).

In this manner, mitochondria gained a central role in the regulation of metabolism, cell proliferation, and apoptosis, while many tasks were transmitted to the host cells (8).

Other than being cell's powerhouses, mitochondria function as signaling organelles. They coordinate distinct metabolic pathways, producing metabolites required for cell survival and proliferation (9). In fact, mitochondria are key players in the calcium-signaling pathway (10). When toxic stimuli damage the cell, mitochondria release pro-apoptotic molecules, such as cytochrome *c*, thus regulating cell death (11). Moreover, mitochondria are established as the major site of production of free radicals, which are major signaling molecules in the cell (12). Recently, it has been shown that mitochondrial metabolites do not only have intermediary roles in energy generation but can also promote regulatory effects on post-translational modifications of proteins (13), as well as affecting chromatin structure and function (14).

Multiple human diseases have been strongly associated with impaired mitochondrial homeostasis. These include liver and cardiovascular diseases, neurological and muscular disorders, seizures, susceptibility to infections, and cancer (15–18). In cancer, mitochondrial roles vary as a function of genetic and environmental differences, as well as the tissue-of-origin of the diverse types of cancer. The main mitochondrial processes contributing to tumorigenesis include mitochondrial biogenesis and mitophagy, fission and fusion dynamics, metabolism, oxidative stress, and cell death (19).

Compared to normal cells, cancer cells show many alterations in energy metabolism. In the 1920s, cancer metabolism studies commenced with Otto Warburg's observation: to produce energy, cancer cells rely less on mitochondrial respiration and more on glycolysis. Warburg hypothesized that mitochondria must be dysfunctional, taking into consideration that glycolysis gives a lot less energy as compared to mitochondrial respiration (20). However, other scientists believed that the reduced mitochondrial activity is due to higher glycolysis. In some cases, Warburg's proposal holds true. Nevertheless, there are reports showing that the mitochondrial function in cancer cells in some cases is intact, or mitochondrial biogenesis is increased (21).

Mitochondrial biogenesis could be described as the division and growth of pre-existing mitochondria. It is regulated at the transcriptional and post-transcriptional levels of gene expression (22). Regulating mitochondrial biogenesis is an attractive target of key oncogenic signaling pathways, since cancer cells induce it to increase ATP production for cellular proliferation. PGC-1 $\alpha$ , through its interactions with numerous transcription factors, is a central regulator of mitochondrial biogenesis (23). It portrays a dual effect on cancer viability. On the one hand, PGC-1 $\alpha$  acts as a tumor suppressor in some cancers, resulting in induced apoptosis upon overexpression. In human epithelial ovarian cancer, apoptosis was induced *via* the organized regulation of Bcl-2 and Bcl-2-associated X protein (BAX) expression by PGC-1 $\alpha$  (24). PGC-1 $\alpha$  is considered a tumor suppressor not only because it induces apoptosis but also because it has been found to suppress the metastatic abilities of tumor cells *via* the direct regulation of transcriptional machinery (25, 26). For example, PGC-1 $\alpha$  directly increases ID2 transcription that binds

to the transcription factor TCF4, rendering it inactive. This in turn leads to a downregulation in metastasis-related genes, such as integrins, that are able to influence metastasis and invasion (25). On the other hand, the ability of PGC-1 $\alpha$  in sustaining metabolic homeostasis can also promote cancer cell survival and tumor metastasis (27). In cancer cells, silencing PGC-1 $\alpha$  resulted in deferred invasive potential and weakened metastatic ability without affecting proliferation and tumor growth. Consistently, the transition from primary lung tumor cells to metastatic cancer cells was coupled with more dependence on mitochondrial respiration, *via* PGC-1 $\alpha$ , leading to an upregulation of PGC-1 $\beta$ , ERR $\alpha$ , and NRF1, which are mitochondrial-related biogenesis genes (28).

Another key activator of mitochondrial biogenesis in cancer is *c-Myc*, a transcription factor regulating cell cycle, proliferation, metabolism and cell death. Studies have demonstrated that the loss or gain of *Myc* decreases or increases mitochondrial mass, respectively. This is due to the fact that over 400 mitochondrial genes are identified as targets of *c-Myc* (29). A third effector of mitochondrial biogenesis is mammalian target of rapamycin (mTOR). It controls mitochondrial gene expression through the activation of PGC-1 $\alpha$ /YY1 and represses the inhibitory 4E-BPs (eukaryotic translation initiation factor 4E-binding protein 1) that downregulates the translation of mitochondrial proteins (30).

During tumorigenesis, mitochondrial dynamics is very important. It determines the equilibrium between cell death programs and mitochondrial energy production. Several studies demonstrated, in cancer, an imbalance in mitochondrial fission and fusion activities, depicted in decreased fusion, and/or elevated fission that resulted in fragmented mitochondrial networks *via* the K-Ras-DRK1/2-Drp1 pathway (31, 32). Also, *c-Myc* affects mitochondrial dynamics by altering the expression of proteins implicated in the fission and fusion processes (33).

Furthermore, mitochondria have a tight relationship with the intrinsic (also called mitochondrial) apoptotic cell death program, since B-cell lymphoma-2 (BCL-2) family of proteins regulates the integrity of the outer mitochondrial membrane (OMM). Mainly two members of this family, BAX and Bcl-2-associated killer (BAK) can break the OMM in response to apoptotic stimuli. This releases apoptogenic factors from inside mitochondria, such as cytochrome *c*, inducing activation of caspases and subsequent cell death. In some cases, mitochondria can also participate in the extrinsic apoptotic pathway, which is initiated by cell membrane death receptors. For example, FAS receptor can truncate Bid protein, another member of the BCL-2 family, *via* caspase 8. Truncated Bid (tBid) can then translocate to mitochondria to induce apoptosis (34).

Mitochondrial morphology is a hallmark for apoptotic susceptibility. Even though fission and fusion do not regulate apoptosis *per se*, the generated mitochondrial morphology supports the interaction with pro-apoptotic Bcl-2 proteins. Thus, mitochondrial hyper-fragmentation causes resistance to apoptosis due to the inability of mitochondrial membranes to interact with pro-apoptotic proteins (35).

Mitochondria play major roles in metabolic reprogramming, including the synthesis of macromolecules and cellular survival (1). One mechanism by which cancer drives these alterations in

metabolism is limiting pyruvate utilization by the mitochondria. This is achieved by regulating pyruvate kinases such as PKM isoforms (36), as well as downregulating mitochondrial pyruvate carriers: MPC1 and MPC2 (37). Moreover, in some tumor types, mutations in the enzymes of the tricarboxylic acid (TCA) cycle render the mitochondria dysfunctional. Cells from such tumors use glutamine-dependent reductive carboxylation rather than oxidative metabolism as the major pathway of citrate formation. This, in turn, leads to the major reprogramming of amino acid metabolism and lipid synthesis (38).

There are multiple levels at which both mitochondrial biology and tumorigenic signaling vastly intersect. First, cellular physiology and tumorigenesis are affected by direct signals from mitochondria. Metabolites generated by the mitochondrial pathways affect gene transcription through chromatin modification, and cytosolic signaling pathways (19). For example, the TCA cycle intermediate  $\alpha$ -ketoglutarate ( $\alpha$ -KG) is a co-substrate for many enzymes in the cytoplasm and nucleus, including families of chromatin-modifying ones. In the case of chromatin regulation, glutamine-derived  $\alpha$ -KG contributes to TET-dependent demethylation reactions (38). Second, many mutations were identified as directly associated with cancer risk (39). Cancer can be caused by mutations in nuclear-encoding genes, such as electron transporter chain (ETC) genes. For example, patients suffering from paraganglioma often presents dysfunctions in succinate dehydrogenase (SDH). Mutations of the same complex have also been found in other cancers, such as gastrointestinal stromal cancer, breast cancer, or renal carcinomas. Other enzymes such as fumarate hydratase (FH) have also found to be mutated in other cancers. When the function of these enzymes is lost, the metabolic intermediates fumarate and succinate accumulate, which in turn function as oncometabolites when found in excess (40, 41). In addition, mitochondrial DNA mutations (amplifications, deletions, point mutations, etc.) have been associated with various cancers (42). For example, point mutations in MT-ND1 gene modify complex I activity, having an influence on the tumorigenic characteristics of cells. Finally, and in order to support tumorigenesis, classical oncogenic signaling pathways alter mitochondrial functions. These include the *c-Myc*, p53, mTOR, and *k-Ras* signaling pathways (19). In addition, a main function of mitochondria is synthesizing aspartate for nucleotide synthesis, inducing cellular proliferation (43).

Mitochondria are complex organelles affecting cancer at many levels: initiation, proliferation, survival, or metastasis. One type of the various organelles that communicate with mitochondria is lysosomes. Mainly, this crosstalk depends on mitochondrial stress and/or destabilization of lysosomal membranes (44).

## THE ROLE OF LYSOSOMES IN CANCER

Also known as “suicidal bags,” lysosomes were first described in 1950s by Christian de Duve as membrane-enclosed vesicles containing hydrolases. Functioning as a digestive system, they are found in all eukaryotic cells, except for mature erythrocytes. The hydrolytic enzymes that they contain include proteases, nucleases, and lipases that can break down proteins, nucleic acids, and lipids, respectively, to their simplest subunits (45).

Lysosomes are formed when material from outside the cell is internalized in clathrin-coated endocytic vesicles forming early endosomes. Endosomal maturation occurs with the delivery of lysosomal acid hydrolases from the trans Golgi network, which contribute lowering of the internal pH to about 5.5. Late endosomes then mature into lysosomes as they acquire a full complement of acid hydrolases, which digest the molecules originally taken up by endocytosis, phagocytosis, and autophagy (46). Nevertheless, many investigations have proved that lysosomes are not only degradative organelles but also participate in metabolism of the entire cell at different levels, and their modifications can promote or repress cell proliferation.

On one hand, lysosomes undergo  $\text{Ca}^{2+}$  regulated exocytosis, which is secreting their content into the extracellular space, and repairing their damaged plasma membranes; when the plasma membrane is injured, lysosomes quickly move to the site of damage and fuse with the plasma membrane. This allows effective resealing (47). On the other hand, they can sense nutrient availability, which controls energy metabolism and mediates the starvation response (48). Zoncu et al. proposed that amino acids have to be detected in the lysosomal lumen, signaling to the Rag GTPases in a manner that is vacuolar  $\text{H}^{+}$ -ATPase (V-ATPase)-dependent. This is known as the “inside-out” mechanism (49). Leucine, among other amino acids, must accumulate in the lumen of the lysosome to trigger the central regulator of cellular and organismal growth, mammalian target of rapamycin complex I (mTORC1) (50). mTORC1 is recruited by Rag GTPases on the lysosomal surface in response to amino acids, the site of activation by Rheb (Ras homolog enriched in brain), when growth factor-stimulated PI3K–Akt signaling is on (51, 52). Upon amino acid and growth factors removal, Rag GTPases releases mTORC1, causing it to become cytoplasmic and inactive. In those conditions, the negative regulator of Rheb, tuberous sclerosis complex 2 (TSC2), is lysosomally localized. Thus, lysosomal proteins change depending on the nutrient status of the cells (53, 54).

Lysosomal biogenesis as well as autophagy is controlled by the main regulator of lysosomal genes, known as TFEB or transcription factor EB; when mTORC1 is active, TFEB remains inactive at the lysosomal membrane. Inactivated mTORC1 induces TFEB localization to the nucleus to activate lysosomal gene transcription (52, 55).

Since lysosomes also serve as platforms of activation of mTORC1, it is important to mention the dysregulation of this pathway in cancer. Indeed, mTORC1 regulates several anabolic processes that are critical for tumorigenesis: it promotes protein synthesis, aerobic glycolysis, *de novo* lipid synthesis, *de novo* nucleotide synthesis, and represses autophagy and lysosomal biogenesis (56–59). Genes that encode components of the PI3K–Akt–mTOR pathway are frequently mutated in cancer, but despite few mutations have been characterized in mTOR, many tumor types present mTOR hyperactivation, thus promoting tumorigenesis (60, 61).

In addition, lysosomal intracellular positioning is important for adhesion and motility (62), and important for mTOR signaling, autophagosome formation, and autophagosome-lysosome fusion, and changes depending on the nutrient availability. During starvation, mTORC1 activity is repressed, which

induces autophagosome formation. Starvation increases pH, causing lysosomes to cluster near the microtubule-organizing center (MTOC), facilitating autophagosome–lysosome fusion. Conversely, nutrient replenishment restores basal pH inducing lysosomal scattering, which brings lysosomal mTORC1 to the cell periphery and stimulates its activity by increasing its coupling to the gradient of signaling molecules emanating from the plasma membrane (63). Given that peripheral lysosomes inside the cell are responsible for cell adhesion and motility, targeting those lysosomes in cancer cells is also a good strategy for cancer treatment (62).

As de Duve already stated in the 1950s, lysosomal membrane permeabilization (LMP), consequently leading to the leakage of lysosomal content into the cytoplasm, induced what is known as “lysosomal cell death” (45, 64). Major players of this mechanism are lysosomal cathepsin proteases. They have apoptotic and/or necrotic features, depending on the cellular context and the extent of leakage occurring into the cytosol (65).

Lysosomes in cancer cells undergo major changes. In some cases, they have an increased volume and protease activity, along with an improved lysosomal protease secretion, as compared to lysosomes in normal cells. Thus, they become hyperactivated as a reaction to fulfill the needs of the challenging microenvironment of the tumorigenic cells (62). For example, they require the ingestion of huge amounts of adhesion molecules and extracellular matrix molecules, leading to an upregulation in exocytosis. Also, they have to move inside the cell to repair damaged membranes (66, 67). Recently, a correlation between lysosomal movement and tumor cell invasion was also established, which was induced by tumor microenvironment stimuli (68). In particular, acidic extracellular pH induced lysosomal movement toward the cell peripheries, successively leading to Cathepsin B exocytosis from the lysosomes. This eventually promoted protease-dependent tumor invasion (69, 70). *In vitro* studies with glioma cells have shown that inhibition of lysosomal exocytosis with vacuolin-1 is a good strategy for fighting against invasion in cancer (71).

As explained above, changes in the lysosomal compartment, in the presence of increased secretions of cysteine cathepsins, render these lysosomes pro-oncogenic. This results in an increased neoplastic progression, *via* proteolytic pathway initiation (72). Other than matrix remodeling, lysosomal role in degradation is crucial in tumorigenesis. This has been observed in reports revealing that specific intracellular cathepsin inhibitors are able to block collagen degradation, promoting tumor viability (73). However, cathepsins are also depicted as proteases with tumor suppressor abilities for their role in inducing cell death through LMP (74, 75).

Due to their role in cell death, autophagy, and deregulating metabolism, targeting lysosomes have a great therapeutic potential in cancer. Lysosomal proteins are indeed good targets for cancer treatment (76), such as lysosome-associated membrane protein 1 (LAMP-1). LAMP-1 is suggested to have a role in cell–cell adhesion and migration, since it was detected on the surface of highly metastatic cancer cells, particularly from colon cancer (77). V-ATPase is another significant lysosomal membrane protein participating in cancer. It functions as a pump of protons to create an acidic pH of lysosomes. Also, it regulates endocytotic

trafficking and affects the tumor microenvironment, by extruding protons into the extracellular matrix (78). Moreover, in tumor malignancy, V-ATPase participates not only in the dysregulation of lysosomal trafficking but also in mTORC1 activation and autophagy (79).

In addition, lysosomes are key players in cancer drug resistance. They can sequester cancer drugs into their acidic milieu, thus, blunting the drugs’ effects (80). This further proves that targeting lysosomes may be a promising new therapeutic strategy for cancer.

Since both organelles, mitochondria and lysosomes, share the power of majorly impacting the process of tumorigenesis, we will next further describe the main crosstalk between these two important organelles, shedding light on their interplay in cancer and their impact on cancer therapy.

## THE MITOCHONDRIAL–LYSOSOMAL INTERPLAY IN CANCER

In cancer, several important changes occur in all the organelles. However, the interplay between mitochondria and lysosomes is of high importance, because both organelles can interact to promote, in some cases cell death and in others tumorigenesis. There are two processes in which mitochondria and lysosomes work together: the first is LMP, a process in which enzymes from lysosomes can induce mitochondrial death pathway, and the second is mitophagy, a process in which lysosomes can degrade mitochondria, resulting in cell survival or cell death. Other than these two processes, there are several common effectors that play important roles in both organelles, which are also affected in cancer.

### Mitochondrial–Lysosomal Mechanisms Lysosomal Membrane Permeabilization

As mentioned above, LMP is a mechanism that induces two types of cell death: apoptosis induced by partial and selective LMP, and necrosis provoked by the complete disruption of lysosomes. One of the causes of apoptosis during LMP is the activation of caspases in the mitochondrial death pathway by mitochondrial outer membrane permeabilization (MOMP) (65).

Reactive oxygen species (ROS) and cathepsins are well-known mediators of LMP-triggered cell death (81). It has been reported that only cathepsin D in the cytoplasm is enough to induce MOMP and apoptosis in human fibroblasts. However, cathepsin D alone is not in all cases of LMP sufficient to induce cell death (65).

As shown in **Figure 1**, MOMP can be triggered by LMP in two manners: either Bid dependent or Bid independent. Bid is known as BH3-interacting-domain death agonist and belongs to the pro-apoptotic BH3-only Bcl-2 family. The Bid-dependent process occurs when Bid is cleaved by the active cathepsins at cytosolic pH (specially cathepsins B and D), after which Bid is capable to form pores at the OMM inducing MOMP and releasing cytochrome *c* from the mitochondria (81). Despite tBid is also known to activate BAX and BAK, in some cases, LMP can induce MOMP in a Bid-independent manner; cathepsins or

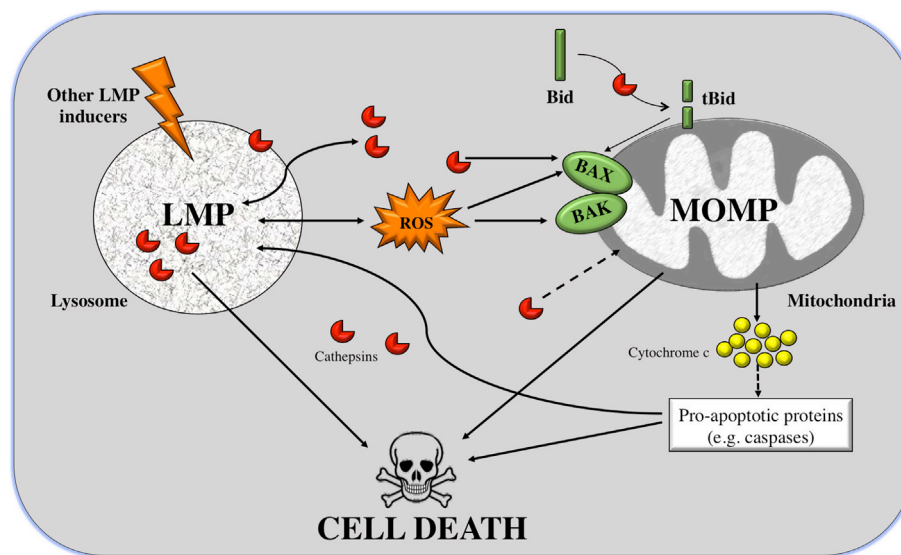


**FIGURE 1** | From lysosomal membrane permeabilization (LMP) to cell death through mitochondrial outer membrane permeabilization (MOMP). LMP is a process in which intralysosomal content (mostly cathepsins but also ROS) is leaked to the cytoplasm. Massive disruption of lysosomes induces cell death by necrosis, but selective LMP can induce apoptosis by MOMP. Cathepsins can promote, on the one hand, the cleavage of the pro-apoptotic protein Bid; and on the other hand, the translocation of Bcl-2-associated killer (BAK) and BAX to the outer mitochondrial membrane (OMM) where they form pores. Truncated Bid (tBid) can itself form pores to the OMM but can also activate BAK/BAK. These two processes can induce apoptosis, *via* release of cytochrome *c* and in a caspase-dependent way or independently of caspases. A positive feedback loop exists given that caspases and cathepsins are also inducers of LMP.

stress stimuli can directly activate the proteins BAX and/or BAK (82, 83). After their activation and translocation to the mitochondria, BAX and BAK make pores at the OMM. This permits the translocation of numerous molecules bigger than 100 kDa, without inducing membrane rupture leading to apoptosis (84–86). Furthermore, cathepsin B has a major role in linking LMP to MOMP *via* the generation of lipid mediators, such as arachidonic acid that induces MOMP (87). Alternatively, other than ROS and cathepsins, there is a large list of agents capable of inducing this mitochondrial membrane permeabilization, such as sphingolipids, phospholipase A2, etc. (64). Some of these stimuli, like the pro-apoptotic proteins or caspases, are derived from mitochondria, suggesting that there is a positive feedback loop: mitochondrial damage also induces LMP (Figure 1).

In addition, the mechanism by which cathepsins are released from the lysosomes is not yet clear. There are three possible hypotheses: (i) through the rupture of the lysosomal membrane, (ii) through specific pores, or (iii) by special transporters. In an attempt to find which of the three hypotheses is valid, fluorescently labeled dextran molecules of different sizes were used. When inducing LMP, it was shown that only small molecules (size of 10 kDa) were released to the cytoplasm in most of the cells. In almost half of the cells, 40-kDa molecules were redistributed to the cytoplasm, and molecules larger than 70 kDa remained inside lysosomes. Based on the fact that cathepsins are relatively small proteins, around 40 kDa in size, it is inferred that cathepsins are among these released molecules. Furthermore, the low intralysosomal pH was maintained, suggesting that lysosomes were still active (88). However, it is still not enough to rule out any of the possible mechanisms.

Until now, several explanations may account for the higher vulnerability to LMP of cancer cell lysosomes. Since lysosomes are relatively large in cancer cells (89), one possibility would be that they are more prone to inducing cell death than lysosomes with normal sizes (90). Another possibility lies in the observation that cancer cells have higher metabolic rates. This is accompanied by an elevated turnover of proteins that contains iron, leading to iron accumulation in the lysosomes. Subsequently, these lysosomes will undergo an iron-mediated predisposition to a ROS-induced LMP (91). In other words, a characteristic of cancer cells is the increased levels of ROS, which is associated with an amplified release of cathepsins from the lysosomes. Since cancer cells appear to be more susceptible to LMP, its induction will eventually facilitate cancer cell death (92).

### Autophagy and Mitophagy

Macroautophagy is a process in which intracellular proteins or organelles are degraded in the lysosomes. Degraded products are then released from lysosomes and recycled into biosynthetic and metabolic pathways. Through the elimination of those damaged components, autophagy basically provides quality control over proteins and organelles, as well as sustains mitochondrial metabolic function and energy homeostasis (93). More than 30 proteins coordinate the autophagic processes, generating autophagosomes from essentially all membrane sources from the cell. Autophagy-related genes (Atg) control the processes of autophagy. The products of Atg genes are regulated by nutrients (mTOR), energy [AMP-activated protein kinase (AMPK)], and stress [hypoxia-inducible factor (HIF)], which can turn the pathway on and off (94). Nevertheless, autophagy may also induce cell

death, known as autophagic cell death (ACD). This specifically occurs when chromatin condensation is absent (95).

Autophagy's role in cancer is still not clear. Some cancers are dependent on autophagy for survival and other cancers use autophagy as a mechanism of cell death. In some models, autophagy suppresses cancer initiation by evading the toxic accumulation of damaged organelles, specifically mitochondria. On the short run, this helps in limiting oxidative stress. On the long run, it restricts chronic tissue damage and oncogenic signaling. So, in this context, autophagy stimulation might help suppress and/or prevent cancer initiation. Though, other cancers depend on autophagy for survival. In order to fit the high metabolic needs of growth and proliferation, cancers (such as the pancreatic) use autophagy-mediated recycling to their own advantage (96). Hence, inhibiting autophagy in this case could be an insight for selective cancer therapy, since these tumors are more dependent on autophagy than normal tissues (93).

Degradation of entire organelles can also occur: mitophagy (mitochondria), reticulophagy (endoplasmic reticulum), lipophagy (lipid droplets), peroxophagy (peroxisomes), and xenophagy (microbes). Mitophagy or autophagy of mitochondria is required to eliminate dysfunctional mitochondria to maintain appropriate metabolic and cell survival signals (97). Here, we will focus only on mitophagy, a key process for the control of mitochondrial quality. It is of substantial importance for the normal development of cells and tissues. The most studied mechanism of mitophagy initiation involves the E3 ubiquitin ligase Parkin and the serine–threonine kinase PINK1 (PTEN-induced putative kinase 1). PINK1 is a mitophagy receptor found at the OMM that accumulates when mitochondria are damaged or undergo any stress leading to mitochondrial membrane potential loss. This PINK1 accumulation at the OMM recruits Parkin from the cytosol. Parkin ubiquitinates proteins at the OMM. These ubiquitinated proteins are recognized by p62, also known as Sequestrome 1 (SQSTM 1). P-62 binds to LC3/Atg8 and takes p62-containing aggregates to the autophagosome to be degraded (98).

In the recent years, the role of mitophagy in cancer has been extensively reviewed. Parkin is frequently genetically inactivated in cancer. Although certain cancers, such as sarcomas and uterine cancer, have amplifications in PARK2 gene, the majority of tumors with lesions in PARK2, including ovarian, breast, and lung cancers, harbor deletions or loss of function mutations. This is mainly because the PARK2 gene is found on a fragile location on chromosome 6 (99). Parkin has been evidenced to control cell cycle regulators, such as cyclin-dependent kinases (CDKs) and cyclins, promoting acceleration of cell cycle progression. It can also lead to the accumulation of damaged mitochondria and elevated ROS production, triggering DNA damage and tumorigenesis (100). In addition, PINK1 and Parkin can promote apoptosis through targeting and ubiquitinating anti-apoptotic Mcl-1 leading to degradation; they operate as molecular switches by dictating cell fate as a response to diverse cellular stresses (101, 102). However, mitophagy can happen in cancer cells without active Parkin, known as mitophagy-independent Parkin function. OMM proteins, such as FUNDC1, BNIP3, and NIX, are autophagy receptors, independently of ubiquitination. Furthermore, other factors such as the phospholipid cardiolipin

can induce mitophagy, as well as ubiquitin ligases, such as SMURF1 and MAPL (103–105).

During hypoxia, HIFs can induce mitophagy through the transcription of NIX and BNIP3. In addition to its transcriptional activation by HIF-1, FoxO3A, PPAR $\alpha$ , RB/E2Fs, NF- $\kappa$ B, oncogenic Ras, and p53 also transcriptionally regulate BNIP3 (103), while NIX is transcriptionally regulated by HIF-1 and p53 (106, 107). Upon hypoxia or high oxidative phosphorylation, the small GTPase Rheb translocates to the OMM, where it can interact with BNIP3 and NIX to induce mitophagy, resulting in mTOR inactivation (108, 109). The role of BNIP3-dependent mitophagy in cancer presents some controversies. BNIP3-dependent mitophagy is required to limit mitochondrial mass and ROS levels in growing tumors; its loss leads to HIF-1 $\alpha$ -dependent increases in tumor growth and increased progression to metastasis (110). However, other studies show that BNIP3 has a pro-tumorigenic role; its inactivation reduced cell migration and its upregulation suppressed the mTOR/S6K1 pathway. It is hypothesized that the dual role of BNIP3 can be explained by alternative splicing or variable transcriptional regulation *via* transcription factor Sp3 (111, 112).

Contrary to BNIP3, the role of NIX and FUNDC1 in tumor progression remains relatively unknown, requiring further investigation. They can induce mitophagy under hypoxic conditions (113). However, their role in cancer mitophagy is still to be revealed (107).

## Signaling Pathways Involved in the Mitochondria–Lysosomal Crosstalk

As shown in **Figure 2**, the master regulator of cell growth and metabolism mTORC1 and proteins of the same pathway are the main linkers of mitochondria and lysosomes. As described

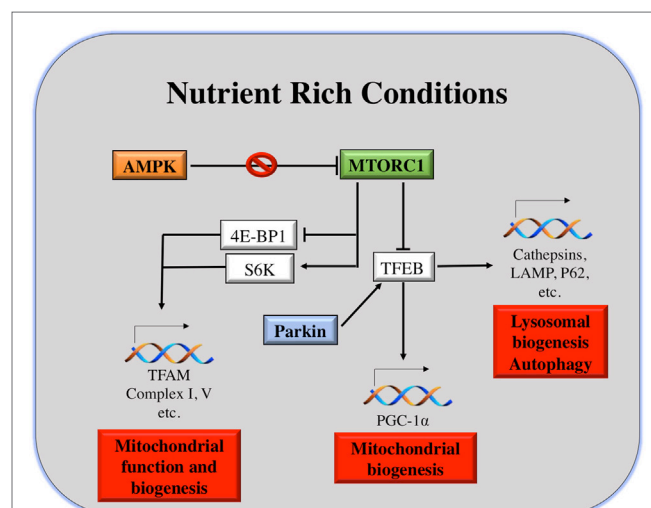


**FIGURE 2** | Mitochondria and lysosomes downstream mammalian target of rapamycin complex I (mTORC1). Under nutrient rich conditions, active mTORC1 can induce the transcription of different genes involved in mitochondrial function and biogenesis. At the same time, it can repress TFEB transcription factor, which is the main responsible for transcription of genes involved in lysosomal and mitochondrial biogenesis, autophagy, etc.

earlier, under nutrient-rich conditions, mTORC1 is activated at the lysosomal surface. mRNA translation of many genes occurs, *via* the activation and repression of S6K and 4E-BP1, respectively. Among the genes repressed by 4E-BP are TFAM, Complex I and Complex V of the mitochondria, regulating mitochondrial activity and biogenesis (114).

On the other hand, under starvation conditions, mTORC1 is inhibited and TFEB positively regulates the expression of lysosomal and autophagy genes, as well as the expression of PGC-1 $\alpha$ . PGC-1 $\alpha$  coactivates numerous biological programs in diverse tissues; it is a key regulator of lipid metabolism (115), but also it promotes mitochondrial biogenesis (30). Notably, TFEB activation can be induced by mitophagy as well, in an attempt to induce mitochondrial biogenesis after eliminating malfunctioning or damaged ones. The mechanism of TFEB activation by mitophagy is different than that under starvation conditions. Parkin promotes TFEB nuclear translocation, inducing lysosomal and mitochondrial biogenesis (98). In addition to that, upon energy depletion, AMPK is activated. AMPK serves as a fuel gage as it becomes active when ATP/AMP ratio is low, thus maintaining energy homeostasis (116). AMPK inhibits mTORC1 by the direct phosphorylation of Raptor, a molecule of the mTORC1 complex. This explains why AMPK has been considered as a tumor suppressor. AMPK activation is essential for increased mitochondrial biogenesis under glucose-limited conditions, since AMPK activation increases the expression of PGC-1 $\alpha$  and TFAM (117) (**Figure 2**).

When mTORC1 is active, there is an increase of mitochondrial biogenesis. This increase in mitochondrial biogenesis will result in a gain of ATP production capacity, a mandatory energy source for translation (114). By contrast, mitochondrial biogenesis induced by AMPK is an attempt to accelerate ATP generation, for restoring its level in favor of cell survival. This takes place under limiting nutrient availability or metabolic stress (118).

To further emphasize the link between mitochondria and lysosomes, it has been shown that mTOR not only binds to lysosomes (when mTORC1 is activated when amino acids are present) but it can also be associated with MOM. This is needed to integrate different stress signals that affect the function of mitochondria and regulate a checkpoint implicating p70S6K, one of the well-known targets of mTORC1 (119). Recent studies link mitochondrial dynamics to the equilibrium between nutrient supply and energy demand, suggesting variations in mitochondrial architecture as an adaptive mechanism to metabolic demands (120).

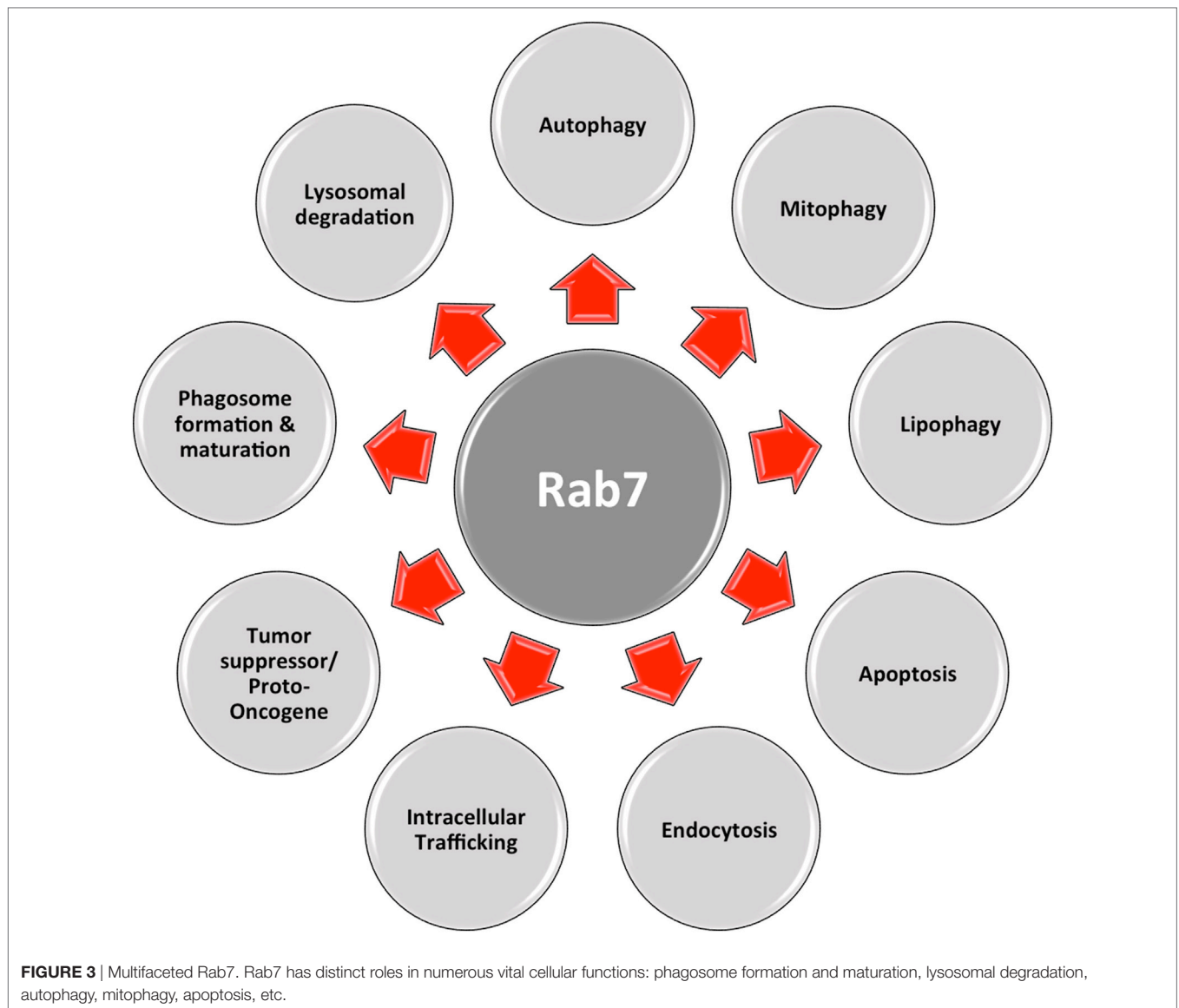
Another important regulator is Rab7, which belongs to the RAB family, a RAS-related group of GTP-binding proteins. This family of proteins includes important regulators of vesicle transportation and is localized in certain intracellular compartments (121). Numerous studies indicate that Rab7 plays major roles in controlling maturation of endosomes and transportation to lysosomes, as well as in phagocytosis, retromere regulation, cytoskeleton regulation, autophagy, and mitophagy (122, 123).

Normally, Rab7 is found on late endosomes and this acquisition is complemented by Rab5 loss, an early endosome marker. The switch from Rab5 to Rab7 is a process in which both proteins cooperate sequentially and dynamically. This determines Rab5 recruitment to early endosomes and Rab7 recruitment

and Rab5 loss at late endosomes (124–126). Late endosomes can fuse with lysosomes and other late endosomes, only if the Rab5 to Rab7 switch is accompanied by variations in fusion and tethering machinery. This allows direct contact in between organelles (127).

Other than being a marker of late endosomes, Rab7 is vital for mitophagy (**Figure 3**), as it is a downstream effector of Parkin (128). This occurs with the help of TBC1D15/17 and Fis1. The first protein belongs to the TBC family (Tre2/Bub2/Cdc16), having RabGAP functions (129, 130), while the latter is a fission protein with cytosolic N-terminal, bound to the OMM at its C-terminal (131, 132). In the absence or inactivity of TBC1D15, membranes that are labeled with LC3 excessively accumulate and lose their cargo orientation. In turn, membrane tubules are sent along microtubule tracks away from the mitochondria. Therefore, it is inferred that, during mitophagy, TBC1D15 binds to Fis1 and LC3 inducing Rab7 activity, which leads to the shaping of the autophagosomal isolation membrane. In fact, besides promoting microtubule-associated trafficking and autophagosomal membrane growth, the activity of Rab7 is affected by TBC1D15/17 activity, inducing autophagosomal membrane expansion to correctly surround the mitochondria (128). This indicates that, in case of Parkin-regulated mitophagy, Rab7 is essential for expanding LC3-labeled isolation membranes. Otherwise, inactive Rab7 might help in mediating the release of LC3-positive membranes from microtubules (133). The above-described model substantially differs from the well-known role of Rab7 in controlling autophagosome maturation and fusion with lysosomes (134, 135). In addition, it was shown an increase in the interaction between Rab7 and Mitofusin2 (MFN2), a mitochondrial fusion-related protein, as a response to starvation. This suggests the contribution of Rab7 during autophagosomal membrane maturation, as an adaptor protein used by MFN2 (136). Hence, Rab7 has a dual role in mitophagy, i.e., autophagosome formation and maturation.

As shown in **Figure 3**, this multifaceted small GTPase also participates in other important processes in the cell, such as in apoptosis and the activation of stress response pathways (137). One of these pathways is the mTORC1 pathway, through which mTORC1 moves toward a Rab7-containing compartment in the presence of amino acids (138). The direct interaction between Rab7 and mTOR has been proved by co-immunoprecipitation experiments (139). During bioenergetic stress, several groups showed a Rab7-dependent lysosomal crosstalk with apoptosis and its regulatory machinery, i.e., intramitochondrial recruitment of endolysosomes mediates apoptosis. As explained before, in the presence of growth factors, mTOR and AKT are activated initiating downstream signaling cascades. Under these conditions, nutrient transporter proteins facilitate the import of extracellular nutrients, supporting cellular bioenergetics by supplying the mitochondria with metabolic substrates. In this case, one important apoptotic mediator, cytochrome *c* is retained at the mitochondrial intermembrane. When there is nutrient starvation, these same signaling cascades are silenced, and genes are no longer transcribed. Existing transporters are trafficked to the lysosomes by Rab7, where they are degraded and removed from the cell. This decrease in cellular bioenergetics results in substrate limitation at the mitochondrial site, loss of homeostasis,



and cytochrome *c* release, eventually leading to apoptosis. This process can be rescued by inhibiting Rab7. For example, transporter proteins destined to enter the endocytic pathway and be trafficked to lysosomes for degradation, instead, are recycled and re-expressed on the cellular surface. As a result, extracellular nutrients are continually imported, and cellular bioenergetics is maintained, as well as mitochondrial homeostasis, in the absence of growth factors (140). In this case, Rab7 has a proapoptotic function, by limiting cell autonomous uptake of extracellular nutrients (141).

In cancer, the specific role of Rab7 is not fully understood. In the literature, Rab7 has been depicted as either a tumor suppressor (68, 141, 142) or a proto-oncogene (143–146), depending on tumor type, morphology, and metastatic and invasive abilities (122) (**Figure 3**). Particularly, synergy between HSP90 inhibition and Rab7 depletion decreases EGFR and Her2 levels, through proteasomal degradation, and promotes apoptosis, depicting

a proto-oncogenic role of Rab7 (147, 148). During melanoma development, Myc is activated, inducing Rab7 overexpression. Subsequently, Rab7 expression is downregulated to support the invasive and metastatic characteristics of melanoma (145). Moreover, the knockdown of Rab7 in prostate cancer cells led to the overexpression of *c-Met*, a protein involved in the promotion of cell invasion and metastasis (149).

In fact, since Rab7 is mainly accountable for intracellular trafficking, which is linked to the metastatic/invasive ability of tumors, and the degradation of many organelles and molecules, such as adhesion molecules and signaling receptors, it is a key regulator in governing cellular homeostasis. Certainly, Rab7 is a central molecule of cell survival, differentiation, and apoptosis. Current data suggest that the regulation of Rab7 expression and activity can reduce several pathologies, such as cancer (122). Of course, further work will be needed to investigate this possibility.

## THERAPEUTIC APPROACHES IN CANCER TREATMENT

Cancer cells exhibit a significant number of metabolic alterations associated with mitochondria, lysosomes, and other sub-cellular organelles. These organelles exhibit a number of deregulations, which have been identified as potential drug targets for successful rational drug design and therapy. For their involvement in bioenergetics, redox balancing, and survival, targeting mitochondria for therapeutic benefits is already in practice to induce apoptotic cell death (150, 151). In addition, the advances in lysosome research have highlighted their importance for degradation, signaling pathways, and cell death in pathophysiological conditions; thus, targeting lysosomes has also been considered a new therapeutic strategy for cancer treatment (76).

In this review, we highlighted the interplay between lysosomes and mitochondria and its importance in cell fate. We propose that targeting this crosstalk between both organelles might be crucial for fighting cancer.

### Inducing LMP

Indeed, many compounds are described to induce LMP and subsequent cell death in various human cancer cells and animal models but are not in clinical use (152, 153). Besides, little is known about the endogenous inhibitors preventing LMP and which mechanisms suppress lysosomal hydrolases in the cytoplasm of both, normal and cancer cells. Inducing LMP-dependent death could activate self-destructive processes in tumor cells, particularly if those cells were dependent on such inhibitors. Future investigations are needed to clarify if antagonists of LMP inducers may be useful synergistically with the current clinical treatments (64).

Interestingly, a minimally invasive anticancer modality called Photodynamic therapy (PDT) is able to induce LMP. PDT combines a drug (a photosensitizing agent) with a precise light wavelength, inducing ROS generation and killing tumor cells (154). The location where the photosensitizing agent is directed is very important, as it determines where the primary damage occurs. Usually photosensitizing agents accumulate either in mitochondria, inducing rapid apoptosis, or in lysosomes, inducing LMP and subsequent cell death (64). To date, PDT is used for treating or relieving the symptoms of non-small cell lung cancer patients and esophageal cancer patients. PDT still presents some limitations, since only tumors on the skin or just underneath it, or in internal organ linings and/or cavities can be treated with this technique. But it cannot be used for treating large tumors or metastasis (155–158).

### Targeting Mitophagy

Targeting mitophagy as an approach to adjuvant chemotherapy has been already questioned by Chourasia et al. (107). They claim that the deletion or inhibition of Parkin and BNIP3 induces the Warburg effect, thus favoring tumorigenesis. Nevertheless, acute chemical inhibition of mitophagy is still an effective approach for advanced tumors that have switched to glycolytic metabolism but still depend on mitochondria for further metabolic purposes (107). Of course, this approach has still to be therapeutically tested.

## Targeting Common Effectors between Mitochondria and Lysosomes

Other than targeting processes in which mitochondria and lysosomes are linked, inhibitors of their main common effectors, i.e., AMPK or mTOR have been already tested for cancer therapy. The role of AMPK in cancer cells is paradoxical. It can be a tumor suppressor, but can also promote tumorigenesis, stimulating cell survival in glucose-deficient situations and preserving metabolic homeostasis (117). Despite that, the use of the anti-diabetic drug Metformin, non-steroidal anti-inflammatory drugs, such as Aspirin, AICAR, and some natural products known to be AMPK activators, has shown to decrease tumorigenesis in animal models and cancer cell lines (159, 160). In addition, preclinical evidence suggests that Metformin appears to prevent the proliferation and growth of certain tumor types. There are currently more than 100 ongoing or clinical studies assessing the role of metformin in the therapy cancer (161, 162). It is well understood that metformin targets the mitochondrial complex I. However, it has been suggested that metformin could directly influence the V-ATPase activity of lysosomes (163), so this fact further supports the importance of lysosomal–mitochondrial link for cancer treatment.

Targeting mTOR may be crucial for cancer treatment not only for cell growth and proliferation but also for reversing the Warburg effect characteristic of tumor cells (164). At the molecular level, mTORC1 inhibition may induce mitochondrial biogenesis *via* PGC-1 $\alpha$ , as well as repression of transcription of mitochondrial genes *via* 4E-BP1 (114) depending on the model. mTORC1 inhibition induces lysosomal biogenesis and also initiates several feedback loops to upstream pathways, activation of which might be beneficial for the survival of tumor cells and metastasis. The best-known mTOR inhibitor is Rapamycin, which does not inhibit directly mTOR's kinase (catalytic) activity. Together with FKBP12, it binds specifically to mTORC1 (at high concentrations also to mTORC2). The binding occurs next to the kinase active site. Consequently, it can only inhibit a number of mTORC1 functions. Given this, and the importance of mTOR for cancer, several groups have developed other inhibitors to target mTOR's catalytic subunit (PP242, Torin 1 and 2, etc.). As reviewed by Xie and al., some mTOR inhibitors are already in clinical trials for treating cancer (165). Despite that, the utility of such inhibitors in oncology still appears to be limited, given that autophagy can be induced by mTOR inhibition, thus promoting cancer cell survival.

As reviewed above, RAB7 is a prominent target for cancer treatment (143). In addition, there are already drugs that target RAB7. It has been shown that liensinine, a major isoquinoline alkaloid that inhibits RAB7A recruitment to lysosomes, not autophagosomes. In this way, autophagy/mitophagy is impaired, enhancing the efficacy of chemotherapy in breast cancer cell lines (166).

## Using Nanomedicine for Inducing Cell Death

Nanotechnology is the science of controlling matter, at the molecular level, to generate devices with new biological, physical, and/or chemical characteristics. It is in the spotlight of therapeutic

innovation. The use of nanomaterial is a particularly promising tool not only to improve the diagnosis but also to generate new cancer treatments and overcome the drawbacks of traditional therapies (167). In particular, the discovery of gold nanorods (GNRs) has provided a new method to induce apoptosis specifically in cancer cells, while posing a negligible impact on normal cells. They are able to induce apoptosis in cancer cells through lysosomal permeability, as indicated by cathepsin D release, and a decrease in mitochondrial membrane potential (168). These findings are promising for the further implementation of nanotechnology at the clinical practice.

## CONCLUSION AND FUTURE PERSPECTIVES

Intracellular organelles, as thoroughly discussed, are the major players of cellular networks. Even though physical contact among these organelles was exhaustively described throughout the years, research is now shifting toward revealing the crosstalk of these entities on the signaling levels, as well as their physiological relevance. Mainly, organelle interactions are needed for metabolite exchange, and more interestingly, in membrane dynamics, intracellular organelle distribution, and the assembly of dynamic signaling platforms depending on cellular requirements.

In tumors, cells significantly display metabolic aberrations, associated directly or indirectly with mitochondria and lysosomes. These anomalies promote cancer cell growth and survival, while exhibiting distinctive properties that render cancer cells vulnerable to specific anticancer agents. In other words, the deregulation of these organelles in cancer cells as compared to their counterparts in healthy cells is a main reason for promising targeted drug therapy. Though substantial advancement has been made regarding elucidating the role of these anomalies in oncogenesis and chemotherapy-resistance, a better interpretation of the main pathophysiological differences between organelles of

normal and tumor cells can undoubtedly compliment the efforts to improve selective targeted anti-cancer agents.

Lysosomes and mitochondria have common regulators and can physically interact to maintain cell homeostasis or induce cell death. However, in cancer everything becomes a paradox; all of the processes in which lysosomes and mitochondria interact, except for LMP, and the common regulators (mTOR, AMPK, Rab7, etc.) present a dual role: on the one hand, they can promote tumorigenesis and, on the other hand, they can induce cell death. The relative contribution of these pathways would depend on tumor type, state, metastatic ability, microenvironment, metabolic reprogramming, etc. This reflects the importance of these two organelles for cancer treatment. New potential targets have been proposed, i.e., PGC-1 $\alpha$ , TFEB, Rab7, etc. However, will these targets overpass the problem of having a paradoxical role in cancer treatment? As we have seen already, every case needs to be studied independently, in order to predict whether the treatment would be beneficial or not. This is known as personalized medicine.

## AUTHOR CONTRIBUTIONS

LC, AN, and LC discussed the ideas and wrote the paper.

## ACKNOWLEDGMENT

We thank Albert Giralt Coll for the critical reading of the manuscript.

## FUNDING

LC was supported by the University of Lausanne. LC and AN performed this work as part of their degree in the University of Lausanne's PhD Programme in Life Sciences, emphasis Cardiovascular and Metabolism.

## REFERENCES

- Pavlova NN, Thompson CB. The emerging hallmarks of cancer metabolism. *Cell Metab* (2016) 23:27–47. doi:10.1016/j.cmet.2015.12.006
- Drabu S, Khatri S, Babu S, Verma D. Nanotechnology: an introduction to future drug delivery system. *J Chem Pharm Res* (2010) 2(1):444–57.
- Sakhrani NM, Padh H. Organelle targeting: third level of drug targeting. *Drug Des Devel Ther* (2013) 7:585–99. doi:10.2147/DDDT.S45614
- Cheng SM, Boddapati SV, D'Souza G, Weissig V. DQAsomes as mitochondria-targeted nanocarriers for anti-cancer drugs. *Nanotechnol Cancer Ther* (2006) 38:787–802. doi:10.1201/9781420006636.ch38
- Rajendran L, Knolker HJ, Simons K. Subcellular targeting strategies for drug design and delivery. *Nat Rev Drug Discov* (2010) 9(1):29–42. doi:10.1038/nrd2897
- Flierl A, Jackson C, Cottrell B, Murdock D, Seibel P, Wallace DC. Targeted delivery of DNA to the mitochondrial compartment via import sequence-conjugated peptide nucleic acid. *Mol Ther* (2003) 7(4):550–7. doi:10.1016/S1525-0016(03)00037-6
- Antico Arciuch VG, Elguero ME, Poderoso JJ, Carreras MC. Mitochondrial regulation of cell cycle and proliferation. *Antioxid Redox Signal* (2012) 16(10):1150–80. doi:10.1089/ars.2011.4085
- Detmer SA, Chan DC. Functions and dysfunctions of mitochondrial dynamics. *Nat Rev Mol Cell Biol* (2007) 8:870–9. doi:10.1038/nrm2275
- Frezza C. Mitochondrial metabolites: undercover signalling molecules. *Interface Focus* (2017) 7:1–6. doi:10.1098/rsfs.2016.0100
- Rizzuto R, De Stefani D, Raffaello A, Mammucari C. Mitochondria as sensors and regulators of calcium signalling. *Nat Rev Mol Cell Biol* (2012) 13:566–78. doi:10.1038/nrm3412
- Tait SWG, Green DR. Mitochondria and cell death: outer membrane permeabilization and beyond. *Nat Rev Mol Cell Biol* (2010) 11:621–32. doi:10.1038/nrm2952
- Schieber M, Chandel NS. ROS function in redox signaling and oxidative stress. *Curr Biol* (2014) 24:453–62. doi:10.1016/j.cub.2014.03.034
- Menzies KJ, Zhang H, Katsyuba E, Auwerx J. Protein acetylation in metabolism – metabolites and cofactors. *Nat Rev Endocrinol* (2016) 12:43–60. doi:10.1038/nrendo.2015.181
- Sullivan LB, Gui DY, Heiden MG. Altered metabolite levels in cancer: implications for tumour biology and cancer therapy. *Nat Rev Cancer* (2016) 16:680–93. doi:10.1038/nrc.2016.85
- Arnoult D, Carneiro L, Tattoli I, Girardin SE. The role of mitochondria in cellular defense against microbial infection. *Semin Immunol* (2009) 21:223–32. doi:10.1016/j.smim.2009.05.009
- Fillano JJ, Goldenthal MJ, Rhodes CH, Marin-Garcia J. Mitochondrial dysfunction in patients with hypotonia, epilepsy, autism, and developmental delay: HEADD syndrome. *J Child Neurol* (2002) 17:435–9. doi:10.1177/088307380201700607

17. Oka T, Hikoso S, Yamaguchi O, Taneike M, Takeda T, Tamai T, et al. Mitochondrial DNA that escapes from autophagy causes inflammation and heart failure. *Nature* (2012) 485:251–5. doi:10.1038/nature10992
18. Zsurka G, Kunz WS. Mitochondrial dysfunction and seizures: the neuronal energy crisis. *Lancet Neurol* (2015) 14:956–66. doi:10.1016/S1474-4422(15)00148-9
19. Vyas S, Zaganjor E, Haigis MC. Mitochondria and cancer. *Cell* (2016) 166:555–66. doi:10.1016/j.cell.2016.07.002
20. Warburg O. The metabolism of carcinoma cells. *J Cancer Res* (1925) 9:148–63. doi:10.1158/jcr.1925.148
21. Senyilmaz D, Teleman AA. Chicken or the egg: Warburg effect and mitochondrial dysfunction. *F1000Prime Rep* (2015) 7(41):1–13. doi:10.12703/P7-41
22. Jornayvaz FR, Shulman GI. Regulation of mitochondrial biogenesis. *Essays Biochem* (2010) 47:69–84. doi:10.1042/bse0470069
23. Puigserver P, Wu Z, Park CW, Graves R, Wright M, Spiegelman BM. A cold-inducible coactivator of nuclear receptors linked to adaptive thermogenesis. *Cell* (1998) 92(6):829–39. doi:10.1016/S0092-8674(00)81410-5
24. Zhang Y, Ba Y, Liu C, Sun G, Ding L, Gao S, et al. PGC-1 $\alpha$  induces apoptosis in human epithelial ovarian cancer cells through a PPAR $\gamma$ -dependent pathway. *Cell Res* (2007) 17(4):363–73. doi:10.1038/cr.2007.11
25. Luo C, Lim JH, Lee Y, Granter SR, Thomas A, Vazquez F, et al. A PGC1 $\alpha$ -mediated transcriptional axis suppresses melanoma metastasis. *Nature* (2016) 537(7620):422–6. doi:10.1038/nature19347
26. Torrano V, Valcarcel-Jimenez L, Cortazar AR, Liu X, Urosecvic J, Castillo-Martin M, et al. The metabolic co-regulator PGC1 $\alpha$  suppresses prostate cancer metastasis. *Nat Cell Biol* (2016) 18(6):645–56. doi:10.1038/ncb3357
27. Tan Z, Luo X, Xiao L, Tang M, Bode AM, Dong Z, et al. The role of PGC1 $\alpha$  in cancer metabolism and its therapeutic implications. *Mol Cancer Ther* (2016) 15:774–82. doi:10.1158/1535-7163.MCT-15-0621
28. LeBleu VS, O'Connell JT, Gonzalez Herrera KN, Wikman H, Pantel K, Haigis MC, et al. PGC1 $\alpha$  mediates mitochondrial biogenesis and oxidative phosphorylation in cancer cells to promote metastasis. *Nat Cell Biol* (2014) 16:992–1015. doi:10.1038/ncb3039
29. Li F, Wang Y, Zeller KI, Potter JJ, Wonsey DR, O'Donnell KA, et al. Myc stimulates nuclear encoded mitochondrial genes and mitochondrial biogenesis. *Mol Cell Biol* (2005) 25:6225–34. doi:10.1128/MCB.25.14.6225-6234.2005
30. Morita M, Gravel SP, Hulea L, Larsson O, Pollak M, St-Pierre J, et al. mTOR coordinates protein synthesis, mitochondrial activity and proliferation. *Cell Cycle* (2015) 14:473–80. doi:10.4161/15384101.2014.991572
31. Senft D, Ronai ZA. Regulators of mitochondrial dynamics in cancer. *Curr Opin Cell Biol* (2016) 39:43–52. doi:10.1016/j.cob.2016.02.001
32. Serasinghe MN, Wieder SY, Renault TT, Elkhohi R, Ascioia JJ, Yao JL, et al. Mitochondrial division is requisite to RAS-induced transformation and targeted by oncogenic MAPK pathway inhibitors. *Mol Cell* (2015) 51:521–36. doi:10.1016/j.molcel.2015.01.003
33. Graves JA, Wang Y, Sims-Lucas S, Cherok E, Rothermund K, Branca MF, et al. Mitochondrial structure, function and dynamics are temporally controlled by c-Myc. *PLoS One* (2012) 7(5):e37699. doi:10.1371/journal.pone.0037699
34. Wang C, Youle RJ. The role of mitochondria in apoptosis. *Annu Rev Genet* (2009) 43:95–119. doi:10.1146/annurev-genet-102108-134850
35. Renault TT, Floros KV, Elkhohi R, Corrigan KA, Kushnareva Y, Wieder SY, et al. Mitochondrial shape governs BAX-induced membrane permeabilization and apoptosis. *Mol Cell* (2015) 57:69–82. doi:10.1016/j.molcel.2014.10.028
36. Christofk HR, Vander Heiden MG, Harris MH, Ramanathan A, Gerszten RE, Wei R, et al. The M2 splice isoform of pyruvate kinase is important for cancer metabolism and tumour growth. *Nature* (2008) 452:230–3. doi:10.1038/nature06734
37. Schell JC, Olson KA, Jiang L, Hawkins AJ, Van Vranken JG, Xie J, et al. A role for the mitochondrial pyruvate carrier as a repressor of Warburg effect and colon cancer cell growth. *Mol Cell* (2014) 56:400–13. doi:10.1016/j.molcel.2014.09.026
38. Mullen AR, Wheaton WW, Jin ES, Chen PH, Sullivan LB, Cheng T, et al. Reductive carboxylation supports growth in tumour cells with defective mitochondria. *Nature* (2011) 481:385–8. doi:10.1038/nature10642
39. van Gisbergen MW, Voets AM, Starmans MH, de Coo IF, Yadak R, Hoffmann RF, et al. How do changes in the mtDNA and mitochondrial dysfunction influence cancer and cancer therapy? Challenges, opportunities and models. *Mutat Res Rev Mutat Res* (2015) 764:16–30. doi:10.1016/j.mrrrev.2015.01.001
40. Dang L, White DW, Gross S, Bennett BD, Bittinger MA, Driggers EM, et al. Cancer-associated IDH1 mutations produce 2-hydroxyglutarate. *Nature* (2009) 462:739–44. doi:10.1038/nature08617
41. Ward PS, Patel J, Wise DR, Abdel-Wahab O, Bennett BD, Collier HA, et al. The common feature of leukemia-associated IDH1 and IDH2 mutations is a neomorphic enzyme activity converting alpha-ketoglutarate to 2-hydroxyglutarate. *Cancer Cell* (2010) 17:225–34. doi:10.1016/j.ccr.2010.01.020
42. Reznik E, Miller ML, Şenbabağlı Y, Riaz N, Sarungbam J, Tickoo SK, et al. Mitochondrial DNA copy number variation across human cancers. *Elife* (2016) 5:1–20. doi:10.7554/eLife.10769
43. Birsoy K, Wang T, Chen WW, Freinkman E, Abu-Remaileh M, Sabatini DM. An essential role of the mitochondrial electron transport chain in cell proliferation is to enable aspartate synthesis. *Cell* (2015) 162(3):540–51. doi:10.1016/j.cell.2015.07.016
44. Aits S, Jaattela M. Lysosomal cell death at a glance. *J Cell Sci* (2013) 126:1905–12. doi:10.1242/jcs.091181
45. de Duve C, Pressman BC, Gianetto R, Wattiaux R, Appelmann F. Tissue fractionation studies: intracellular distribution patterns of enzymes in rat-liver tissue. *Biochem J* (1955) 60(4):604–17. doi:10.1042/bj0600604
46. Cooper GM. *The Cell: A Molecular Approach*. Sunderland, MA: Sinauer Associates (2000).
47. Morgan AJ, Platt FM, Lloyd-Evans E, Galione A. Molecular mechanisms of endolysosomal Ca<sup>2+</sup> signalling in health and disease. *Biochem J* (2011) 439(3):349–74. doi:10.1042/BJ20110949
48. Settembre C, Fraldi A, Medina DL, Ballabio A. Signals from the lysosome: a control centre for cellular clearance and energy metabolism. *Nat Rev Mol Cell Biol* (2013) 14:283–96. doi:10.1038/nrm3565
49. Zoncu R, Bar-Peled L, Efeyan A, Wang S, Sancak Y, Sabatini DM. mTORC1 senses lysosomal amino acids through an inside-out mechanism that requires the vacuolar H(+)-ATPase. *Science* (2011) 334(6056):678–83. doi:10.1126/science.1207056
50. Bar-Peled L, Sabatini DM. Regulation of mTORC1 by amino acids. *Trends Cell Biol* (2014) 24(7):400–6. doi:10.1016/j.tcb.2014.03.003
51. Dibble CC, Cantley LC. Regulation of mTORC1 by PI3K signaling. *Trends Cell Biol* (2015) 25(9):545–55. doi:10.1016/j.tcb.2015.06.002
52. Shimobayashi M, Hall MN. Multiple amino acid sensing inputs to mTORC1. *Cell Res* (2016) 26:7–20. doi:10.1038/cr.2015.146
53. Demetriades C, Doumpas N, Teleman AA. Regulation of TORC1 in response to amino acid starvation via lysosomal recruitment of TSC2. *Cell* (2014) 156(4):786–99. doi:10.1016/j.cell.2014.01.024
54. Zheng L, Zhang W, Zhou Y, Li F, Wei H, Peng J. Recent advances in understanding amino acid sensing mechanisms that regulate mTORC1. *Int J Mol Sci* (2016) 17(10):1635–50. doi:10.3390/ijms17101636
55. Sardiello M, Palmieri M, di Ronza A, Medina DL, Valenza M, Gennarino VA, et al. A gene network regulating lysosomal biogenesis and function. *Science* (2009) 325(5939):473–7. doi:10.1126/science.1174447
56. Pópulo H, Lopes JM, Soares P. The mTOR signalling pathway in human cancer. *Int J Mol Sci* (2012) 13(2):1886–918. doi:10.3390/ijms13021886
57. Dibble CC, Manning BD. Signal integration by mTORC1 coordinates nutrient input with biosynthetic output. *Nat Cell Biol* (2013) 15:555–64. doi:10.1038/ncb2763
58. Francipane MG, Lagasse E. mTOR pathway in colorectal cancer: an update. *Oncotarget* (2014) 5(1):49–66. doi:10.18632/oncotarget.1548
59. Hare SH, Harvey AJ. mTOR function and therapeutic targeting in breast cancer. *Am J Cancer Res* (2017) 7(3):383–404.
60. Tardy C, Codogno P, Autefage H, Levade H, Andrieu-Abadie N. Lysosomes and lysosomal proteins in cancer cell death (new players of an old struggle). *Biochim Biophys Acta* (2006) 1765(2):101–25. doi:10.1016/j.bbcan.2005.11.003
61. Alayev A, Holz MK. mTOR signaling for biological control and cancer. *J Cell Physiol* (2013) 228(8):1658–64. doi:10.1002/jcp.24351
62. Hämalistö S, Jäättelä M. Lysosomes in cancer—living on the edge (of the cell). *Curr Opin Cell Biol* (2016) 39:69–76. doi:10.1016/j.cob.2016.02.009
63. Korolchuk VI, Saiki S, Lichtenberg M, Siddiqui FH, Roberts EA, Imarisio S, et al. Lysosomal positioning coordinates cellular nutrient responses. *Nat Cell Biol* (2011) 13(4):453–60. doi:10.1038/ncb2204
64. Boya P, Kroemer G. Lysosomal membrane permeabilization in cell death. *Oncogene* (2008) 27:6434–51. doi:10.1038/ncb2008.310

65. Kirkegaard T, Jäättelä M. Lysosomal involvement in cell death and cancer. *BBA Mol Cell Res* (2009) 1793(4):746–54. doi:10.1016/j.bbamcr.2008.09.008
66. Kallunki T, Olsen OD, Jaattela M. Cancer-associated lysosomal changes: friends or foes? *Oncogene* (2013) 32:1995–2004. doi:10.1038/onc.2012.292
67. Xu H, Ren D. Lysosomal physiology. *Ann Rev Physiol* (2015) 77:57–80. doi:10.1146/annurev-physiol-021014-071649
68. Steffan JJ, Dykes SS, Coleman DT, Adams LK, Rogers D, Carroll JL, et al. Supporting a role for the GTPase Rab7 in prostate cancer progression. *PLoS One* (2014) 9(2):e87882. doi:10.1371/journal.pone.0087882
69. Friedl P, Wolf K. Tumor-cell invasion and migration: diversity and escape mechanisms. *Nat Rev Cancer* (2003) 3(5):362–74. doi:10.1038/nrc1075
70. Friedl P, Wolf K. Tube travel: the role of proteases in individual and collective cancer cell invasion. *Cancer Res* (2008) 68(18):7247–9. doi:10.1158/0008-5472.CAN-08-0784
71. Liu Y, Zhou Y, Zhu K. Inhibition of glioma cell lysosome exocytosis inhibits glioma invasion. *PLoS One* (2012) 7:e45910. doi:10.1371/journal.pone.0045910
72. Mohamed MM, Sloane BF. Cysteine cathepsins: multifunctional enzymes in cancer. *Nat Rev Cancer* (2006) 6(10):764–75. doi:10.1038/nrc1949
73. Sameni M, Moin K, Sloane BF. Imaging proteolysis by living human breast cancer cells. *Neoplasia* (2000) 2:496–504. doi:10.1038/sj.neo.7900116
74. Lopez-Otin C, Matrisian LM. Emerging roles of proteases in tumour suppression. *Nat Rev Cancer* (2007) 7:800–8. doi:10.1038/nrc2228
75. Jäättelä M. Multiple cell death pathways as regulators of tumour initiation and progression. *Oncogene* (2004) 23:2746–56. doi:10.1038/sj.onc.1207513
76. Piao S, Amaravadi RK. Targeting the lysosome in cancer. *Ann N Y Acad Sci* (2016) 1371(1):45–54. doi:10.1111/nyas.12953
77. Furuta K, Ikeda M, Nakayama Y, Nakamura K, Tanaka M, Hamasaki N, et al. Expression of lysosome-associated membrane proteins in human colorectal neoplasms and inflammatory diseases. *Am J Pathol* (2001) 159(2):449–55. doi:10.1016/S0002-9440(10)61716-6
78. Dettmer J, Hong-Hermesdorf A, Stierhof YD, Schumacher K. Vacuolar H<sup>+</sup>-ATPase activity is required for endocytic and secretory trafficking in arabidopsis. *Plant Cell* (2006) 18(3):715–30. doi:10.1105/tpc.105.037978
79. Meo-Evoli N, Almacellas E, Massucci FA, Gentilella A, Ambrosio S, Kozma SC, et al. V-ATPase: a master effector of E2F1-mediated lysosomal trafficking, mTORC1 activation and autophagy. *Oncotarget* (2015) 6(29):28057–70. doi:10.18632/oncotarget.4812
80. Gotink KJ, Broxterman HJ, Labots M, de Haas RR, Dekker H, Honeywell RJ, et al. Lysosomal sequestration of sunitinib: a novel mechanism of drug resistance. *Clin Cancer Res* (2011) 17(23):7337–46. doi:10.1158/1078-0432.CCR-11-1667
81. Cirman T, Oresić K, Mazovec GD, Turk V, Reed JC, Myers RM, et al. Selective disruption of lysosomes in HeLa cells triggers apoptosis mediated by cleavage of Bid by multiple papain-like lysosomal cathepsins. *J Biol Chem* (2004) 279(5):3578–87. doi:10.1074/jbc.M308347200
82. Kroemer G, Jäättelä M. Lysosomes and autophagy in cell death control. *Nat Rev Cancer* (2005) 5:886–97. doi:10.1038/nrc1738
83. Boya P, Andreau K, Poncet D, Zamzami N, Perfettini JL, Metivier D, et al. Lysosomal membrane permeabilization induces cell death in a mitochondrion-dependent fashion. *J Exp Med* (2003) 197(10):1323–34. doi:10.1084/jem.20021952
84. Kuwana T, Bouchier-Hayes L, Chipuk JE, Bonzon C, Sullivan BA, Green DR, et al. BH3 domains of BH3-only proteins differentially regulate Bax-mediated mitochondrial membrane permeabilization both directly and indirectly. *Mol Cell* (2005) 17(4):525–35. doi:10.1016/j.molcel.2005.02.003
85. Kågedal K, Johansson AC, Johansson U, Heimlich G, Roberg K, Wang NS, et al. Lysosomal membrane permeabilization during apoptosis— involvement of Bax? *Int J Exp Pathol* (2005) 86(5):309–21. doi:10.1111/j.0959-9673.2005.00442.x
86. Feldstein AE, Werneburg NW, Li Z, Bronk SF, Bronk SF, Gores GJ. Bax inhibition protects against free fatty acid-induced lysosomal permeabilization. *Am J Physiol Gastrointest Liver Physiol* (2006) 290(6):G1339–46. doi:10.1152/ajpgi.00509.2005
87. Jäättelä M, Tschopp J. Caspase-independent cell death in T lymphocytes. *Nat Immunol* (2003) 4(5):416–23. doi:10.1038/ni0503-416
88. Bidère N, Lorenzo HK, Carmona S, Laforge M, Harper F, Dumont C, et al. Cathepsin D triggers bax activation, resulting in selective apoptosis-inducing factor (AIF) relocation in T lymphocytes entering the early commitment phase to apoptosis. *J Biol Chem* (2003) 278(33):31401–11. doi:10.1074/jbc.M301911200
89. Glunde K, Guggino SE, Solaiyappan M, Pathak AP, Ichikawa Y, Bhujwala ZM. Extracellular acidification alters lysosomal trafficking in human breast cancer cells. *Neoplasia* (2003) 5(6):533–45. doi:10.1016/S1476-5586(03)80037-4
90. Ono K, Kim SO, Han J. Susceptibility of lysosomes to rupture is a determinant for plasma membrane disruption in tumor necrosis factor alpha-induced cell death. *Mol Cell Biol* (2003) 23(2):665–76. doi:10.1128/MCB.23.2.665-676.2003
91. Eaton JW, Qian M. Molecular bases of cellular iron toxicity. *Free Radic Biol Med* (2002) 32(9):833–40. doi:10.1016/S0891-5849(02)00772-4
92. Gyrud-Hansen M, Nylandsted J, Jäättelä M. Heat shock protein 70 promotes cancer cell viability by safeguarding lysosomal integrity. *Cell Cycle* (2004) 3(12):1484–5. doi:10.4161/cc.3.12.1287
93. White E, Mehnert JM, Chan CS. Autophagy, metabolism, and cancer. *Clin Cancer Res* (2015) 21(22):5037–46. doi:10.1158/1078-0432.CCR-15-0490
94. Lorin S, Hamai A, Mehrpour M, Codogno P. Autophagy regulation and its role in cancer. *Semin Cancer Biol* (2013) 23:361–79. doi:10.1016/j.semcancer.2013.06.007
95. Kroemer G, Levine B. Autophagic cell death: the story of a misnomer. *Nat Rev Mol Cell Biol* (2008) 9(12):1004–10. doi:10.1038/nrm2529
96. Yang S, Wang X, Contino G, Liesa M, Sahin E, Ying H, et al. Pancreatic cancers require autophagy for tumor growth. *Genes Dev* (2011) 25(7):717–29. doi:10.1101/gad.2016111
97. Klionsky DJ, Cuervo AM, Seglen PO. Methods for monitoring autophagy from yeast to human. *Autophagy* (2007) 3(3):181–206. doi:10.4161/auto.3678
98. Pankiv S, Clausen TH, Lamark T, Brech A, Bruun JA, Outzen H, et al. p62/SQSTM1 binds directly to Atg8/LC3 to facilitate degradation of ubiquitinated protein aggregates by autophagy. *J Biol Chem* (2007) 282(33):24131–45. doi:10.1074/jbc.M702824200
99. Gong Y, Zack TI, Morris LG, Lin K, Hukkelhoven E, Raheja R, et al. Pan-cancer genetic analysis identifies PARK2 as a master regulator of G1/S cyclins. *Nat Genet* (2014) 46:588–94. doi:10.1038/ng.2981
100. Palikaras K, Tavernarakis N. Measuring oxygen consumption rate in caenorhabditis elegans. *Bio Protoc* (2016) 6:23. doi:10.21769/BioProtoc.2049
101. Zhang C, Lee S, Peng Y, Bunker E, Giaime E, Shen J, et al. PINK1 triggers autocatalytic activation of parkin to specify cell fate decisions. *Curr Biol* (2014) 18(24):1854–65. doi:10.1016/j.cub.2014.07.014
102. Esteban-Martínez L, Doménech E, Boya P, Salazar-Roa M, Malumbres M. Mitophagy in mitosis: more than a myth. *Autophagy* (2015) 11(12):2379–80. doi:10.1080/15548627.2015.1108509
103. Chourasia AH, Macleod KF. Tumor suppressor functions of BNIP3 and mitophagy. *Autophagy* (2015) 11(10):1937–8. doi:10.1080/15548627.2015.1085136
104. Bernardini JP, Lazarou M, Dewson G. Parkin and mitophagy in cancer. *Oncogene* (2017) 36(10):1315–27. doi:10.1038/onc.2016.302
105. Drake LE, Springer MZ, Poole LP, Kim CJ, Macleod KF. Expanding perspectives on the significance of mitophagy in cancer. *Semin Cancer Biol* (2017) S1044-579X(17):30102–5. doi:10.1016/j.semcancer.2017.04.008
106. Palikaras K, Lionaki E, Tavernarakis N. Mitophagy: in sickness and in health. *Mol Cell Oncol* (2016) 3(1):1–2. doi:10.1080/23723556.2015.1056332
107. Chourasia AH, Boland ML, Macleod KF. Mitophagy and cancer. *Cancer Metab* (2015) 3(4):1–11. doi:10.1186/s40170-015-0130-8
108. Melder S, Chatelain EH, Lavie J, Mahfouf W, Jose C, Obre E, et al. Rheb regulates mitophagy induced by mitochondrial energetic status. *Cell Metab* (2013) 17(5):719–30. doi:10.1016/j.cmet.2013.03.014
109. Li Y, Wang Y, Kim E, Beemiller P, Wang CY, Swanson J, et al. Bnip3 mediates the hypoxia-induced inhibition on mTOR by interacting with Rheb. *J Biol Chem* (2007) 282(49):35803–13. doi:10.1074/jbc.M705231200
110. Palikaras K, Daskalakis I, Markaki M, Tavernarakis N. Mitophagy and age-related pathologies: development of new therapeutics by targeting mitochondrial turnover. *Pharmacol Ther* (2017). doi:10.1016/j.pharmthera.2017.04.005
111. Chang JY, Yi HS, Kim HW, Shong M. Dysregulation of mitophagy in carcinogenesis and tumor progression. *Biochim Biophys Acta* (2017) 1858(8):633–40. doi:10.1016/j.bbabi.2016.12.008

112. Huang Y, Shen P, Chen X, Chen Z, Zhao T, Chen N, et al. Transcriptional regulation of BNIP3 by Sp3 in prostate cancer. *Prostate* (2015) 75(14):1556–67. doi:10.1002/pros.23029
113. Kulikov AV, Luchkina EA, Gogvadze V, Zhivotovsky B. Mitophagy: link to cancer development and therapy. *Biochem Biophys Res Commun* (2017) 482(3):432–9. doi:10.1016/j.bbrc.2016.10.088
114. Morita M, Gravel SP, Chénard V, Sikström K, Zheng L, Alain T, et al. Mtorc1 controls mitochondrial activity and biogenesis through 4E-BP-dependent translational regulation. *Cell Metab* (2013) 18(5):698–711. doi:10.1016/j.cmet.2013.10.001
115. Settembre C, De Cegli R, Mansueto G, Saha PK, Vetrini F, Visvikis O, et al. TFEB controls cellular lipid metabolism through a starvation-induced autoregulatory loop. *Nat Cell Biol* (2013) 15(6):647–58. doi:10.1038/ncb2718
116. Hardie DG, Carling D. The AMP-activated protein kinase – fuel gauge of the mammalian cell? *Eur J Biochem* (1997) 246(2):259–73. doi:10.1111/j.1432-1033.1997.00259.x
117. Chaube B, Malvi P, Singh SV, Mohammad N, Violle B, Bhat MK. AMPK maintains energy homeostasis and survival in cancer cells via regulating p38/PGC-1ALPHA-mediated mitochondrial biogenesis. *Cell Death Discov* (2015) 1(15063):1–11. doi:10.1038/cddiscovery.2015.63
118. Kahn BB, Alquier T, Carling D, Hardie DG. AMP-activated protein kinase: ancient energy gauge provides clues to modern understanding of metabolism. *Cell Metab* (2005) 1(1):15–25. doi:10.1016/j.cmet.2004.12.003
119. Desai BN, Myers BR, Schreiber SL. FKBP12-rapamycin-associated protein associates with mitochondria and senses osmotic stress via mitochondrial dysfunction. *Proc Natl Acad Sci U S A* (2002) 99(7):4319–24. doi:10.1073/pnas.261702698
120. Liesa M, Shirihai OS. Mitochondrial dynamics in the regulation of nutrient utilization and energy expenditure. *Cell Metab* (2013) 17(4):491–506. doi:10.1016/j.cmet.2013.03.002
121. Agola JO, Jim PA, Ward HH, Basuray S, Wandering-Ness A. Rab GTPases as regulators of endocytosis, targets of disease and therapeutic opportunities. *Clin Genet* (2011) 80(4):305–18. doi:10.1111/j.1399-0004.2011.01724.x
122. Guerra F, Bucci C. Multiple roles of the small GTPase Rab7. *Cells* (2016) 5(3):34–62. doi:10.3390/cells5030034
123. Zhang M, Chen L, Wang S, Wang T. Rab7: roles in membrane trafficking and disease. *Biosci Rep* (2009) 29(3):193–209. doi:10.1042/BSR20090032
124. Rink J, Ghigo E, Kalaidzidis Y, Zerial M. Rab conversion as a mechanism of progression from early to late endosomes. *Cell* (2005) 122(5):735–49. doi:10.1016/j.cell.2005.06.043
125. Vonderheit A, Helenius A. Rab7 associates with early endosomes to mediate sorting and transport of Semliki orest virus to late endosomes. *PLoS Biol* (2005) 3(7):e233. doi:10.1371/journal.pbio.0030233
126. Poteryaev D, Datta S, Ackema K, Zerial M, Spang A. Identification of the switch in early-to-late endosome transition. *Cell* (2010) 141(3):497–508. doi:10.1016/j.cell.2010.03.011
127. Luzzio JP, Pryor PR, Bright NA. Lysosomes: fusion and function. *Nat Rev Mol Cell Biol* (2007) 8:622–32. doi:10.1038/nrm2217
128. Yamano K, Fogel AI, Wang C, van der Blik AM, Youle RJ. Mitochondrial Rab GAPs govern autophagosome biogenesis during mitophagy. *Elife* (2014) 3:1–24. doi:10.7554/eLife.01612
129. Frasa MA, Koessmeier KT, Ahmadian MR, Braga VM. Illuminating the functional and structural repertoire of human tbc/rabgaps. *Nat Rev Mol Cell Biol* (2013) 13(476):67–73. doi:10.1038/nrm3267
130. Fukuda M. Tbc proteins: GAPs for mammalian small GTPase Rab? *Biosci Rep* (2011) 31(3):159–68. doi:10.1042/BSR20100112
131. Mozdy AD, McCaffery JM, Shaw JM. Dnm1p GTPase-mediated mitochondrial fission is a multi-step process requiring the novel integral membrane component Fis1p. *J Cell Biol* (2000) 151(2):367–80. doi:10.1083/jcb.151.2.367
132. Suzuki M, Jeong SY, Karbowski M, Youle RJ, Tjandra N. The solution structure of human mitochondria fission protein Fis1 reveals a novel TPR-like helix bundle. *J Mol Biol* (2003) 334(3):445–58. doi:10.1016/j.jmb.2003.09.064
133. Pankiv S, Alemu EA, Brech A, Bruun JA, Lamark T, Overvatn A, et al. FYCO1 is a Rab7 effector that binds to LC3 and PI3P to mediate microtubule plus end-directed vesicle transport. *J Cell Biol* (2010) 188(2):253–69. doi:10.1083/jcb.200907015
134. Jager S, Bucci C, Tanida I, Ueno T, Kominami EL. Role for Rab7 in maturation of late autophagic vacuoles. *J Cell Sci* (2004) 117(20):4837–48. doi:10.1242/jcs.01370
135. Zhou J, Tan SH, Nicolas V, Bauvy C, Yang ND, Zhang J, et al. Activation of lysosomal function in the course of autophagy via mTORC1 suppression and autophagosome-lysosome fusion. *Cell Res* (2013) 23(4):508–23. doi:10.1038/cr.2013.11
136. Zhao T, Huang X, Han L, Wang X, Cheng H, Zhao Y, et al. Central role of mitofusin 2 in autophagosome-lysosome fusion in cardiomyocytes. *J Biol Chem* (2012) 287(28):23615–25. doi:10.1074/jbc.M112.379164
137. Snider MD. A role for Rab7 GTPase in growth factor-regulated cell nutrition and apoptosis. *Mol Cell* (2003) 12(4):796–7. doi:10.1016/S1097-2765(03)00401-5
138. Sancak Y, Bar-Peled L, Zoncu R, Markhard AL, Nada S, Sabatini DM. Regulator-Rag complex targets mTORC1 to the lysosomal surface and is necessary for its activation by amino acids. *Cell* (2010) 141(2):290–303. doi:10.1016/j.cell.2010.02.024
139. Ding X, Zhang W, Zhao T, Yan C, Du H. Rab7 GTPase controls lipid metabolic signaling in myeloid-derived suppressor cells. *Oncotarget* (2017) 8(18):30123–37. doi:10.18632/oncotarget.16280
140. Edinger AL. Growth factors regulate cell survival by controlling nutrient transporter expression. *Biochem Soc Trans* (2005) 33(1):225–7. doi:10.1042/BS0330225
141. Edinger AL, Cinalli RM, Thompson CB. Rab7 prevents growth factor-independent survival by inhibiting cell-autonomous nutrient transporter expression. *Dev Cell* (2003) 5(4):571–82. doi:10.1016/S1534-5807(03)00291-0
142. Steffan JJ, Cardelli JA. Thiazolidinediones induce Rab7-RILP-MAPK-dependent juxtannuclear lysosome aggregation and reduce tumor cell invasion. *Traffic* (2010) 11(2):274–86. doi:10.1111/j.1600-0854.2009.01012.x
143. Wang T, Zhang M, Ma Z, Guo K, Tergaonkar V, Zeng Q, et al. A role of Rab7 in stabilizing EGFR-HER2 and in sustaining Akt survival signal. *J Cell Physiol* (2012) 227(6):2788–97. doi:10.1002/jcp.23023
144. Williams KC, Coppolino MG. Phosphorylation of membrane type 1-matrix metalloproteinase (mt1-mmp) and its vesicle-associated membrane protein 7 (Vamp7)-dependent trafficking facilitate cell invasion and migration. *J Biol Chem* (2011) 286(50):43405–16. doi:10.1074/jbc.M111.297069
145. Alonso-Curbelo D, Riveiro-Falkenbach E, Pérez-Guijarro E, Cifdaloz M, Karras P, Osterloh L, et al. Rab7 controls melanoma progression by exploiting a lineage-specific wiring of the endolysosomal pathway. *Cancer Cell* (2014) 26(1):61–76. doi:10.1016/j.ccr.2014.04.030
146. Lackner MR, Kindt RM, Carroll PM, Brown K, Cancilla MR, Chen C, et al. Chemical genetics identifies Rab geranylgeranyl transferase as an apoptotic target of farnesyl transferase inhibitors. *Cancer Cell* (2005) 7(4):325–36. doi:10.1016/j.ccr.2005.03.024
147. Ceresa BP, Bahr SJ. Rab7 activity affects epidermal growth factor: epidermal growth factor receptor degradation by regulating endocytic trafficking from the late endosome. *J Biol Chem* (2006) 281(2):1099–106. doi:10.1074/jbc.M504175200
148. Sakane A, Hatakeyama S, Sasaki T. Involvement of Rab7 in EGF receptor degradation as an E3 ligase. *Biochem Biophys Res Commun* (2007) 357(4):1058–64. doi:10.1016/j.bbrc.2007.04.052
149. Benvenuti S, Comoglio PM. The MET receptor tyrosine kinase in invasion and metastasis. *J Cell Physiol* (2007) 213(2):316–25. doi:10.1002/jcp.21183
150. Ubah OC, Wallace HM. Cancer therapy: targeting mitochondria and other sub-cellular organelles. *Curr Pharm Des* (2014) 20:201–22. doi:10.2174/13816128113199990031
151. Wen S, Zhu D, Huang P. Targeting cancer cell mitochondria as a therapeutic approach. *Future Med Chem* (2013) 5(1):53–67. doi:10.4155/fmc.12.190
152. Rigo A, Vinante F. The antineoplastic agent  $\alpha$ -bisabolol promotes cell death by inducing pores in mitochondria and lysosomes. *Apoptosis* (2016) 21(8):917–27. doi:10.1007/s10495-016-1257-y
153. Erdal H, Berndtsson M, Castro J, Brunk U, Shoshan MC, Linder S. Induction of lysosomal membrane permeabilization by compounds that activate p53-independent apoptosis. *Proc Natl Acad Sci U S A* (2005) 102(1):192–7. doi:10.1073/pnas.0408592102
154. Buytaert E, Dewaele M, Agostinis P. Molecular effectors of multiple cell death pathways initiated by photodynamic therapy. *Biochim Biophys Acta* (2007) 1776(1):86–107. doi:10.1016/j.bbcan.2007.07.001

155. Capella MA, Capella LS. A light in multidrug resistance: photodynamic treatment of multidrug-resistant tumors. *J Biomed Sci* (2003) 10(4):361–6. doi:10.1159/000071155
156. Vrouenraets MB, Visser GW, Snow GB, van Dongen GA. Basic principles, applications in oncology and improved selectivity of photodynamic therapy. *Anticancer Res* (2003) 23(1B):505–22.
157. Gudgin Dickson EF, Goyan RL, Pottier RH. New directions in photodynamic therapy. *Cell Mol Biol* (2002) 48(8):939–54.
158. Dougherty TJ, Gomer CJ, Henderson BW, Jori G, Kessel D, Korbelik M, et al. Photodynamic therapy. *J Natl Cancer Instit* (1998) 90(12):889–905. doi:10.1093/jnci/90.12.889
159. Li W, Saud SM, Young MR, Chen G, Hua B. Targeting AMPK for cancer prevention and treatment. *Oncotarget* (2015) 6(10):7365–78. doi:10.18632/oncotarget.3629
160. Luo Z, Zang M, Guo W. AMPK as a metabolic tumor suppressor: control of metabolism and cell growth. *Future Oncol* (2010) 6(3):457–70. doi:10.2217/fon.09.174
161. Griss T, Vincent EE, Egnatchik R, Chen J, Ma EH, Faubert B, et al. Metformin antagonizes cancer cell proliferation by suppressing mitochondrial-dependent biosynthesis. *PLoS Biol* (2015) 13(12):e1002309. doi:10.1371/journal.pbio.1002309
162. Kasznicki J, Sliwinska A, Drzewos J. Metformin in cancer prevention and therapy. *Ann Transl Med* (2014) 2(6):57–68. doi:10.3978/j.issn.2305-5839.2014.06.01
163. Kim J, You YJ. Regulation of organelle function by metformin. *IUBMB Life* (2017) 69(7):459–69. doi:10.1002/iub.1633
164. Lu CL, Qin L, Liu HC, Candas D, Fan M, Li JJ. Tumor cells switch to mitochondrial oxidative phosphorylation under radiation via mTOR-mediated hexokinase II inhibition – a Warbourg-Reversing effect. *PLoS One* (2015) 10(3):e0121046. doi:10.1371/journal.pone.0121046
165. Xie J, Wang X, Proud CG. mTOR inhibitors in cancer therapy. *F1000 Fac Rev* (2016) 5(2078):1–11. doi:10.12688/f1000research.9207.1
166. Zhou J, Li G, Zheng Y, Shen HM, Hu X, Ming QL, et al. A novel autophagy/mitophagy inhibitor liensinine sensitizes breast cancer cells to chemotherapy through DNMI1-mediated mitochondrial fission. *Autophagy* (2015) 11(8):1259–79. doi:10.1080/15548627.2015.1056970
167. Kodiha M, Wang YM, Hutter E, Maysinger D, Stochaj U. Off to the organelles – killing cancer cells with targeted gold nanoparticles. *Theranostics* (2015) 5(4):357–70. doi:10.7150/thno.10657
168. Zhang F, Zhu X, Gong J, Sun Y, Chen D, Wang J, et al. Lysosome-mitochondria-mediated apoptosis specifically evoked in cancer cells induced by gold nanorods. *Nanomedicine* (2016) 11(15):1993–2006. doi:10.2217/nmm-2016-0139

**Conflict of Interest Statement:** The authors declare that the research was conducted in the absence of any commercial or financial relationships that could be construed as a potential conflict of interest.

Copyright © 2017 Martinez-Carreres, Nasrallah and Fajas. This is an open-access article distributed under the terms of the Creative Commons Attribution License (CC BY). The use, distribution or reproduction in other forums is permitted, provided the original author(s) or licensor are credited and that the original publication in this journal is cited, in accordance with accepted academic practice. No use, distribution or reproduction is permitted which does not comply with these terms.

---

## *Appendix B*

---

### **CDK4 Phosphorylates AMPK $\alpha$ 2 to Inhibit Its Activity and Repress Fatty Acid Oxidation**

(Lopez-Mejia et al., 2017)

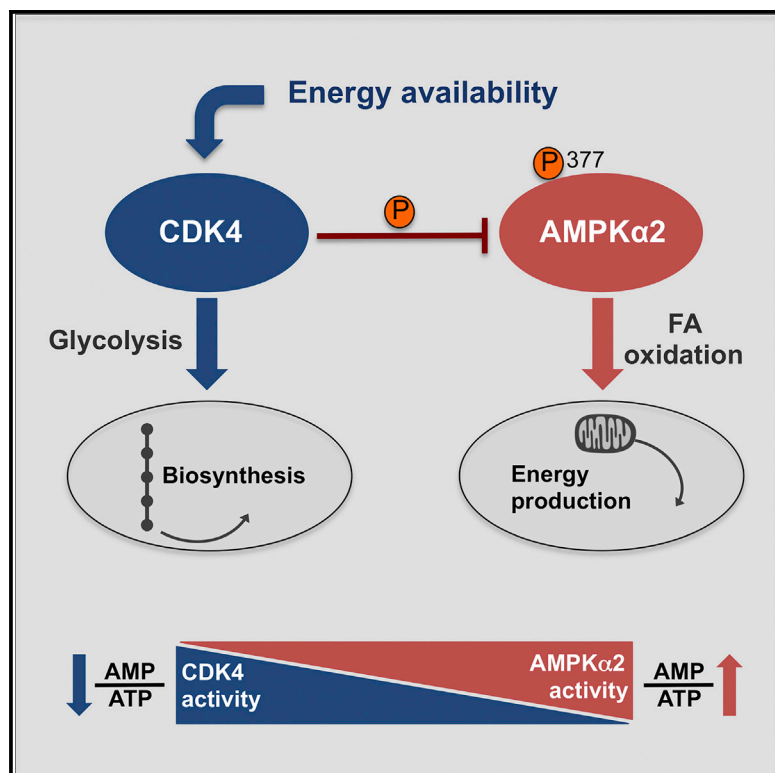
Apart from the review, I had the chance to help other colleagues with their research. In this paper, we explain how CDK4 promotes anabolism by blocking catabolic processes (fatty acid oxidation) that are activated by AMPK.

I have helped with the in vivo experimentations, as well as tissue collection and sample preparation.



# CDK4 Phosphorylates AMPK $\alpha$ 2 to Inhibit Its Activity and Repress Fatty Acid Oxidation

## Graphical Abstract



## Authors

Isabel C. Lopez-Mejia,  
Sylviane Lagarrigue, Albert Giralt, ...,  
Benoît Viollet, D. Grahame Hardie,  
Lluís Fajas

## Correspondence

lluis.fajas@unil.ch

## In Brief

Lopez-Mejia et al. show in this study that CDK4, a protein that is usually involved in the control of cell division, is an important regulator of the energy balance of the cell through the direct inhibition of the activity of AMPK, which is a major regulator of energy consuming processes.

## Highlights

- CDK4 promotes glycolysis and inhibits fatty acid oxidation
- CDK4 inhibits AMPK activity through direct phosphorylation of the AMPK- $\alpha$ 2 subunit
- Mice treated with CDK4 inhibitor have AMPK-dependent increased oxidative metabolism



# CDK4 Phosphorylates AMPK $\alpha$ 2 to Inhibit Its Activity and Repress Fatty Acid Oxidation

Isabel C. Lopez-Mejia,<sup>1,2</sup> Sylviane Lagarrigue,<sup>2</sup> Albert Giralt,<sup>1</sup> Laia Martinez-Carreres,<sup>1</sup> Nadège Zanou,<sup>2,3</sup> Pierre-Damien Denechaud,<sup>1,2</sup> Judit Castillo-Armengol,<sup>1</sup> Carine Chavey,<sup>4</sup> Meritxell Orpinell,<sup>2</sup> Brigitte Delacuisine,<sup>1,2</sup> Anita Nasrallah,<sup>1</sup> Caterina Collodet,<sup>5,6</sup> Lianjun Zhang,<sup>7</sup> Benoît Viollet,<sup>8,9,10</sup> D. Grahame Hardie,<sup>11</sup> and Lluís Fajas<sup>1,2,12,\*</sup>

<sup>1</sup>Center for Integrative Genomics, University of Lausanne, 1015 Lausanne, Switzerland

<sup>2</sup>Department of Physiology, University of Lausanne, 1005 Lausanne, Switzerland

<sup>3</sup>Institute of Sport Sciences, University of Lausanne, 1015 Lausanne, Switzerland

<sup>4</sup>IGMM, Université de Montpellier, UMR 5535 CNRS, 34293 Montpellier, France

<sup>5</sup>Nestlé Institute of Health Sciences SA, EPFL Innovation Park, 1015 Lausanne, Switzerland

<sup>6</sup>École Polytechnique Fédérale de Lausanne, School of Life Sciences, 1015 Lausanne, Switzerland

<sup>7</sup>Ludwig Center for Cancer Research, University of Lausanne, 1066 Epalinges, Switzerland

<sup>8</sup>Institut Cochin, INSERM U1016, Paris, France

<sup>9</sup>CNRS, UMR 8104, Paris, France

<sup>10</sup>Université Paris Descartes, Sorbonne Paris Cité, Paris, France

<sup>11</sup>School of Life Sciences, University of Dundee, Dundee, Scotland, UK

<sup>12</sup>Lead Contact

\*Correspondence: [lluis.fajas@unil.ch](mailto:lluis.fajas@unil.ch)

<https://doi.org/10.1016/j.molcel.2017.09.034>

## SUMMARY

The roles of CDK4 in the cell cycle have been extensively studied, but less is known about the mechanisms underlying the metabolic regulation by CDK4. Here, we report that CDK4 promotes anaerobic glycolysis and represses fatty acid oxidation in mouse embryonic fibroblasts (MEFs) by targeting the AMP-activated protein kinase (AMPK). We also show that fatty acid oxidation (FAO) is specifically induced by AMPK complexes containing the  $\alpha$ 2 subunit. Moreover, we report that CDK4 represses FAO through direct phosphorylation and inhibition of AMPK $\alpha$ 2. The expression of non-phosphorylatable AMPK $\alpha$ 2 mutants, or the use of a CDK4 inhibitor, increased FAO rates in MEFs and myotubes. In addition, *Cdk4*<sup>-/-</sup> mice have increased oxidative metabolism and exercise capacity. Inhibition of CDK4 mimicked these alterations in normal mice, but not when skeletal muscle was AMPK deficient. This novel mechanism explains how CDK4 promotes anabolism by blocking catabolic processes (FAO) that are activated by AMPK.

## INTRODUCTION

Promitotic signals such as growth factors increase the levels of D-type cyclins (cyclins D1, D2, and D3), which bind and activate CDK4/6 to trigger the phosphorylation of the retinoblastoma-associated protein pRB and other pocket proteins (i.e., p107 and p130) (Malumbres and Barbacid, 2005). Rb phosphorylation enables release of the E2F transcription factors that promote the

transcription of genes necessary for the replication of the genome (Malumbres and Barbacid, 2005). The role of CDK4 in the regulation of cell-cycle progression has been extensively studied in eumetazoan organisms, and alterations in CDK4 activity have been associated with cancer development and progression (Malumbres and Barbacid, 2001, 2009; O'Leary et al., 2016). For example, the R24C mutation, which is used in this study, renders CDK4 resistant to inhibition by INK4 inhibitors and has been reported to confer a genetic predisposition to melanoma (Rane et al., 1999, 2002; Wölfel et al., 1995).

Cell division requires substantial amounts of ATP, and numerous metabolic intermediates to support biosynthesis of essential molecules, such as lipids and nucleic acids. Proliferating cells preferentially use anaerobic glycolysis to generate large amounts of ATP and provide metabolic intermediates to support cell growth (Jones and Thompson, 2009). Growing evidence demonstrates that regulatory crosstalk exists between metabolic pathways and regulators of cell-cycle progression. Mitochondrial respiration and metabolism are coordinated with cell-cycle progression by cell-cycle regulators (Lopez-Mejia and Fajas, 2015; Salazar-Roa and Malumbres, 2016). Our laboratory and others have demonstrated that CDK4 is one such "metabolic" cell-cycle regulator (Blanchet et al., 2011; Icreverzi et al., 2012; Lagarrigue et al., 2016; Lee et al., 2014). Indeed, we have previously shown that CDK4 regulates oxidative metabolism via the E2F1 transcription factor in muscle and brown adipose tissue (Blanchet et al., 2011) and promotes the insulin-signaling pathway in mature adipocytes (Lagarrigue et al., 2016). Overall, the participation of cell-cycle regulators in the control of energy homeostasis occurs mainly through the activation of anabolic processes (Aguilar and Fajas, 2010). The AMP-activated protein kinase (AMPK) is a central inhibitor of such anabolic processes and might therefore be repressed by cell-cycle regulators. Under conditions of low cellular energy, AMP and ADP are increased relative to ATP, and this is sensed by AMPK.

AMPK exists as heterotrimeric complexes composed of a catalytic subunit ( $\alpha$ ) and two regulatory subunits ( $\beta$  and  $\gamma$ ); the  $\alpha$  and  $\beta$  subunits exist as two isoforms ( $\alpha1/\alpha2$  and  $\beta1/\beta2$ , encoded by the *PRKAA1/2* and *PRKAB1/2* genes), and the  $\gamma$  subunit exists as three isoforms ( $\gamma1/\gamma2/\gamma3$ , encoded by *PRKAG1/2/3*), thus generating up to 12 combinations of heterotrimeric complex (Carling, 2004; Grahame Hardie, 2016; Hardie et al., 2012; Ross et al., 2016b). AMPK is regulated both by phosphorylation/dephosphorylation and by the relative cellular concentrations of adenine nucleotides, with the two mechanisms being intimately linked. First, the upstream kinases LKB1 (liver kinase B1) (Hawley et al., 2003; Shaw et al., 2004; Woods et al., 2003) or CaMKK2 (calmodulin-dependent kinase kinase-2/- $\beta$ ) (Hawley et al., 2005; Hurley et al., 2005; Woods et al., 2005) activate AMPK through the phosphorylation of Thr<sup>172</sup> of the  $\alpha$  subunit (Hawley et al., 1996). Second, AMPK is regulated through the competitive binding of ATP or AMP and ADP at up to three sites on the  $\gamma$  subunit. When cellular energy levels are low, binding of AMP or ADP enhances Thr<sup>172</sup> phosphorylation by LKB1 and inhibits Thr<sup>172</sup> dephosphorylation by protein phosphatases, while binding of AMP (but not ADP) causes further allosteric activation (Ross et al., 2016a). Metabolic stresses that reduce intracellular ATP concentrations are therefore the best-characterized activators of AMPK, although it has recently been shown that glucose deprivation can activate AMPK by an adenine nucleotide-independent mechanism (Zhang et al., 2017). Once activated, AMPK promotes catabolic pathways that generate ATP (e.g., fatty acid oxidation [FAO]) while switching off anabolic pathways and other ATP-requiring processes to restore cellular ATP levels (Carling, 2004; Grahame Hardie, 2016; Hardie et al., 2012; Ross et al., 2016b).

Other kinase activities that are induced by growth stimuli are known to inhibit AMPK. This includes AKT a key effector of the insulin/insulin growth factor 1 (IGF1)-signaling pathway that antagonizes the AMPK pathway through phosphorylation of AMPK $\alpha1$  on Ser<sup>487</sup> (Horman et al., 2006), or extracellular signal-regulated kinase (ERK), which was shown to phosphorylate the same residue (López-Cotarelo et al., 2015). The cyclic-AMP-dependent protein kinase (PKA) also phosphorylates and negatively regulates AMPK (Djouder et al., 2010; Hurley et al., 2006), and Thr<sup>481</sup> and Ser<sup>477</sup> on AMPK $\alpha1$  are phosphorylated by glycogen synthase kinase 3 (GSK3) (Suzuki et al., 2013), following a “priming” phosphorylation of Ser<sup>487</sup> by AKT.

Muscle function requires a finely tuned balance between anabolism and catabolism in order to respond to physiological challenges within the available energy supply. AMPK is a major coordinator of energy intake and utilization in exercising muscle (Hoffman et al., 2015), functioning to enhance energy availability. Among other effects, AMPK promotes FAO to maintain ATP cellular stores, although the exact role of AMPK in regulation of muscle FAO has been controversial (Mounier et al., 2015).

In this study, we sought to determine whether CDK4 participates in energy homeostasis by inhibiting catabolic processes. The mechanisms by which the activity of AMPK is inhibited under anabolic conditions, such as during cell-cycle progression or in resting muscle, have not been thoroughly studied. We report

here that CDK4 enhances anaerobic glycolysis and represses fatty acid oxidation. Surprisingly, the AMPK $\alpha1$  and  $\alpha2$  subunits play distinct roles. We provide here a molecular mechanism whereby CDK4-CycD3 complexes directly repress  $\alpha2$ -containing complexes to inhibit FAO. We show that chemical and genetic inhibition of CDK4 also promotes oxidative metabolism *in vivo*, as evidenced by decreased respiratory exchange ratio (RER) and increased exercise performance in mice lacking CDK4 activity.

## RESULTS

### CDK4 Modulates FAO in an E2F1-Independent Manner

We previously demonstrated that CDK4 is a major mediator of insulin signaling and therefore contributes to the positive regulation of biosynthetic processes, such as fatty acid synthesis, and the inhibition of catabolic pathways, such as lipolysis (Lagarigue et al., 2016). To further investigate the contribution of CDK4 to metabolic regulation, Seahorse analyses were performed. *Cdk4*<sup>R24C/R24C</sup> mouse embryonic fibroblasts (MEFs), which express a hyperactive CDK4 mutant, exhibited a significant increase in anaerobic glycolysis, as measured by the extracellular acidification rate (ECAR), whereas *Cdk4*<sup>-/-</sup> MEFs had impaired anaerobic glycolysis (Figures 1A and 1B). In contrast, CDK4 activity was inversely correlated with FAO. *Cdk4*<sup>R24C/R24C</sup> MEFs metabolized palmitate at a low rate, whereas *Cdk4*<sup>-/-</sup> MEFs showed increased palmitate oxidation (Figures 1C and 1D). Interestingly, the effects of CDK4 on substrate use were independent of E2F1 activity, since deletion of E2F1 in *Cdk4*<sup>R24C/R24C</sup> MEFs failed to reverse the effects of *Cdk4*<sup>R24C</sup> on anaerobic glycolysis or palmitate oxidation (Figures 1E–1H). These results suggest that CDK4 controls substrate utilization in MEFs independently of E2F1.

### CDK4 Regulation of FAO Is AMPK Dependent

The decrease in FAO observed in response to constitutive activation of CDK4 is the opposite of the effect seen with AMPK activation (Fullerton et al., 2013; Hardie, 2015; Hardie and Pan, 2002; O'Neill et al., 2014). Therefore, we analyzed the involvement of AMPK in the CDK4-mediated regulation of FAO in MEFs. Basal levels of phosphorylated ACC (pACC), which is a known target and marker of AMPK activity, were decreased in *Cdk4*<sup>R24C/R24C</sup> MEFs but increased 3-fold in the *Cdk4*<sup>-/-</sup> cells (Figures 2A, 2B, S1A, and S1B), suggesting that CDK4 antagonizes AMPK function. Moreover, the activation of AMPK by the specific activator A769662 (Göransson et al., 2007; Moreno et al., 2008) was reduced in *Cdk4*<sup>R24C/R24C</sup> MEFs (Figures 2A and 2B), suggesting that CDK4 can prevent AMPK activation. In addition, increased AMP/ATP and ADP/ATP ratios were observed in MEFs expressing the hyperactive CDK4 mutant, which suggested a lower catabolic rate (Figures 2C and 2D). Interestingly, in *Cdk4*<sup>-/-</sup> MEFs, comparable pACC levels were measured both in the basal state and upon AMPK stimulation (Figures 2A and 2B). This finding implies that in the absence of CDK4, AMPK reaches its activated state without need for any further stimulation. Likewise in *Cdk4*<sup>-/-</sup> cells and wild-type (WT) MEFs treated with A769662, we observed a significant decrease of AMP/ATP and ADP/ATP ratios (Figures 2C–2F).

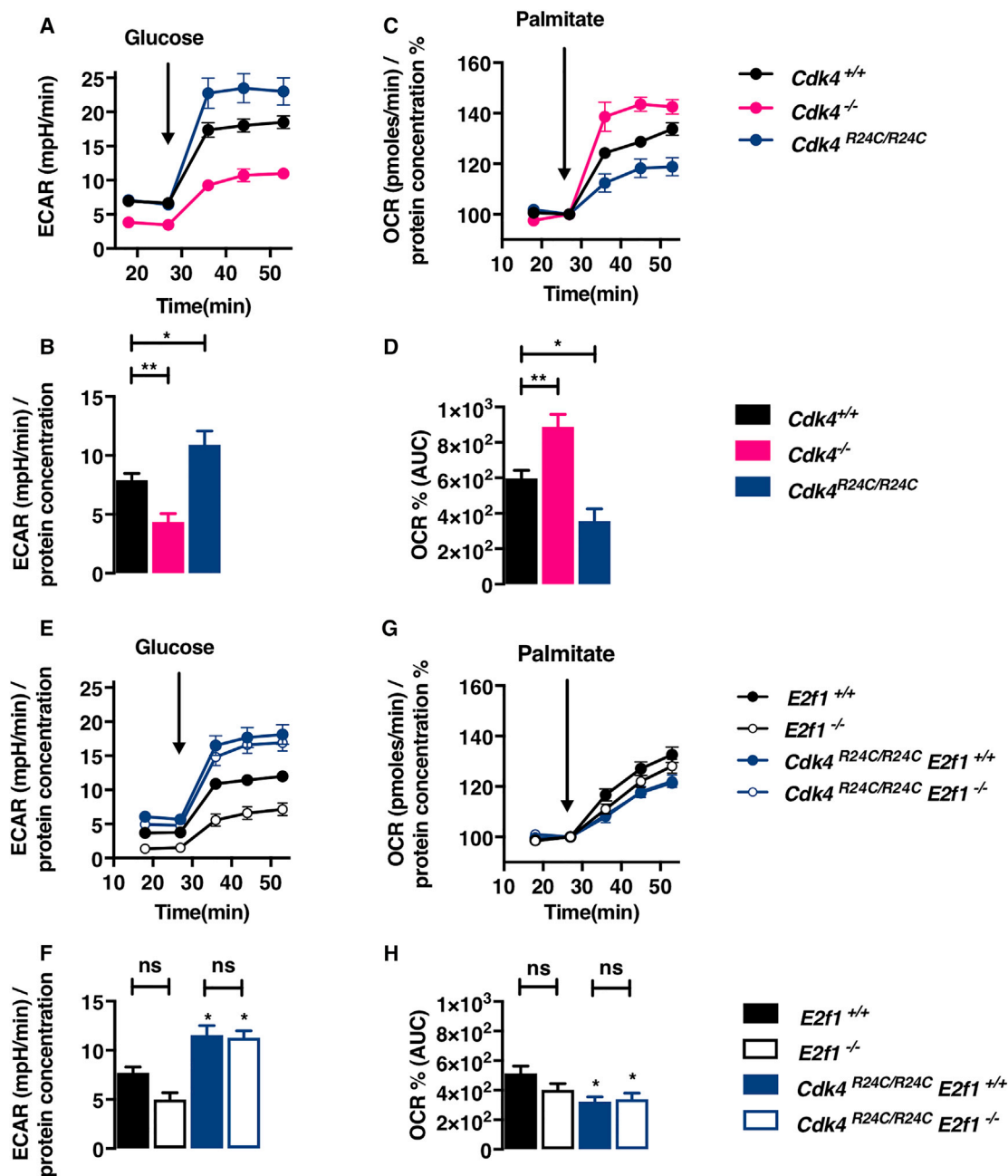


**Figure 1. CDK4 Modulates FAO in an E2F1-Independent Manner**

(A–D) *Cdk4*<sup>+/+</sup>, *Cdk4*<sup>-/-</sup>, and *Cdk4*<sup>R24C/R24C</sup> MEFs were submitted to a glycolysis assay, during which ECAR was measured at the basal level and upon glucose injection (A), or to a FAO assay, in which the palmitate induced OCR was measured (in % OCR compared to the basal OCR) (C). The glycolytic rate was calculated (B). The area under curve of the palmitate induced OCR was quantified (D).

(E–H) *E2f1*<sup>+/+</sup>, *E2f1*<sup>-/-</sup>, *Cdk4*<sup>R24C/R24C</sup> *E2f1*<sup>+/+</sup>, and *Cdk4*<sup>R24C/R24C</sup> *E2f1*<sup>-/-</sup> MEFs were submitted to a glycolysis assay, during which ECAR was measured at the basal level and upon glucose injection (E), or to a FAO assay, in which the palmitate induced OCR was measured (in % OCR compared to the basal OCR) (G). The glycolytic rate was calculated in (F). The area under curve of the palmitate induced OCR was quantified in (H).

Data are expressed as mean ± SEM.

Next, we studied the physiological relevance of the increase in AMPK activity in *Cdk4*<sup>-/-</sup> cells using FAO assays in MEFs treated with A769662 and with the non-selective AMPK inhibitor compound C. As expected, the levels of palmitate oxidation in

WT MEFs were at least 25% higher in A769662-treated cells (Figures 2G, S1C, and S1D). However, *Cdk4*<sup>-/-</sup> cells did not respond in the same assay to A769662 treatment. By contrast, AMPK activation by A769662 in *Cdk4*<sup>R24C/R24C</sup> MEFs was only able to

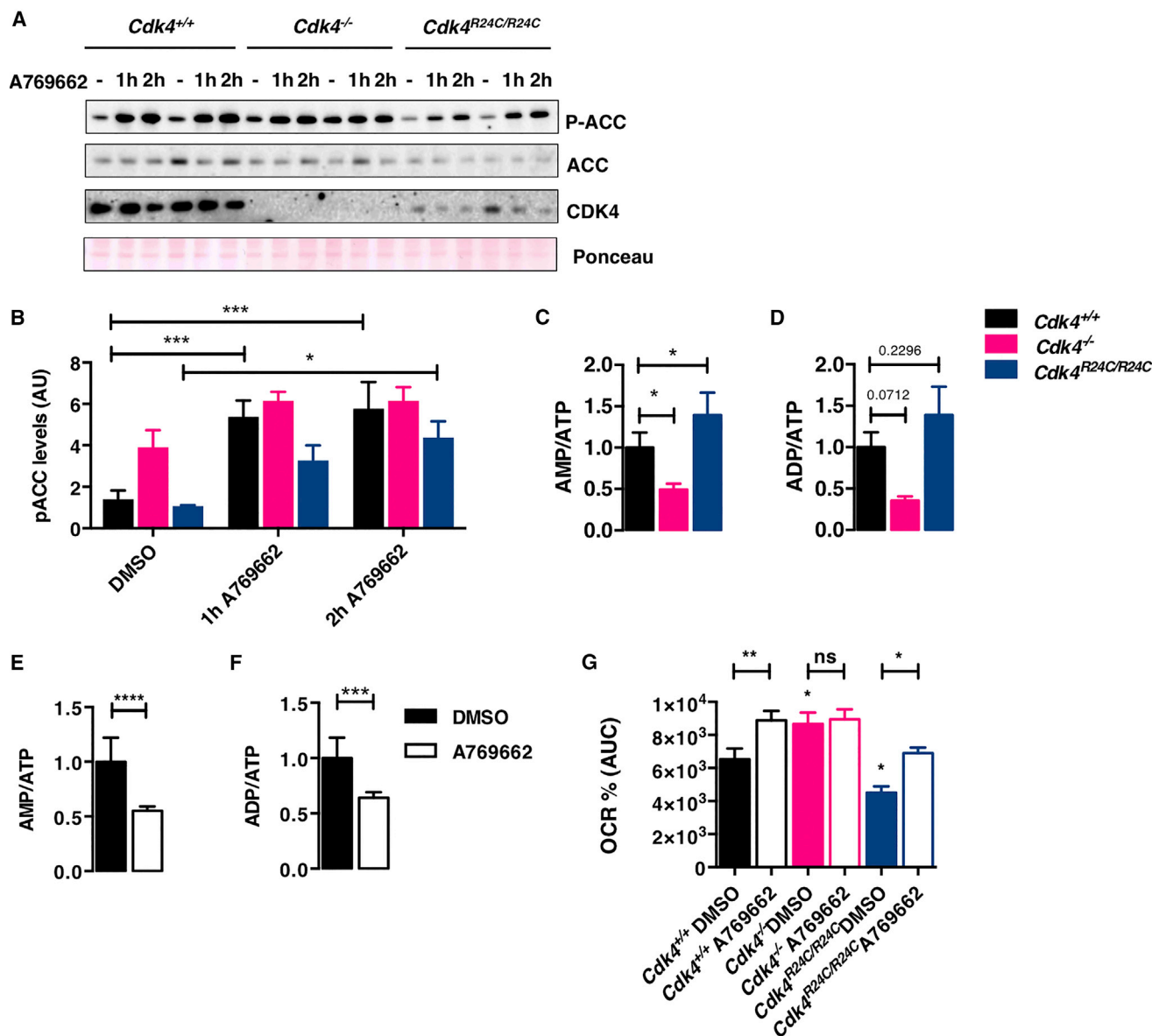


### Figure 2. CDK4 Regulation of FAO Is AMPK Dependent

(A) *Cdk4*<sup>+/+</sup>, *Cdk4*<sup>-/-</sup>, and *Cdk4*<sup>R24C/R24C</sup> MEFs were starved for 3 hr and then stimulated with 50  $\mu$ M A769662; western blot analysis shows the A769662-induced ACC phosphorylation in *Cdk4*<sup>+/+</sup>, *Cdk4*<sup>-/-</sup>, and *Cdk4*<sup>R24C/R24C</sup> cells.

(B) Quantification of pACC levels.

(C and D) SV40 immortalized cells were placed in KHB medium containing 1.5 mM carnitine and 300  $\mu$ M oleate for AMP, ADP, and ATP quantification by HPLC, and AMP/ATP (C) and ADP/ATP (D) ratios are shown.

(E and F) AMP/ATP (E) and ADP/ATP (F) ratios of WT SV40 immortalized cells treated with 50  $\mu$ M A769662 for 8 hr.

(G) *Cdk4*<sup>+/+</sup>, *Cdk4*<sup>-/-</sup>, and *Cdk4*<sup>R24C/R24C</sup> MEFs were treated with DMSO or 50  $\mu$ M A769662 for 2 hr in KHB medium and submitted to a FAO assay in which the palmitate induced OCR was measured (in % OCR compared to the basal OCR). The area under curve of the palmitate-induced OCR was quantified.

Data are expressed as mean  $\pm$  SEM. See also Figure S1.

restore WT levels of FAO (Figures 2G, S1C, and S1D). AMPK inhibition in *Cdk4*<sup>-/-</sup> cells (albeit by the non-selective inhibitor compound C) produced consistent results. The levels of pACC in CDK4-null MEFs, as well as the increased FAO levels, were restored back to basal levels (Figures S1E–S1G). Taken together, these results suggest that CDK4 inhibits the AMPK pathway.

### The AMPK $\alpha$ 2 Subunit Is Required for Efficient FAO in MEFs

Our results suggested that CDK4 has a negative effect on FAO via the regulation of AMPK activity, raising the question of which AMPK subunits contribute to this effect. Interestingly, the deletion of either AMPK $\alpha$  subunit in MEFs resulted in increased

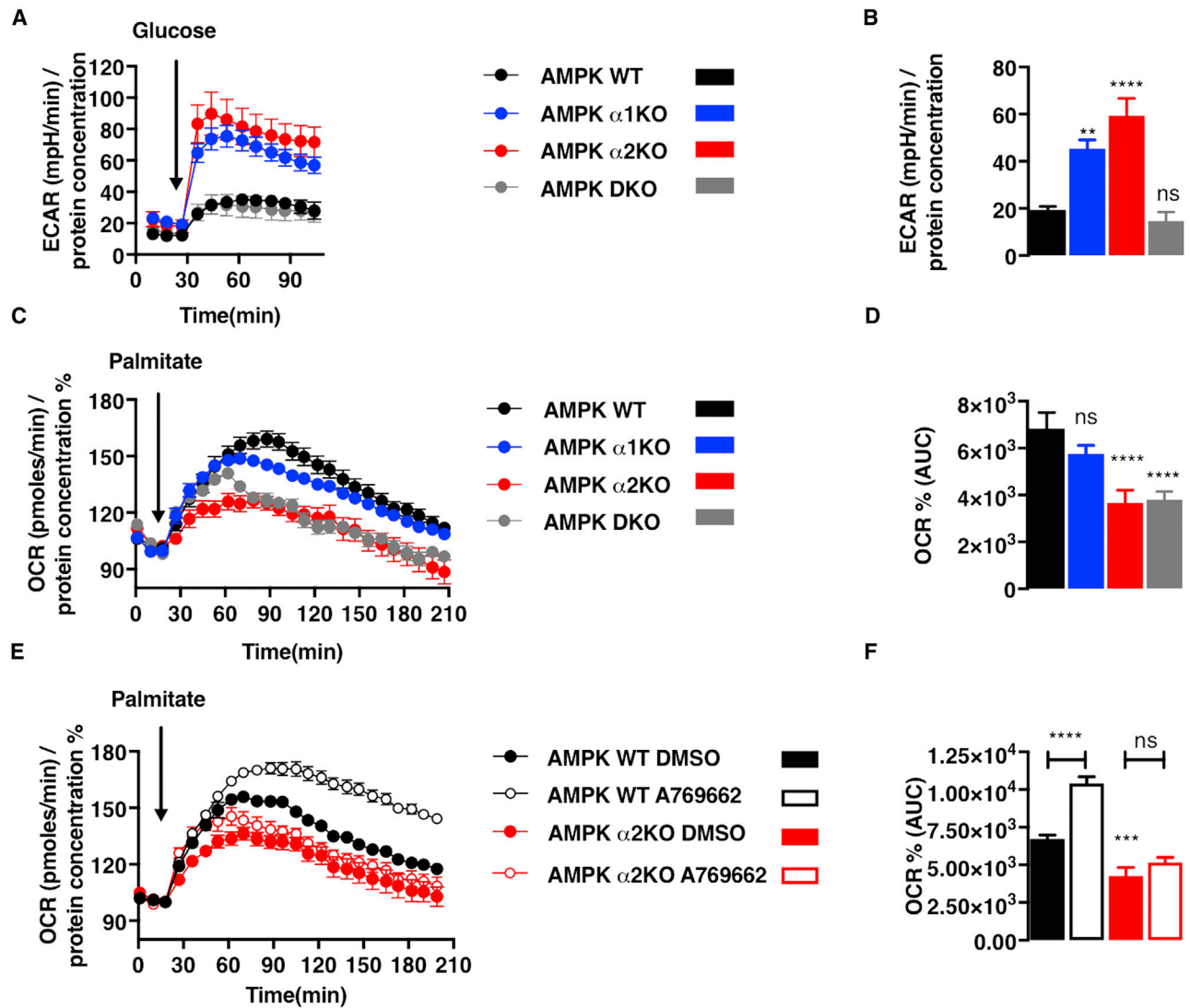


**Figure 3. The AMPK $\alpha2$  Subunit Is Required for Efficient Fatty Acid Oxidation in MEFs**

(A–D) AMPK WT, AMPK  $\alpha1$  KO, AMPK  $\alpha2$  KO, and AMPK DKO SV40-immortalized MEFs were submitted to a glycolysis assay, during which ECAR was measured at the basal level and upon glucose injection (A), or to a FAO assay, in which the palmitate induced OCR was measured (in % OCR compared to the basal OCR) (C). The glycolytic rate was calculated (B). The area under curve of the palmitate induced OCR was quantified (D).

(E and F) AMPK WT and AMPK  $\alpha2$  KO SV40-immortalized MEFs were treated for 2 hr with DMSO or 50  $\mu$ M A769662 for 2 hr in KHB medium and submitted to a FAO assay in which the palmitate induced OCR was measured (in % OCR compared to the basal OCR) (E). The area under curve of the palmitate induced OCR was quantified (F).

Data are expressed as mean  $\pm$  SEM. See also Figure S2.

ECAR, indicating increased glycolysis, whereas the complete abrogation of AMPK activity had no effect, perhaps due to disruption of glucose transport into the cells (Figures 3A and 3B). However, although AMPK $\alpha1$  knockout (KO) MEFs metabolized palmitate as efficiently as control cells, both AMPK $\alpha2$ KO and AMPK  $\alpha1/\alpha2$  double-knockout (DKO) cells exhibited significantly reduced levels of FAO (Figures 3C and 3D). Consistently, A769662 failed to trigger FAO in cells lacking the  $\alpha2$  subunit (both  $\alpha2$ KO and DKO). Thus, despite being more abundant in MEFs (Morizane et al., 2011), the AMPK $\alpha1$  subunit cannot substitute for the  $\alpha2$  subunit in the control of FAO, even when allosterically

activated by A769662 (Figures 3E, 3F, S1H, and S1I). In addition, ACC phosphorylation could be detected upon stimulation with A769662 in both AMPK  $\alpha1$ KO and AMPK  $\alpha2$ KO MEFs (Figure S1J), suggesting that both AMPK subunits can phosphorylate ACC1 and therefore inhibit lipid synthesis, but only AMPK $\alpha2$  can promote FAO. Taken together, these results suggest that AMPK complexes containing  $\alpha2$  specifically control FAO.

#### CDK4 Phosphorylates the AMPK $\alpha2$ Subunit

The inhibition of AMPK $\alpha2$ -dependent FAO could be the result of a direct phosphorylation by CDK4. *In vitro* kinase assays showed

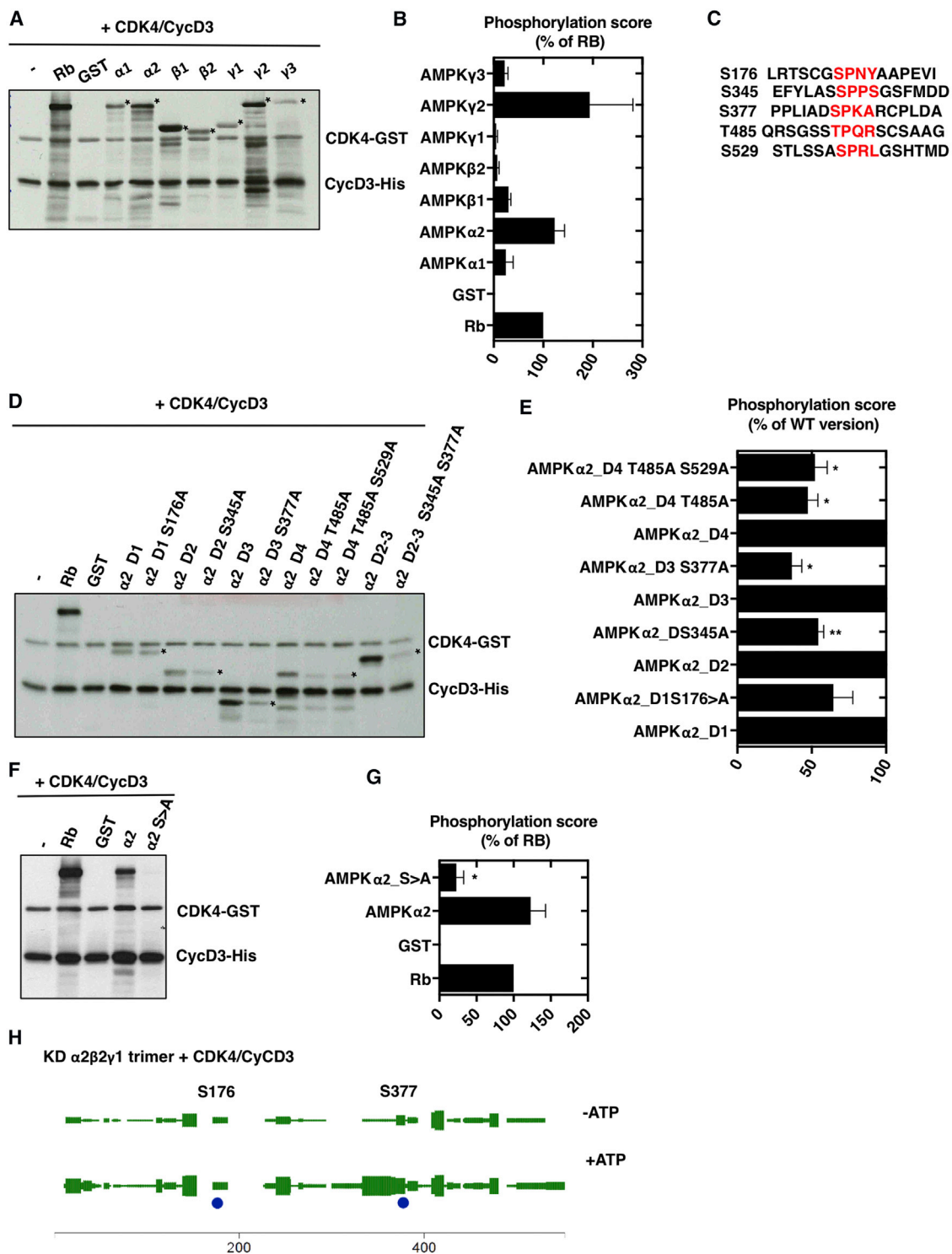


**Figure 4. CDK4 Phosphorylates the AMPK $\alpha$ 2 Subunit**

(A) Cyclin D3-CDK4 directly phosphorylates full-length GST-AMPK subunits *in vitro* (n = 3). Asterisks mark the proteins of interest.

(B) Phosphorylation score (in percentage of RB phosphorylation).

(C) CDK consensus sites in human AMPK $\alpha$ 2 (PRKAA2).

(D) *In vitro* phosphorylation of WT and mutated (Ser or Thr to Ala) GST-AMPK  $\alpha$ 2 fragments (D1, 1–245 aa; D2, 246–356 aa; D3, 357–422 aa; D4, 432–522; and D2–D3, 246–422 aa) by cyclin D3/CDK4 (n = 3).

(legend continued on next page)

that recombinant CDK4/CycD3 phosphorylated all glutathione S-transferase (GST) fusions of AMPK subunits tested at different levels (Figure 4A; loading control in Figure S2A). Interestingly, AMPK $\alpha$ 2 and AMPK $\gamma$ 2 were phosphorylated by CDK4 to a greater extent than pRB, which is the canonical CDK4 substrate (Figure 4B). Since the specificity of CDKs is partially determined by substrate docking on the cyclin subunit, kinase assays were also performed using recombinant CDK4/CycD1 instead of CDK4/CycD3. The phosphorylation of the AMPK subunits was very low under these conditions (Figure S2B), suggesting that AMPK phosphorylation by CDK4 requires recognition by cyclin D3.

AMPK $\alpha$ 2 was predicted to contain 6 CDK4 phosphorylation sites (Thr<sup>85</sup>, Ser<sup>176</sup>, Ser<sup>345</sup>, Ser<sup>377</sup>, Thr<sup>485</sup>, and Ser<sup>529</sup>). Out of these six potential sites, five were listed in the phosphoNET database (Figure 4C). Site-directed mutagenesis (S > A or T > A) combined with protein truncation studies (Figure S3C) identified Ser<sup>345</sup>, Ser<sup>377</sup>, Thr<sup>485</sup>, and Ser<sup>529</sup> as CDK4 phosphorylation sites (Figures 4D and 4E; loading control in Figure S3D). Phosphorylation by CDK4 was completely abrogated in a full-length recombinant protein carrying Ser to Ala or Thr to Ala mutations at the four CDK4 phosphosites ( $\alpha$ 2 S > A mutant), suggesting that the four newly identified residues account for all sites phosphorylated on GST-AMPK $\alpha$ 2 by CDK4 in cell-free assays (Figure 4F and 4G; loading control in Figure S2E). The phosphorylation of Ser<sup>377</sup> and Thr<sup>485</sup> has been previously described in proteomic studies (Figure S2F) (Dinkel et al., 2011; Gnad et al., 2011; Hornbeck et al., 2015), including cell-cycle-related phosphoproteomes (Daub et al., 2008; Kettenbach et al., 2011), and in liver upon insulin stimulation (Humphrey et al., 2015), suggesting that the regulation of AMPK by CDK4 is important for cell-cycle progression and for the insulin signaling pathway. Moreover, we found the four newly identified CDK4 phosphosites to be conserved among the AMPK $\alpha$ 2 subunits of several mammalian species (Figure S3A), but not between the AMPK $\alpha$ 1 and AMPK $\alpha$ 2 isoforms (Figure S3B).

In intact cells, AMPK is found as a heterotrimeric complex; therefore recombinant kinase-inactive  $\alpha$ 2 $\beta$ 2 $\gamma$ 1 complexes were also used as substrate for recombinant CDK4-CycD3 complexes. After mass spectrometry analysis, we obtained 83% coverage of the AMPK $\alpha$ 2 subunit and observed the phosphorylation in Ser<sup>176</sup> and Ser<sup>377</sup> (Figure 4H). A targeted analysis to increase coverage showed phosphorylation of Thr<sup>485</sup> and Ser<sup>529</sup> with low detectability. The phosphorylation of Ser<sup>345</sup> and Ser<sup>377</sup> was also detected in myotubes and muscle tissue, which express high levels of the  $\alpha$ 2 subunit (Figures S4A and S4B; Table S1). Interestingly, our results suggest that these phosphorylations are present when AMPK is inactive, since the activating Thr<sup>172</sup> phosphorylation was not found in 5 out of 6 experiments

(Figures S4A and S4B). Taken together, these data indicate that the  $\alpha$ 2 subunit of AMPK is a substrate for CDK4-CycD3 complexes in cell-free assays and that some of these phosphorylations occur *in vivo*, in conditions in which CDK4 is active (Blanchet et al., 2011; Lagarrigue et al., 2016) but AMPK is inactive.

### AMPK $\alpha$ 2 Phosphorylation Is Necessary and Sufficient for FAO Repression by CDK4

To elucidate the functional relevance of the phosphorylation of AMPK $\alpha$ 2 by CDK4, we compared the regulatory activities of AMPK $\alpha$ 2 S > A, AMPK $\alpha$ 2, and AMPK $\alpha$ 1 in the context of FAO. Transfection of AMPK DKO MEFs with the AMPK $\alpha$ 2 S > A mutant conferred ACC phosphorylation levels that were higher than those observed in AMPK $\alpha$ 1- or  $\alpha$ 2-transfected cells in the basal state and upon stimulation by A769662 (Figure 5A). Similarly, ectopic expression of the AMPK $\alpha$ 2 S > A mutant in the FAO-defective AMPK DKO MEFs rescued palmitate oxidation to a greater extent than that observed upon transfection with WT AMPK $\alpha$ 2 (Figures 5B and S5A). Taken together, these results indicate that defective targeting of AMPK $\alpha$ 2 by CDK4 at Ser<sup>345</sup>, Ser<sup>377</sup>, Thr<sup>485</sup>, and Ser<sup>529</sup> results in increased AMPK $\alpha$ 2 FAO-promoting activity.

In order to demonstrate that CDK4 represses FAO by inhibiting AMPK activity, WT and AMPK mutant cells were treated with CDK4 inhibitors. Inhibition of CDK4 activity by LY2835219 significantly increased FAO after 24 hr (Figures 5C and S5B) or 2 hr (Figure S5C) of treatment. Strikingly, the CDK4 inhibitor failed to increase FAO in both AMPK  $\alpha$ 2KO and AMPK DKO cells, but not in AMPK  $\alpha$ 1KO cells, demonstrating that CDK4 targets AMPK $\alpha$ 2 to alter cellular metabolism (Figures 5C, S5B, and S5E–S5G). The overall positive effect of CDK4 inhibition on AMPK activity was confirmed by analyzing ACC phosphorylation. Indeed, LY2835219 treatment induced a dose-dependent increase in the phosphorylation of ACC (Figures S5H and S5I). This effect correlated with decreased CDK4 activity given that phosphorylation of RB Ser<sup>780</sup> was also reduced (Figure S5I). Of note, increased ACC phosphorylation and increased FAO could be detected after 2 hr of CDK4 inhibition, whereas inhibition of RB phosphorylation required longer treatments. Moreover, LY2835219 had an effect comparable to that of A769662, significantly decreasing AMP/ATP and ADP/ATP ratios in WT MEFs (Figures 2E, 2F, 5D, and 5E). The use of LY2835219 suggests that CDK4 inhibition promotes catabolic processes in an AMPK $\alpha$ 2-subunit-dependent manner.

We next decided to validate our findings in a more physiological cellular model. LY2835219 treatment induced an increase in FAO in C2C12 myotubes, which are known to express high levels of AMPK $\alpha$ 2 (Figures S6A and S6B). In this model, CDK4 inhibition correlated with a dose-dependent increase of the

(E) Phosphorylation score (in percentage of the WT fragment).

(F) *In vitro* phosphorylation of full-length WT GST-AMPK $\alpha$ 2 and full-length S > A GST-AMPK $\alpha$ 2 by cyclin D3/CDK4 (n = 3).

(G) Phosphorylation score (in percentage of RB phosphorylation).

(H) Kinase-dead AMPK  $\alpha$ 2 $\beta$ 2 $\gamma$ 1 trimers were used as a substrate for cyclin D3-CDK4 complex and analyzed by mass spectrometry. A graphical overview of the sequence coverage of AMPK $\alpha$ 2 human protein in samples displayed by MsViz is depicted. The thickness of the green bars is a function of the number of spectra matching the sequence region, while modification sites are labeled and shown as circles with size proportional to the number of spectra matching a given position. A truncated form of RB (hRB; 379–928 aa) was used as a positive control. A representative autoradiography for each kinase assay is shown. See also Figure S3.

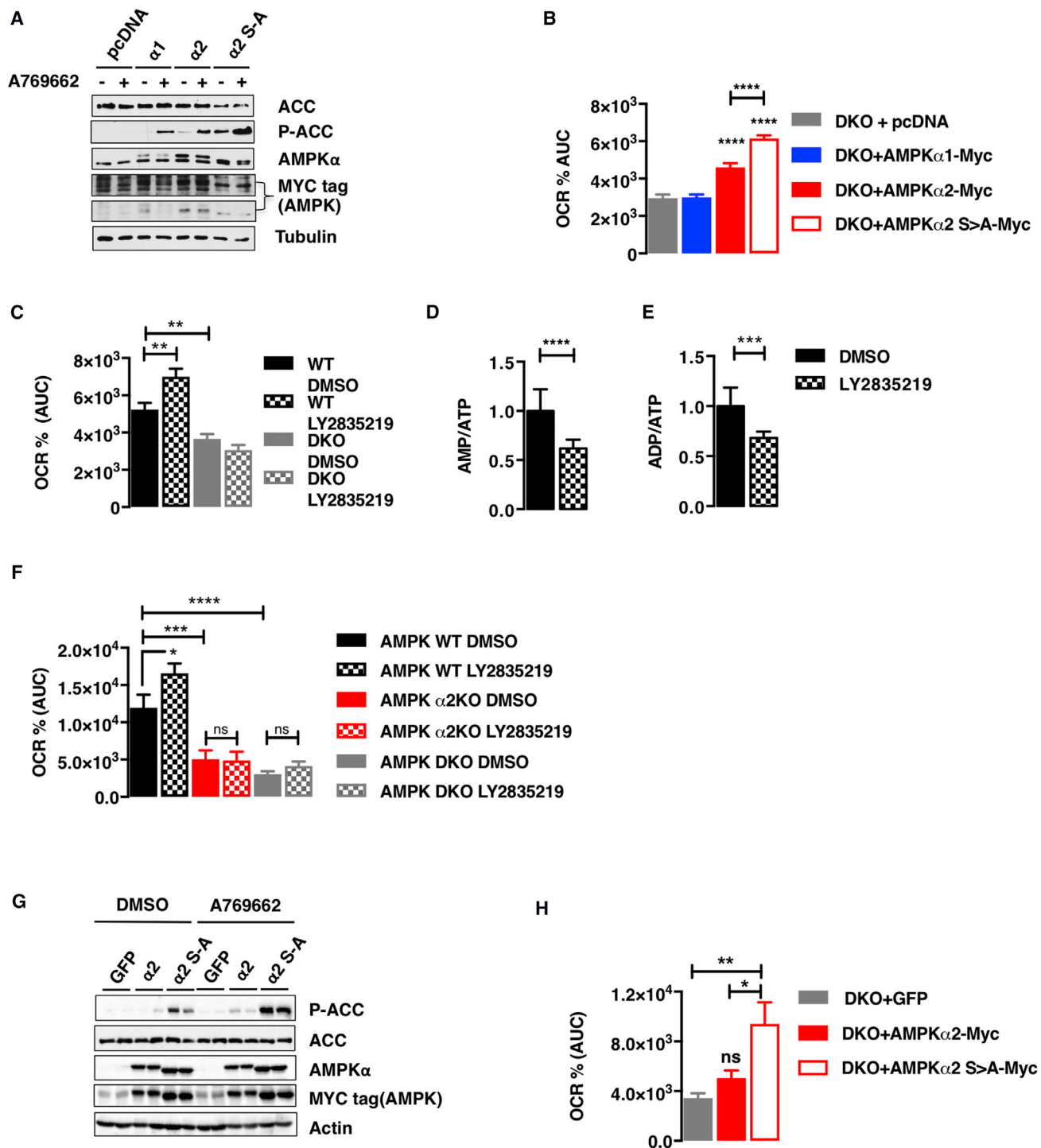


**Figure 5. AMPK $\alpha 2$  Phosphorylation Is Necessary and Sufficient for FAO Repression by CDK4**

(A) AMPK DKO SV40-immortalized MEFs were electroporated with plasmids encoding Myc-tagged AMPK  $\alpha 1$ , Myc-tagged AMPK  $\alpha 2$  and Myc-tagged AMPK  $\alpha 2$  S > A. 48 hr later, MEFs were starved for 3 hr and treated for 2 hr with DMSO or 50  $\mu$ M A769662 before protein extraction. Western blot analysis shows the A769662-induced ACC phosphorylation in transfected cells.

(B) Electroporated MEFs were submitted to a FAO assay 48 hr after transfection, in which the palmitate induced OCR was measured (in % OCR compared to the basal OCR). The area under curve of the palmitate induced OCR was quantified.

(C) AMPK WT and AMPK DKO SV40-immortalized MEFs were treated with DMSO or LY2835219 (1.5  $\mu$ M) for 24 hr and submitted to a FAO assay, in which the palmitate-induced OCR was measured (in % OCR compared to the basal OCR). The area under curve of the palmitate induced OCR was quantified.

(legend continued on next page)

phosphorylation of ACC, without significant increase of AMPK Thr<sup>172</sup> phosphorylation (Figures S6C–S6E). The direct involvement of AMPK $\alpha$ 2 was confirmed by analyzing myotubes lacking AMPK $\alpha$ 2 or both the  $\alpha$ 1 and  $\alpha$ 2 subunits (Lantier et al., 2010). Like in MEFs, FAO was impaired in the  $\alpha$ 2KO and DKO myotubes. Similarly, the CDK4 inhibitor failed to increase FAO in  $\alpha$ 2KO and DKO myotubes (Figures 5F and S6F). Rescue of AMPK DKO myotubes with the AMPK $\alpha$ 2 S > A mutant triggered ACC phosphorylation levels that were higher than those observed in AMPK  $\alpha$ 2-transfected cells both in the basal state or upon stimulation with A769662 (Figure 5G). Similarly, ectopic expression of the AMPK $\alpha$ 2 S > A mutant in the FAO-defective AMPK DKO myotubes rescued palmitate oxidation to levels similar to those of WT myotubes (Figures 5H and S6G). Taken together, these results in muscle cells confirm that CDK4 modulates FAO through the specific inhibition of AMPK $\alpha$ 2 activity and that a non-phosphorylatable AMPK $\alpha$ 2 mutant has a FAO-promoting activity.

#### CDK4 Modulates Oxidative Metabolism and Exercise Capacity *In Vivo*

We next investigated the contribution of CDK4 to oxidative metabolism and muscle function *in vivo*. Isolated mitochondria from *Cdk4*<sup>-/-</sup> muscles showed increased oxygen consumption, suggesting increased fatty acid oxidation capacity (Figures 6A and 6B). Increased FAO was further demonstrated by using intact muscle fibers from flexor digitorum brevis (FDB) muscle (Figure 6C). Fibers from *Cdk4*<sup>-/-</sup> FDB muscle metabolized palmitate at a higher rate (Figures 6C and 6D) and were capable to reach a higher maximal respiration (Figures 6C and 6E). The increased capacity of the muscles of *Cdk4*<sup>-/-</sup> mice to oxidize fatty acids suggested an overall metabolic phenotype in these mice.

*Cdk4*<sup>-/-</sup> mice have decreased body weight (Figure 6F). Consistent with increased AMPK activity, *Cdk4*<sup>-/-</sup> mice exhibit increased exercise capacity and decreased RER, indicating a preference toward fat oxidation (Figures 6G–6I). An 8-day treatment with LY2835219 did not trigger significant alterations in body weight and food intake (Figures 6J and S7D), although it induced a consistent albeit non-significant decrease in fat mass (Figure S7C) and a modest but significant increase in exercise performance (Figure 6K). A decrease in RER was observed after 4–5 days of treatment (Figures 6L and 6M). *In vivo*, the inhibition of CDK4 triggered an increase in the phosphorylation of ACC in quadriceps muscle (Figures S7E and S7G), suggesting increased AMPK activity. This was accompanied by an increase of the slow-twitch fiber marker MyHC I (Figure S7I). MyHC I mRNA levels were also increased in gastrocnemius and tibialis muscles from LY2835219-treated animals (Figures S7H–S7J).

Overall, these data suggest that CDK4 is a negative regulator of exercise capacity and whole-body oxidative metabolism in mice.

#### CDK4 Regulation of Oxidative Metabolism and Exercise Capacity *In Vivo* Requires Muscle AMPK

To determine if the effects of CDK4 inhibition in exercise performance and whole-body oxidative metabolism require muscle AMPK, we treated muscle-specific AMPK  $\alpha$ 1/ $\alpha$ 2 KO mice (MDKO) (Lantier et al., 2014) with the CDK4 inhibitor. Consistently, treatment with LY2835219 did not trigger significant alterations in body weight or food intake (Figures 7A and S7M) in control or in AMPK MDKO animals. In control animals, LY2835219 was sufficient to trigger a decrease (albeit not significant [ $p = 0.1243$ ]) in fat mass, a modest increase in exercise performance, and a decrease in RER (Figures 7B–7D and S7L). In agreement with previous reports (Lantier et al., 2014; O'Neill et al., 2011), AMPK MDKO animals showed decreased RER and decreased exercise capacity (Figures 7B–7D). However, they were not affected by the treatment with LY2835219 under our experimental conditions (Figures 7A–7D and S7K–S7M). Taken together, these results show that the negative effects of CDK4 in oxidative metabolism and exercise performance *in vivo* involve muscle AMPK activity.

#### DISCUSSION

The contribution of CDK4 to the control of cell-cycle progression, via pocket proteins and E2F transcription factors, has been extensively studied (Malumbres, 2014) for more than two decades. However, the CDK4/6-pRB/E2F1 pathway was only recently implicated in metabolic regulation (Aguilar and Fajas, 2010; Blanchet et al., 2011; Denechaud et al., 2016; Lagarrigue et al., 2016; Lee et al., 2014; Lopez-Mejia and Fajas, 2015; Petrov et al., 2016; Salazar-Roa and Malumbres, 2016). Our study provides evidence that the cell-cycle kinase CDK4 is a key player in the control of cellular energy homeostasis and can also act independently of E2F1 to regulate metabolic pathways.

Three major findings are described here. First, we found that CDK4 negatively regulates the AMPK pathway and thus inhibits FAO through phosphorylation of the AMPK $\alpha$ 2 subunit. Indeed, *Cdk4*<sup>-/-</sup> MEFs behaved like cells treated with an AMPK activator and exhibited high FAO levels and low levels of anaerobic glycolysis. Consistently, *Cdk4*<sup>R24C/R24C</sup> cells exhibited increased anaerobic glycolysis and very low FAO levels. A similar phenotype was observed in AMPK  $\alpha$ 2KO MEFs. Therefore, CDK4 activity is inversely correlated with AMPK $\alpha$ 2-dependent activity. These findings indicate that CDK4 plays a central role in

(D and E) AMPK WT SV40 immortalized cells were treated for 8 hr with DMSO or LY2835219 (1.5  $\mu$ M). AMP, ADP, and ATP were quantified by HPLC. The AMP/ATP (D) and ADP/ATP (E) ratios are shown.

(F–H) AMPK WT, AMPK  $\alpha$ 2 KO and AMPK DKO myotubes were treated with DMSO or 1.5  $\mu$ M LY2835219 for 24, and submitted to a FAO assay, in which the palmitate induced OCR was measured (in % OCR compared to the basal OCR). The area under curve of the palmitate induced OCR was quantified in (F). AMPK DKO myotubes were transfected with plasmids encoding Myc-tagged AMPK  $\alpha$ 2 and Myc-tagged AMPK  $\alpha$ 2 S > A. B. 48 hr later, myotubes were treated for 2 hr with DMSO or 50  $\mu$ M A769662 before protein extraction; western blot analysis shows the A769662-induced ACC phosphorylation in transfected cells (G). Transfected myotubes were submitted to a FAO assay in which the palmitate-induced OCR was measured (in % OCR compared to the basal OCR). The area under curve of the palmitate-induced OCR was quantified in (H).

Data are expressed as mean  $\pm$  SEM. See also Figure S4 and S5.

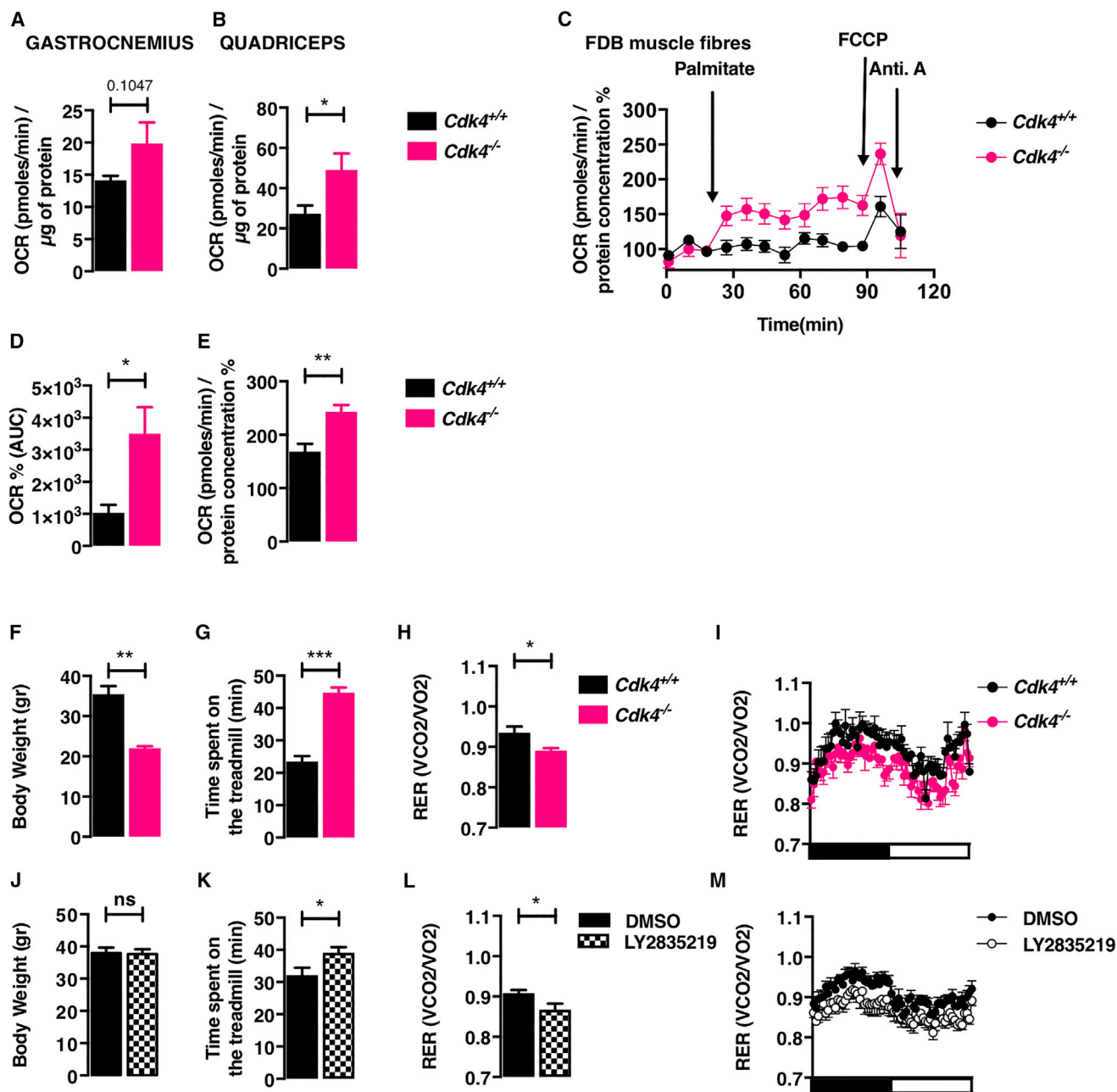


**Figure 6. CDK4 Modulates Oxidative Metabolism and Exercise Capacity In Vivo**

(A–E) Mitochondria isolated from gastrocnemius (A) and quadriceps (B) muscle from *Cdk4*<sup>+/+</sup> and *Cdk4*<sup>-/-</sup> mice were submitted to a respiration assay using fatty acids as a substrate. Isolated FDB muscle fibres from *Cdk4*<sup>+/+</sup> and *Cdk4*<sup>-/-</sup> mice were submitted to a FAO assay in which the palmitate-induced OCR was measured (in % OCR compared to the basal OCR) (C). The area under curve of the palmitate-induced OCR is shown (D). The maximal respiration was induced by FCCP (E).

(F) Body weight of 25- to 30-week-old male *Cdk4*<sup>+/+</sup> and *Cdk4*<sup>-/-</sup> mice was measured.

(G) *Cdk4*<sup>+/+</sup> and *Cdk4*<sup>-/-</sup> were submitted to an exercise capacity testing on treadmill, and the time before exhaustion was recorded.

(H and I) RER of the aforementioned mice is depicted.

(J and K) 30-week-old WT mice were gavaged with 37 mg/kg LY2835219 or vehicle for 8 days. Body weight (K) and exercise capacity (K) were measured the day after the last treatment.

(L and M) RER of the aforementioned mice after 5 days of treatment is depicted.

Data are expressed as mean  $\pm$  SEM. See also Figure S6.

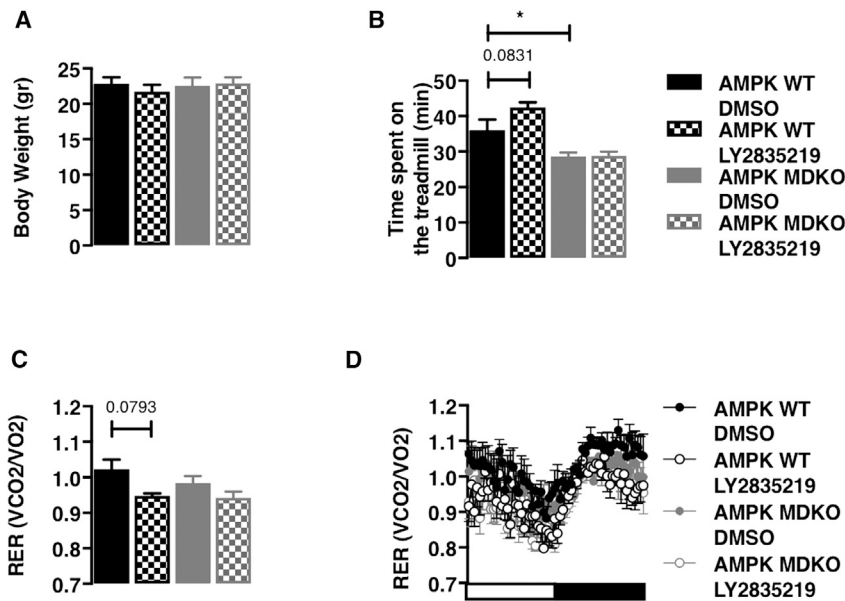


**Figure 7. CDK4 Regulation of Oxidative Metabolism and Exercise Capacity *In Vivo* Requires Muscle AMPK**

(A) Body weight of 12- to 16-week-old AMPK WT and AMPK MDKO females gavaged with 37 mg/kg LY2835219 or vehicle for 8 days was measured. (B–D) Body weight of 12–16 weeks old AMPK WT and AMPK MDKO females gavaged with 37mg/kg of LY2835219 or vehicle for 8 days was measured in (A). To measure exercise capacity on treadmill, the time before exhaustion was recorded in (B). RER of the aforementioned mice is depicted in (C) and (D). Data are expressed as mean  $\pm$  SEM. See also Figure S7.

mitochondrial FAO that involves AMPK $\alpha$ 2 inhibition and is independent of other downstream effectors, such as E2F1.

Cell division requires high cellular energy levels. Despite the recent evidence that underscores the existence of a crosstalk between cell-cycle regulators and energy metabolism (Lopez-Mejia and Fajas, 2015; Salazar-Roa and Malumbres, 2016), the molecular mechanisms coupling energy production and cell-cycle progression remain to be elucidated. Based on our results, we propose that to exert its role in both cell-cycle progression and the insulin-signaling pathway, CDK4 represses catabolism by directly targeting at least one of the catalytic subunits of AMPK, namely the  $\alpha$ 2 subunit. Interestingly, AKT, another key player of the insulin-signaling pathway, phosphorylates the  $\alpha$ 1 subunit of AMPK, thus reducing  $\alpha$ 1 Thr172 phosphorylation and the subsequent activation of the AMPK heterotrimer (Hawley et al., 2014; Horman et al., 2006). Remarkably, previous evidence from our laboratory demonstrates that CDK4 is a key effector of the AKT pathway (Lagarrigue et al., 2016). Surprisingly, GSK3 has been reported to inhibit AMPK activity after phosphorylation of the  $\alpha$  subunit by AKT (Suzuki et al., 2013). This finding is somehow unexpected, since GSK3 activity is negatively regulated via phosphorylation by AKT upon insulin stimulation. Moreover, GSK3 is known to inhibit rather than promote anabolic pathways, like the synthesis of glycogen (Cohen and Frame, 2001).

The second major finding in our study is the observation that the function of AMPK heterotrimers can differ depending on their  $\alpha$  subunit isoform. Few studies have focused on the specific function of each AMPK subunit (but see a recent review by Ross et al., 2016b), and models completely lacking AMPK activity are often used to study the function of AMPK. Liver-specific deletion or overexpression of the AMPK $\alpha$ 2 subunit suggested that this isoform is involved in regulating the balance between lipid synthesis and FAO (Andreelli et al., 2006; Foretz et al., 2005), but these studies did not assess the differences in spec-

ificity between  $\alpha$ 1 and  $\alpha$ 2. Interestingly, leptin was shown to directly trigger FAO in muscle (Minokoshi et al., 2002) and trigger an anorexigenic response in hypothalamus (Minokoshi et al., 2004) in an AMPK $\alpha$ 2-dependent manner. The effect on food intake may be triggered through AKT signaling via phosphorylation of AMPK $\alpha$ 2 by p70S6K (Dagon et al., 2012). Other positive energy balance signals can also reduce food intake via AMPK $\alpha$ 2 activity in the brain (Claret et al., 2007; Kim et al., 2004). The isoform-specific roles of the different AMPK subunits in whole-body energy homeostasis were further highlighted by the fact that the AMPK $\alpha$ 2 subunit is essential for nicotine-triggered lipolysis in adipocytes (Wu et al., 2015). However, the specific regulation of energy homeostasis by AMPK $\alpha$ 2, and the molecular mechanisms regulating  $\alpha$ 2-isoform specific AMPK activity have remained largely unknown.

The third major finding in our study is that the modulation of CDK4 activity *in vivo* can result in modifications in whole-body energy homeostasis and exercise performance. These modifications require the expression of AMPK in skeletal muscle. Our results are in agreement with previous studies demonstrating that the use of 5-aminoimidazole-4-carboxamide ribonucleotide (AICAR) can increase exercise performance in sedentary mice while increasing the proportion of slow-twitch fibers (Narkar et al., 2008). However, the exact mechanisms that mediate this phenotype remain to be studied. Global approaches to determine muscle reprogramming at the proteomics and gene expression level will allow further study of the involvement of CDK4 in muscle biology, particularly during exercise. Given that muscle expresses the AMPK $\alpha$ 2 subunit highly and responds to exercise by downregulating CDK activity (Hoffman et al., 2015), we believe that the study of the CDK4-AMPK $\alpha$ 2 interaction in skeletal muscle will be very relevant to the discovery of pharmacological interventions to promote or enhance the beneficial effects of exercise on general health.

By identifying 4 new specific CDK4 phosphosites in the  $\alpha$ 2 subunit of AMPK, we have discovered a specific role for this subunit in the control of fatty acid metabolism that we could not demonstrate for the  $\alpha$ 1 subunit. Interestingly, we detected the phosphorylation of two of these residues, Ser<sup>377</sup> and Ser<sup>345</sup>, in

muscle samples from resting mice and myotubes stimulated with insulin or IGF1.

FAO repression by CDK4 emerges as an additional level of metabolic regulation by this kinase, which also mediates other effects of the insulin-signaling pathway (Lagarrigue et al., 2016), including lipid synthesis, glycolysis (Denechaud et al., 2016), and proliferation (Malumbres and Barbacid, 2005).

In conclusion, our results demonstrate that CDK4 is a major regulator of cellular energy homeostasis. By combining experimental data from cellular metabolism analyses, biochemistry and molecular biology studies, and *in vivo* experiments, our work provides insights into the complex regulation of anabolic and catabolic pathways. These novel findings can have broad implications not only in the regulation of cell metabolism during proliferation but also in the control of energy utilization at the level of the whole organism. Moreover, they highlight the need to delve deeper into the specific functions of the different AMPK heterotrimers, as well as in the regulation of AMPK inactivation.

## STAR★METHODS

Detailed methods are provided in the online version of this paper and include the following:

- KEY RESOURCES TABLE
- CONTACT FOR REAGENT AND RESOURCE SHARING
- EXPERIMENTAL MODEL AND SUBJECT DETAILS
  - Cell culture
  - Animal studies
- METHOD DETAILS
  - Materials
  - Immunoblot
  - Plasmid constructs and mutagenesis
  - GST production
  - CDK4 Kinase assay
  - Mitochondrial isolation
  - Isolation of adult skeletal muscle fibers
  - Seahorse analyses
  - Immunoprecipitation
  - Mass spectrometry
  - HPLC
  - mRNA analysis
- QUANTIFICATION AND STATISTICAL ANALYSES

## SUPPLEMENTAL INFORMATION

Supplemental Information includes seven figures and three tables and can be found with this article online at <https://doi.org/10.1016/j.molcel.2017.09.034>.

## AUTHOR CONTRIBUTIONS

I.C.L.-M. and L.F. designed this study. I.C.L.-M. guided and performed most experiments, with assistance from S.L., A.G., L.M.-C., P.-D.D., N.Z., C. Chavey, B.D., J.C.-A., A.N., L.Z., and C. Collodet. M.O. performed HPLC analysis for AMP-ADP-ATP quantification. B.V. generated the *Prkaa1*<sup>-/-</sup>, *Prkaa2*<sup>-/-</sup> individual KOs and *Prkaa1*<sup>-/-</sup>; *Prkaa2*<sup>-/-</sup> double-KO MEF cells and myoblasts, as well as the muscle-specific *Prkaa1*<sup>-/-</sup>; *Prkaa2*<sup>-/-</sup> double-KO mice. D.G.H. helped to design the experiments and provided AMPK constructs. I.C.L.-M. and L.F. wrote the manuscript.

## ACKNOWLEDGMENTS

We acknowledge all of the members of the Fajas laboratory for support and discussions. We thank P. Waridel and M. Quadroni (from the Protein Analysis Facility, Center for Integrative Genomics, Faculty of Biology and Medicine, University of Lausanne, Switzerland) for their help with mass spectrometry analysis. We thank M. Barbacid for providing the *Cdk4*<sup>R24C/R24C</sup> and *Cdk4*<sup>-/-</sup> mice that were used to prepare MEFs. This work was supported by the Swiss National Science Foundation. C. Collodet is an employee of the Nestlé Institute of Health Sciences SA (Switzerland).

Received: November 14, 2016

Revised: July 17, 2017

Accepted: September 22, 2017

Published: October 19, 2017

## REFERENCES

- Aguilar, V., and Fajas, L. (2010). Cycling through metabolism. *EMBO Mol. Med.* *2*, 338–348.
- Andreelli, F., Foretz, M., Knauf, C., Cani, P.D., Perrin, C., Iglesias, M.A., Pillot, B., Bado, A., Tronche, F., Mithieux, G., et al. (2006). Liver adenosine monophosphate-activated kinase- $\alpha$ 2 catalytic subunit is a key target for the control of hepatic glucose production by adiponectin and leptin but not insulin. *Endocrinology* *147*, 2432–2441.
- Blanchet, E., Annicotte, J.S., Lagarrigue, S., Aguilar, V., Clapé, C., Chavey, C., Fritz, V., Casas, F., Apparailly, F., Auwerx, J., and Fajas, L. (2011). E2F transcription factor-1 regulates oxidative metabolism. *Nat. Cell Biol.* *13*, 1146–1152.
- Carling, D. (2004). Ampk. *Curr. Biol.* *14*, R220.
- Claret, M., Smith, M.A., Batterham, R.L., Selman, C., Choudhury, A.I., Fryer, L.G., Clements, M., Al-Qassab, H., Heffron, H., Xu, A.W., et al. (2007). AMPK is essential for energy homeostasis regulation and glucose sensing by POMC and AgRP neurons. *J. Clin. Invest.* *117*, 2325–2336.
- Cohen, P., and Frame, S. (2001). The renaissance of GSK3. *Nat. Rev. Mol. Cell Biol.* *2*, 769–776.
- Dagon, Y., Hur, E., Zheng, B., Wellenstein, K., Cantley, L.C., and Kahn, B.B. (2012). p70S6 kinase phosphorylates AMPK on serine 491 to mediate leptin's effect on food intake. *Cell Metab.* *16*, 104–112.
- Daub, H., Olsen, J.V., Bairlein, M., Gnad, F., Oppermann, F.S., Körner, R., Greff, Z., Kéri, G., Stemmann, O., and Mann, M. (2008). Kinase-selective enrichment enables quantitative phosphoproteomics of the kinome across the cell cycle. *Mol. Cell* *31*, 438–448.
- Denechaud, P.D., Lopez-Mejia, I.C., Giralt, A., Lai, Q., Blanchet, E., Delacuisine, B., Nicolay, B.N., Dyson, N.J., Bonner, C., Pattou, F., et al. (2016). E2F1 mediates sustained lipogenesis and contributes to hepatic steatosis. *J. Clin. Invest.* *126*, 137–150.
- Dinkel, H., Chica, C., Via, A., Gould, C.M., Jensen, L.J., Gibson, T.J., and Diella, F. (2011). Phospho.ELM: a database of phosphorylation sites—update 2011. *Nucleic Acids Res.* *39*, D261–D267.
- Djouder, N., Tuerk, R.D., Suter, M., Salvioni, P., Thali, R.F., Scholz, R., Vaahtomeri, K., Auchli, Y., Rechsteiner, H., Brunisholz, R.A., et al. (2010). PKA phosphorylates and inactivates AMPK $\alpha$  to promote efficient lipolysis. *EMBO J.* *29*, 469–481.
- Foretz, M., Ancellin, N., Andreelli, F., Saintillan, Y., Grondin, P., Kahn, A., Thorens, B., Vaulont, S., and Viollet, B. (2005). Short-term overexpression of a constitutively active form of AMP-activated protein kinase in the liver leads to mild hypoglycemia and fatty liver. *Diabetes* *54*, 1331–1339.
- Fullerton, M.D., Galic, S., Marcinko, K., Sikkema, S., Pulinilkunnil, T., Chen, Z.P., O'Neill, H.M., Ford, R.J., Palanivel, R., O'Brien, M., et al. (2013). Single phosphorylation sites in *Acc1* and *Acc2* regulate lipid homeostasis and the insulin-sensitizing effects of metformin. *Nat. Med.* *19*, 1649–1654.
- Gnad, F., Gunawardena, J., and Mann, M. (2011). PHOSIDA 2011: the post-translational modification database. *Nucleic Acids Res.* *39*, D253–D260.

- Göransson, O., McBride, A., Hawley, S.A., Ross, F.A., Shpiro, N., Foretz, M., Viollet, B., Hardie, D.G., and Sakamoto, K. (2007). Mechanism of action of A-769662, a valuable tool for activation of AMP-activated protein kinase. *J. Biol. Chem.* *282*, 32549–32560.
- Grahame Hardie, D. (2016). Regulation of AMP-activated protein kinase by natural and synthetic activators. *Acta Pharm. Sin. B* *6*, 1–19.
- Hardie, D.G. (2015). AMPK: positive and negative regulation, and its role in whole-body energy homeostasis. *Curr. Opin. Cell Biol.* *33*, 1–7.
- Hardie, D.G., and Pan, D.A. (2002). Regulation of fatty acid synthesis and oxidation by the AMP-activated protein kinase. *Biochem. Soc. Trans.* *30*, 1064–1070.
- Hardie, D.G., Ross, F.A., and Hawley, S.A. (2012). AMPK: a nutrient and energy sensor that maintains energy homeostasis. *Nat. Rev. Mol. Cell Biol.* *13*, 251–262.
- Hawley, S.A., Davison, M., Woods, A., Davies, S.P., Beri, R.K., Carling, D., and Hardie, D.G. (1996). Characterization of the AMP-activated protein kinase kinase from rat liver and identification of threonine 172 as the major site at which it phosphorylates AMP-activated protein kinase. *J. Biol. Chem.* *271*, 27879–27887.
- Hawley, S.A., Boudeau, J., Reid, J.L., Mustard, K.J., Udd, L., Mäkelä, T.P., Alessi, D.R., and Hardie, D.G. (2003). Complexes between the LKB1 tumor suppressor, STRAD alpha/beta and MO25 alpha/beta are upstream kinases in the AMP-activated protein kinase cascade. *J. Biol.* *2*, 28.
- Hawley, S.A., Pan, D.A., Mustard, K.J., Ross, L., Bain, J., Edelman, A.M., Frenguelli, B.G., and Hardie, D.G. (2005). Calmodulin-dependent protein kinase kinase-beta is an alternative upstream kinase for AMP-activated protein kinase. *Cell Metab.* *2*, 9–19.
- Hawley, S.A., Ross, F.A., Gowans, G.J., Tibarewal, P., Leslie, N.R., and Hardie, D.G. (2014). Phosphorylation by Akt within the ST loop of AMPK- $\alpha$ 1 down-regulates its activation in tumour cells. *Biochem. J.* *459*, 275–287.
- Hoffman, N.J., Parker, B.L., Chaudhuri, R., Fisher-Wellman, K.H., Kleinert, M., Humphrey, S.J., Yang, P., Holliday, M., Trefely, S., Fazakerley, D.J., et al. (2015). Global phosphoproteomic analysis of human skeletal muscle reveals a network of exercise-regulated kinases and AMPK substrates. *Cell Metab.* *22*, 922–935.
- Horman, S., Vertommen, D., Heath, R., Neumann, D., Mouton, V., Woods, A., Schlattner, U., Wallimann, T., Carling, D., Hue, L., and Rider, M.H. (2006). Insulin antagonizes ischemia-induced Thr172 phosphorylation of AMP-activated protein kinase alpha-subunits in heart via hierarchical phosphorylation of Ser485/491. *J. Biol. Chem.* *281*, 5335–5340.
- Hornbeck, P.V., Zhang, B., Murray, B., Kornhauser, J.M., Latham, V., and Skrzypek, E. (2015). PhosphoSitePlus, 2014: mutations, PTMs and recalibrations. *Nucleic Acids Res.* *43*, D512–D520.
- Humphrey, S.J., Azimifar, S.B., and Mann, M. (2015). High-throughput phosphoproteomics reveals in vivo insulin signaling dynamics. *Nat. Biotechnol.* *33*, 990–995.
- Hurley, R.L., Anderson, K.A., Franzone, J.M., Kemp, B.E., Means, A.R., and Witters, L.A. (2005). The Ca<sup>2+</sup>/calmodulin-dependent protein kinase kinases are AMP-activated protein kinase kinases. *J. Biol. Chem.* *280*, 29060–29066.
- Hurley, R.L., Barré, L.K., Wood, S.D., Anderson, K.A., Kemp, B.E., Means, A.R., and Witters, L.A. (2006). Regulation of AMP-activated protein kinase by multisite phosphorylation in response to agents that elevate cellular cAMP. *J. Biol. Chem.* *281*, 36662–36672.
- Icreverzi, A., de la Cruz, A.F., Van Voorhies, W.A., and Edgar, B.A. (2012). Drosophila cyclin D/Cdk4 regulates mitochondrial biogenesis and aging and sensitizes animals to hypoxic stress. *Cell Cycle* *11*, 554–568.
- Jones, R.G., and Thompson, C.B. (2009). Tumor suppressors and cell metabolism: a recipe for cancer growth. *Genes Dev.* *23*, 537–548.
- Kettenbach, A.N., Schweppe, D.K., Faherty, B.K., Pechenick, D., Pletnev, A.A., and Gerber, S.A. (2011). Quantitative phosphoproteomics identifies substrates and functional modules of Aurora and Polo-like kinase activities in mitotic cells. *Sci. Signal.* *4*, rs5.
- Kim, M.S., Park, J.Y., Namkoong, C., Jang, P.G., Ryu, J.W., Song, H.S., Yun, J.Y., Namgoong, I.S., Ha, J., Park, I.S., et al. (2004). Anti-obesity effects of alpha-lipoic acid mediated by suppression of hypothalamic AMP-activated protein kinase. *Nat. Med.* *10*, 727–733.
- Laderoute, K.R., Amin, K., Calaoagan, J.M., Knapp, M., Le, T., Orduna, J., Foretz, M., and Viollet, B. (2006). 5'-AMP-activated protein kinase (AMPK) is induced by low-oxygen and glucose deprivation conditions found in solid-tumor microenvironments. *Mol. Cell. Biol.* *26*, 5336–5347.
- Lagarrigue, S., Lopez-Mejia, I.C., Denechaud, P.D., Escoté, X., Castillo-Armengol, J., Jimenez, V., Chavey, C., Giralt, A., Lai, Q., Zhang, L., et al. (2016). CDK4 is an essential insulin effector in adipocytes. *J. Clin. Invest.* *126*, 335–348.
- Lantier, L., Mounier, R., Leclerc, J., Pende, M., Foretz, M., and Viollet, B. (2010). Coordinated maintenance of muscle cell size control by AMP-activated protein kinase. *FASEB J.* *24*, 3555–3561.
- Lantier, L., Fentz, J., Mounier, R., Leclerc, J., Trebak, J.T., Pehmoller, C., Sanz, N., Sakakibara, I., Saint-Amand, E., Rimbaud, S., et al. (2014). AMPK controls exercise endurance, mitochondrial oxidative capacity, and skeletal muscle integrity. *FASEB J.* *28*, 3211–3224.
- Lee, Y., Dominy, J.E., Choi, Y.J., Jurczak, M., Tolliday, N., Camporez, J.P., Chim, H., Lim, J.H., Ruan, H.B., Yang, X., et al. (2014). Cyclin D1-Cdk4 controls glucose metabolism independently of cell cycle progression. *Nature* *510*, 547–551.
- López-Cotarelo, P., Escribano-Díaz, C., González-Bethencourt, I.L., Gómez-Moreira, C., Deguiz, M.L., Torres-Bacete, J., Gómez-Cabañas, L., Fernández-Barrera, J., Delgado-Martín, C., Mellado, M., et al. (2015). A novel MEK-ERK-AMPK signaling axis controls chemokine receptor CCR7-dependent survival in human mature dendritic cells. *J. Biol. Chem.* *290*, 827–840.
- Lopez-Mejia, I.C., and Fajas, L. (2015). Cell cycle regulation of mitochondrial function. *Curr. Opin. Cell Biol.* *33*, 19–25.
- Malumbres, M. (2014). Cyclin-dependent kinases. *Genome Biol.* *15*, 122.
- Malumbres, M., and Barbacid, M. (2001). To cycle or not to cycle: a critical decision in cancer. *Nat. Rev. Cancer* *1*, 222–231.
- Malumbres, M., and Barbacid, M. (2005). Mammalian cyclin-dependent kinases. *Trends Biochem. Sci.* *30*, 630–641.
- Malumbres, M., and Barbacid, M. (2009). Cell cycle, CDKs and cancer: a changing paradigm. *Nat. Rev. Cancer* *9*, 153–166.
- Manfredi, G., Yang, L., Gajewski, C.D., and Mattiazzi, M. (2002). Measurements of ATP in mammalian cells. *Methods* *26*, 317–326.
- Martín-Campos, T., Mylonas, R., Masselot, A., Waridel, P., Petricevic, T., Xenarios, I., and Quadroni, M. (2017). MsViz, a graphical software tool for in-depth manual validation and quantitation of post-translational modifications. *J. Proteome Res.* *16*, 3092–3101.
- Minokoshi, Y., Kim, Y.B., Peroni, O.D., Fryer, L.G., Müller, C., Carling, D., and Kahn, B.B. (2002). Leptin stimulates fatty-acid oxidation by activating AMP-activated protein kinase. *Nature* *415*, 339–343.
- Minokoshi, Y., Alquier, T., Furukawa, N., Kim, Y.B., Lee, A., Xue, B., Mu, J., Fofelle, F., Ferré, P., Birbaumer, M.J., et al. (2004). AMP-kinase regulates food intake by responding to hormonal and nutrient signals in the hypothalamus. *Nature* *428*, 569–574.
- Moreno, D., Knecht, E., Viollet, B., and Sanz, P. (2008). A769662, a novel activator of AMP-activated protein kinase, inhibits non-proteolytic components of the 26S proteasome by an AMPK-independent mechanism. *FEBS Lett.* *582*, 2650–2654.
- Morizane, Y., Thanos, A., Takeuchi, K., Murakami, Y., Kayama, M., Trichonas, G., Miller, J., Foretz, M., Viollet, B., and Vavvas, D.G. (2011). AMP-activated protein kinase suppresses matrix metalloproteinase-9 expression in mouse embryonic fibroblasts. *J. Biol. Chem.* *286*, 16030–16038.
- Mounier, R., Thérêt, M., Lantier, L., Foretz, M., and Viollet, B. (2015). Expanding roles for AMPK in skeletal muscle plasticity. *Trends Endocrinol. Metab.* *26*, 275–286.

- Narkar, V.A., Downes, M., Yu, R.T., Embler, E., Wang, Y.X., Banayo, E., Mihaylova, M.M., Nelson, M.C., Zou, Y., Juguilon, H., et al. (2008). AMPK and PPARdelta agonists are exercise mimetics. *Cell* 134, 405–415.
- Nesvizhskii, A.I., Keller, A., Kolker, E., and Aebersold, R. (2003). A statistical model for identifying proteins by tandem mass spectrometry. *Analytical Chemistry* 75, 4646–4658.
- O’Leary, B., Finn, R.S., and Turner, N.C. (2016). Treating cancer with selective CDK4/6 inhibitors. *Nat. Rev. Clin. Oncol.* 13, 417–430.
- O’Neill, H.M., Maarbjerg, S.J., Crane, J.D., Jeppesen, J., Jørgensen, S.B., Schertzer, J.D., Shyroka, O., Kiens, B., van Denderen, B.J., Tarnopolsky, M.A., et al. (2011). AMP-activated protein kinase (AMPK) beta1beta2 muscle null mice reveal an essential role for AMPK in maintaining mitochondrial content and glucose uptake during exercise. *Proc. Natl. Acad. Sci. USA* 108, 16092–16097.
- O’Neill, H.M., Lally, J.S., Galic, S., Thomas, M., Azizi, P.D., Fullerton, M.D., Smith, B.K., Puliniikunnil, T., Chen, Z., Samaan, M.C., et al. (2014). AMPK phosphorylation of ACC2 is required for skeletal muscle fatty acid oxidation and insulin sensitivity in mice. *Diabetologia* 57, 1693–1702.
- Petrov, P.D., Ribot, J., López-Mejía, I.C., Fajas, L., Palou, A., and Bonet, M.L. (2016). Retinoblastoma protein knockdown favors oxidative metabolism and glucose and fatty acid disposal in muscle cells. *J. Cell. Physiol.* 231, 708–718.
- Rane, S.G., Dubus, P., Mettus, R.V., Galbreath, E.J., Boden, G., Reddy, E.P., and Barbacid, M. (1999). Loss of Cdk4 expression causes insulin-deficient diabetes and Cdk4 activation results in beta-islet cell hyperplasia. *Nat. Genet.* 22, 44–52.
- Rane, S.G., Cosenza, S.C., Mettus, R.V., and Reddy, E.P. (2002). Germ line transmission of the Cdk4(R24C) mutation facilitates tumorigenesis and escape from cellular senescence. *Mol. Cell. Biol.* 22, 644–656.
- Ross, F.A., Jensen, T.E., and Hardie, D.G. (2016a). Differential regulation by AMP and ADP of AMPK complexes containing different  $\gamma$  subunit isoforms. *Biochem. J.* 473, 189–199.
- Ross, F.A., MacKintosh, C., and Hardie, D.G. (2016b). AMP-activated protein kinase: a cellular energy sensor that comes in 12 flavours. *FEBS J.* 283, 2987–3001.
- Salazar-Roa, M., and Malumbres, M. (2016). Fueling the cell division cycle. *Trends Cell Biol.* 27, 69–81.
- Schindelin, J., Arganda-Carreras, I., Frise, E., Kaynig, V., Longair, M., Pietzsch, T., Preibisch, S., Rueden, C., Saalfeld, S., Schmid, B., et al. (2012). Fiji: an open-source platform for biological-image analysis. *Nat. Methods* 9, 676–682.
- Shaw, R.J., Kosmatka, M., Bardeesy, N., Hurley, R.L., Witters, L.A., DePinho, R.A., and Cantley, L.C. (2004). The tumor suppressor LKB1 kinase directly activates AMP-activated kinase and regulates apoptosis in response to energy stress. *Proc. Natl. Acad. Sci. USA* 101, 3329–3335.
- Suzuki, T., Bridges, D., Nakada, D., Skiniotis, G., Morrison, S.J., Lin, J.D., Saltiel, A.R., and Inoki, K. (2013). Inhibition of AMPK catabolic action by GSK3. *Mol. Cell* 50, 407–419.
- Wölfel, T., Hauer, M., Schneider, J., Serrano, M., Wölfel, C., Klehmann-Hieb, E., De Plaen, E., Hankeln, T., Meyer zum Büschenfelde, K.H., and Beach, D. (1995). A p16INK4a-insensitive CDK4 mutant targeted by cytolytic T lymphocytes in a human melanoma. *Science* 269, 1281–1284.
- Woods, A., Johnstone, S.R., Dickerson, K., Leiper, F.C., Fryer, L.G., Neumann, D., Schlattner, U., Wallimann, T., Carlson, M., and Carling, D. (2003). LKB1 is the upstream kinase in the AMP-activated protein kinase cascade. *Curr. Biol.* 13, 2004–2008.
- Woods, A., Dickerson, K., Heath, R., Hong, S.P., Momcilovic, M., Johnstone, S.R., Carlson, M., and Carling, D. (2005). Ca<sup>2+</sup>/calmodulin-dependent protein kinase kinase-beta acts upstream of AMP-activated protein kinase in mammalian cells. *Cell Metab.* 2, 21–33.
- Wu, Y., Song, P., Zhang, W., Liu, J., Dai, X., Liu, Z., Lu, Q., Ouyang, C., Xie, Z., Zhao, Z., et al. (2015). Activation of AMPK $\alpha$ 2 in adipocytes is essential for nicotine-induced insulin resistance in vivo. *Nat. Med.* 21, 373–382.
- Zhang, C.S., Hawley, S.A., Zong, Y., Li, M.Q., Wang, Z.C., Gray, A., Ma, T., Cui, J.W., Feng, J.W., Zhu, M.J., et al. (2017). Fructose-1,6-bisphosphate and aldolase mediate glucose sensing by AMPK. *Nature* 548, 112–116.

## STAR★METHODS

## KEY RESOURCES TABLE

REAGENT or RESOURCE	SOURCE	IDENTIFIER
<b>Antibodies</b>		
Rabbit polyclonal anti-ACC	Cell Signaling Technology	Cat#3662
Rabbit polyclonal anti-Phospho-ACC	Cell Signaling Technology	Cat#3661
Rabbit polyclonal anti-AMPKa	Cell Signaling Technology	Cat#2532
Rabbit monoclonal anti-Phospho-AMPKa(Thr172)(40H9)	Cell Signaling Technology	Cat#2535
Mouse monoclonal anti-Myc-Tag (9B11)	Cell Signaling Technology	Cat#2276
Rabbit monoclonal anti-Phospho Rb (ser780)(D59B7)	Cell Signaling Technology	Cat#8180
Rabbit polyclonal anti-Cdk4 (C-22)	Santa Cruz biotechnology	Sc-260
Mouse monoclonal anti-Rb (C-2)	Santa Cruz biotechnology	Sc-74562
Goat polyclonal anti-AMPK a2 (C-20)	Santa Cruz biotechnology	Sc-19131
Goat polyclonal anti-Actin (C11)	Santa Cruz biotechnology	Sc-1615
Rabbit polyclonal anti-Myc-Tag	Abcam	Ab9106
Mouse monoclonal anti- $\alpha$ -Tubulin	Sigma-Aldrich	T6199
<b>Chemicals, Peptides, and Recombinant Proteins</b>		
LY2835219	MedChemExpress	HY-16297
PD0332991	MedChemExpress	HY-50767
LEE011	MedChemExpress	HY-15777
A769662	MedChemExpress	HY-50662
Compound C	MedChemExpress	HY-13418
FCCP	Sigma Aldrich	C2920
Antimycine A	Sigma Aldrich	A8674
CDK4/CycD3	ProQinase	0142-0373-1
CDK4/CycD1	ProQinase	0142-0143-1
Recombinant kinase dead AMPK trimers ( $\alpha 2\beta 2\gamma 1$ )	DG. Hardie lab.	
<b>Experimental Models: Cell Lines</b>		
C2C12	ATCC	CRL-1772
Primary and SV40 immortalized <i>Cdk4</i> <sup>-/-</sup> MEFs	This paper	N/A
Primary and SV40 immortalized <i>Cdk4</i> <sup>+/+</sup> MEFs,	This paper	N/A
Primary and SV40 immortalized <i>Cdk4</i> <sup>R24C/R24C</sup> MEFs	This paper	N/A
Primary <i>E2f1</i> <sup>+/+</sup> MEFs	This paper	N/A
Primary <i>E2f1</i> <sup>-/-</sup> MEFs	This paper	N/A
Primary <i>Cdk4</i> <sup>R24C/R24C</sup> <i>E2f1</i> <sup>+/+</sup> MEFs	This paper	N/A
Primary <i>Cdk4</i> <sup>R24C/R24C</sup> <i>E2f1</i> <sup>-/-</sup> MEFs	This paper	N/A
<i>Prkaa1</i> <sup>-/-</sup> SV40 immortalized MEFs	(Laderoute et al., 2006)	N/A
<i>Prkaa2</i> <sup>-/-</sup> SV40 immortalized MEFs	(Laderoute et al., 2006)	N/A
<i>Prkaa1</i> <sup>-/-</sup> ; <i>Prkaa2</i> <sup>-/-</sup> double KO SV40 immortalized MEFs	(Laderoute et al., 2006)	N/A
AMPK alpha2 KO Myoblasts	(Lantier et al., 2010)	N/A
AMPK alpha1, alpha2 double KO Myoblasts	(Lantier et al., 2010)	N/A
AMPK WT Myoblasts	(Lantier et al., 2010)	N/A
<b>Experimental Models: Organisms/Strains</b>		
Skeletal muscle AMPK-deficient mice [AMPK_1fl/fl_2fl/fl human skeletal actin (HSA)-Cre_ mice on a C57Bl6-129Sv mixed background]	(Lantier et al., 2014)	N/A
The generation of <i>Cdk4</i> <sup>-/-</sup> , that lack CDK4 in all tissues except pancreatic beta cells and were referred as <i>Cdk4</i> <sup>nc/nc</sup> in our previous study.	(Lagarrigue et al., 2016)	N/A
C57BL/6JRj mice.		Janvier Labs

(Continued on next page)

**Continued**

REAGENT or RESOURCE	SOURCE	IDENTIFIER
Oligonucleotides		
See <a href="#">Table S2</a>		N/A
See <a href="#">Table S3</a>		N/A
Recombinant DNA		
pDONR223-hPRKAA1	Addgene	(ref:23871)
pDONR223-hPRKAA2	Addgene	(ref:23671)
pDONR223-hPRKAB1	Addgene	(ref:23360)
pDONR223-hPRKAB2	Addgene	(ref:23647)
pDONR223-hPRKAG1,	Addgene	(ref:23718)
pDONR223-hPRKAG2	Addgene	(ref:23689)
pDONR223-hPRKAG3	Addgene	(ref:23549)
pDEST pGEX-2T-hPRKAA1	This paper	N/A
pDEST pGEX-2T -hPRKAA2	This paper	N/A
pDEST pGEX-2T -hPRKAB1	This paper	N/A
pDEST pGEX-2T -hPRKAB2	This paper	N/A
pDEST pGEX-2T -hPRKAG1,	This paper	N/A
pDEST pGEX-2T -hPRKAG2	This paper	N/A
pDEST pGEX-2T -hPRKAG3	This paper	N/A
pDEST pGEX-2T -hPRKAA2 D1	This paper	N/A
pDEST pGEX-2T -hPRKAA2 D1 S176A	This paper	N/A
pDEST pGEX-2T -hPRKAA2 D2	This paper	N/A
pDEST pGEX-2T -hPRKAA2 D2 S345A	This paper	N/A
pDEST pGEX-2T -hPRKAA2 D3	This paper	N/A
pDEST pGEX-2T -hPRKAA2 D3 S377A	This paper	N/A
pDEST pGEX-2T -hPRKAA2 D4	This paper	N/A
pDEST pGEX-2T -hPRKAA2 D4 T485A	This paper	N/A
pGEX-2T -hPRKAA2 D4 T485A S529A	This paper	N/A
pDEST pGEX-2T -hPRKAA2 D2-D3	This paper	N/A
pDEST pGEX-2T -hPRKAA2 D2-D3 S345A S377A	This paper	N/A
pDEST pGEX-2T -hPRKAA2 S377A S345A T485A S529A	This paper	N/A
pCDNA3 MYC hPRKAA1	This paper	N/A
pCDNA3 MYC hPRKAA2	This paper	N/A
pCDNA3 MYC hPRKAA2 S377A S345A T485A S529A	This paper	N/A
Software and Algorithms		
Protein Prophet algorithm	( <a href="#">Nesvizhskii et al., 2003</a> )	N/A
MsViz software	( <a href="#">Martin-Campos et al., 2017</a> )	N/A
Fiji image processing package	( <a href="#">Schindelin et al., 2012</a> ).	N/A

**CONTACT FOR REAGENT AND RESOURCE SHARING**

Further information and requests for resources and reagents should be directed to and will be fulfilled by Lluís Fajas ([lluis.fajas@unil.ch](mailto:lluis.fajas@unil.ch)).

**EXPERIMENTAL MODEL AND SUBJECT DETAILS****Cell culture**

MEFs were derived from embryos that were dissected 13.5 days after vaginal plugs. The *Cdk4*<sup>-/-</sup> (*Cdk4*<sup>nc</sup>), *Cdk4*<sup>R24C/R24C</sup> and *E2f1*<sup>-/-</sup> mice have been previously described ([Denechaud et al., 2016](#); [Lagarrigue et al., 2016](#)).

*Prkaa1*<sup>-/-</sup>, *Prkaa2*<sup>-/-</sup> individual KOs; and *Prkaa1*<sup>-/-</sup>; *Prkaa2*<sup>-/-</sup> double KO SV40 immortalized MEF cells were prepared as described (Laderoute et al., 2006). They are referred in the manuscript as AMPK  $\alpha$ 1KO, AMPK  $\alpha$ 2KO and AMPK DKO.

MEFs were cultured in DMEM/F12 supplemented with 10% fetal bovine serum (FBS, PAA Laboratories), glutamax (1mM), sodium pyruvate (1mM), non-essential amino-acids, 2-Mercapto-ethanol (50 $\mu$ M) and antibiotics in 5% CO<sub>2</sub> 37°C incubator.

C2C12 myoblasts were obtained from ATCC and were cultured in low-glucose DMEM with 10% FBS in 5% CO<sub>2</sub> 37°C incubator. For myotube differentiation, when the cells reached 80%–90% confluency, the culture medium was switched to DMEM containing 2% horse serum. The medium was changed every 2 days until day 5 to 7 of differentiation.

Primary myoblasts were grown in collagen coated plates cultured DMEM/F12 supplemented with 20% fetal bovine serum, 2mM Glutamine and FGF (5ng/ml) in 5% CO<sub>2</sub> 37°C incubator. For myotube differentiation, cells were plated on matrigel-coated plates when the cells reached 80%–90% confluency, the culture medium was switched to DMEM/F12 supplemented with 2% horse serum and 2mM Glutamine. The medium was changed every 2 days until day 4–5 of differentiation. For rescue experiments, myotubes were transfected using lipofectamine 3000 (Thermo Fisher Scientific), at day 1 and day 3 of differentiation. The cells were assayed 48 hr after the 2<sup>nd</sup> round of transfection.

Primary *Cdk4*<sup>+/+</sup>, *Cdk4*<sup>-/-</sup> and *Cdk4*<sup>R24C/R24C</sup> MEFs, as well as primary *E2f1*<sup>+/+</sup>, *E2f1*<sup>-/-</sup>, *Cdk4*<sup>R24C/R24C</sup> *E2f1*<sup>+/+</sup> and *Cdk4*<sup>R24C/R24C</sup> *E2f1*<sup>-/-</sup> MEFs, between P2 and P5, were used for Figures 1 and 2. SV40 immortalized MEFs were used for all other figures.

### Animal studies

The generation of *Cdk4*<sup>-/-</sup>, that lack CDK4 in all tissues except pancreatic beta cells and were referred as *Cdk4*<sup>nc/nc</sup> in our previous study, was described in (Lagarrigue et al., 2016). Male mice were used.

For gavage experiments, C57BL/6J male mice were obtained from Janvier Labs. Animals were gavaged daily with 37mg/kg of LY2835219 or vehicle for 8 days. Mice were acclimated and submitted to indirect calorimetry between day 4 and day 6. Exercise capacity testing was performed the day after the last gavage. Body weight was controlled daily. Food intake was measured in the metabolic cages.

To obtain skeletal muscle AMPK-deficient mice [AMPK<sub>1fl/fl</sub> <sub>2fl/fl</sub> human skeletal actin (HSA)-Cre<sub>1</sub> mice on a C57Bl6-129Sv mixed background], AMPK<sub>1<sup>fl/fl</sup>2<sup>fl/fl</sup></sub> mice were interbred with transgenic mice expressing Cre recombinase under the control of the HSA promoter. Female mice were used.

The mice were housed in a facility on a 12-h light-dark cycle with free access to standard rodent chow and water.

Mice were familiarized to the motorized rodent treadmill (Columbus Instruments, Columbus OH) on the J-2 and J-1 before the evaluation of exercise capacity. Familiarization consisted of an initial 10 min period where the treadmill speed and incline were set to zero with a slight electric shock grid at the back of the carpet set to 20 V, 0.34 mA, and 2 Hz. The treadmill speed was then increased steadily to 10 m/min (J-2) and 12 m/min (J-1) for an additional 10 min.

The day immediately following familiarization to the treadmill, mice were subjected to an exercise capacity test. For this, the mice were acclimated to the treadmill for 10 min, with the speed and incline set initially to zero. The treadmill speed was then increase to 8.5 m/min with an angle of inclination set to 0° for 9 min. Next, the treadmill speed and incline was increased to 10 m/min and 5°, respectively, for 3 min. The speed was then increased by 2.5 m/min every 3 min to a maximum speed of 40 m/min, while inclination was increased by 5° every 9 min until a maximum incline of 15°.

Strict a priori criteria for exercise-induced exhaustion consisted in: (1) 10 consecutive seconds on the electric grid; (2) spending more than 50% of time on the grid; and/or (3) lack of motivation to manual prodding. Mice were immediately removed from their respective lane once one or more of these criteria were reached.

Following the protocol, mice were killed by cervical dislocation and skeletal muscles were isolated for analysis.

All animal care and treatment procedures were performed in accordance with Swiss guidelines and were approved by the Canton of Vaud, Service de la Consommation et des Affaires Vétérinaires (SCAV) (authorization VD 3121.a).

## METHOD DETAILS

### Materials

All cell culture reagents were purchased from GIBCO (Thermo Fisher Scientific). All chemicals, except if stated otherwise, were purchased from Sigma-Aldrich. The CDK4 inhibitor (LY2835219) and Compound C. were purchased from MedChem Express. Experiments were done using 1 $\mu$ M of LY2835219, unless stated otherwise. The AMPK allosteric activator was purchased from Abcam or MedChem Express. Unless stated otherwise, A769662 was used at a concentration of 50 $\mu$ M.  $\gamma$ -<sup>33</sup>P-ATP was purchased from Perkin Elmer.

### Immunoblot

For western blot analysis, the cells were seeded in 6-well plates 48 hr before the experiment, serum starved for 3 hr, and treated with either LY2835219 or A769662 for 2 hr.

Total proteins extracts were subjected to SDS-PAGE analysis and transferred to nitrocellulose membranes for immunoblotting. The following antibodies were obtained from Cell Signaling Technology: ACC (no. 3662), phosphorylated ACC (ser79) (no. 3661), AMPK (no.2532), phosphorylated AMPK (Thr172) (no 2535), Myc-tag (no. 2276), phosphorylated RB (Ser780) (no. 8180). The

following antibodies were obtained from Santa Cruz Technology: Cdk4 (C-22; sc-260), Rb (C-2; sc-74562), AMPK  $\alpha$ 2 (sc-19131). A second Myc-tag antibody was used to analyze myotube samples (Abcam ab9106)

The  $\alpha$  Tubulin (no. T6199) antibody was obtained from Sigma Aldrich, the actin (sc-1615) was obtained from Santa Cruz Technology.

The levels of total proteins and the levels of phosphorylation of proteins were analyzed on separate gels. The band intensities on developed films, fusion FX images or chemidoc images or were quantified using Fiji image processing package (Schindelin et al., 2012).

### Plasmid constructs and mutagenesis

pDONR223-hPRKAA1 (ref:23871), pDONR223-hPRKAA2 (ref:23671), pDONR223-hPRKAB1 (ref:23360), pDONR223-hPRKAB2 (ref:23647), pDONR223-hPRKAG1 (ref:23718), pDONR223-hPRKAG2 (ref:23689), pDONR223-hPRKAG3 (ref:23549) were provided from Addgene. The different GST subunits of human AMPK were obtained using the pDEST pGEX-2T vector of Gateway Cloning Technology (Invitrogen) starting from previously described pDONR223AMPK constructs. The different serine-to-alanine mutants of GST-hPRKAA2 were generated using a Quick-Change Site-Directed Mutagenesis kit (Stratagene) with the following primers (Table S2). A similar strategy was used to obtain the truncated versions of GST-hPRKAA2 and the different serine-to-alanine mutants using the following primers (Table S2).

The Myc-hPRKAA1, the Myc-hPRKAA2 and the Myc-hPRKAA2-S345A-S377A-T485A-S529A were obtained using the pDEST pCDNA3 MYC vector previously and the above described pDONR223-human AMPK constructs. pDONR-hRB 379-928aa was subcloned from pCMV human RB and generated using the pDONR221 vector of Gateway Cloning Technology. The pGEX-2T hRB 379-928aa was obtained using the pDEST pGEX-2T from Gateway Cloning Technology.

### GST production

Independent AMPK subunits were cloned in the pDEST pGEX-2T and expressed in BL21 bacteria. GST-purified proteins were re-suspended in 50mM Tris.HCl [pH 8], 100 mM NaCl, 5 mM DTT and 20% glycerol buffer.

### CDK4 Kinase assay

Kinase assays were performed using independent AMPK subunits proteins and 500ng of recombinant RB protein (Santa Cruz) as a substrate in kinase buffer (25 mM Tris.HCl [pH 7.5], 150 mM NaCl, 10 mM MgCl<sub>2</sub>, 1 mM DTT, 5 mM Na<sub>4</sub>P<sub>2</sub>O<sub>7</sub>, 50 mM NaF, 1 mM vanadate and protease inhibitor cocktail) with 40  $\mu$ M ATP and 8  $\mu$ Ci  $\gamma$ -<sup>33</sup>PATP (Perkin Elmer) for 30 min at 30°C. Recombinant CDK4/cyclin D3 kinase and CDK4/Cyclin D1 (ProKinase) were used. RB was used as a positive control.

Boiling the samples for 5 min in the presence of denaturing sample buffer stopped the reaction. Samples were subsequently subjected to SDS-PAGE, and transferred to a nitrocellulose membrane before being exposed to an X-ray film at -80°C during 4 hr or over night. Recombinant protein loading was confirmed by SYPRO Ruby protein Blot Staining (Life Technologies).

For mass spectrometry, recombinant kinase dead AMPK trimers ( $\alpha$ 2 $\beta$ 2 $\gamma$ 1) were used as a substrate for CDK4/CyCD3. Recombinant kinase dead AMPK trimers ( $\alpha$ 2 $\beta$ 2 $\gamma$ 1) were produced by the DG. Hardie lab.

### Mitochondrial isolation

Quadriceps muscle from *Cdk4*<sup>+/+</sup> or *Cdk4*<sup>-/-</sup> mice were homogenized in 2ml cold buffer I. Tissue homogenization was obtained at 1500rpm after 30 strokes. The homogenized extract was then centrifuged at 600 g for 10 min at 4°C in order to remove cellular debris. This step was performed three times. The mitochondrial fraction was pelleted at 10000 g for 10 min at 4°C and subsequently washed using buffer II. The mitochondrial pellet was suspended in 80ul cold buffer II. Mitochondria were immediately used for Seahorse analysis. Buffers I composition is as follows: 210 mM mannitol, 70 mM sucrose, 5 mM HEPES, 1 mM EGTA, 0.5% BSA pH to 7.4. Buffer II composition is as follows: 210 mM mannitol, 70 mM sucrose, 10 mM MgCl<sub>2</sub>, 5 mM MK<sub>2</sub>HPO<sub>4</sub>, 10 mM MOPS, 1 mM EGTA pH to 7.4.

### Isolation of adult skeletal muscle fibers

Flexor digitorum brevis (FDB) muscles were incubated for 45 min at 37°C in an oxygenated 'Krebs-HEPES' solution containing 0.2% collagenase type IV (GIBCO). Muscles were then washed twice in DMEM/F12 supplemented with 2% fetal bovine serum and mechanically dissociated by repeated passages through fire-polished Pasteur pipettes of progressively decreasing diameter. Dissociated fibers were plated directed onto Seahorse XF24 tissue culture dishes coated with Matrigel and allowed to adhere to the bottom of the dish for 2h. After checking the adhesion of the fibers, a Seahorse Fatty acid oxidation was performed as described

The Krebs-HEPES solution contains NaCl 135.5mM, MgCl<sub>2</sub> 1.2mM, KCl 5.9mM, glucose 11.5mM, HEPES 11.5mM and CaCl<sub>2</sub> mM.

### Seahorse analyses

For Seahorse analysis, the cells were seeded 16 hr before the experiment.

Mitochondrial function was determined with an XF-24 extracellular flux analyzer (Seahorse Bioscience). Oxygen consumption Rate (OCR) and Extracellular acidification rate (ECAR) was measured in adherent MEFs. Control and mutant fibroblast cells were seeded in an XF 24-well cell culture microplate at a density of  $7 \times 10^5$  cells per cell in 200  $\mu$ L DMEM/F12 media. Cells were incubated for 16 hr at 37°C in 5% CO<sub>2</sub> before the assay. OCR was expressed as pmol of O<sub>2</sub> per minute and was normalized by protein content a Pierce BCA

Protein Assay protocol (Thermo Fisher Scientific). ECAR was expressed as mpH per minute and was normalized by protein content a Pierce BCA Protein Assay protocol (Thermo Fisher Scientific).

For glycolysis experiments, just before the experiment the cells were washed, and the growth medium was replaced with DMEM medium containing only 2mM Glutamine. Cells were then pre-incubated for 1 hr at 37°C without CO<sub>2</sub> to allow cells to pre-equilibrate with the assay media before starting the glycolysis test procedure. After measuring baseline ECAR, ECAR was measured after an acute injection of 25mM Glucose. The glycolytic rate was calculated as glucose dependent ECAR. It was calculated as follows: Glucose induced ECAR-basal ECAR.

For fatty acid oxidation experiments, just before the experiment the cells are washed, and the growth medium was replaced with KHB containing 2.5mM Glucose and 1.5mM of carnitine. Cells were then pre-incubated for 1 hr at 37°C without CO<sub>2</sub> to allow cells to pre-equilibrate with the assay media before starting the fatty acid oxidation procedure. After measuring baseline OCR as an indication of basal respiration, OCR was measured after an acute injection of 400μM or 150μM of palmitate coupled to BSA (for MEFs and myotubes respectively).

For FDB muscle fibers 125μM of palmitate coupled to BSA, 400nM of FCCP and 1μM of Antimycine A were injected directly onto the fibers using the Seahorse analyzer. Fatty acid oxidation was induced by the palmitate injection. The uncoupling agent FCCP induced the maximal respiration.

OCR was expressed as pmol of O<sub>2</sub> per minute and was normalized by total DNA content.

For mitochondrial respiration, 50 μL of mitochondrial suspension (containing 10μg of freshly isolated mitochondria) were used per well. The XF24 cell culture microplate was centrifuged at 2000 g for 20 min at 4°C. The assay medium contained 250 mM sucrose, 15 mM KCl, 1 mM EGTA, 5 mM MgCl<sub>2</sub>, 30 mM K<sub>2</sub>HPO<sub>4</sub>, 2mM HEPES and 0.2% FFA-Free BSA. 0.5mM Malate, 80μM PalmitoylCoA, 240μM Carnitine and 4mM ADP diluted in assay medium were added after the centrifugation of the mitochondria to obtain a final volume of 525μl per well. After 10 min of incubation at 37°C without CO<sub>2</sub> the mitochondrial respiration was measured using the Seahorse analyzer.

### Immunoprecipitation

Myotubes or liquid N2 grinded muscle samples were lysed in M-PER buffer (Thermo Fisher Scientific) and incubated in agitation for one hour at 4°C. 2-5 mg of protein was immunoprecipitated overnight with an AMPKα2 antibody (Santa Cruz, sc-19131) and Protein G coupled with magnetic beads (Sigma, 1004D) in the following buffer (IP buffer): 25 mM TRIS pH 7.9, 5 mM MgCl<sub>2</sub>, 10% Glycerol, 100 mM KCl, 0.1% NP40, 0.3 mM DTT. Next day, beads were washed for times with the IP buffer and frozen. Samples were used for mass spectrometry.

### Mass spectrometry

In the *in vitro* assays, protein samples were loaded on a 12% mini polyacrylamide gel and migrated about 3 cm, while in the immunoprecipitation experiments proteins were loaded on an 8% gel and fully migrated. After Coomassie staining, visible band between 50 and 75 kDa corresponding to AAKP2 was excised and digested with sequencing-grade trypsin (Promega). Extracted tryptic peptides were dried and resuspended in 0.05% trifluoroacetic acid, 2% (v/v) acetonitrile for mass spectrometry analyses.

Tryptic peptide mixtures were injected on an Ultimate RSLC 3000 nanoHPLC system (Dionex, Sunnyvale, CA, USA) interfaced via a nanospray source to a high resolution mass spectrometer based on Orbitrap technology: Fusion Tribrid or QExactive Plus (Thermo Fisher, Bremen, Germany), depending on the experiments considered. Peptides were loaded onto a trapping microcolumn Acclaim PepMap100 C18 (20 mm x 100 μm ID, 5 μm, Dionex) before separation on a C18 reversed-phase analytical nanocolumn at a flowrate of 0.25 μl/min, using a gradient from 4 to 76% acetonitrile in 0.1% formic acid (total time: 65min).

The *in vitro* experiments were analyzed with a Fusion mass spectrometer interfaced to a custom packed 40-cm C18 column (75 μm ID, 100Å, Reprosil Pur 1.9 μm particles). Full MS survey scans were performed at 120'000 resolution. Data-dependent acquisition was controlled by Xcalibur 3.0 software (Thermo Fisher) and applied a top speed precursor selection strategy to maximize acquisition of peptide tandem MS spectra with a maximum cycle time of 3 s. Multiple-charge precursor ions were isolated in the quadrupole with a window of 1.6 m/z width and then dynamically excluded from further selection during 60 s. HCD fragmentation was performed in the ion routing multipole with 32% normalized collision energy and fragment ions were measured in the ion trap.

The immunoprecipitation experiments were analyzed with a Q-Exactive Plus instrument interfaced to an Easy Spray C18 PepMap column (50cm x 75μm ID, 2μm, 100Å, Dionex). Full MS survey scans were performed at 70'000 resolution. In data-dependent acquisition controlled by Xcalibur 3.1 software (Thermo Fisher), the 10 most intense multiple-charge precursor ions detected in the full MS survey scan were selected for higher energy collision-induced dissociation (HCD, normalized collision energy NCE = 27%) and analysis in the orbitrap at 17'500 resolution. The window for precursor isolation was of 1.5 m/z units around the precursor and selected fragments were excluded for 60 s from further analysis.

MS data were analyzed using Mascot 2.6 (Matrix Science, London, UK) set up to search the UniProt database ([www.uniprot.org](http://www.uniprot.org)) restricted to *Homo sapiens* (*in vitro* experiments) or *Mus musculus* (immunoprecipitation experiments) taxonomy (SwissProt, November 2016 version: 20'130 and 16'846 sequences, respectively). Trypsin (cleavage at K,R) was used as the enzyme definition, allowing 3 missed cleavages. Mascot was searched with a parent ion tolerance of 10 ppm and a fragment ion mass tolerance of 0.5

(Fusion MS data) or 0.02 Da (QExactive MS data). Iodoacetamide derivative of cysteine was specified in Mascot as a fixed modification. N-terminal acetylation of protein, oxidation of methionine, and phosphorylation of serine, threonine or tyrosine were specified as variable modifications.

Scaffold software (version 4.7.5, Proteome Software Inc., Portland, OR) was used to validate MS/MS based peptide and protein identifications, and to perform dataset alignment. Peptide identifications were accepted if they could be established at greater than 90.0% probability by the Scaffold Local FDR algorithm. Protein identifications were accepted if they could be established at greater than 95.0% probability and contained at least 2 identified peptides. Protein probabilities were assigned by the Protein Prophet algorithm. Proteins that contained similar peptides and could not be differentiated based on MS/MS analysis alone were grouped to satisfy the principles of parsimony. Proteins sharing significant peptide evidence were grouped into clusters.

MsViz software (Martín-Campos et al., 2017) was used to compare sequence coverage and phosphorylation of the AMPK alpha 2 protein in the *in vitro* experiments.

### HPLC

Cells were grown in 10 cm dishes and treated as indicated in the figure legends. Culture medium was removed by aspiration, rinsed with ultra pure water, flash frozen with liquid nitrogen, thawed on ice, and followed by immediate addition of ice-cold 0.4M perchloric acid (500  $\mu$ l). Cells were scrapped off thoroughly, and transferred to 1.5 mL microfuge eppendorf tubes. Samples were incubated at 4°C for 45 min, and centrifuged at 14,000 rpm at 4C for 10 min. The supernatant (500  $\mu$ l) was collected, mixed with 500 $\mu$ l K<sub>2</sub>CO<sub>3</sub> 4M, and incubated at least 1h at -80°C. The samples were again centrifugated at 4C for 10 min, the supernatant collected and tested on HPLC.

External standards stocks were prepared in ultra pure water, at 10 mg/ml, and treated in exactly the same way as the samples.

For normalization, protein measurements were performed using a Pierce BCA Protein Assay protocol (Thermo Fisher Scientific). In parallel DNA was extracted from the pellets and quantified.

The gradient elution was performed as described (Manfredi et al., 2002) on a 4.6-mm.i.d, 150-mm, Kinetex 5u EVO C18 100A HPLC column (Phenomenex) with two buffers at a rate of 0.5 ml/min. Buffer A contained 25mM NaH<sub>2</sub>PO<sub>4</sub>, 100 mg/liter tetrabutylammonium hydrogen sulfate, pH 5. Organic buffer B was composed of 10% (v/v) acetonitrile in 200mM NaH<sub>2</sub>PO<sub>4</sub>, 100 mg/liter tetrabutylammonium hydrogen sulfate, pH 4.0. Buffers were filtered and degassed. The gradient was 100% buffer A from 0–5 min, 100% buffer A to 100% buffer B from 5–20 min, and 100% buffer A from 20 to 31 min for column reequilibration, which was sufficient to achieve stable baseline conditions. 25  $\mu$ l of prepared sample was autoinjected and UV monitored at 260nm from 0 to 31 min for phosphorylated nucleotides. Peaks were identified by their retention times and by using co-chromatography with standards.

Each standard of interest was first subjected to chromatography individually to obtain its retention time (Manfredi et al., 2002) and to be able to later identify each compound in a standard mixture. A standard curve for each compound was constructed by plotting peakheight s (IV) versus concentration. Linear curves were obtained with R<sup>2</sup> values > 0.95. The quantification of nucleotides in the sample was performed using the external standard calibration, integrating sample peak heights against corresponding standard curves.

### mRNA analysis

Muscle tissues were grinded to powder in liquid nitrogen. mRNAs from muscle was isolated using TRIAGENT according to the manufacturer's protocol. One microgram of the RNA was subsequently reverse-transcribed (Superscript II, Life Technologies) and quantified via real-time quantitative PCR using an ABI 7900HT instrument. qPCR analysis was performed using a 7900HT Fast Real-Time PCR System (Applied Biosystems) and SYBR Green detection of the amplified products. The relative quantification for a given gene was corrected to RS9 mRNA values (oligonucleotide sequences are provided in Table S3).

### QUANTIFICATION AND STATISTICAL ANALYSES

The results were expressed as means  $\pm$  standard error of the means (s.e.m). Comparisons between 2 groups were performed with an unpaired 2-tailed Student's t test and multiple group comparisons were performed by unpaired 1-way ANOVA followed by Tukey's test and 2-way ANOVA, followed by Tukey's test. All *p-values* below 0.05 were considered significant. Statistical significance values were represented by asterisks corresponding to \**p* < 0.05, \*\**p* < 0.01, \*\*\**p* < 0.001 and \*\*\*\**p* < 0.0001.



---

## *Appendix C*

---

### **Global Kinome Analysis in Obese Subjects Reveal PIM-1 as a Novel Target for the Treatment of Insulin Resistance**

(submitted to Nature Metabolism)

The main part of my thesis is based on this manuscript. As previously stated, we show that PIM-1 is implicated in adipose tissue insulin resistance. The full mechanism is yet to be studied, however, we know that it is through induction of pro-inflammatory macrophages and their recruitment in the adipose tissue.

I have performed most of the experiments and analyzed all the data with the help of other lab members, as well as our collaborators. This work is submitted to Nature Metabolism.



# **Global kinome analysis in obese subjects reveals PIM-1 as a novel target for the treatment of insulin resistance.**

Anita Nasrallah<sup>1</sup>, Pu-Ste Liu<sup>2,3,4</sup>, Eric-Aria Fernandez<sup>1</sup>, Xiaoyun Li<sup>2,3</sup>, Miriam Ejarque<sup>5,6</sup>, Tiziana Caputo<sup>1</sup>, Judit Castillo-Armengol<sup>1</sup>, Laia Martinez-Carreres<sup>1</sup>, Enrique Calvo<sup>5,6</sup>, Wan-Chen Cheng<sup>2,3</sup>, Amel Bekkar<sup>7</sup>, Ioannis Xenarios<sup>7,8,9</sup>, Federica Gilardi<sup>1,10</sup>, Silvia Pellitero<sup>6,11</sup>, Sonia Fernandez-Veledo<sup>5,6</sup>, Francisco José Tinahones<sup>12,13</sup>, Joan Vendrell-Ortega<sup>5,6,14</sup>, Ping Chih Ho<sup>2,3</sup>, Isabel C. Lopez-Mejia<sup>1\*</sup>, and Lluís Fajas<sup>1\*</sup>

<sup>1</sup> Center for Integrative Genomics, University of Lausanne, 1015 Lausanne, Switzerland

<sup>2</sup> Department of Fundamental Oncology, University of Lausanne, 1066 Epalinges, Switzerland

<sup>3</sup> Ludwig Cancer Center, Lausanne Branch, Epalinges, Switzerland

<sup>4</sup> Institute of Cellular and System Medicine, National Health Research Institutes, Miaoli County, Taiwan

<sup>5</sup> Institut d'Investigació Sanitària Pere Virgili; Hospital Universitari de Tarragona Joan XXIII-Tarragona Spain.

<sup>6</sup> CIBER de Diabetes y Enfermedades Metabólicas Asociadas (CIBERDEM)-Instituto de Salud Carlos III, Madrid, Spain.

<sup>7</sup> Vital-IT group, SIB Swiss Institute of Bioinformatics, 1015 Lausanne, Switzerland

<sup>8</sup> Swiss-Prot group, SIB Swiss Institute of Bioinformatics, 1211 Geneva, Switzerland

<sup>9</sup> Swiss Institute of Bioinformatics CITY: Lausanne Switzerland

<sup>10</sup> Faculty Unit of Toxicology, University Center of Legal Medicine, Lausanne University Hospital (CHUV), 1000 Lausanne, Switzerland

<sup>11</sup> Department of Endocrinology and Nutrition. Germans Trias i Pujol Research Institute, Barcelona, Spain

<sup>12</sup> Unidad de Gestión Clínica Endocrinología y Nutrición. Instituto de Investigación Biomédica de Málaga (IBIMA), Complejo Hospitalario de Málaga (Virgen de la Victoria) Málaga (Spain)

<sup>13</sup> CIBER Fisiopatología de la Obesidad y Nutrición (CB06/03), Málaga, Spain.

<sup>14</sup> Universitat Rovira i Virgili, Tarragona, Spain.

\* Corresponding authors: Isabel C. Lopez-Mejia and Lluís Fajas, University of Lausanne, Center for Integrative Genomics, Quartier UNIL-Sorge, Bâtiment Génopode, CH-1015 Lausanne, Switzerland

E-mail: [lluis.fajas@unil.ch](mailto:lluis.fajas@unil.ch), [isabel.lopezmejia@unil.ch](mailto:isabel.lopezmejia@unil.ch)

## Summary

Obesity, the accumulation of excess body fat, is an epidemic leading to numerous human metabolic diseases, such as type 2 diabetes (T2D). T2D is mainly characterized by hyperglycemia, accompanied by local (adipose tissue) and systemic insulin resistance. In the adipose tissue, insulin resistance involves alterations in the cross-talk of various signaling cascades, implicating numerous kinases and phosphatases. To identify molecular changes that occur during the development of insulin resistance, we have used here a new activity-based method to study the global kinase activity in human adipose tissue. Our study is based on the observation that some obese subjects do not develop insulin resistance. This population represents our control group, which avoids confounding results due to obesity by itself rather than to insulin resistance. We found that a specific set of kinase activities are representative of insulin resistance in the obese population. In particular, we found that the Serine/Threonine kinase (STK) PIM-1 has increased activity in the visceral adipose tissue (VAT) of morbid obese diabetic (MOD) insulin resistant (IR) patients. We further show that PIM-1 inhibition decreases the inflammatory capacity of bone marrow-derived macrophages *in vitro*, and leads to a decrease in the inflammatory profile in visceral adipose tissue (VAT), as well as to an increase in insulin sensitivity in diabetic mice.

Key words: PamGene, PIM-1, obesity, T2D, VAT, inflammation

## **Introduction**

The World Health Organization (WHO) has recently announced that worldwide obesity has almost tripled since 1975 (16 February 2018). Obesity is linked to numerous health problems, including insulin resistance, type 2 diabetes, hypertension, dyslipidemia, atherosclerosis, and cancer, among others (Arroyo-Johnson & Mincey, 2016; Y. C. Wang, McPherson, Marsh, Gortmaker, & Brown, 2011; Weitzman & Gordon, 1990). Together, the rising prevalence of obesity and the frequent co-morbidities in affected patients is an important challenge for health care systems. Nevertheless, recent data suggest that the total amount of body fat does not entirely explain the predisposition to cardio-metabolic risk (Goossens, 2017; Wajchenberg, Giannella-Neto, da Silva, & Santos, 2002). Indeed, metabolic complications can be observed in a significant number of non-obese individuals. In sharp contrast, 10 to 35% of obese patients do not appear to develop such complications and are thus considered metabolically healthy (Wildman et al., 2008).

In adipose tissue, insulin resistance is tightly correlated with inflammation as well as with the accumulation of pro-inflammatory macrophages (Lackey & Olefsky, 2016; McLaughlin, Ackerman, Shen, & Engleman, 2017). Adipose tissue consists of mature adipocytes and stromal vascular cells (SVCs). SVCs include premature adipocytes, endothelial cells and immune cells. These immune cells include myeloid cells like macrophages and granulocytes, effector and memory T cells, regulatory T cells and others (Huh, Park, Ham, & Kim, 2014). Macrophages, classified into anti-inflammatory (M2-like) and pro-inflammatory (M1-like) macrophages (Rosen & Spiegelman, 2014), are especially important for adipose tissue homeostasis. Indeed, it is well known that, upon obesity, pro-inflammatory macrophages are recruited (Hotamisligil, Shargill, & Spiegelman, 1993; Nguyen et al., 2007; Weisberg et al., 2003; Xu et al., 2003). Thus, an inflammatory reaction is a pre-requisite for insulin

resistance, locally in the adipose tissue and systemically in the whole organism (Kanda et al., 2006; Patsouris et al., 2008).

Insulin exerts its actions through a cascade of phosphorylation/dephosphorylation reactions of intra-cellular proteins. Insulin signaling in adipocytes has been extensively studied *in vitro* and in animal models, with a particular focus on the effects of insulin receptor, Insulin receptor substrates 1 and 2 (IRS1 and IRS2), and PI3K-protein kinase B (AKT) (Copps & White, 2012). Other known protein kinases that have been involved in the onset of insulin resistance include, but are not limited to, AMP-activated protein kinase (AMPK), I $\kappa$ B kinase (IKK), protein kinase C (PKC), or mitogen-activated protein kinases (MAPKs) (Ye, 2013; Zhang, Zhou, & Li, 2009). However, an extensive study of protein phosphorylation or kinase function alterations in IR has not been performed in human visceral white adipose tissue (VAT).

Describing the changes in the kinome is key to understanding the contributions of signaling cascades in normal or dysfunctional conditions, and therefore for the identification of signaling alterations leading to systemic diseases. The rapid development of techniques, such as genome-wide association study (GWAS), RNA sequencing, or chromatin immunoprecipitation (ChIP) sequencing has paved the way for several scientific breakthroughs (Andersen et al., 2019; Gupta & Vadde, 2019; Ke et al., 2017; Sun et al., 2018). We have chosen now to use a novel technology developed by PamGene to perform a whole kinase activity profiling of human visceral adipose tissue from morbid obese non-diabetic subjects (MOND), compared to morbid-obese diabetic (MOD) patients. Identifying new and specific protein kinases involved in adipose tissue chronic inflammation and insulin resistance may help in developing targeted drug therapies and treatment strategies to minimize insulin resistance in patients.

While analyzing the differences in the kinome of VAT, we found that the activity of the serine/threonine kinase PIM-1 was increased in the VAT of obese insulin resistant patients, compared to metabolically healthy obese subjects. PIM-1 is a member of the PIM family, that is composed of three kinases: PIM-1, PIM-2 and PIM-3. The PIM family plays roles in numerous cellular functions, such as proliferation, cell cycle progression, differentiation, apoptosis, and tumorigenesis (J. Li, Loveland, & Xing, 2011; Narlik-Grassow, Blanco-Aparicio, & Carnero, 2014; Warfel & Kraft, 2015). PIM kinases are important for growth factor signaling (Mikkers et al., 2004) by regulating B- and T- cell responses to cytokines and hematopoietic growth factors (An, Kraft, & Kang, 2013), and are thus known for their role supporting tumor cell growth and survival (Brault et al., 2010). PIM-1 has been specially studied in hematological malignancies and is known to be a major target for cytokine induced STAT signaling (Brault et al., 2010).

We show in this study that PIM-1 activity in the macrophage fraction of adipose tissue mediates their pro-inflammatory effects, thus promoting insulin resistance and type II diabetes. Moreover, we demonstrate that the pharmacological inhibition of PIM-1 alters macrophage polarization *in vitro* and ameliorates insulin resistance in a mouse model of diabetes.

## Results

### **Kinome profiling reveals distinct kinase activities in human visceral adipose tissue from morbid obese diabetic, compared to non-diabetic subjects**

The main goal of our study was to identify novel kinases inducing insulin resistance in obese subjects. The insulin signaling cascade is dependent on the rapid activation of a series of tyrosine and serine/threonine protein kinases. We used a technology developed by PamGene to determine differential global kinase activity in human VAT from morbid obese non-diabetic (MOND) and morbid obese diabetic (MOD) patients (Table 1) (Supplemental Figure 1). We used arrays that consist of 140 immobilized serine/threonine containing peptides (STK PamChips). These chips were incubated with the different adipose tissue lysates. Differentially phosphorylated peptides, whose phosphorylation varied significantly between the MOND and MOD samples, were indicative of differential specific kinase activities. More than 60 peptides were highly phosphorylated specifically in the VAT of MOD patients, as compared to MOND patients (Figure 1A and Table S4). Putative upstream kinase analysis was done using the “STK upstream kinase analysis” pipeline from the Bionavigator software. This method takes into account the multiple parallel changes in peptide phosphorylation and both experimental kinase-substrate relationships ([Uniprot](#), [HPRD](#), [PhosphositePlus](#), [Phospho.ELM](#), and [Reactome](#) databases), and in silico predictions for upstream kinases ([phosphoNET](#) database). The kinases that were identified with “more confidence” using this method were AKT1/PKB $\alpha$ , AKT2/PKB $\beta$ , AMPK $\alpha$ 1, ANP $\alpha$ , CHK2, mTOR/FRAP, PIM1, PIM2, PIM3, PKA $\alpha$ , PKC ( $\alpha$ ,  $\delta$ ,  $\epsilon$ ,  $\eta$ ,  $\theta$ ), PKD1, PKG1, PKG2, PRKX and p70S6K $\beta$  (Figure 1B-C). Even though PRKY is shown as a kinase hit in the kinexus-based analysis (Figure 1B), however it is considered as a pseudogene, which is why it is not depicted in the String Plot (Figure 1C). Of note, during the course of this study it was shown that the knockout of PKG1 in TNF $\alpha$ -induced mature adipocytes reverted the insulin resistant phenotype, by rescuing glucose uptake impairment

(Ando et al., 2015), and the adipose tissue specific knockout of PKC $\epsilon$  improves diet induced glucose intolerance in mice (Brandon et al., 2019). Importantly, PKA, PKC $\beta$ , AKT and AMPK have already been described as involved in the onset of insulin resistance (Huang, Liu, Guo, & Su, 2018; Mehta, 2014). These findings validated our experimental approach, and suggested that the increased activity of the above-mentioned kinases can be either a cause or a consequence of the insulin resistance characterizing MOD subjects.

***Pim-1* expression in VAT positively correlates with IR markers and is increased in different mouse models of insulin resistance.**

Next, we focused on the PIM family of kinases, because they were not previously described to be involved in insulin resistance or diabetes. PIM kinase activity is constitutively active (Warfel & Kraft, 2015). Thus, unlike other kinases, PIM kinase activity is regulated primarily at the transcriptional level, then by translation efficiency, and finally by proteasomal degradation (Amaravadi & Thompson, 2005). Functional redundancy, at the *in vitro* and *in vivo* levels, between the PIM kinases have been shown (Mikkers et al., 2004; Narlik-Grassow et al., 2012).

Thus, we used their transcriptional level as a readout for activity and measured the expression of the different novel kinases in the VAT of more than 80 human patients (Table 2). mRNA levels were correlated to the different IR markers, i.e. body mass index (BMI), insulinemia, and glycemia (Supplemental Figure 2A-I). Of all the identified kinases, *PIM-1* was the only one to show a positive correlation with all 3 variables (Figure 2 A-C). *PIM-2* was only correlated to BMI (Figure 2D-F), while *PIM-3* did not correlate to any of the 3 parameters (Figure 2G-I).

To validate if the increased expression of *PIM-1* upon insulin resistance is conserved in mice, we quantified mRNA levels in two different mouse models of insulin resistance: mice

under high-fat diet (HFD), and db/db mice. Based on RNA sequencing data, *Pim-1* gene expression was significantly increased in the VAT of mice fed a HFD for 8 weeks, as compared to mice under normal chow diet (CD), which has the exact same composition as the HFD but with lower fat content, otherwise known as low fat diet (LFD) (Figure 2J). This was further increased after 20 weeks of HFD (Figure 2J). It is important to note here that 60% of the calories of the HFD is coming from fat. *Pim-2* expression did not change between the groups (Figure 2K), while *Pim-3* expression significantly decreased in the VAT of mice under HFD (Figure 2L). RTqPCR data showed that *Pim-1* mRNA is also significantly higher in VAT of db/db mice (Figure 2M). However, *Pim-2* expression was also increased in VAT of db/db mice (Figure 2N), while *Pim-3* expression was significantly decreased in the VAT of db/db mice (Figure 2O). Overall, these results prove that *PIM-1* gene expression is increased in adipose tissue from diabetic human subjects and from mouse models of diabetes, suggesting that PIM-1 participates in the development of insulin resistance.

### **The effects of Pim-1 in insulin resistance are not mediated by adipocytes.**

Next, we wanted to analyze the participation of PIM-1 in the onset of insulin-resistance in cellular models of white adipose tissue. Indeed, *Pim-1* is increasingly expressed during adipocyte differentiation in the 3T3L1 model (Figure 3A). Mature 3T3L1 adipocytes treated with TNF $\alpha$  for 72h were used as a model for insulin resistance (Stephens, Lee, & Pilch, 1997). We stimulated these cells with 100nM insulin for 20 minutes and saw a significant decrease in the phosphorylation of AKT at Threonine 308, which is a readout of IS (Figure 3B-C). We treated these insulin-resistant adipocytes with the Pim-1 inhibitor SGI-1776. The inhibition of Pim-1 activity was validated by showing a dose-dependent decrease in the phosphorylation of Bad at Serine 112, which is a target of Pim-1, upon SGI-1776 treatment starting from 0.25 $\mu$ M (Figure 3D-F). The phosphorylation levels of AKT were, however, not increased with any of

the tested doses of Pim-1 inhibitor, showing no rescue of the insulin resistant phenotype of TNF $\alpha$  treated 3T3L1 mature adipocytes (Figure 3D-F). These results suggested that Pim-1 does not directly act on adipocytes to induce insulin resistance in the adipose tissue of obese subjects.

### ***Pim-1* expression and activity are increased in pro-inflammatory macrophages.**

Our initial kinome analysis was performed in whole VAT. In addition to adipocytes VAT contains fibroblasts, endothelial cells, and inflammatory cells. Out of those non-adipocyte cells, pro-inflammatory macrophages play a major role in the development of insulin resistance in this tissue. Therefore, we used bone marrow-derived macrophages (BMDMs) treated with lipopolysaccharide (LPS) for 6h, as an *in vitro* model of pro-inflammatory macrophages. Protein extracts from naïve and 6h-LPS-stimulated cells were then submitted to PamChip serine/threonine kinase analyses (Supplemental Figure 4). Pim-1 was among the kinases with increased activity in response to LPS treatment (Figure 4A). Consistently, RNA sequencing data from naïve and LPS-treated macrophages showed an increase in *Pim-1* mRNA levels in the pro-inflammatory macrophages (Figure 4B). Moreover, the expression of *Pim-1* was also increased in FACS sorted CD11c<sup>+</sup> adipose tissue-derived pro-inflammatory macrophages from mice under HFD, when compared to CD11c<sup>+</sup> macrophages from mice under chow diet (Figure 4C), suggesting that our observations in BMDMs can be extended to adipose tissue macrophages.

### **SGI-1776 decreases pro-inflammatory markers in LPS-stimulated macrophages.**

BMDMs were stimulated with LPS for 6h or 24h to induce a pro-inflammatory phenotype. As expected, pro-inflammatory markers (*IL-1 $\beta$* , *IL-6*, *TNF $\alpha$* , *MCP-1* and *iNOS*) were significantly increased in LPS treated macrophages as compared to naïve macrophages

(Figure 5A). *Pim-1* expression was also increased upon LPS-stimulation in BMDMs, both at the mRNA and protein levels (Figure 5B-D). The phosphorylation of the known Pim-1 targets pS112 Bad and pT146 p21 was also increased upon LPS stimulation (Figure 5E), suggesting an increase in Pim-1 activity in pro-inflammatory macrophages.

The treatment of macrophages with the Pim-1 inhibitor SGI-1776 prior to LPS stimulation decreased the mRNA expression of several pro-inflammatory cytokines, such as *IL-1 $\beta$* , *TNF $\alpha$* , *MCP-1* and *iNOS* (Figure 5F), as well as the expression of *Pim-1* (Figure 5G). These results proved that Pim-1 has a direct role on pro-inflammatory macrophages, and this may participate in the onset of insulin resistance in VAT.

### **Pim-1 inhibition improves insulin sensitivity in diabetic mice**

We next wanted to test the clinical relevance of our findings by treating the db/db diabetic mouse model with the SGI-1776 Pim-1 inhibitor. After 3 weeks of treatment, we did not observe changes in the food intake (Figure 6A) or body weight (Figure 6B). In contrast, the treatment resulted in alterations in body composition; an increase of lean mass and a decrease of fat mass (Figure 6C-D). This correlated with a decreased weight of WAT depots in SGI-1776-treated mice, whereas no differences were observed in the weight of other tissues, such as liver, heart or muscle (Figure 6E). This suggests a specific effect of SGI-1776 on adipose tissue depots. Most important was the finding that the fasting glycemia of the db/db mice treated with the Pim-1 inhibitor was reduced after 3 weeks of treatment, when compared to the vehicle-treated group (Figure 6F). Moreover, SGI-1776 treatment resulted in enhanced insulin sensitivity and glucose disposal, as measured by insulin and glucose tolerance tests (Figure 6G-J).

Gene expression of several cytokines was next assessed. Pro-inflammatory markers, such as *MCP-1*, *TNF $\alpha$*  and *iNOS* decreased in the VAT of SGI-1776-treated mice (Figure 6K).

A higher expression of pro-inflammatory cytokines is often correlated with the aggregation of pro-inflammatory macrophages around dead adipocytes, and is a characteristic feature of inflammation in this tissue. These so-called crown-like structures were indeed apparent in the adipose tissue of vehicle-treated mice (Figure 6L-M), but were much decreased in the VAT of db/db mice treated with SGI-1776 (Figure 6L-M). These results proved that the inhibition of Pim-1 improves adipose tissue inflammation and the overall diabetic phenotype in the db/db mouse model.

## Discussion

The use of genomic, proteomic, and transcriptomic techniques in the study of human pathologies has been rapidly expanding. Indeed, the recent identification of new key players in human type 2 diabetes mellitus (T2DM) is based on high throughput techniques. These approaches study potentially pathogenic mutations or SNPs, as well as the expression of protein coding genes and actual protein abundance, whereas functional proteomic methodologies bring more insight on protein activity and how cell signaling works. Actually, in the past five years, proteomic studies have confirmed the importance of inflammatory pathways and cellular stress in the alterations found in adipose tissue of obese subjects (Garrison, Lastwika, Zhang, Li, & Lampe, 2017). A first prediction of upregulated kinases in adipose tissue in conditions of obesity and insulin resistance in mice was performed using phosphoproteomics. However, this study shows very limited overlap with our dataset (Shaik et al., 2016). The kinase activity-based assay from PamGene allows us to detect kinase function directly in order to perform kinome profiling on patients' biopsies.

The aim of our study was to discover new kinases whose activities are deregulated during the development of insulin resistance in obese subjects, independently of adiposity. To implement our strategy, we took advantage of a population of obese subjects that are protected from the development insulin resistance and other obesity-derived pathologies (Wildman et al., 2008). Comparing the global kinase activities in the adipose tissue of these subjects with the kinase activities of the obese diabetic patients allowed us to discover new kinases, specifically active in the adipose tissue of the pathological group. This strategy allows us to overcome any confounding factors that could be related to obesity *per se*, and not to insulin resistance. Moreover, our results shed light on the mechanism behind the ability of a certain population of obese subjects to maintain metabolic health and evade metabolic complications.

We used three criteria to select specific kinase activities for further *in vivo* studies. First, the kinase activity should be significantly modified in validation studies. Second, specific kinase inhibitors should be available for further preclinical testing. And third, a role for the identified kinase in diabetes should not have been previously described. By performing an upstream putative kinase analysis of the differentially phosphorylated peptides in MOD and MOND VAT samples, we identified PIM-1 as a potentially upregulated kinase in diabetic patients. We consequently validated our finding and proposed a mechanism by which Pim-1 modulates insulin sensitivity by integrating cellular models, diabetic mouse models and clinical data from our human cohort.

Emerging evidence proves that PIM-1 is a promising drug target against many types of cancer. It is correlated with tumor aggressiveness and is a marker of poor prognosis in several tumor types, such as prostate cancer and leukemia (Dhanasekaran et al., 2001; Liu, Wang, Wang, & Li, 2010; Shah et al., 2008). Interestingly, in ovarian cancer cells, PIM-1 phosphorylates c-Myc, which in turn induces the expression of several metabolic enzymes: PGK1, LDHA, GLUT1, etc. (Wu et al., 2018), providing a first observation linking PIM-1 activity to the regulation of metabolism, at least in the context of cancer. Moreover, PIM-1 has been shown to play a role in diabetic cardiomyopathy and diabetic nephropathy, which are severe complications associated with diabetes (Agrawal & Kant, 2014; Kannel, Hjortland, & Castelli, 1974). However, PIM-1 has never been directly associated with adipose tissue insulin resistance in the context of T2D. An important role of PIM-1 that strongly places this kinase as a novel target for insulin resistance is its role in the inflammatory response. Indeed, PIM-1 has been linked to placental inflammation (Liong, Barker, & Lappas, 2017), to the stabilization of the p65 subunit of NF $\kappa$ B (Nihira et al., 2009), and to the immunosuppressive activity of human regulatory T cells (Z. Li et al., 2014). It is well established that pro-inflammatory cytokines, such as IL-6 and TNF- $\alpha$ , affect insulin signaling, which in turn is essential to

maintain glucose homeostasis and regulate its metabolism in adipose tissue. We show here that PIM-1 kinase does not mediate cytokine-induced insulin resistance in adipocytes (Figure 3A-D), but rather plays a key role in another cell type mediating insulin resistance in adipose tissue: pro-inflammatory macrophages.

PIM kinases are arising as significant mediators in cytokine signaling pathways. *Pim-1* is highly expressed in the bone marrow, spleen, thymus, fetal liver, and non-hematopoietic tissues such as hippocampus, prostate, and epithelia (Eichmann, Yuan, Breant, Alitalo, & Koskinen, 2000). *Pim-1* transcription is activated in response to numerous cytokines through JAK-STAT signaling (Brault et al., 2010). PIM-1 is also involved in myeloid cell differentiation, indeed when the levels of active PIM-1 are manipulated, the rate of differentiation of U937 cells is altered (Z. Wang et al., 2001). Importantly, PIM-1 has been shown to promote NF $\kappa$ B transactivation by preventing its degradation in HeLa cells (Nihira et al., 2009), and by promoting RANKL-induced NF $\kappa$ B transcriptional activity in osteoclasts (Kim, Kim, Youn, Jin, & Kim, 2010). We propose here an additional role for PIM-1 in macrophage polarization in response to pro-inflammatory stimuli.

In conclusion, this study has identified a subset of novel kinases potentially involved in adipose tissue insulin resistance through an activity-based screen and elucidated yet another important role of PIM-1 kinase, linking its canonical role in cancer and inflammation to metabolism, specifically insulin resistance in diabetic patients. This will now pave the way for more studies, investigating the mechanisms by which PIM-1 participates in adipose tissue inflammation in obese subjects, and thus in the onset of T2D. This will also help develop new targeted drug therapies in the field of diabetes, a worldwide epidemic, with no clear therapeutic strategies yet.

## Tables

*Table 1: Cohort 1 (discovery cohort)*

Morbid obese non-diabetic (MOND) and morbid obese type 2 diabetic (MOD) patients used for PamGene data analysis

Patients	n	Females	Males	Age (years)	BMI (kg/m <sup>2</sup> )	Insulinemia (mIU/mL)	Glycaemia (mg/dL)	HOMA-IR
MOND	23	16	7	47 ± 2	46.3 ± 1.0	17.8 ± 2.3	94.6 ± 2.6	4.4 ± 0.6
MOD	21	11	10	52 ± 2	48.5 ± 1.7	25.4 ± 4.8	133.5 ± 9.8	10.7 ± 2.7

*Table 2: Cohort 2 (confirmatory cohort)*

Lean (L), obese (O) and morbid obese (MO) patients that are diabetic and non-diabetic used for the correlations between mRNA expression and IR markers (BMI, Glycemia, and Insulinemia)

Patients	n	Females	Males	Age (years)	BMI (kg/m <sup>2</sup> )	Insulinemia (mIU/mL)	Glycaemia (mg/dL)	HOMA-IR
L	20	13	7	55 ± 3	23.7 ± 0.4	7.5 ± 1.2	100.8 ± 4.2	1.9 ± 0.3
O	23	12	11	59 ± 3	32.8 ± 0.4	11.1 ± 1.4	110.8 ± 5.1	3.0 ± 0.4
MO	43	33	10	49 ± 1	46.6 ± 0.9	19.9 ± 2.3	114.4 ± 5.0	6.2 ± 1.0

*Table S 1: Primers used for qPCR analysis of housekeeping genes (human and mouse)*

Gene	Forward	Reverse
RS9	CACACTCTCCCAACGTTCT	ACCACCTGCTTGCGGACCCTGATA
Actin	TCCATCATGAAGTGTGACGT	TACTCCTGCTTGCTGATCCAC

*Table S 2: Primers used for qPCR analysis of kinases upregulated in VAT of MOD patients*

Gene	Forward	Reverse
Pim-1 (human)	CCTGGGGATCCTGCTGTATG	CAGGGCCAAGCACCATCTAA
Pim-1 (mouse)	GCGGCGAAATCAAACCTCA	TCATAGAGCAGGATCCCAAG

Pim-2 (human)	AGCTCATCGACTTCGGTTCG	TATCGTAGAGAAGCACGCCC
Pim-2 (mouse)	AGCTTTCGAGGCCGAATA	GGTTCCGGGAGATTACTTTG
Pim-3 (human)	GTTCTGGTGCCCTGCTTCAT	TGCATGGTACTGGTGTCGAG
Pim-3 (mouse)	AGCTGAAGCTCATCGACT	GTAGAGCAGTACACCCAGA
PRKG1 (human)	ATCAGGCAAGGTGCAAGAGG	CCTGCAAGGCTTTCTCTCCA
PRKG2 (human)	TCCTGCACAATGGGAAGAGG	ATGGGGTAGCCTCTAGCAGT
CHK2 (human)	GCAGGTTTAGCGCCACTCTG	TCCGACTCCCGAGACATCAC

*Table S 3: Primers used for qPCR analysis of pro-inflammatory markers (mouse)*

<b>Gene</b>	<b>Forward</b>	<b>Reverse</b>
IL-1 $\beta$	GCAACTGTTTCCTGAACTCAACT	ATCTTTTGGGGTCCGTCAACT
IL-6	TAGTCCTTCCTACCCCAATTTCC	TTGGTCCTTAGCCACTCCTTC
iNOS	CCAAGCCCTCACCTACTTCC	CTCTGAGGGCTGACACAAGG
MCP-1	CCACTCACCTGCTGCTACTCA	TGGTGATCCTCTTGTAGCTCTCC
TNF $\alpha$	ACGGCATGGATCTCAAAGAC	AGATAGCAAATCGGCTGACG

Table S 4: Peptides highly phosphorylated in hVAT of MOD as compared to MOND patients

Rank	ID	UniprotAccession	Sequence	Ser	Thr	p-value
1	NCF1_296_308	P14598	RGAPRRSSIRNA	[303, 304]	[]	1.42E-03
2	NCF1_321_333	P14598	QDAYRRNSVRFLQ	[328]	[]	2.09E-03
3	SCN7A_898_910	Q01118	KNGCRRGSSLGQI	[905, 906]	[]	3.31E-03
4	PTN12_32_44	Q05209	FMRLRRLSTKYRT	[39]	[40, 44]	3.84E-03
5	VTNC_390_402	P04004	NQNSRRPSRATWL	[393, 397]	[400]	4.14E-03
6	ADRB2_338_350	P07550	ELLCLRRSSLKAY	[345, 346]	[]	5.74E-03
7	GBRB2_427_439	P47870	SRLRRRASQLKIT	[427, 434]	[439]	5.74E-03
8	CAC1C_1974_1986	Q13936	ASLGRRASFHLEC	[1975, 1981]	[]	6.50E-03
9	BAD_69_81	Q92934	IRSRHSSYPAGTE	[71, 74, 75]	[80]	6.59E-03
10	EPB42_241_253	P16452	LLNKRRGSVPILR	[248]	[]	6.59E-03
11	GPSM2_394_406	P81274	PKLGRRHSMENME	[401]	[]	6.70E-03
12	MYPC3_268_280	Q14896	LSAFRRTSLAGGG	[269, 275]	[274]	6.71E-03
13	NFKB1_330_342	P19838	FVQLRRKSDLETS	[337, 342]	[341]	6.76E-03
14	VASP_150_162	P50552	EHIERRVSNAGGP	[157]	[]	7.15E-03
15	DESP_2842_2854	P15924	RSGSRRGSFDTG	[2843, 2845, 2849]	[2853]	7.76E-03
16	VASP_271_283	P50552	LARRRKATQVGEK	[]	[278]	8.65E-03
17	CGHB_109_121	P01233	QCALCRRSTTDCG	[116]	[117, 118]	8.97E-03
18	KPB1_1011_1023	P46020	QVEFRRLSISAES	[1018, 1020, 1023]	[]	9.05E-03
19	CFTR_730_742	P13569	EPLERRLSLVPDS	[737, 742]	[]	9.24E-03
20	LIPS_944_956	Q05469	GFHPRRSSQGATQ	[950, 951]	[955]	9.53E-03
21	KAP2_92_104	P13861	SRFNRRVSVCAET	[92, 99]	[104]	9.63E-03
22	KCNA6_504_516	P17658	ANRERRPSYLPTP	[511]	[515]	1.00E-02

23	CREB1_126_138	P16220	EILSRRPSYRKIL	[129, 133]	[]	1.01E-02
24	ANDR_785_797	P10275	VRMRHLSQEFQWL	[791]	[]	1.11E-02
25	RYR1_4317_4329	P21817	VRRLRRLTAREAA	[]	[4324]	1.15E-02
26	KAP3_107_119	P31323	NRFTRRASVCAEA	[114]	[110]	1.20E-02
27	E1A_ADE05_212_224	P03255	AILRRPTSPVSRE	[219, 222]	[218]	1.20E-02
28	F263_454_466	Q16875	NPLMRRNSVTPLA	[461]	[463]	1.27E-02
29	ANXA1_209_221	P04083	AGERRRKGTDVNVF	[]	[216]	1.29E-02
30	RAP1B_172_184	P61224	PGKARKKSSCQLL	[179, 180]	[]	1.29E-02
31	KCNA1_438_450	Q09470	DSDLSRRSSSTMS	[439, 442, 445, 446, 447, 450]	[448]	1.31E-02
32	CENPA_1_14	P49450	MGPRRRSRKPEAPR	[7]	[]	1.32E-02
33	REL_260_272	Q04864	KMQLRRPSDQEVS	[267, 272]	[]	1.35E-02
34	TY3H_65_77	P07101	FIGRRQSLIEDAR	[71]	[]	1.35E-02
35	STMN2_90_102	Q93045	AAGERRKSQEAQV	[97]	[]	1.42E-02
36	NMDZ1_890_902	Q05586	SFKRRRSSKDTST	[890, 896, 897, 901]	[900, 902]	1.47E-02
37	PPR1A_28_40	Q13522	QIRRRRPTPATLV	[]	[35, 38]	1.51E-02
38	PLM_76_88	O00168	EEGTFRSSIRRLS	[82, 83, 88]	[79]	1.57E-02
39	NOS3_1171_1183	P29474	SRIRTQSFSLQER	[1171, 1177, 1179]	[1175]	1.57E-02
40	GPR6_349_361	P46095	QSKVPFRSRSPSE	[350, 356, 358, 360]	[]	1.60E-02
41	CSF1R_701_713	P07333	NIHLEKKYVRRDS	[713]	[]	1.74E-02
42	RS6_228_240	P62753	IAKRRRLSSLRAS	[235, 236, 240]	[]	1.85E-02
43	PTK6_436_448	Q13882	ALRERLSSFTSYE	[442, 443, 446]	[445]	1.98E-02
44	FRAP_2443_2455	P42345	RTRTDSYSAGQSV	[2448, 2450, 2454]	[2444, 2446]	2.02E-02
45	PDE5A_95_107	O76074	GTPTRKISASEFD	[102, 104]	[96, 98]	2.09E-02

46	TOP2A_1463_1475	P11388	RRKRKPSTSDSD	[1469, 1471, 1474]	[1470]	2.10E-02
47	H32_3_18	Q71DI3	RTKQTARKSTGGKAPR	[11]	[4, 7, 12]	2.12E-02
48	KCNA2_442_454	P16389	PDLKKSRSASTIS	[447, 449, 451, 454]	[452]	2.13E-02
49	K6PL_766_778	P17858	LEHVTRRTLMDK	[775]	[770, 773]	2.15E-02
50	COF1_17_29	P23528	DMKVRKSSTPEEV	[23, 24]	[25]	2.36E-02
51	ADDB_706_718	P35612	KKKFRTPSFLKKS	[713, 718]	[711]	2.38E-02
52	ESR1_160_172	P03372	GGRERLASTNDKG	[167]	[168]	2.42E-02
53	STK6_283_295	O14965	SSRRTLCLGTLDY	[283, 284]	[287, 288, 292]	2.45E-02
54	H2B1B_27_40	P33778	GKKRKRSRKESYSI	[33, 37, 39]	[]	2.47E-02
55	KIF2C_105_118_S106G	Q99661	EGLRSRSTRMSTVS	[109, 111, 115, 118]	[112, 116]	2.57E-02
56	RAF1_253_265	P04049	QRQRSTSTPNVHM	[257, 259]	[258, 260]	2.62E-02
57	PLEK_106_118	P08567	GQKFARKSTRRSI	[113, 117]	[114]	2.63E-02
58	KPCB_19_31_A25S	P05771	RFARKGSLRQKNV	[25]	[]	2.88E-02
59	BAD_93_105	Q92934	FRGRSRSAPPNLW	[97, 99]	[]	3.08E-02
60	BAD_112_124	Q92934	RELRRMSDEFVDS	[118, 124]	[]	3.30E-02
61	RBL2_655_667	Q08999	GLGRSITSPTTLY	[659, 662]	[661, 664, 665]	3.37E-02
62	KCNA3_461_473	P22001	EELRKARSNSTLS	[468, 470, 473]	[471]	3.40E-02
63	GYS2_1_13	P54840	MLRGRSLSVTSLG	[6, 8, 11]	[10]	3.81E-02
64	RB_242_254	P06400	AVIPINGSRTPR	[249]	[252]	4.66E-02
65	ACM1_444_456	P11229	KIPKRPGSVHRTPT	[451]	[455]	4.93E-02

## Figure Legends

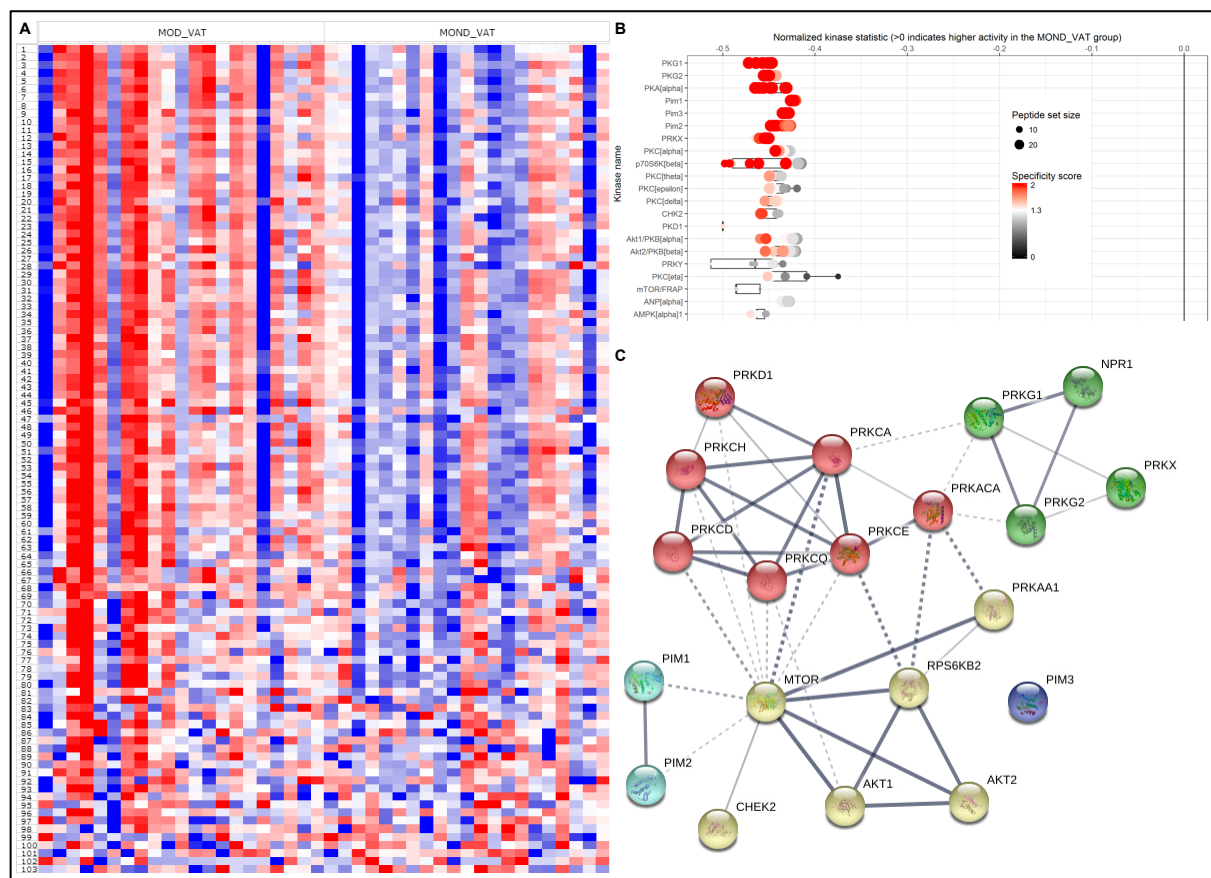


Figure 1: *Pim-1* kinase activity is upregulated in human visceral adipose tissue (hVAT) of morbid obese diabetic (MOD) patients as seen in upstream score plot using kinexus-based analysis.

The heatmap shows that more than 60 peptides were highly phosphorylated in visceral adipose tissue samples from morbid obese diabetic (IR) as compared to samples from morbid obese non-diabetic (IS) patients (A). Upstream kinase analysis was done using the Bionavigator software of the PamGene, which bases its assumption on kinexus. Peptide set size corresponding to each kinase is denoted by the size of the dot. As for the specificity of these peptides to the kinase, it ranges from black (0) to red (2). The darker the red color, the higher the specificity of the peptide set to the kinase. Negative values indicate higher kinase activity in the MOD group. As seen in this score plot, PKG1, PKG2, PKA, Pim-1, Pim-2, Pim-3, PRKX, PKC, p70S6K $\beta$ , CHK2, PKD1, Akt1/PKB, etc. have higher kinase activity in the

hVAT samples from MOD patients, as compared to the hVAT samples from morbid obese non-diabetic (MOND) patients (B). An interaction network was constructed using the STRING tool and the selected kinases as input. The width of the interactions depends on the confidence score to each association in STRING, i.e. the thickness of the lines indicates the strength of the data support. Each color group of the kinases is attributed to a kinase cluster, giving a total of 5 different groups of interacting kinases (C). More detailed information is found in the Materials and Methods section. n = 21-24.

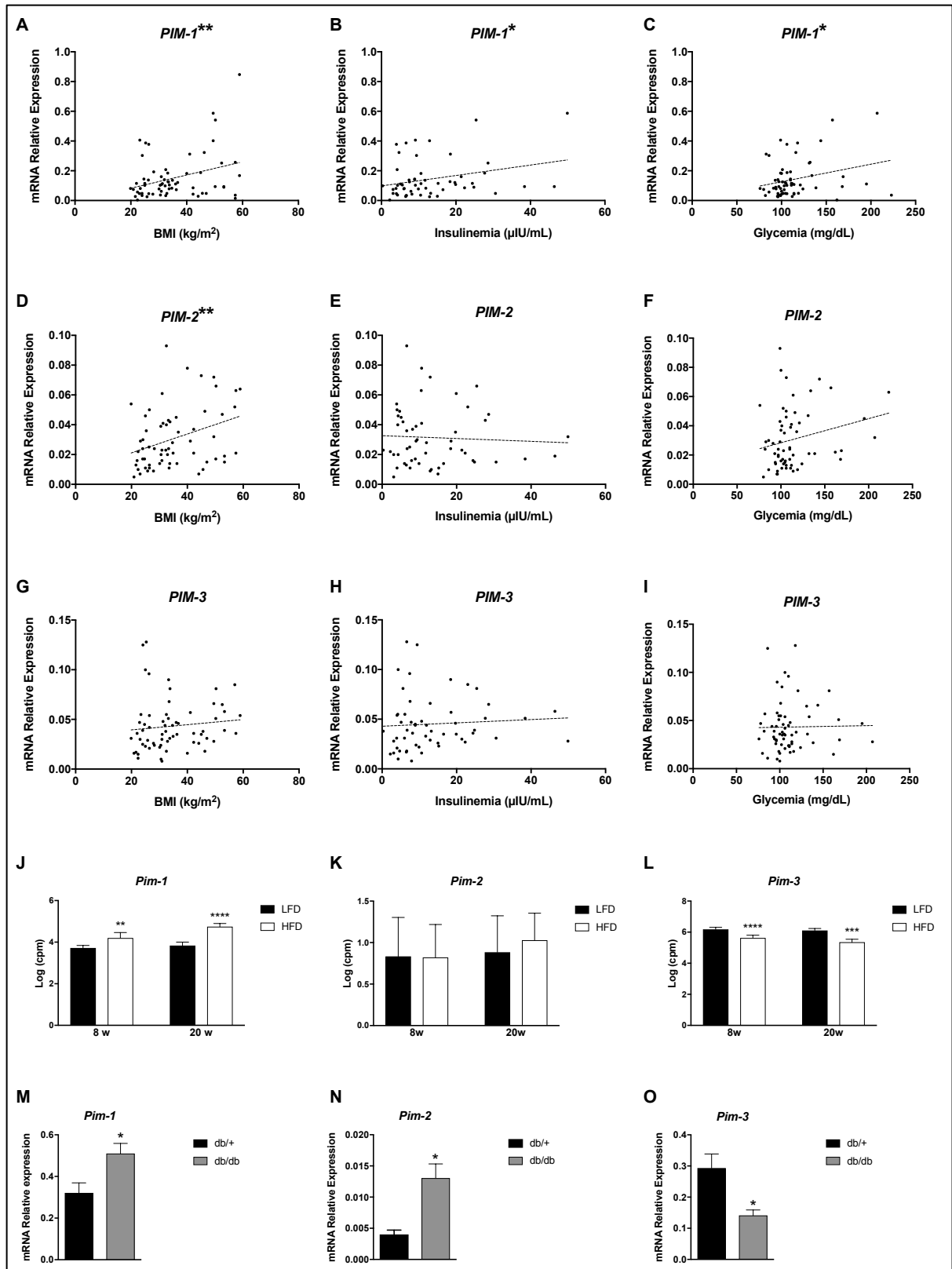


Figure 2: *Pim-1* gene expression positively correlates to IR markers in hVAT and is upregulated in mVAT of 2 IR mouse models.

RTqPCR was performed on visceral adipose tissue samples taken from more than 80 lean, obese, and morbid obese healthy and diabetic patients. Pim-1 relative gene expression positively correlates with BMI (A), insulinemia (B), and glycemia (C). Pim-2 positively correlates with BMI (D), but not with insulinemia (E) or glycemia (F). Pim-3 does not correlate with any of the three markers (G-I). Pim expression was also checked in visceral adipose tissue from 2 mouse models of insulin resistance (J-O). RNA sequencing data of VAT from male mice under CHOW or HFD (8 or 20 weeks) show that Pim-1 expression was significantly increased in VAT of mice under HFD, with higher values in the 20 weeks' duration (J), Pim-2 does not differ (K), and Pim-3 significantly decreases in mice under HFD (L). Pim-1 and Pim-2 gene expression significantly increase in VAT of male db/db mice (M-N), while Pim-3 significantly decreases (O). RS9 and 18S were used as housekeeping genes. Significance of the correlation data was determined using the Pearson correlation coefficients, with \*  $p < 0.05$ , \*\*  $p < 0.01$ . Results of panels D-E represent the average  $\pm$  SEM.  $n = 5-7$  mice. Significance was determined using the Bonferroni-Dunn method, with \*  $p < 0.05$ , \*\*  $p < 0.01$ , \*\*\*  $p < 0.001$ , \*\*\*\*  $p < 0.0001$ .



0.25, 0.5, and 1  $\mu$ M of the inhibitor (E). pT308 Akt was not rescued with the inhibitor treatment (F). RS9 and 18S were used as housekeeping genes in RTqPCR experiments. 10  $\mu$ g of extracted protein was blotted, and  $\alpha$ -Tubulin was used as the loading control. Western blot quantification is done using ImageJ. Results represent the average  $\pm$  SEM, with n=3. Significance was determined using the Bonferroni-Dunn method, with \* p < 0.05, \*\* p < 0.01, \*\*\* p < 0.001, \*\*\*\* p < 0.0001.

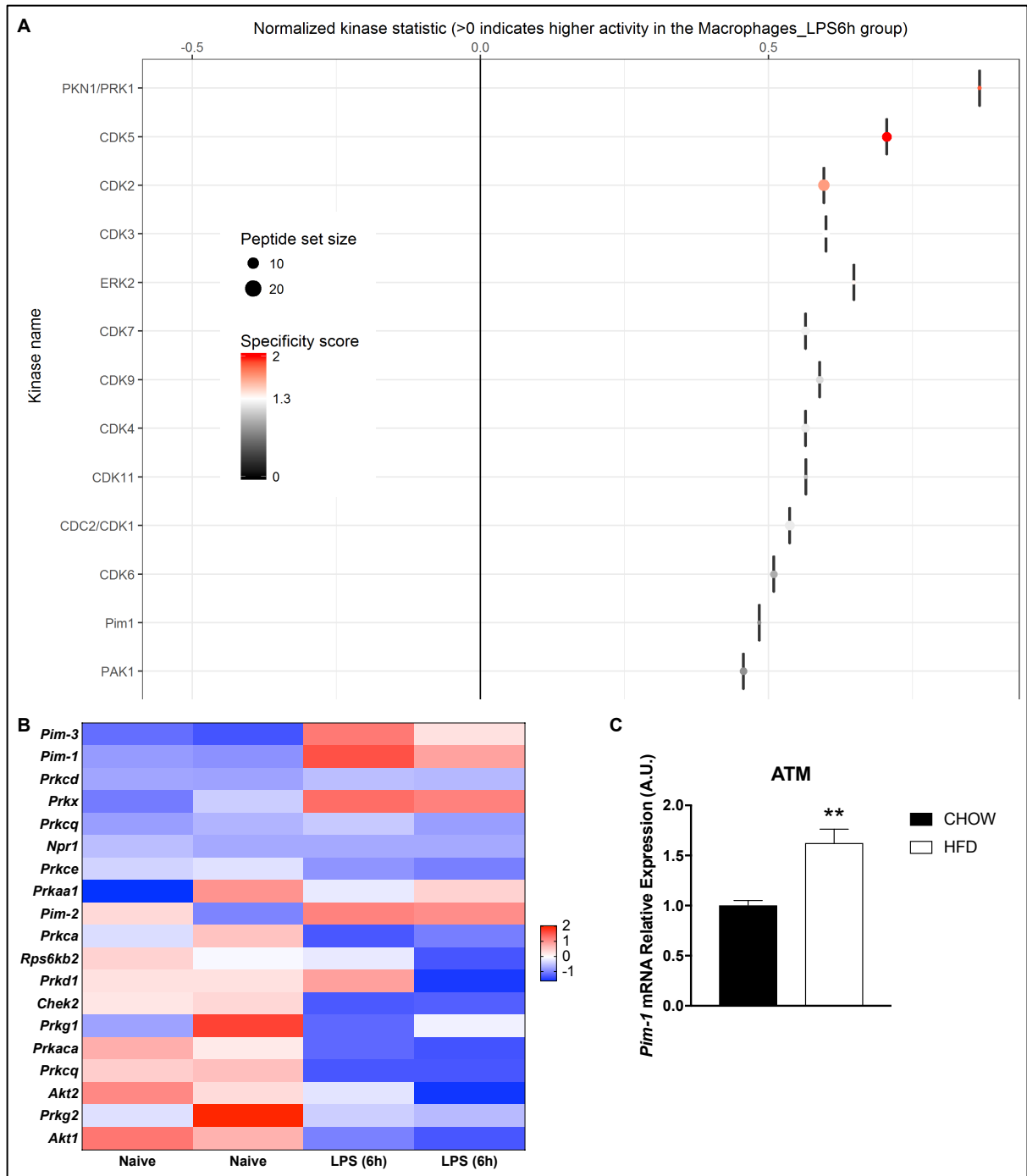


Figure 4: *Pim-1* kinase activity and gene expression are upregulated in pro-inflammatory macrophages.

Protein was extracted from naive and 6h-LPS-stimulated pro-inflammatory BMDMs, and then incubated on PamChip Serine/Threonine kinase microarrays to detect peptide phosphorylation. Upstream kinase analysis was done using the Bionavigator software of the PamGene, which bases its assumption on kinexus. Peptide set size corresponding to each kinase is denoted by

the size of the dot. As for the specificity of these peptides to the kinase, it ranges from black (0) to red (2). The darker the red color, the higher the specificity of the peptide set to the kinase. Positive values indicate higher kinase activity in LPS-stimulated macrophages. As seen in the score plot, PKA, AMPK, several CDKs, and Pim-1 have higher kinase activity in the pro-inflammatory LPS-stimulated macrophages (A). Heat map of the RNA sequencing data from naive and LPS-treated macrophages show that PRKX, Pim-1, and Pim-2 genes are significantly high in the pro-inflammatory as compared to naïve BMDMs (B). RTqPCR data show that Pim-1 mRNA expression is significantly higher in M1-sorted macrophages from VAT of HFD mice (C). PamGene results are the average of 3 independent experiments, each with 4 replicates. B2M was used as the housekeeping gene in RTqPCR experiments, and results represent the average  $\pm$  SEM, n = 6. Significance was determined using the Bonferroni-Dunn method, with \* p < 0.05, \*\* p < 0.01, \*\*\* p < 0.001, \*\*\*\* p < 0.0001.

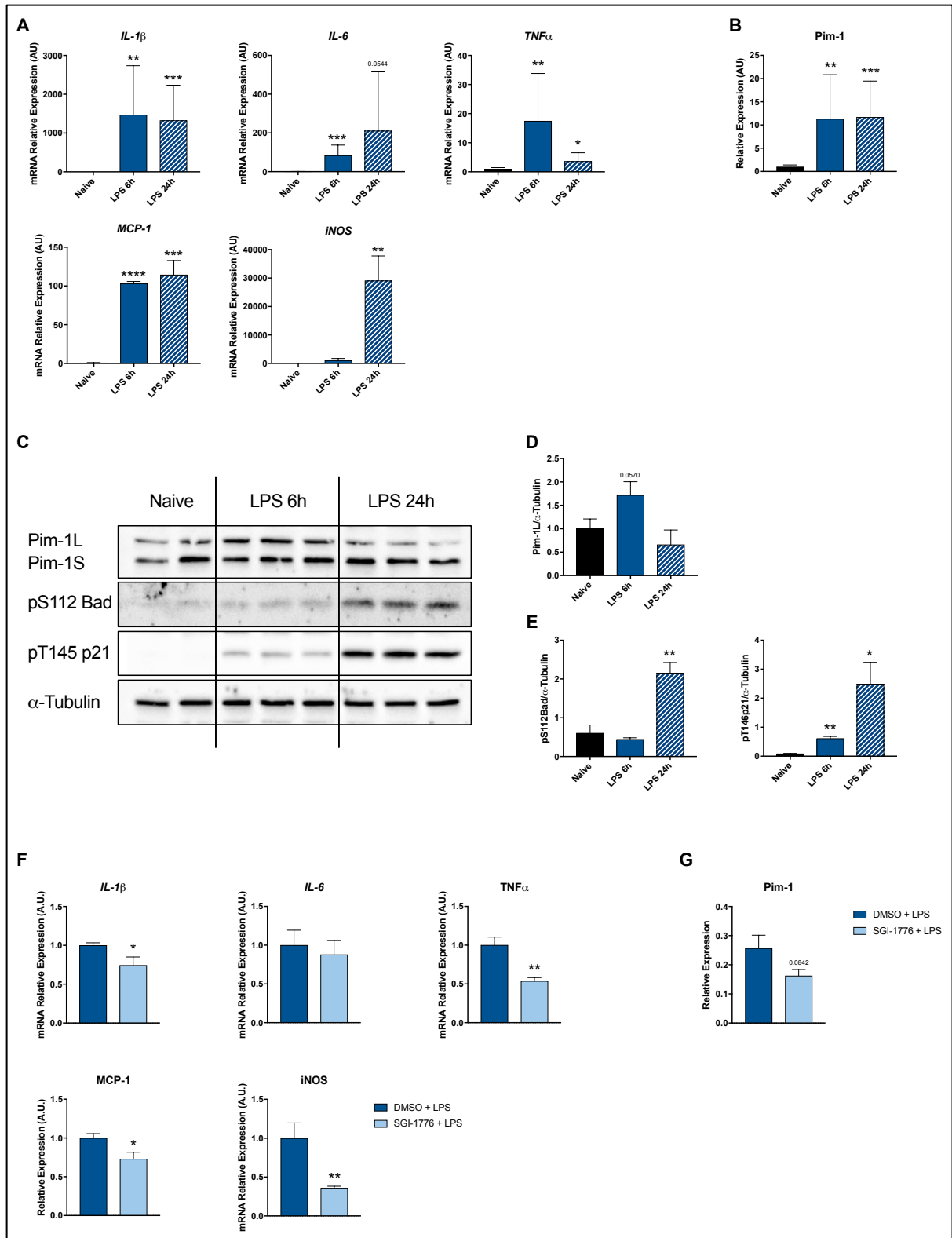


Figure 5: Pim-1 expression is high in LPS-stimulated macrophages, and its inhibition decreases the expression of pro-inflammatory markers.

RTqPCR was performed on naïve and LPS-stimulated (6h, 24h) macrophages (A-B). Expression of pro-inflammatory markers IL-1 $\beta$ , IL-6, TNF $\alpha$ , and MCP-1 significantly increase in LPS-treated macrophages for 6h (A). Pim-1 expression is significantly high in LPS-treated pro-inflammatory macrophages (B). Western blot analysis of naïve and LPS-stimulated macrophages (6h, 24h) against Pim-1, pS112 Bad, and pT145p21 (C). Pim-1 protein expression decreases in LPS-treated macrophages for 6h, while it increases back to normal levels in LPS-treated macrophages for 24h (D). pS112 Bad and pT145p21, Pim-1 phospho targets, significantly increase in LPS-treated macrophages (E). Pro-inflammatory macrophages that are LPS-stimulated for 6h were treated with DMSO or 0.25 $\mu$ M SGI-1776 for 24h. Pro-inflammatory markers IL-1 $\beta$ , TNF $\alpha$ , MCP-1, and iNOS gene expression significantly decrease upon inhibitor treatment (F). Pim-1 gene expression tends to decrease upon inhibitor treatment (G). RS9 and actin were used as housekeeping genes in RTqPCR experiments. 10 $\mu$ g of extracted protein was blotted, and  $\alpha$ -Tubulin was used as the loading control. Western blot quantification is done using ImageJ. Results represent the average  $\pm$  SEM, with n = 3. Significance was determined using the Bonferroni-Dunn method, with \* p < 0.05, \*\* p < 0.01, \*\*\* p < 0.001.

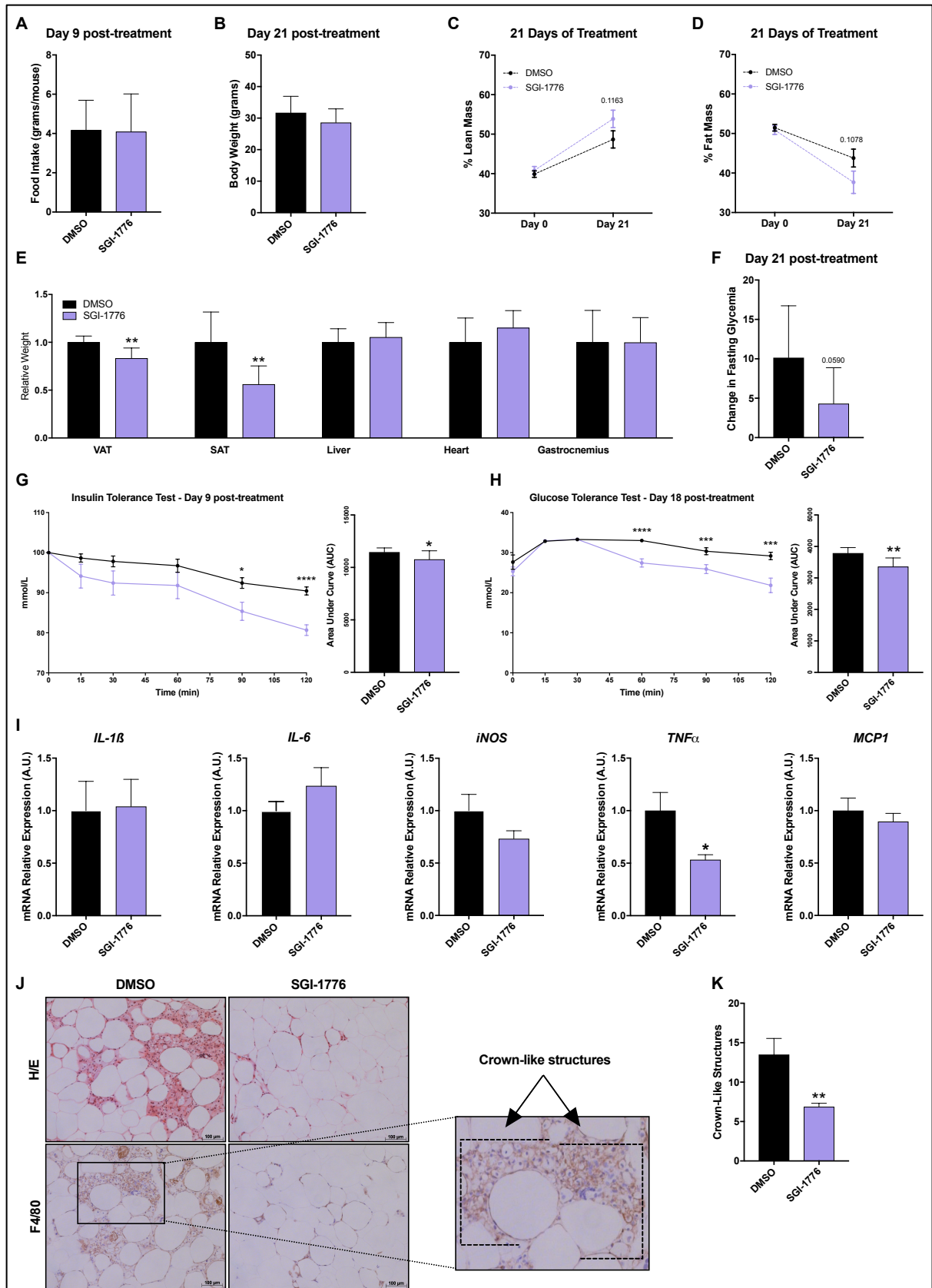
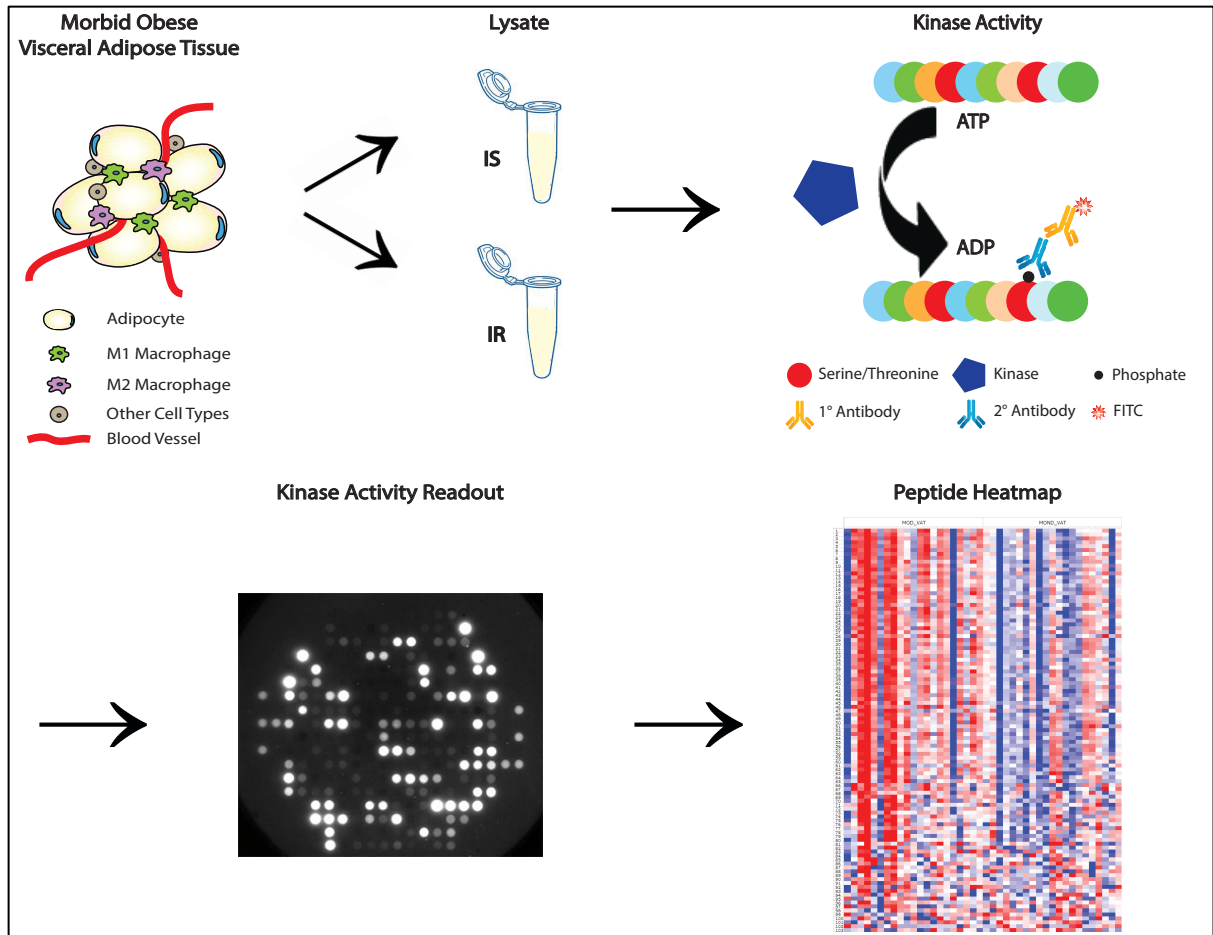


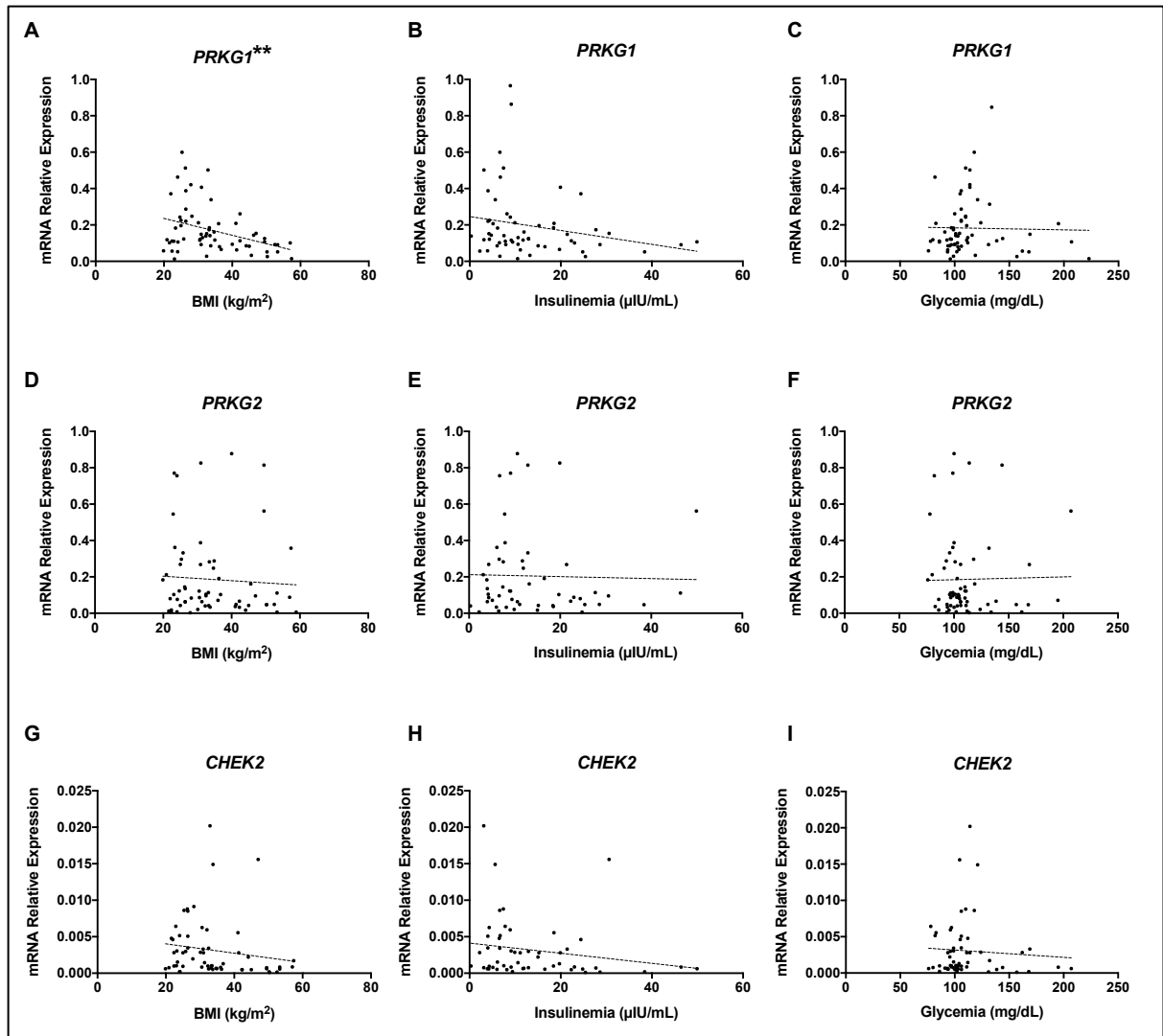
Figure 6: *db/db* mice treated with SGI-1776 for 3 weeks have lower fat mass, increased glucose and insulin sensitivity, and decreased VAT inflammation.

Gavaged mice with DMSO or the Pim-1 inhibitor do not differ in food intake (A) or total body weight (B). However, their % lean mass increases (C), and their % fat mass decreases (D) as compared to the control group. The relative masses of VAT and SAT of treated mice significantly decrease in the treated group, while the relative masses of the liver, heart, and gastrocnemius do not change between the groups (E). The % change in fasting glycemia before and after treatment tends to decrease in the treated group (F). Mice underwent an insulin tolerance test at day 9 post-treatment, in which the treated db/db mice became more insulin sensitive after 1h of insulin injection (G), and had a significant decrease in the Area Under Curve (H). Glucose tolerance test was done on both groups at day 18 post-treatment. Treated mice became more glucose tolerant after 30' of glucose injection (I), and had a significant decrease in the area under curve in SGI-1776-gavaged mice (J). RTqPCR was done on VAT of all mice, and gene expression of several pro-inflammatory macrophage markers was measured. iNOS, TNF $\alpha$ , and MCP-1 decrease in the SGI-1776-gavaged group, while IL-1 $\beta$  and IL-6 tend to increase (K). Cross-sections of the mVAT of control and treated mice were stained for H/E and F4/80, a macrophage marker (L). An example of a crown-like structure is depicted in the magnified image. For each mVAT sample, 20 images were taken and all crown-like structures were counted, and shown to be significantly decreased in mVAT of treated mice (M). Results represent the average  $\pm$  SEM, n = 8-9 mice. Significance was determined using the Bonferroni-Dunn method, with \* p < 0.05, \*\* p < 0.01, \*\*\* p < 0.001, \*\*\*\* p < 0.0001.



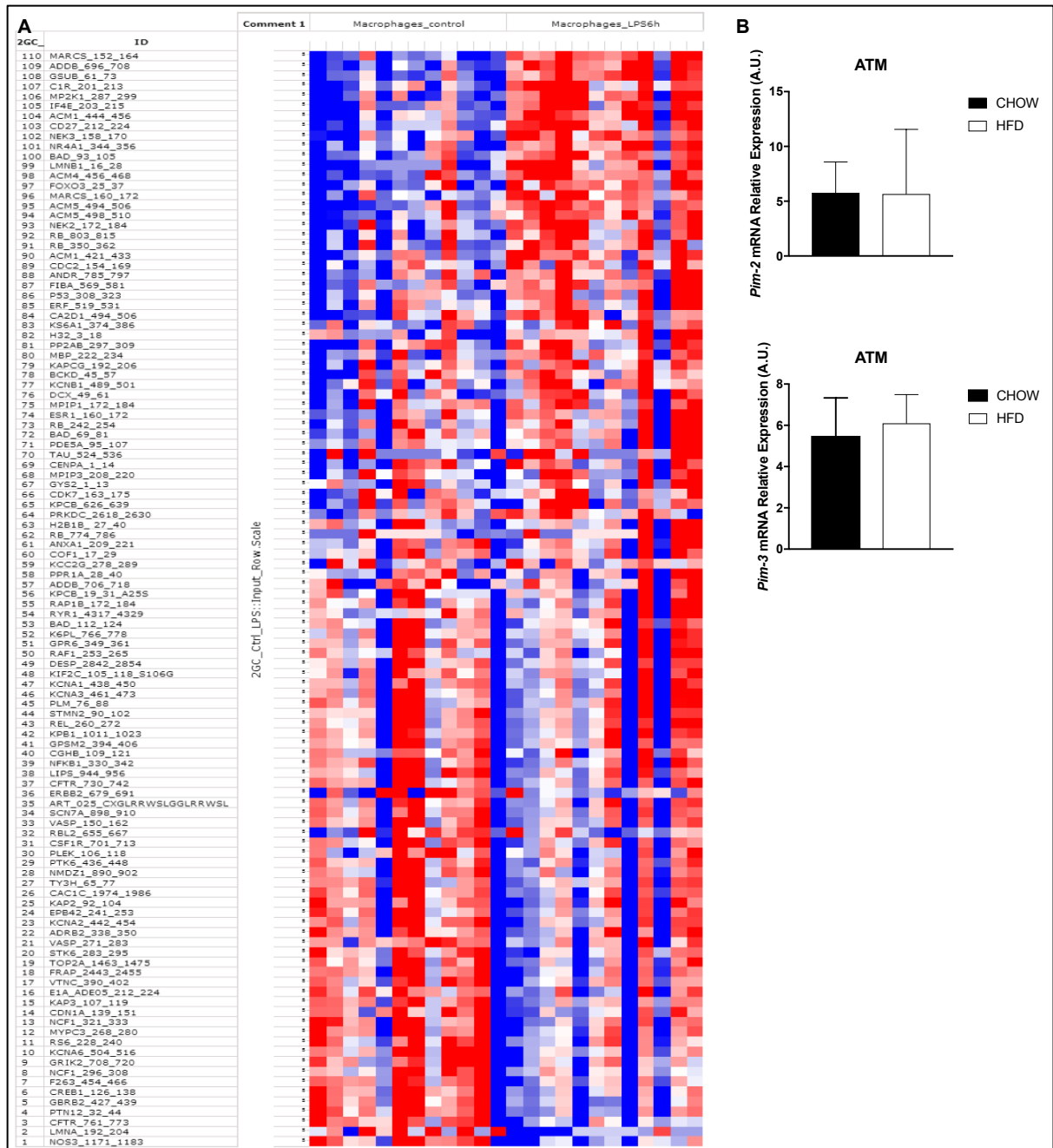
*Supplemental Figure 1: Kinome profiling of human visceral adipose tissue (hVAT) samples from morbid obese diabetic (MOD) and morbid obese non-diabetic (MOND) patients.*

The protein lysate was extracted from morbid obese visceral adipose tissue from IS and IR patients, and were passed into the PamStation, where the samples were incubated on PamChip Serine/Threonine kinase microarrays to detect kinase activity readout, by peptide phosphorylation and FITC labelling. The Log Data is then displayed as a heat map showing that more than 60 peptides were highly phosphorylated in visceral adipose tissue samples from morbid obese diabetic (IR) as compared to samples from morbid obese non-diabetic (IS) patients. The darker the red color, the higher the phosphorylation. The darker the blue color, the lower the phosphorylation. n = 21-24.



Supplemental Figure 2: Gene expression correlations to IR markers in *hVAT* and kinase activity validation of *Pim* family in *mVAT*.

RTqPCR was performed on visceral adipose tissue samples taken from more than 80 lean, obese, and morbid obese healthy and diabetic patients (A-I). *PRKG1* relative gene expression negatively correlates with BMI (A) not insulinemia (B) or glycemia (C). *PRKG2* (D-F) and *CHK2* (G-I) do not correlate with any of the IR markers. *RS9* and *18S* were used as housekeeping genes. Significance was determined using the Pearson correlation coefficients, with \*  $p < 0.05$ , \*\*  $p < 0.01$ .



Supplemental Figure 3: Kinome profiling of naïve and pro-inflammatory macrophages.

Protein was extracted from naïve and 6h-LPS-stimulated pro-inflammatory macrophages. Samples were then incubated on PamChip Serine/Threonine kinase microarrays to detect peptide phosphorylation. As seen in this heat map, the upper 45 peptides were highly phosphorylated in the pro-inflammatory LPS-stimulated macrophages. The darker the red color, the higher the phosphorylation, and the darker the blue color, the lower the phosphorylation (A). RTqPCR data show that Pim-2 and Pim-3 mRNA expression does not

change in M1-sorted macrophages from VAT of HFD mice as compared to mice under CHOW diet (B). PamGene results are the average of 3 independent experiments, each with 4 replicates. B2M was used as the housekeeping gene in RTqPCR experiments, and results represent the average  $\pm$  SEM, with n = 5.

## **Materials and Methods**

### *Human Samples*

Cohort 1: Patients scheduled for a bariatric surgery procedure were recruited from the obesity outpatient clinic of Hospital Universitari Germans Trias, Badalona (Spain) and from the Hospital Universitario Virgen de la Victoria, Malaga (Spain). The study was conducted according to the principles of the Declaration of Helsinki. All patients signed an informed consent form approved by the corresponding institutional ethics committee. Inclusion criteria were as follows: age between 18 and 60 years, BMI >35 kg/m<sup>2</sup>. Exclusion criteria were type 1 diabetes or positivity for GAD autoantibodies, secondary forms of diabetes, acute metabolic complications, liver disease, renal dysfunction or patients under anticoagulant treatment, pregnancy and corticoid use by oral or intravenous route for more than 14 consecutive days in the last 3 months. Patients were classified as having type 2 diabetes (MOD) according to ADA criteria (American Diabetes, 2010) or as morbid obese non-diabetic subjects (MOND). A physical examination with determination of anthropometrical parameters and a complete biochemical analysis was performed before bariatric surgery (Table 1). A sample of visceral fat was obtained during the surgical bariatric procedure.

Cohort 2: lean (20), obese (23) and morbid obese (43) patients were included in the study from a biobank adipose tissue collection (registry number C.0001665 from the national registry of biobank collections at the Instituto de Salud Carlos III (ISCIII) (Spain) managed by the Institut d'Investigacio Sanitaria Pere Virgili (IISPV). Visceral adipose tissue samples with clinical and analytical variables were obtained from this collection and registry. All samples had the corresponding informed consent approved by the IISPV ethics committee. The main clinical and analytical characteristics are shown in table 2.

Glucose, cholesterol and triglycerides were determined using standard enzymatic methods. Plasma insulin was analyzed by immunoassay (Coat-A-Count Insulin; Diagnostic Products Corp., Los Angeles, CA). Glycated haemoglobin (HbA1c) was measured by high-pressure liquid chromatography using a fully automated analyzer system (Hitachi L-9100). The homeostatic model assessment insulin resistance index (HOMA-IR) was calculated by the formula: (plasma glucose (mmol/l) x serum insulin (mU/L)) / 22.5).

#### *Isolation of mature adipocytes and stromal vascular fraction*

SVF was obtained from human adipose tissue biopsies as described (Ceperuelo-Mallafre et al., 2016; Serena et al., 2016; Serena et al., 2017). Briefly, sub-cutaneous white adipose tissue (scWAT) and visceral white adipose tissue (vWAT) was washed extensively with PBS to remove debris and treated with 0.1% collagenase in PBS and 1% BSA for 1 hr at 37°C with gentle agitation. Digested samples were centrifuged at  $300 \times g$  at 4°C for 5 min to separate adipocytes from the SVF. Adipocytes were directly used for RNA isolation and the cell pellet containing the SVF was resuspended in red-blood-cell lysis buffer (10 mM KHCO<sub>3</sub>, 150 mM NH<sub>4</sub>Cl, 0.1 mM EDTA) for 2 min, then washed with PBS and passed through a 40- $\mu$ m filter (Fisher Scientific). To isolate ultrapure ATMs, the SVF was incubated with F4/80 MicroBeads (130-110-443, MiltenyiBiotec S.L. Madrid, Spain) for 30 min and positive selection was performed with an autoMACS separator (MiltenyiBiotec).

#### *Flow cytometry*

The SVF from scWAT and vWAT was isolated as described above. To isolate myeloid lineage cells, SVF was incubated with CD11b MicroBeads (130-049-601, MiltenyiBiotec) for 30 min, and positive selection was performed with an autoMACS separator. Magnetically isolated CD11b<sup>+</sup> cells were washed and incubated with the desired combination of fluorochrome-conjugated monoclonal antibodies, including FITC-anti-F4/80 (clone BM8), APC-anti-CD11c

(clone N418), PE-anti-CD206 (clone MR6F3) and PE-Cy7-anti-Ly-6G (clone RB6-8C5) (all from eBiosciences, San Diego, CA) for 20 min. Data were acquired on a FACS Aria III (BD Biosciences) and analysis was performed using FACSDiva™ software (BD Biosciences).

#### *Kinome Profiling (PamGene):*

For kinome analysis, serine/threonine (STK) kinase microarrays were purchased from PamGene International BV. Each array contained 140 phosphorylatable peptides, as well as 4 control peptides. Sample incubation, detection, and analysis were performed according to the manufacturer's instructions in a PamStation 12. Briefly, extracts from human adipose tissue were made using M-PER mammalian extraction buffer (Thermo Scientific) containing 1:50 Halt phosphatase inhibitor cocktail (Thermo Scientific) and 1:50 Halt protease inhibitor cocktail EDTA-free (Thermo Scientific) for 20 min on a spinning wheel at 4°C. The lysates were then centrifuged at 13,000 r.p.m. for 20 min to remove all debris. The supernatant was aliquoted, snap-frozen in liquid nitrogen, and stored at -80°C until further processing. Prior to incubation with the kinase reaction mix, the arrays were blocked with 2% BSA for 30 cycles and washed three times with PK assay buffer. Kinase reactions were performed over 1 h with 5 µg total extract and 400 µM ATP at 30°C. Phosphorylated peptides were detected with a secondary anti rabbit-FITC antibody that recognizes a pool of anti-phospho serine/threonine antibodies. The instrument contains a 12-bit CCD camera suitable for imaging of FITC-labelled arrays. The images obtained from the phosphorylated arrays were quantified using the bionavigator software (PamGene International BV). Generated heat maps and kinexus plots are further explained in the results and figures sections.

#### *STRING Analysis*

Based on the kinexus plot generated by the bionavigator software (PamGene International BV), we chose the top 20 kinases. The hit kinases were then used as input in the [STRING](#) software. A kinase interaction network was constructed with a minimum required interaction score or medium confidence of 0.4 and several criteria for linkage, i.e. co-expression, experimental evidence, existing databases, text mining, as well as co-occurrence and neighborhood. Further explanation is found in the figure legend.

#### *Mouse Strains and Diet Information*

BKS(D)-Lepr db/+JOrlRj and BKS(D)-Lepr db/db JOrlRj male mice were obtained from Janvier Labs. Mice had free access to standard rodent chow diet and water, unless stated otherwise. They were housed 5 mice per cage in a 12h-day 12h-night cycle, unless stated differently. Animals were gavaged daily with 75mg/kg of vehicle or SGI-1776 (HY-13287) purchased from MedChemTronics, the European branch of MedChemExpress, for 21 consecutive days. Mice were acclimated and submitted to the PhenoMaster (metabolic phenocage) throughout the treatment, by which food intake was measured. Body weight was controlled daily. Following the protocol, mice were killed by cervical dislocation and tissues were isolated for analysis.

Male C57Bl6 mice were fed with HFD with 60% calories from fat (Research Diet D12492) or matched control diet (D12450J) starting from 5 weeks of age.

All animal care and treatment procedures were performed in accordance with Swiss guidelines and were approved by the Canton of Vaud, Service de la Consommation et des Affaires Vétérinaires (SCAV) (authorization VD 3371.b).

#### *Glucose and Insulin Tolerance Tests*

For the Glucose Tolerance Test, mice were starved for 16h and then injected intraperitoneally with glucose (2g/kg). Tail vein blood glucose was checked at the indicated time points. For the

Insulin Tolerance Test, mice were fasted for 6h, after which they were injected intraperitoneally with 1.125 U/kg insulin, and tail vein blood glucose was then measured at the indicated time.

#### *Metabolic Phenocage of the PhenoMaster*

This special automated cage construct separates, collects, and quantifies urine and feces of mice or rats, and thus provides important information about the animal's energy balance. Dedicated urine and feces collection funnels direct urine and feces into standard lab tubes. Weighing sensors below the collection containers quantify urine and feces by amount and time. Before measurement, mice were adapted for five days, after which the mice stayed throughout the whole period of treatment. Individual mice were housed in a single test chamber (size, 8" x 5" x 4"). Animals had free access to food and water during the entire experiment period.

#### *Body Composition Analysis Using the EchoMRI*

Lean body mass, fat mass, free water, and total water were measured on live animals by quantitative magnetic resonance (QMR) using an EchoMRI instrument. Mice were not restrained nor anesthetized.

#### *Immunohistochemistry*

Adipose Tissue samples were fixed overnight at 4°C with 4% paraformaldehyde, and then washed 3 times with cold PBS and embedded in paraffin. 4µm sections cut at 50µm intervals were mounted on charged glass slides, deparaffinized in xylene, and stained for expression of F4/80 as described by (Cecchini et al., 1994) with anti-F4/80 monoclonal antibody (ab6640) from Abcam, and hematoxylin and eosin as described in (Ni et al., 2018). Histological observation was done using light microscopy (Olympus Upright Motorized Microscope, Olympus Corporation, Tokyo, Japan). Image acquisition and processing was performed using the AxioVision software. 2 tissue sections were selected from each mouse, and 20 random non-

overlapping fields at 10x magnification were taken. In a blinded manner, crown-like structures of the F4/80 staining were manually counted.

### *3T3L1 Differentiation*

3T3-L1 were cultured in Dulbecco's modified Eagle's medium (DMEM) with 10% foetal bovine serum (FBS, PAA Laboratories) in 5% CO<sub>2</sub>. Two days after reaching confluence, they were differentiated with DMEM, 10% FBS, 0.5 mM 3-isobutyl-1-methylxanthine (IBMX), 1.7  $\mu$ M insulin, 1  $\mu$ M dexamethasone, and 1  $\mu$ M rosiglitazone for 2 days. From day 3 onward, cells were incubated with DMEM, 10% FBS, 10  $\mu$ g/ml insulin. Media was changed every 2 days until day 8 of differentiation. 3T3-L1 mature adipocytes were maintained in medium containing 10% FBS only.

### *3T3L1 Insulin Resistance Models and Treatment*

After differentiation, mature 3T3L1 adipocytes were washed with PBS and incubated with or without 20 ng/ml TNF $\alpha$  in DMEM containing 0.2% bovine serum albumin (BSA). Insulin resistant mature adipocytes were treated overnight with DMSO, 0.1 $\mu$ M, 0.25 $\mu$ M, 0.5 $\mu$ M or 1 $\mu$ M SGI-1776. Then, cells were starved and stimulated with or without insulin, at 100 nM. Cells were washed with cold PBS and lysed as described later.

### *BMDM Treatment*

Bone marrow-derived macrophages (BMDMs) were seeded in 10cm petri-dishes. After cells attached, they were treated with control or 100ng/mL LPS for 6h or 24h. As for treatment with the inhibitor, BMDMs were seeded in 6-well plates. After they attached, BMDMs were treated with DMSO or 0.25 $\mu$ M SGI-1776 for 24h, and then 100ng/mL LPS was added for 6h.

### *Protein Extraction and Western Blotting:*

For Western blot (WB) analysis, protein extraction from different mouse tissues, cell lysates, and human adipose tissue samples was obtained with M-PER mammalian extraction buffer

(Thermo Scientific, USA) containing 1:100 Halt phosphatase inhibitor cocktail (Thermo Scientific, USA) and 1:100 Halt protease inhibitor cocktail, EDTA-free (Thermo Scientific, USA). Membranes were incubated over night at 4°C with the corresponding primary antibodies. The following day, membranes were washed and incubated with the corresponding secondary antibodies, washed and revealed with ECL in the fusion Fx. WB bands were quantified using ImageJ or Fiji software.

The following antibodies were used for Western blot analysis: anti-phospho AKT-T308 (4056), anti AKT (9272), anti-phospho IKK $\alpha/\beta$ -S176/180 (2697) and anti IKK $\beta$  (8943) from cell signaling, anti-phospho Bad-S112 (ab129192) and anti-phospho p21-T145 (ab135553) from Abcam, anti-PIM1 (AP7932d) from Abgent, and anti-Tubulin (T6199) from Sigma.

#### *RNA Extraction and RTqPCR:*

Samples were lysed using TRI-reagent (T9424, Sigma Aldrich), according to the manufacturer's instructions. An additional centrifugation step immediately after lysis was included in order to remove the lipid layer when adipose tissue samples or mature 3T3L1 adipocytes were extracted. For adipose tissue samples, a second chloroform wash step, followed by an overnight precipitation using ammonium acetate and absolute ethanol, was performed to remove phenol contaminations. Quality check and quantification of the RNA was done using the Nanodrop. cDNA was prepared using 1 $\mu$ g of total RNA (unless stated otherwise), using Superscript II (Invitrogen). cDNAs were diluted 20 times and used for qPCR. qPCR experiments were done using the FastStart Universal SYBR Green Master (Rox) from Roche and a 7900HT Fast Real-Time PCR System (Applied Biosystems), with a mix of 10 $\mu$ M forward and reverse primers of the targeted genes. Relative mRNA expression levels were calculated from the comparative threshold cycle (Ct) values of the gene of interest relative to RS9 and actin mRNA (unless stated otherwise). Specific primer sequences are listed in Table S1, S2 and S3.

*Data Analysis:*

All statistics are described in the figure legends. All *P*-values below 0.05 were considered significant. The results were expressed as means  $\pm$  standard error of the means (s.e.m). Statistical significance values were represented by asterisks corresponding to \**p*<0.05, \*\**p*<0.01, \*\*\**p*<0.001, and \*\*\*\**p*<0.0001.

## **Acknowledgements**

The authors would like to thank the previous and current lab members of Prof. Lluís Fajas group for the helpful discussions, Prof. Béatrice Desvergne for the sharing of unpublished information, the main animal facility and the Mouse Experimental Facility (MEF) at the Center for Integrative Genomics (CIG), and Catherine Moret from the Histology platform at the CIG. We want to particularly acknowledge the patients and the BioBank IISPV (PT17/0015/0029) integrated in the Spanish National Biobanks Network for its collaboration.

This work was supported by the University of Lausanne, the Novartis Foundation for medical-biological Research (#16C2176), the Fundació La Marató de TV3, and the Spanish Ministry of Science, Innovation and Universities (PI17/01503 to J.V-O. and SAF2015-65019-R to S.F-V) co-financed by the European Regional Development Fund (ERDF). The Spanish Biomedical Research Center in Diabetes and Associated Metabolic Disorders (CIBERDEM) (CB07708/0012) is an initiative of the Instituto de Salud Carlos III. I.C.L-M is supported by the Swiss National Science Foundation (Ambizione PZ00P3\_168077). P-C.H. is supported in part by Swiss Cancer League (grant KFS-3949-08-2016), Swiss National Science Foundation (31003A\_163204 and 31003A\_182470) and Cancer Research Institute (CLIP award). E.C. and M.E. are recipients of postdoctoral fellowships from ISCIII, Spain (Sara Borrell program, CD15/00173) and AGAUR, Generalitat de Catalunya (SLT002/16/00120), respectively. S.F-V. acknowledges support from the Miguel Servet tenure-track program (CP10/00438 and CPII16/00008) from the Fondo de Investigación Sanitaria, co-financed by the ERDF.

## **Author Contributions**

A.N., I.C.L-M and L.F. designed the study. A.N. and I.C.L-M performed kinome experiments. A.N., I.C.L-M., A.B. and I.X. analyzed the kinome experiments. A.N. performed *in vitro* and

*in vivo* experiments and their analysis, with the help of I.C.L-M. P-S.L., X.L, W-C.C. and P-C.H performed BMDM cultures and provided BMDM RNA Sequencing data for the top 20 kinase candidates. M.E. and S.F-V. performed the ATM sorting. E-A.F., J.C-A, L.M-C. and E.C. provided technical assistance. T.C. and F.G. provided mouse VAT RNA Sequencing data for the top 20 kinase candidates. F-J.T. and J.V-O. and S.P. provided the human samples, performed anthropometric studies and classified metabolic status of cohorts. A.N., I.C.L-M and L.F. wrote the manuscript.

### **Declaration of Interests**

The authors declare no competing interests.

## References

- Agrawal, N. K., & Kant, S. (2014). Targeting inflammation in diabetes: Newer therapeutic options. *World J Diabetes*, 5(5), 697-710. Retrieved from <https://www.ncbi.nlm.nih.gov/pubmed/25317247>. doi:10.4239/wjd.v5.i5.697
- Amaravadi, R., & Thompson, C. B. (2005). The survival kinases Akt and Pim as potential pharmacological targets. *J Clin Invest*, 115(10), 2618-2624. Retrieved from <https://www.ncbi.nlm.nih.gov/pubmed/16200194>. doi:10.1172/JCI26273
- American Diabetes, A. (2010). Diagnosis and classification of diabetes mellitus. *Diabetes Care*, 33 Suppl 1, S62-69. Retrieved from <https://www.ncbi.nlm.nih.gov/pubmed/20042775>. doi:10.2337/dc10-S062
- An, N., Kraft, A. S., & Kang, Y. (2013). Abnormal hematopoietic phenotypes in Pim kinase triple knockout mice. *J Hematol Oncol*, 6, 12. Retrieved from <https://www.ncbi.nlm.nih.gov/pubmed/23360755>. doi:10.1186/1756-8722-6-12
- Andersen, E., Ingerslev, L. R., Fabre, O., Donkin, I., Altintas, A., Versteyhe, S., . . . Barres, R. (2019). Preadipocytes from obese humans with type 2 diabetes are epigenetically reprogrammed at genes controlling adipose tissue function. *Int J Obes (Lond)*, 43(2), 306-318. Retrieved from <https://www.ncbi.nlm.nih.gov/pubmed/29511320>. doi:10.1038/s41366-018-0031-3
- Ando, Y., Shinozawa, Y., Iijima, Y., Yu, B. C., Sone, M., Ooi, Y., . . . Takahashi, S. (2015). Tumor necrosis factor (TNF)-alpha-induced repression of GKAP42 protein levels through cGMP-dependent kinase (cGK)-Ialpha causes insulin resistance in 3T3-L1 adipocytes. *J Biol Chem*, 290(9), 5881-5892. Retrieved from <https://www.ncbi.nlm.nih.gov/pubmed/25586176>. doi:10.1074/jbc.M114.624759
- Arroyo-Johnson, C., & Mincey, K. D. (2016). Obesity Epidemiology Worldwide. *Gastroenterol Clin North Am*, 45(4), 571-579. Retrieved from <https://www.ncbi.nlm.nih.gov/pubmed/27837773>. doi:10.1016/j.gtc.2016.07.012
- Brandon, A. E., Liao, B. M., Diakanastasis, B., Parker, B. L., Raddatz, K., McManus, S. A., . . . Schmitz-Peiffer, C. (2019). Protein Kinase C Epsilon Deletion in Adipose Tissue, but Not in Liver, Improves Glucose Tolerance. *Cell Metab*, 29(1), 183-191 e187. Retrieved from <https://www.ncbi.nlm.nih.gov/pubmed/30318338>. doi:10.1016/j.cmet.2018.09.013
- Brault, L., Gasser, C., Bracher, F., Huber, K., Knapp, S., & Schwaller, J. (2010). PIM serine/threonine kinases in the pathogenesis and therapy of hematologic malignancies and solid cancers. *Haematologica*, 95(6), 1004-1015. Retrieved from <https://www.ncbi.nlm.nih.gov/pubmed/20145274>. doi:10.3324/haematol.2009.017079
- Cecchini, M. G., Dominguez, M. G., Mocci, S., Wetterwald, A., Felix, R., Fleisch, H., . . . Stanley, E. R. (1994). Role of colony stimulating factor-1 in the establishment and regulation of tissue macrophages during postnatal development of the mouse. *Development*, 120(6), 1357-1372. Retrieved from <https://www.ncbi.nlm.nih.gov/pubmed/8050349>.
- Ceperuelo-Mallafre, V., Ejarque, M., Serena, C., Duran, X., Montori-Grau, M., Rodriguez, M. A., . . . Fernandez-Veledo, S. (2016). Adipose tissue glycogen accumulation is associated with obesity-linked inflammation in humans. *Mol Metab*, 5(1), 5-18. Retrieved from <https://www.ncbi.nlm.nih.gov/pubmed/26844203>. doi:10.1016/j.molmet.2015.10.001
- Copps, K. D., & White, M. F. (2012). Regulation of insulin sensitivity by serine/threonine phosphorylation of insulin receptor substrate proteins IRS1 and IRS2. *Diabetologia*,

- 55(10), 2565-2582. Retrieved from <http://www.ncbi.nlm.nih.gov/pubmed/22869320>. doi:10.1007/s00125-012-2644-8
- Dhanasekaran, S. M., Barrette, T. R., Ghosh, D., Shah, R., Varambally, S., Kurachi, K., . . . Chinnaiyan, A. M. (2001). Delineation of prognostic biomarkers in prostate cancer. *Nature*, 412(6849), 822-826. Retrieved from <https://www.ncbi.nlm.nih.gov/pubmed/11518967>. doi:10.1038/35090585
- Eichmann, A., Yuan, L., Breant, C., Alitalo, K., & Koskinen, P. J. (2000). Developmental expression of pim kinases suggests functions also outside of the hematopoietic system. *Oncogene*, 19(9), 1215-1224. Retrieved from <https://www.ncbi.nlm.nih.gov/pubmed/10713710>. doi:10.1038/sj.onc.1203355
- Garrison, C. B., Lastwika, K. J., Zhang, Y., Li, C. I., & Lampe, P. D. (2017). Proteomic Analysis, Immune Dysregulation, and Pathway Interconnections with Obesity. *J Proteome Res*, 16(1), 274-287. Retrieved from <https://www.ncbi.nlm.nih.gov/pubmed/27769113>. doi:10.1021/acs.jproteome.6b00611
- Goossens, G. H. (2017). The Metabolic Phenotype in Obesity: Fat Mass, Body Fat Distribution, and Adipose Tissue Function. *Obes Facts*, 10(3), 207-215. Retrieved from <https://www.ncbi.nlm.nih.gov/pubmed/28564650>. doi:10.1159/000471488
- Gupta, M. K., & Vadde, R. (2019). Identification and characterization of differentially expressed genes in Type 2 Diabetes using in silico approach. *Comput Biol Chem*, 79, 24-35. Retrieved from <https://www.ncbi.nlm.nih.gov/pubmed/30708140>. doi:10.1016/j.compbiolchem.2019.01.010
- Hotamisligil, G. S., Shargill, N. S., & Spiegelman, B. M. (1993). Adipose expression of tumor necrosis factor- $\alpha$ : direct role in obesity-linked insulin resistance. *Science*, 259(5091), 87-91. Retrieved from <https://www.ncbi.nlm.nih.gov/pubmed/7678183>.
- Huang, X., Liu, G., Guo, J., & Su, Z. (2018). The PI3K/AKT pathway in obesity and type 2 diabetes. *Int J Biol Sci*, 14(11), 1483-1496. Retrieved from <https://www.ncbi.nlm.nih.gov/pubmed/30263000>. doi:10.7150/ijbs.27173
- Huh, J. Y., Park, Y. J., Ham, M., & Kim, J. B. (2014). Crosstalk between adipocytes and immune cells in adipose tissue inflammation and metabolic dysregulation in obesity. *Mol Cells*, 37(5), 365-371. Retrieved from <https://www.ncbi.nlm.nih.gov/pubmed/24781408>. doi:10.14348/molcells.2014.0074
- Kanda, H., Tateya, S., Tamori, Y., Kotani, K., Hiasa, K., Kitazawa, R., . . . Kasuga, M. (2006). MCP-1 contributes to macrophage infiltration into adipose tissue, insulin resistance, and hepatic steatosis in obesity. *J Clin Invest*, 116(6), 1494-1505. Retrieved from <https://www.ncbi.nlm.nih.gov/pubmed/16691291>. doi:10.1172/JCI26498
- Kannel, W. B., Hjortland, M., & Castelli, W. P. (1974). Role of diabetes in congestive heart failure: the Framingham study. *Am J Cardiol*, 34(1), 29-34. Retrieved from <https://www.ncbi.nlm.nih.gov/pubmed/4835750>.
- Ke, M., Wu, H., Zhu, Z., Zhang, C., Zhang, Y., & Deng, Y. (2017). Differential proteomic analysis of white adipose tissues from T2D KKAY mice by LC-ESI-QTOF. *Proteomics*, 17(5). Retrieved from <https://www.ncbi.nlm.nih.gov/pubmed/27995753>. doi:10.1002/pmic.201600219
- Kim, K., Kim, J. H., Youn, B. U., Jin, H. M., & Kim, N. (2010). Pim-1 regulates RANKL-induced osteoclastogenesis via NF- $\kappa$ B activation and NFATc1 induction. *J Immunol*, 185(12), 7460-7466. Retrieved from <https://www.ncbi.nlm.nih.gov/pubmed/21068407>. doi:10.4049/jimmunol.1000885

- Lackey, D. E., & Olefsky, J. M. (2016). Regulation of metabolism by the innate immune system. *Nat Rev Endocrinol*, 12(1), 15-28. Retrieved from <https://www.ncbi.nlm.nih.gov/pubmed/26553134>. doi:10.1038/nrendo.2015.189
- Li, J., Loveland, B. E., & Xing, P. X. (2011). Anti-Pim-1 mAb inhibits activation and proliferation of T lymphocytes and prolongs mouse skin allograft survival. *Cell Immunol*, 272(1), 87-93. Retrieved from <https://www.ncbi.nlm.nih.gov/pubmed/21974958>. doi:10.1016/j.cellimm.2011.09.002
- Li, Z., Lin, F., Zhuo, C., Deng, G., Chen, Z., Yin, S., . . . Li, B. (2014). PIM1 kinase phosphorylates the human transcription factor FOXP3 at serine 422 to negatively regulate its activity under inflammation. *J Biol Chem*, 289(39), 26872-26881. Retrieved from <https://www.ncbi.nlm.nih.gov/pubmed/25096571>. doi:10.1074/jbc.M114.586651
- Liong, S., Barker, G., & Lappas, M. (2017). Placental Pim-1 expression is increased in obesity and regulates cytokine- and toll-like receptor-mediated inflammation. *Placenta*, 53, 101-112. Retrieved from <https://www.ncbi.nlm.nih.gov/pubmed/28487013>. doi:10.1016/j.placenta.2017.04.010
- Liu, H. T., Wang, N., Wang, X., & Li, S. L. (2010). Overexpression of Pim-1 is associated with poor prognosis in patients with esophageal squamous cell carcinoma. *J Surg Oncol*, 102(6), 683-688. Retrieved from <https://www.ncbi.nlm.nih.gov/pubmed/20544717>. doi:10.1002/jso.21627
- McLaughlin, T., Ackerman, S. E., Shen, L., & Engleman, E. (2017). Role of innate and adaptive immunity in obesity-associated metabolic disease. *J Clin Invest*, 127(1), 5-13. Retrieved from <https://www.ncbi.nlm.nih.gov/pubmed/28045397>. doi:10.1172/JCI88876
- Mehta, K. D. (2014). Emerging role of protein kinase C in energy homeostasis: A brief overview. *World J Diabetes*, 5(3), 385-392. Retrieved from <https://www.ncbi.nlm.nih.gov/pubmed/24936260>. doi:10.4239/wjd.v5.i3.385
- Mikkers, H., Nawijn, M., Allen, J., Brouwers, C., Verhoeven, E., Jonkers, J., & Berns, A. (2004). Mice deficient for all PIM kinases display reduced body size and impaired responses to hematopoietic growth factors. *Mol Cell Biol*, 24(13), 6104-6115. Retrieved from <https://www.ncbi.nlm.nih.gov/pubmed/15199164>. doi:10.1128/MCB.24.13.6104-6115.2004
- Narlik-Grassow, M., Blanco-Aparicio, C., & Carnero, A. (2014). The PIM family of serine/threonine kinases in cancer. *Med Res Rev*, 34(1), 136-159. Retrieved from <https://www.ncbi.nlm.nih.gov/pubmed/23576269>. doi:10.1002/med.21284
- Narlik-Grassow, M., Blanco-Aparicio, C., Cecilia, Y., Peregrina, S., Garcia-Serelde, B., Munoz-Galvan, S., . . . Carnero, A. (2012). The essential role of PIM kinases in sarcoma growth and bone invasion. *Carcinogenesis*, 33(8), 1479-1486. Retrieved from <https://www.ncbi.nlm.nih.gov/pubmed/22623646>. doi:10.1093/carcin/bgs176
- Nguyen, M. T., Favelyukis, S., Nguyen, A. K., Reichart, D., Scott, P. A., Jenn, A., . . . Olefsky, J. M. (2007). A subpopulation of macrophages infiltrates hypertrophic adipose tissue and is activated by free fatty acids via Toll-like receptors 2 and 4 and JNK-dependent pathways. *J Biol Chem*, 282(48), 35279-35292. Retrieved from <https://www.ncbi.nlm.nih.gov/pubmed/17916553>. doi:10.1074/jbc.M706762200
- Ni, X., Zhang, L., Peng, M., Shen, T. W., Yu, X. S., Shan, L. Y., . . . Ma, K. T. (2018). Hydrogen Sulfide Attenuates Hypertensive Inflammation via Regulating Connexin Expression in Spontaneously Hypertensive Rats. *Med Sci Monit*, 24, 1205-1218. Retrieved from <https://www.ncbi.nlm.nih.gov/pubmed/29485979>.

- Nihira, K., Ando, Y., Yamaguchi, T., Kagami, Y., Miki, Y., & Yoshida, K. (2009). Pim-1 controls NF- $\kappa$ B signalling by stabilizing RelA/p65. *Cell Death And Differentiation*, 17, 689. Retrieved from <https://doi.org/10.1038/cdd.2009.174>. doi:10.1038/cdd.2009.174  
<https://www.nature.com/articles/cdd2009174#supplementary-information>
- Patsouris, D., Li, P. P., Thapar, D., Chapman, J., Olefsky, J. M., & Neels, J. G. (2008). Ablation of CD11c-positive cells normalizes insulin sensitivity in obese insulin resistant animals. *Cell Metab*, 8(4), 301-309. Retrieved from <https://www.ncbi.nlm.nih.gov/pubmed/18840360>. doi:10.1016/j.cmet.2008.08.015
- Rosen, E. D., & Spiegelman, B. M. (2014). What we talk about when we talk about fat. *Cell*, 156(1-2), 20-44. Retrieved from <https://www.ncbi.nlm.nih.gov/pubmed/24439368>. doi:10.1016/j.cell.2013.12.012
- Serena, C., Keiran, N., Ceperuelo-Mallafre, V., Ejarque, M., Fradera, R., Roche, K., . . . Fernandez-Veledo, S. (2016). Obesity and Type 2 Diabetes Alters the Immune Properties of Human Adipose Derived Stem Cells. *Stem Cells*, 34(10), 2559-2573. Retrieved from <https://www.ncbi.nlm.nih.gov/pubmed/27352919>. doi:10.1002/stem.2429
- Serena, C., Keiran, N., Madeira, A., Maymo-Masip, E., Ejarque, M., Terron-Puig, M., . . . Vendrell, J. (2017). Crohn's Disease Disturbs the Immune Properties of Human Adipose-Derived Stem Cells Related to Inflammasome Activation. *Stem Cell Reports*, 9(4), 1109-1123. Retrieved from <https://www.ncbi.nlm.nih.gov/pubmed/28966116>. doi:10.1016/j.stemcr.2017.07.014
- Shah, N., Pang, B., Yeoh, K. G., Thorn, S., Chen, C. S., Lilly, M. B., & Salto-Tellez, M. (2008). Potential roles for the PIM1 kinase in human cancer - a molecular and therapeutic appraisal. *Eur J Cancer*, 44(15), 2144-2151. Retrieved from <https://www.ncbi.nlm.nih.gov/pubmed/18715779>. doi:10.1016/j.ejca.2008.06.044
- Shaik, A. A., Qiu, B., Wee, S., Choi, H., Gunaratne, J., & Tergaonkar, V. (2016). Phosphoprotein network analysis of white adipose tissues unveils deregulated pathways in response to high-fat diet. *Sci Rep*, 6, 25844. Retrieved from <https://www.ncbi.nlm.nih.gov/pubmed/27180971>. doi:10.1038/srep25844
- Stephens, J. M., Lee, J., & Pilch, P. F. (1997). Tumor necrosis factor-alpha-induced insulin resistance in 3T3-L1 adipocytes is accompanied by a loss of insulin receptor substrate-1 and GLUT4 expression without a loss of insulin receptor-mediated signal transduction. *J Biol Chem*, 272(2), 971-976. Retrieved from <https://www.ncbi.nlm.nih.gov/pubmed/8995390>.
- Sun, W., Yao, S., Tang, J., Liu, S., Chen, J., Deng, D., & Zeng, C. (2018). Integrative analysis of super enhancer SNPs for type 2 diabetes. *PLoS One*, 13(1), e0192105. Retrieved from <https://www.ncbi.nlm.nih.gov/pubmed/29385209>. doi:10.1371/journal.pone.0192105
- Wajchenberg, B. L., Giannella-Neto, D., da Silva, M. E., & Santos, R. F. (2002). Depot-specific hormonal characteristics of subcutaneous and visceral adipose tissue and their relation to the metabolic syndrome. *Horm Metab Res*, 34(11-12), 616-621. Retrieved from <http://www.ncbi.nlm.nih.gov/pubmed/12660870>. doi:10.1055/s-2002-38256
- Wang, Y. C., McPherson, K., Marsh, T., Gortmaker, S. L., & Brown, M. (2011). Health and economic burden of the projected obesity trends in the USA and the UK. *Lancet*, 378(9793), 815-825. Retrieved from <https://www.ncbi.nlm.nih.gov/pubmed/21872750>. doi:10.1016/S0140-6736(11)60814-3

- Wang, Z., Bhattacharya, N., Meyer, M. K., Seimiya, H., Tsuruo, T., Tonani, J. A., & Magnuson, N. S. (2001). Pim-1 negatively regulates the activity of PTP-U2S phosphatase and influences terminal differentiation and apoptosis of monoblastoid leukemia cells. *Arch Biochem Biophys*, 390(1), 9-18. Retrieved from <https://www.ncbi.nlm.nih.gov/pubmed/11368509>. doi:10.1006/abbi.2001.2370
- Warfel, N. A., & Kraft, A. S. (2015). PIM kinase (and Akt) biology and signaling in tumors. *Pharmacol Ther*, 151, 41-49. Retrieved from <https://www.ncbi.nlm.nih.gov/pubmed/25749412>. doi:10.1016/j.pharmthera.2015.03.001
- Weisberg, S. P., McCann, D., Desai, M., Rosenbaum, M., Leibel, R. L., & Ferrante, A. W., Jr. (2003). Obesity is associated with macrophage accumulation in adipose tissue. *J Clin Invest*, 112(12), 1796-1808. Retrieved from <https://www.ncbi.nlm.nih.gov/pubmed/14679176>. doi:10.1172/JCI19246
- Weitzman, S. A., & Gordon, L. I. (1990). Inflammation and cancer: role of phagocyte-generated oxidants in carcinogenesis. *Blood*, 76(4), 655-663. Retrieved from <https://www.ncbi.nlm.nih.gov/pubmed/2200535>.
- Wildman, R. P., Muntner, P., Reynolds, K., McGinn, A. P., Rajpathak, S., Wylie-Rosett, J., & Sowers, M. R. (2008). The obese without cardiometabolic risk factor clustering and the normal weight with cardiometabolic risk factor clustering: prevalence and correlates of 2 phenotypes among the US population (NHANES 1999-2004). *Arch Intern Med*, 168(15), 1617-1624. Retrieved from <http://www.ncbi.nlm.nih.gov/pubmed/18695075>. doi:10.1001/archinte.168.15.1617
- World Health Organization (16 February 2018). Obesity and overweight. Retrieved from: <https://www.who.int/en/news-room/fact-sheets/detail/obesity-and-overweight>.
- Wu, Y., Deng, Y., Zhu, J., Duan, Y., Weng, W., & Wu, X. (2018). Pim1 promotes cell proliferation and regulates glycolysis via interaction with MYC in ovarian cancer. *Onco Targets Ther*, 11, 6647-6656. Retrieved from <https://www.ncbi.nlm.nih.gov/pubmed/30349298>. doi:10.2147/OTT.S180520
- Xu, H., Barnes, G. T., Yang, Q., Tan, G., Yang, D., Chou, C. J., . . . Chen, H. (2003). Chronic inflammation in fat plays a crucial role in the development of obesity-related insulin resistance. *J Clin Invest*, 112(12), 1821-1830. Retrieved from <https://www.ncbi.nlm.nih.gov/pubmed/14679177>. doi:10.1172/JCI19451
- Ye, J. (2013). Mechanisms of insulin resistance in obesity. *Front Med*, 7(1), 14-24. Retrieved from <https://www.ncbi.nlm.nih.gov/pubmed/23471659>. doi:10.1007/s11684-013-0262-6
- Zhang, B. B., Zhou, G., & Li, C. (2009). AMPK: an emerging drug target for diabetes and the metabolic syndrome. *Cell Metab*, 9(5), 407-416. Retrieved from <https://www.ncbi.nlm.nih.gov/pubmed/19416711>. doi:10.1016/j.cmet.2009.03.012



---

## *Appendix D*

---

### **PamgeneAnalyzeR open and reproducible pipeline for kinase profiling**

(BioRxiv. Doi: <https://doi.org/10.1101/589838>)

This is mainly the PamGene analysis part of my kinome project. We have collaborated with the SIB and the Vital IT. Here, we present “pamgeneAnalyzeR”, an R package developed as an alternative to the manual steps necessary to extract the data from PamChip® peptide microarrays images in a reproducible and robust manner. The extracted data can be directly used for downstream analysis.



## PamgeneAnalyzeR open and reproducible pipeline for kinase profiling

Amel Bekkar<sup>1</sup>, Anita Nasrallah<sup>2</sup>, Nicolas Guex<sup>1</sup>, Lluís Fajas<sup>2</sup>, Ioannis Xenarios<sup>2</sup> and Isabel C. Lopez-Mejia<sup>2</sup>

<sup>1</sup> Swiss Institute of Bioinformatics SIB

<sup>2</sup> University of Lausanne UNIL

### Abstract

Protein phosphorylation – catalyzed by protein kinases - is the most common post-translational modification. It increases the functional diversity of the proteome and influences various aspects of normal physiology and can be altered in disease states. High throughput profiling of kinases is becoming an essential experimental approach to investigate their activity and this can be achieved using technologies such as PamChip® arrays provided by PamGene for kinase activity measurement. Here we present "pamgeneAnalyzeR", an R package developed as an alternative to the manual steps necessary to extract the data from PamChip® peptide microarrays images in a reproducible and robust manner. The extracted data can be directly used for downstream analysis.

**Availability and implementation:** PamgeneAnalyzeR is implemented in R and can be obtained from <https://github.com/amelbek/pamgeneAnalyzeR>.

### Introduction

Analytical pipelines are at the heart of several research endeavors, improving and providing transparent mechanisms for the analysis of complex data. One of the challenges we are facing in today technology providers is the increased necessity for a direct transfer from raw data to an analytical framework. This challenge has been taken on the technology called PamGene that enables the parallel analysis of over 500 kinases and their substrates<sup>1</sup>.

Protein phosphorylation, which consists of a reversible transfer of a phosphoryl group onto specific amino acids on target proteins, is the most common post-translational modification. This mechanism increases the functional diversity of the proteome and influences various aspects of normal physiology by activating and deactivating enzymes, receptors and regulatory proteins. Enzymes known as protein kinases catalyze these events. Protein phosphorylation is often altered in pathological conditions, like cancer, metabolic diseases and neurodegenerative diseases<sup>2, 3, 4</sup>. Kinases phosphorylate their specific targets on specific serine, threonine, and tyrosine residues. Protein kinases can function as receptors on the cell surface or as intracellular mediators. They are essential players in signal transduction and participate in the regulation of all cellular functions, such as proliferation, metabolism, survival and apoptosis.

Unlike methods such as transcriptomics, which only assess the transcribed quantity of each kinase, PamChip® arrays allow a direct examination of kinases at an activity level (kinome profiling). High throughput kinome profiling is becoming an essential experimental approach to investigate aspects of cell and tissue function in physiologic and pathologic conditions. Several techniques,

known as phosphoproteomics, have been developed as adaptations of traditional proteomics, to survey protein phosphorylation on a large scale<sup>5,6</sup>. However, phosphoproteomics only measure steady state protein phosphorylation and do not directly reflect cellular dynamics. Alternative approaches using peptide arrays allow the measurement of direct kinase function. Several peptide arrays were developed to measure kinase activity<sup>1,7</sup>. One of those technologies, developed by PamGene, provides PamChip<sup>®</sup> arrays for kinase activity measurement. PamChip<sup>®</sup> arrays contain peptides with one or several phosphorylatable residues. Upon incubation with a biological sample this technology enables to measure kinase activity using phosphorylated peptides as readout.

### **PamGene PamChip<sup>®</sup> arrays**

PamChip arrays consists of 144 distinct peptides, each composed of 12–15 amino acids, with one or more phospho-sites. PamGene proposes two different types of arrays with peptides containing tyrosine or serine/threonine phosphorylation sites. The PamChips were designed to capture the activity of upstream kinases of either the tyrosine kinome (protein tyrosine kinase or PTK) or the serine/threonine kinome (serine/threonine kinase or STK) respectively. Peptides are printed onto the array in ‘spots’, and like for other microarray technologies, FITC-conjugated antibodies are used to quantify the phosphorylation signal by quantifying the image pixel brightness at each spot. To capture the kinetic of the reactions, the sample fluid is pumped during several cycles. Images are taken at fixed cycle intervals over the course of a reaction. Depending on the chosen experimental design images can be taken at a fix or a varying camera exposure time (10ms, 20ms, 50ms, 100ms, 200ms).

PamGene experiments can generate substantial amounts of data in the form of images taken at different cycles and camera exposure times. Those images have to be explored carefully with the aim of removing and identifying failed chips, which is tedious and prone to operator variation. To enable an operator independent reproducible analysis, we propose “pamgeneAnalyzeR”, an open-source R package that extracts the raw data signal from the PamChip images. The extracted data quantification can be used subsequently for downstream analyses such as kinetic exploration or differentially phosphorylated peptides detection. The pamgeneAnalyzeR is an alternative approach to BioNavigator (licensed by PamGene) that aims to automate the data analysis.

### **Methodology**

The proposed R package is composed of a set of functions that are used to extract data from the images and prepare it for further analysis (figure 1). Raw images acquired by the camera are directly used as input of this package. One reference image is selected to detect the centers of peptides spots as well as the right and left controls. The reference image should have at least clear bright left and right control spots, which are used to identify the optimal parameter for the radius of the spot during quantification. This parameter is necessary, since bleaching and spreading of the signal can occur depending on the acquisition

protocol. At this step, QC images showing the radius of the spots overlaid onto raw images can be generated. The centers of the spots are used thereafter with the chosen radius to draw a circle on each spot, inside which the pixel brightness values are captured. The pipeline then automatically aligns all the other images onto the chosen reference image and the signal of each spot of each image is extracted. As an assessment of the quality of the process, a synthetic image can be reconstructed from the extracted signal and compared to the original one to ensure that the pixel values were extracted correctly and no drift or shift is observable. Summary statistics of pixel brightness (mean, median, standard deviation and sum) are collected for each peptide spot, the left and right control point as well as 8 control background points.

All collected signals are then merged in a unique R data frame. By default, the median pixel brightness value of each spot is used since it represents a robust measure of the spot signal once aligned to the reference. For background normalization we subtract from each spot the mean of background control spots. A Z'-factor is calculated for each sample representing the dynamic range between positive and negative controls contained by each PamGene chip. Z'-factor values between 0.5 and 1 are considered excellent, values between 0 and 0.5 may be acceptable, and values less than 0 indicate the assay is unlikely to be usable, since positive and negative control readout overlap heavily, indicating that the chip for a given experiment has had some failure.

## Conclusion

Kinome profiling to investigate biological processes is becoming easily accessible thanks to methods such as PamGene PamChip® arrays that provide a valuable tool for direct exploration of cellular kinase activities<sup>8,9,10</sup>. The ability to develop bioinformatic tools to extract and analyze the data in a reproducible and robust manner is critical. We have developed "pamgeneAnalyzeR", an automated R package as an alternative to the manual steps commonly used to analyze such arrays, with the idea to implement this technique in pipelines applied to cancer and diabetes research. The extracted data can be directly used for downstream analysis. Other tools are also developed allowing downstream analysis of PamChip data, such as the Kinomics toolbox<sup>11</sup>, indicating the interest for this technology and the need for analysis frameworks. The aim of providing this software as an open-source GPL license is to help researchers take full advantage of the technology and also integrate it more in their complex data acquisition environment.

## Acknowledgments

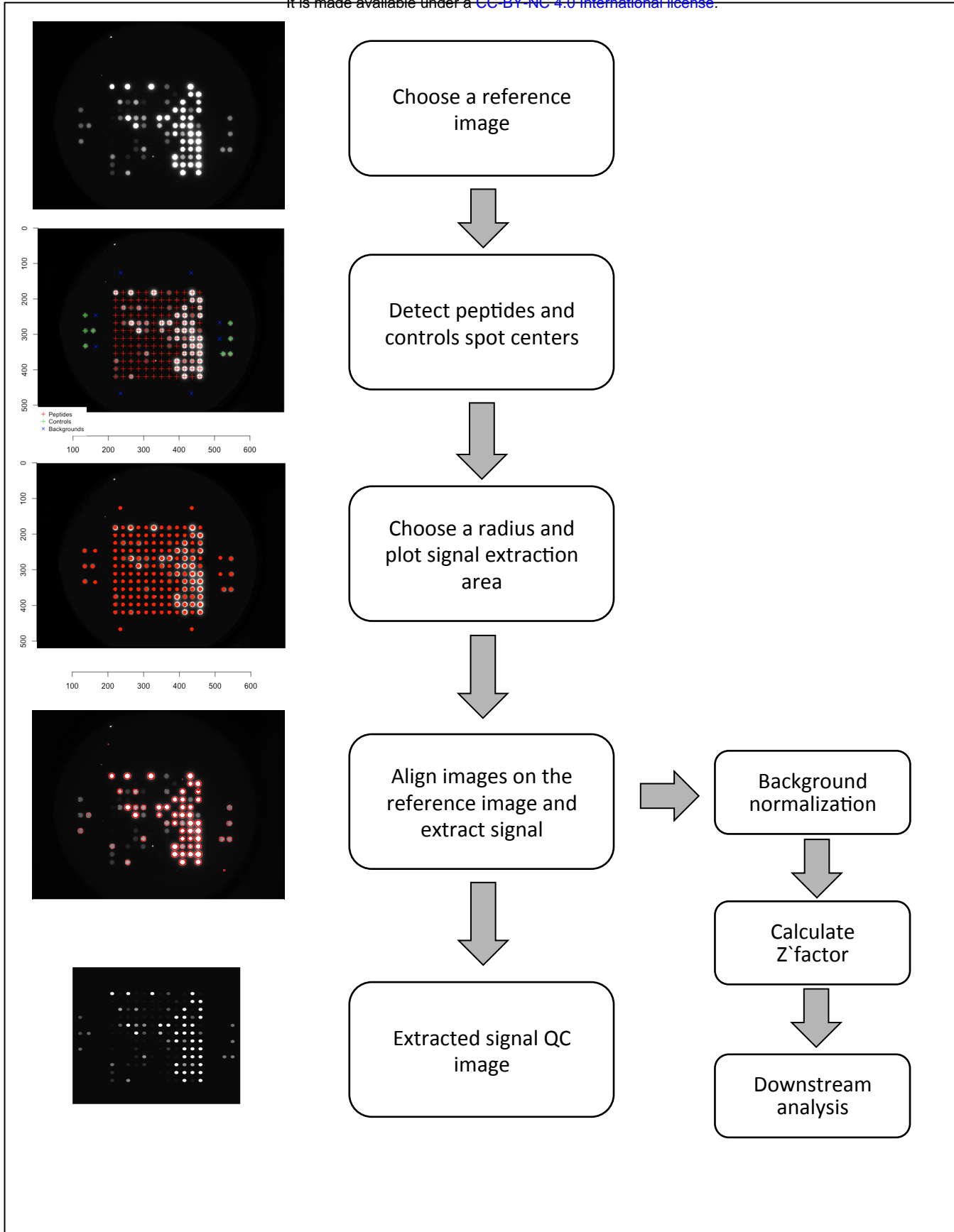
We are thankful to Julien Dorier for his advice.

## References

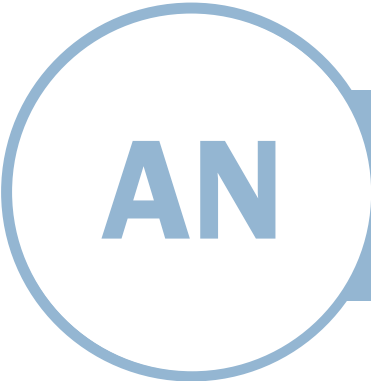
1. Arsenault R, Griebel P, Napper S. Peptide arrays for kinome analysis: New opportunities and remaining challenges. *Proteomics*. 2011;11(24):4595-4609. doi:10.1002/pmic.201100296.

2. Ardito F, Giuliani M, Perrone D, Troiano G, Lo Muzio L. The crucial role of protein phosphorylation in cell signaling and its use as targeted therapy (Review). *Int J Mol Med*. 2017;40(2):271-280. doi:10.3892/ijmm.2017.3036.
3. Humphrey SJ, James DE, Mann M, James DEM, De M, Mann ). Special Issue: Systems Approach to Metabolic Disease Protein Phosphorylation: A Major Switch Mechanism for Metabolic Regulation. *Trends Endocrinol Metab*. 2015;26(12). doi:10.1016/j.tem.2015.09.013.
4. Scurfield AK. Reviewing the Diverse Effects of Protein Phosphorylation in Neural Signaling Transduction. *J Undergrad Neurosci Educ*. 2018;16(2):R54-R56. Available at: <http://www.ncbi.nlm.nih.gov/pubmed/30057512>. Accessed February 25, 2019.
5. White FM, Wolf-Yadlin A. Methods for the Analysis of Protein Phosphorylation-Mediated Cellular Signaling Networks. *Annu Rev Anal Chem*. 2016;9(1):295-315. doi:10.1146/annurev-anchem-071015-041542.
6. Jünger MA, Aebersold R. Mass spectrometry-driven phosphoproteomics: patterning the systems biology mosaic. *Wiley Interdiscip Rev Dev Biol*. 2014;3(1):83-112. doi:10.1002/wdev.121.
7. Baharani A, Trost B, Kusalik A, Napper S. Technological advances for interrogating the human kinome. *Biochem Soc Trans*. 2017;45(1):65-77. doi:10.1042/BST20160163.
8. Schwill M, Tamaskovic R, Gajadhar AS, Kast F, White FM, Plückthun A. Systemic analysis of tyrosine kinase signaling reveals a common adaptive response program in a HER2-positive breast cancer. *Sci Signal*. 2019;12(565):eaau2875. doi:10.1126/scisignal.aau2875.
9. Rabhi N, Hannou SA, Gromada X, et al. Cdkn2a deficiency promotes adipose tissue browning. *Mol Metab*. 2018;8:65-76. doi:10.1016/j.molmet.2017.11.012.
10. Lagarrigue S, Lopez-Mejia IC, Denechaud P-D, et al. CDK4 is an essential insulin effector in adipocytes. *J Clin Invest*. 2015;126(1):335-348. doi:10.1172/JCI81480.
11. Dussaq AM, Kennell T, Eustace NJ, Anderson JC, Almeida JS, Willey CD. Kinomics toolbox—A web platform for analysis and viewing of kinomic peptide array data. Gupta D, ed. *PLoS One*. 2018;13(8):e0202139. doi:10.1371/journal.pone.0202139.

Figure1: General package workflow. From raw images to extracted signal.







AN

# ANITA NASRALLAH

+41 79 951 87 59 | E: ANITA.NASRALLAH@UNIL.CH  
CHEMIN DE BOSTON 9C, 1004 LAUSANNE, VAUD, SWITZERLAND

## PROFESSIONAL SUMMARY

Results-oriented research scientist, successful at contributing to research, mentoring students and teaching classes in a productive and efficient manner. Methodical professional with an analytical approach. Passionate about metabolism and its crosstalk with other fields.

## AWARDS

- 1<sup>st</sup> place winner – EMBO Molecular Medicine Poster Prize – Oct 2017
- 2<sup>nd</sup> place winner – 5<sup>th</sup> Annual Conference in Biology and Biomedical Sciences – May 2012
- Honor Society (LAU) – Academic Excellence – 2007-2010

## WORK

**TEACHING INSTRUCTOR**  
2015-2019 | UNIL

**ORGANIZING COMMITTEE MEMBER**  
2018 | LIMNA

**ACADEMIC COORDINATOR**  
2012-2014 | LAU

## SKILLS

- Excellent interpersonal skills, ability to work under pressure, and optimum time management
- Highly committed and self-driven team player, with the ability to multitask
- In depth experience in written and oral communication, and international collaborations
- In depth knowledge in working with animal models (metabolic phenotyping, explants, xenografts, etc.) and cell culture
- In depth proficiency in research training techniques: molecular techniques (RNAi, RTqPCR), microscopy, flow cytometry, cancer motility (invasion, adhesion), plasmid construction, etc.
- Highly competent in data management and analysis: PamGene, BioNavigator, Illustrator, Photoshop, FIJI, ImageJ, GraphPad, Serial Cloner, etc.
- Languages: Arabic and English (mother languages), and French (oral and written)

## EDUCATION

**PHD • 2019 • UNIVERSITY OF LAUSANNE (UNIL)**  
Life Sciences – Cardiovascular and Metabolism (Diabetes)

**MSC • 2013 • LEBANESE AMERICAN UNIVERSITY (LAU)**  
Molecular Biology (Cancer)

**BSC • 2010 • LEBANESE AMERICAN UNIVERSITY (LAU)**  
Biology

## CERTIFICATES

- Data Management Plan and Open Data – Nov 2018
- Public Dissemination Skills – Sept 2018
- Biostatistics for Non-Statisticians – Jan 2016
- Transgenic Mice and their Application in Biomedical Research – Mar 2015

## PUBLICATIONS

---

### 2017

- **CDK4 Phosphorylates AMPK $\alpha$ 2 to Inhibit Its Activity and Repress Fatty Acid Oxidation.** Lopez-Mejia IC, Lagarrigue S, Giralt A, Martinez-Carreres L, Zanou N, Denechaud PD, Castillo-Armengol J, Chavey C, Orpinell M, Delacuisine B, [Nasrallah A](#), Collodet C, Zhang L, Viollet B, Hardie DG, Fajas L.
- **Cancer: Linking Powerhouses to Suicidal Bags.** [Nasrallah A](#)\*, Martinez-Carreres L\*, Fajas L.

### 2014

- **Daucus carota Pentane/Diethyl Ether Fraction Inhibits Motility and Reduces Invasion of Cancer Cells.** Zgheib P, Daher CF, Mroueh M, [Nasrallah A](#), Taleb RI, El-Sibai M.
- **StarD13 is a tumor suppressor in breast cancer that regulates cell motility and invasion.** Hanna S, Khalil B, [Nasrallah A](#), Saykali BA, Sobh R, Nasser S, El-Sibai M.
- **The regulation of RhoA at focal adhesions by StarD13 is important for astrocytoma cell motility.** Khalil BD, Hanna S, Saykali BA, El-Sitt S, [Nasrallah A](#), Marston D, El-Saban M, Hahn KM, Symons M, El-Sibai M.
- **Effect of StarD13 on colorectal cancer proliferation, motility and invasion.** [Nasrallah A](#), Saykali BA, Al Dimassi S, Khoury N, Hanna S, El-Sibai M.

## MANUSCRIPTS UNDER REVISION/IN SUBMISSION

---

### Under Revision

- **CDK4 regulates lysosomal function and mTORC1 activation to promote cancer cells survival.** Martínez-Carreres L, Orpinell M, Puyal J, Castillo-Armengol J, Giralt A, Moret C, Barquissau V, [Nasrallah A](#), Pabois A, Zhang L, Coukos G, Romero P, Lopez-Mejia IC and Fajas L. (**Cancer Research**)

### In Submission

- **Global kinome analysis in obese subjects reveals PIM-1 as a novel target for the treatment of insulin resistance.** [Nasrallah A](#), Liu PS, Aria Fernandez E, Li X, Ejarque M, Caputo T, Castillo-Armengol J, Martinez-Carreres L, Gilardi F, Tinahones FJ, Fernandez-Veledo S, Vendrell J, Ho PC, Lopez-Mejia IC, Fajas L. (**Cell Metabolism**)
- **PamGeneAnalyzeR open and reproducible pipeline for kinase profiling.** Bekkar A, [Nasrallah A](#), Dorier J, Guex N, Fajas L, Xenarios I, Lopez-Mejia IC. (**Bioinformatics**)

## SELECTED CONFERENCES/WORKSHOPS

---

- Thematic LIMNA Symposium: Central Regulation of Metabolism and Feeding (UNIL – Nov 2018)
- Journée Scientifique G2L2: 2018 Symposium in Metabolism (UNIGE – Oct 2018)
- Cardiovascular and Metabolism Mini-Symposium : Bioinformatics for Personalized Health (CHUV – May 2018)
- Tarraco-Malacca V Joint Workshop ( HUJ23, Tarragona, Spain – Jan 2018)
- Frontiers in Metabolism – EMBO (EPFL – Oct 2017)
- Journée Scientifique G2L2 ( CHLS, Lyon, France – May 2017)

## REFERENCES

---

LLUIS FAJAS COLL, Full Professor, UNIL, Lausanne, [lluis.fajas@unil.ch](mailto:lluis.fajas@unil.ch), +41 76 611 16 75

JOAN VENDRELL ORTEGA, MD Professor, HUJ23, Tarragona, Spain, [jvortega2002@gmail.com](mailto:jvortega2002@gmail.com), +34 97 729 58 00

MIRVAT EL SIBAI, Associate Professor, LAU Beirut, [mirvat.elsibai@lau.edu.lb](mailto:mirvat.elsibai@lau.edu.lb), + 961 3 473 008